Chapter 2 · CO_2 LASERS

P. K. CHEO†

BELL TELEPHONE LABORATORIES, INC.
WHIPPANY. NEW JERSEY

I. Historical Review

Early in 1964, Patel et al. (*I*) first reported the observation of CW laser action in CO_2 gas at approximately 10 μ. This discovery came at a time when the search for new laser transitions from ionic and molecular species was near its peak, and this particular laser did not attract any more attention than hundreds of other laser transitions

†*Present address:* United Aircraft Research Laboratories, East Hartford, Connecticut.

reported at that time. A few months later, Patel(*2*) published a detailed study of both the CW (~ 1 mW) and pulsed output power spectra of the CO_2 laser and also presented an interpretation(*3*) of previously reported results. Similar studies were made independently by a group of French scientists(*4–6*) whose interests were primarily in molecular spectroscopic research.

Within a two-year period, two great advances were made. The first was the use of a mixture of nitrogen and CO_2 as the active medium, which was suggested almost simultaneously by Legay and Legay-Sommaire(*7*) and by Patel(*8*). Patel(*9*) later demonstrated that resonant transfer of the vibrational energy from the N_2 metastable state ($v = 1$) to the upper CO_2 laser level ($00^0 1$) increased the CO_2 laser output from the milliwatts range up to about 10 W. The other advance was made by Moeller and Rigden(*10*), who showed that helium can enhance the laser output as well as nitrogen, although the mechanism was not well understood at that time. In the meantime, Patel et al.(*11*) obtained from a CO_2 laser a very impressive CW output power in excess of 100 W by using a flowing CO_2–N_2–He gas mixture. This was a significant achievement in view of the fact that good optical quality IR components were not available at that time. It was then evident that the efficiency and average output power of this laser are unique when compared with all other existing lasers. Recently(*11a*), CW laser output in excess of 11 kW and multijoule Q-switched laser pulse have been obtained from a compact CO_2 laser with a 1-m discharge length. A short sealed-off CO_2 laser (~ 1 ft in length) with a long-term stability better than one part in 10^{10} or a short term of only a few cycles at optical frequency has been achieved and can provide a single frequency and single mode output greater than 1 W with about 15% efficiency. Also short and fast-rise pulses on the order of nanoseconds can be generated by an electrooptic technique. Clearly this laser can be useful in basic research and in important communication, military, and industrial applications.

Recently (1966–1969), very intensive research and development activities on the CO_2 laser and related areas were carried out in industrial, government, and university laboratories. These can be categorized as follows:

1. Investigation of mechanisms responsible for high efficiency and high gain or power. This involves mainly the studies of relaxation (*12–15*) and electronic excitation(*16–18*) processes. In addition to the well-known resonant transfer(*7,8*), much information has been obtained concerning the low-lying CO_2 molecular vibrational levels

pertinent to the CO_2 laser and about the effects of foreign gases (*19,20*) on the population inversion. In this area a series of theoretical papers by Russian scientists (*21,22*) also appeared in the literature.

2. Measurement of CO_2 molecular lifetimes. This includes both the vibrational (*23–25*) and rotational (*26,27*) lifetimes as well as the rate constants (*14,15,23–28*) of kinetic equations for various collisional processes.

3. Studies of linewidth (*29–31*), line shape (*32,33*), rotational-level competition (*26,27,33*), gain characteristics (*19,34–39*), and saturation effects (*40–43*).

4. Work on active (*44–46*) and passive (*47–51*) Q switching, mode locking (*52,53,56*), modulation (*54,55*), and cavity dumping (*56*) of the CO_2 laser.

5. Development of CO_2 lasers (*57–63*) and laser amplifiers (*19,34, 35,43,64,65*) for both the flowing and nonflowing gas systems. In the related areas, effort was made in the studies of the characteristics (*66–68*), operating lifetime (*69–73*), and stability (*74,75*) of a sealed-off CO_2 laser, as well as the development of IR optical components (*76*) with high power capabilities.

6. Research and development work on various novel systems including thermal (*77–82*), chemical (*83*), high-speed transverse-gas-flow CO_2 laser systems (*84–87*), and high-pressure discharges (*88,89*).

7. Research and evaluation of CO_2 lasers for use in terrestrial and deep space communication (*90,91*), radar systems (*92*), and various industrial applications (*93*) such as cutting, drilling, welding, and hot plasma generation.

8. Studies of nonlinear optical phenomena (*94–98*) and coherent interactions between short CO_2 laser pulses and resonant media (*99–107*).

9. Deployment of CO_2 laser communication satellite ATS-F experiment (Applications Technology Satellite scheduled for launch in early 1973).

The above references are not a complete list of all the advances involving the CO_2 laser during the years 1966–1969. However, they represent most of the important contributions and achievements, and provide a broad perspective of the field. It should also be pointed out that several new areas of research—i.e., laser-induced fluorescence (*108*), infrared–infrared (*109*), and infrared–microwave (*110*) double resonance molecular spectroscopy—have recently become very active as a result of the advances with the CO_2 laser.

II. Introduction

To date, there are nearly 200 CO_2 laser oscillations resulting from vibration–rotation transitions among a number of low-lying ($E_v < 1$ eV) vibrational levels in the ground electronic $^1\Sigma$ state of the CO_2 molecule. These oscillations cover the spectral range from 9 to 18 μ. Among them, two of the strongest groups arise from the $00^0 1$–$10^0 0$ and $00^0 1$–$02^0 0$ bands with the band edges at 10.4 and 9.4 μ, respectively. With present-day optical technology in this IR wavelength range, one can easily construct a stable, single frequency, and single-mode CO_2 laser, operating on a number of the vibration–rotation transitions with a CW output power greater than 20 W ($\simeq$ 100 W multimode output) or $\simeq$ 10 kW Q-switched laser pulses from a 1-m-long gas discharge tube.

Mainly because its gain and efficiency are high, the CO_2 laser is by far the simplest of all gas lasers to fabricate and process. Neither the ultracleanliness required for He–Ne lasers nor the elaborate structural design required for high-power ($\sim$ 10 W) CW ion lasers is needed in the construction of CO_2 lasers. In fact, impurities often are helpful to the gain and power output of CO_2 lasers. The laser medium commonly consists of either a continuously flowing CO_2–N_2–He or a static CO_2–N_2–He–H_2–Xe gas mixture excited by either a dc or an rf electric discharge with water-cooled walls. For sealed-off CO_2 lasers, the power output can be as high as 60% of that obtainable from a flowing system but the operating life of the laser is limited to 1–2 khr. Because of the large number of impurities involved in this laser, the collisional processes in the active medium may be complicated. Investigation of these kinetic processes has led to some of the most significant advances in laser technology in recent years, particularly in the achievement of the highest efficiency ($\gtrsim$ 20%) and average power (more than 11 kW/m of active medium) ever obtained from a laser.

The CO_2 laser field has grown so enormously and is still expanding at such a fast rate that it is inappropriate to cover all aspects in one chapter. For this reason emphasis will be placed on the chemical physics and performance characteristics of CO_2 lasers and only incidental reference will be made to engineering techniques and systems involving the use of CO_2 lasers. Discussion of these topics will stress fundamental principles and concepts.

In general, the basic mechanisms of various types of CO_2 laser systems are fairly well understood. Since this laser involves a large number of collisional processes (i.e., electronic, atomic, and molecular) and in some cases involves chemical and fluid dynamic reactions, the exact analysis can be extremely complex. In many instances, there-

fore, assumptions are made to simplify the existing problem and treatments are limited to semiquantitative aspects. A number of review papers 111-113) are available in the literature but most of them are brief.

The remaining text of this chapter is divided as follows: Section III gives a brief review of CO, molecular structure and IR spectra with emphasis on those arising from low-lying vibration-rotation levels pertinent to CO, lasers. Also included in Section III are a summary of CO, laser transitions, the measurements of absorption and transmission spectroscopy, and determination of some molecular fine-structure constants by means of lasers. Section IV deals with excitation and relaxation processes leading to the achievement of population inversion in the CO, molecules. Data are presented on the inelastic collision cross section between CO, and N_2 with electrons, electron temperature in various gaseous discharges, and the collisional relaxation rates of 00^01, 10^00, 02^00, and 01^10 levels of CO, in various gas mixtures. The resonant process involving vibrational-vibrational energy exchange among CO_2, molecules and between CO_2, and other excited molecules also are detailed. These materials are extremely important for the understanding of CO_2, laser systems. Finally, Sections V and VI are devoted to various aspects involving both the properties and performance of conventional and novel laser systems. Conventional lasers refer to either the sealed-off or the slow longitudinal-flow (< I m/sec) lasers, whereas novel systems include transverse-subsonic-flow, supersonic-flow (or gasdynamic lasers), thermal, chemical, and high-pressure CO_2, lasers. A comprehensive discussion on gain and power output from various types of lasing media is given. Emphasis is placed on the mechanisms responsible for the observed results. For the conventional laser systems, the gain saturation and power output are analyzed by rate equations utilizing previously measured results on collisional and excitation cross sections and relaxation-rate constants. -These calculations are found to provide reasonably good physical models. In the cases of high-speed transverse-flow lasers, agreement between experiment and analysis is not as good as for the conventional laser systems owing mainly to the lack of precise information about the rate constants involved in these high-speed flowing systems. Other topics such as linewidth, lineshape, rotational level and mode competitions, Q switching and mode locking, stabilization, and life of a sealed-off CO_2, laser are discussed in detail. Techniques , for design and construction of various CO_2, laser devices; performance of various CO_2, laser components such as detectors, modulators, mirrors, beam splitters, interference filters, polarizers, and low-

absorption IR transmitting materials for windows and so on; and satellite applications in space-qualified laser communication systems will be subjects of a subsequent article.

III. CO, Molecular Structure and Laser Spectroscopy

Carbon dioxide is a simple polyatomic molecule and, therefore, has been extensively studied (114). A brief review of the CO, molecular structure is presented in this section with only a minimum of mathematical detail. The main purpose is to build a clear picture of the laser medium and to make the subsequent presentation of the properties of CO, lasers more meaningful. Since our interest is in lasers, we shall consider only the IR spectra which arise from low-lying vibration-rotation levels in the ground electronic Σ_g^+ state. We shall first consider, as an approximation, the vibrational and rotational motion separately, and later consider briefly the mutual interactions of these motions. Readers who are already familiar with these topics and terminology may proceed onto Section I I I. D.

A. NORMAL MODES OF VIBRATION

For ease in visualization, we shall first examine the vibrational structure classically, and later extend it to the quantum mechanical description. The CO, is a linear symmetric molecule which has an axis of symmetry, C_{oo} and a plane of symmetry perpendicular to the C_{oo} axis. There are three normal modes of vibration, ν_1, ν_2 and ν_3 which are associated with the species Σ_g^+ Σ_u^+ and π_u respectively (Fig. I). The designations of species for the CO, molecule are chosen in the usual way as for electronic states of homonuclear diatomic molecules. The species π_u corresponds to $l = 2$ representing a doubly degenerate vibration, usually indicated by ν_{2a} and ν_{2b} which occurs with equal frequency both in the plane and perpendicular to the plane of the paper. As shown in Fig. 1, the S_i's are the symmetry coordinates (115) which in the case of CO, are identical to the normal coordinates. The potential V and kinetic T energies expressed in these coordinates are

$$2V = \sum_{ik} C_{ik} S_i S_k$$

$$= C_{11} S_{12} \quad C_{22}(S^2_{2a} + S^2_{2b}) + C_{33} S_3^2 \qquad (1)$$

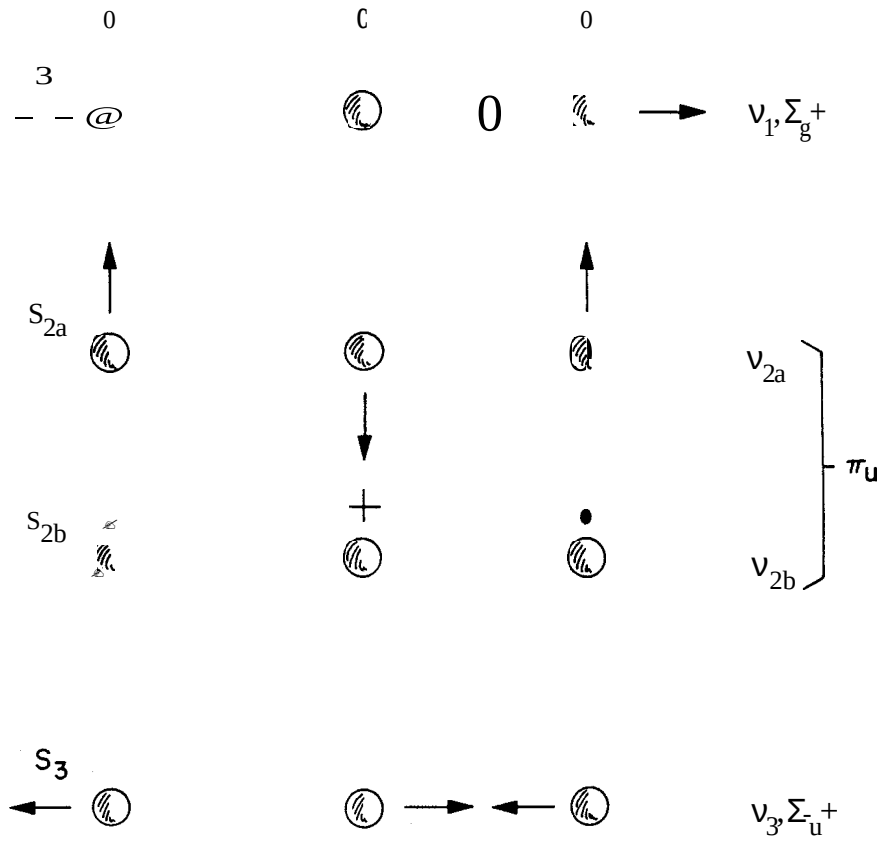

Fig. 1. Normal vibration of CO, molecule: symmetric (ν_1) bent (ν_2) and asymmetric (ν_3) modes.

$$2T = \sum_{ik} D_{ik} S_i S_k$$

$$= D_{11} S_1^2 + D_{22}(S_{2a}^2 + S_{2b}^2) + D_{22} S_3^2 \qquad (2)$$

where S_{2a} and S_{2b} are the doubly degenerate and orthogonal symmetry coordinates of specie π_u and C_{ik} and D_{ik} are related to the force constants aik in the internuclear or internal coordinate system (116) as

$$C_{11} = 2(a_{11} + a_{12})$$

$$C_{22} = \frac{4a_{33}(1+n)^2}{l^2} \qquad (3)$$

$$C_{33} = 2(1+\mu)^2(a_{11} - a_{12})$$

where a_{11} is the force constant of C-O bond, a_{12} is the force constant that gives the interaction of the two bonds, a_{33} is the force constant for the bending mode of the molecule, $\mu = M_C/2M_O$ and l is the equilibrium internuclear distance between C and O. From Eqs. (1) and (2),

the secular determinan $\{C_{ik} - \lambda D_{ik}\} = 0$ resolves into three equations,

$$\begin{aligned} C_{11} - \lambda_1 D_{11} &= 0 \\ C_{22} - \lambda_2 D_{22} &= 0 \\ C_{33} - \lambda_3 D_{33} &= 0 \end{aligned} \tag{4}$$

From Eqs. (3) and (4) the frequencies of the normal vibration are obtained as follows:

$$\begin{aligned} \omega_1^2 &= \frac{a_{11} + a_{12}}{M_O} \\ \omega_2^2 &= \left[\frac{2(M_C + 2M_O)}{M_C M_O}\right]\left(\frac{a_{33}}{l^2}\right) \\ \omega_3^2 &= \left[\frac{(M_C + 2M_O)}{M_C M_O}\right](a_{11} - a_{12}) \end{aligned} \tag{5}$$

For almost all linear symmetric molecules the force constants must be determined experimentally from the observed fundamental frequencies. Except a few cases, the number of force constants assumed over all symmetry types is larger than the number of normal modes and, therefore, the former cannot be determined from the latter. To overcome this difficulty, one usually uses isotopic molecules, for which the force constants are the same but the frequencies are different, thus providing additional equations. Another method is to make certain assumptions about the force fields in the molecule such that the number of force constants can be reduced. The most commonly used force field is the "central" force; however, for a linear triatomic molecule (symmetric or not) the assumption of central force would lead to zero frequency for the perpendicular (degenerate) vibration except in the higher order. Therefore the central force assumption is not always suitable. There are other force types, such as "valence" force which is often used by assuming a strong restoring force in the line of every valence bond if the distance of two atoms formed by this bond is changed, and also a restoring force opposing a change of angle between two valence bonds.

Application of valence forces to the CO, molecule yields the frequencies of three normal vibrations as

$$\begin{aligned} \omega_1^2 &= \frac{K_1}{M_O} \\ \omega_2^2 &= \left(1 + \frac{2M_O}{M_C}\right)\frac{2K_\delta}{M_O \ell^2} \\ \omega_3^2 &= \left(1 + \frac{2M_O}{M_C}\right)\frac{K_1}{M_O} \end{aligned} \tag{6}$$

where K_1 and K_δ are the two valence-force constants. Note that Eqs. (6) and (5) are identical when

$$a_{11} = K_1 \qquad a_{12} = 0 \qquad a_{33} = K_\delta \tag{7}$$

Table 1 gives the observed (117-119) frequencies for CO_2, and values for K_1 and K_δ/l^2 obtained from ν_1 or ν_3 The two values of K_1 in Table 1 are fairly close indicating that the valence force is a reasonably good model. Using isotopic molecules, one can obtain additional equations for the force constants. In addition, information about the geometric structure and effects of Fermi resonance (120) also may be obtained, but these topics will not be discussed here.

TABLE I

Fundamental Frequencies and Force Constants of CO, Molecule (117-119)

$\nu_1(cm^{-1})$	$\nu_2(cm^{-1})$	$\nu_3(cm^{-1})$	($\times 10^5$ dynes/cm)		
			K_1 from ν_1	K_2 from ν_2	K_δ/l^2
1337	667	2349	16.8	14.2	0.57

It should be emphasized that the concept of normal vibrations rests on the assumption that the amplitudes of oscillations are infinitesimally small. Actually the amplitudes of the quantized oscillations, though small, are by no means infinitesimal and therefore the oscillations are more or less anharmonic. In other words, in addition to the quadratic terms, higher-order terms in the potential must be introduced into the wave equation. As a consequence, the energy is no longer a sum of independent terms corresponding to the different normal vibrations but contains cross terms corresponding to the vibrational quantum numbers of two or more normal vibrations. Classical analysis of anharmonic vibrations is rather lengthy and since it would not yield much more useful information relevant to this discussion, it will not be included here. However, the effects of anharmonicity on energy levels and on the determination of transition probabilities between CO_2, laser levels will be discussed later in a quantum mechanical treatment. It may be worth pointing out that the anharmonic corrections to the vibrational energy levels, in most cases, increase monotonically with increasing vibrational quantum numbers. Fortunately, CO_2, laser transitions involve the lowest vibrational levels, namely, ν_3-ν_1 and ν_3-$2\nu_2$ therefore the anharmonic corrections are not very large. It will be shown, however, that

they are important in the calculation of transition probabilities. Certain IR bands which are forbidden in the harmonic approximation are partially allowed when anharmonic force constants are taken into account.

B. Energy Levels

In this section we shall present quantum mechanical results of the vibrational-rotational structure of the CO_2 molecule. For simplicity, we shall first consider the rotational and vibrational motions separately and then treat the mutual interaction of the two motions as a perturbation.

1. Rotational Energy Levels

In the electronic ground state of the CO_2, molecule, the angular momentum of the electrons about the internuclear axis is zero. Therefore, one can use the same treatment as for a diatomic molecule rotating about its equilibrium position. The energy levels are simply given by the well known formula as

$$E_r/hc = F(J) = BJ(J+1) + DJ^2(J+1)^2 + \ldots \tag{8}$$

where *Er* is the rotational energy, F(J) is the term value (in cm-1 *J* is the rotational quantum number, and B is the rotational constant. The DJ^2 $(J+1)^2$ and higher-order terms enter Eq. (8) because of the nonrigidity of the molecule and other effects which are small compared with the first term.

The population n_J of the various rotational levels can be described by the Boltzmann distribution as

$$n_J \simeq n_T\left(\frac{hcB}{kT}\right)g(J)\exp-\left\{F(J)\frac{hc}{kT}\right\} \tag{9}$$

where g(J) is the statistical weight. For the CO_2, molecule or molecules belonging to point group $D_{\infty h}$ alternate rotational levels have different statistical weights. In the case of CO_2 spins of identical nuclei are zero. Therefore, the antisymmetric rotational levels are missing entirely. That is, for Σ_g^+ electronic states, the odd rotational levels are absent in accordance with Bose statistics Therefore g(*J)* = *(2J* + 1). The thermal distribution of the rotational levels in the 00°1 upper vibrational state for $B = 0.38714$ cm^{-1} and $T = 400°K$ is shown in Fig. 2. The J_{max} at

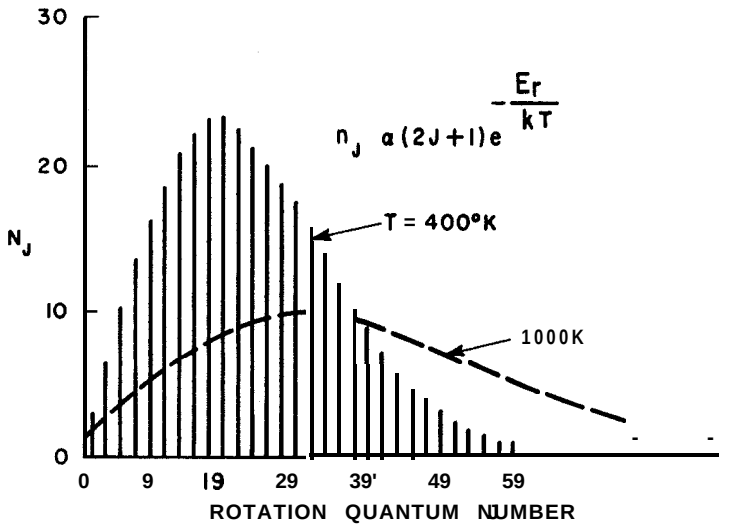

Fig. 2. Thermal distribution of rotational level population in the 00°1 upper laser state.

which n_J is a maximum is obtained from Eq. (9) and is given by

$$J_{\max} = \left(\frac{kT}{hcB}\right) - \frac{1}{2} \tag{10}$$

At $T = 400°\mathrm{K}$, $J_{max} \simeq 19$, while at $T = 1000°\mathrm{K}$, $J_{max} \simeq 29$, and the distribution of rotational level population spreads over a wider range of J values with correspondingly decreasing amplitude.

The rotational eigenfunction Ψ_r of CO, associated with these eigenstates are the surface harmonics such as

$$\Psi_r = \Theta_{JM}(\theta)e^{iM\Phi} \tag{11}$$

where θ is the angle made by the axes of an inclined spinning top with respect to a spatially fixed z axis through the equilibrium position, and ϕ is its azimuth angle about the z axis; M is the magnetic quantum number which gives the components of J in the direction of the z axis in units of $h/2\pi$, and can have the values $J, J-1 \ldots, -J$; $\Theta_{JM}(\theta)$ represents the Jacobi (hypergeometric) polynomials. The selection rules for rotational transitions are $\Delta J = \pm 1$ for molecules having permanent dipole moment. Since the CO, molecule has no permanent dipole moment, transitions between rotational levels in a given vibrational state are forbidden.

2. *Vibrational Energy Levels*

In the harmonic approximation (displacements are small) the Schrodinger equation can be resolved into three uncoupled equations

in terms of normal coordinates ei:

$$\frac{1}{\Psi_i}\frac{d^2\Psi_i}{d\xi_i^2}+\frac{8\pi^2}{h^2}\left(E_i-\frac{1}{2}\lambda_i\xi_i^2\right)=0 \tag{12}$$

The solution of Eq. (12) is well known,

$$\Psi_i(\xi_i)=N_{v_i}H_{v_i}(\sqrt{\alpha}_i\xi_i)\exp\left(\frac{-\alpha_i}{2}\right)\xi_i^2 \tag{13}$$

where H_{v_i} is the Hermite polynomials of degree v_i, $\alpha_i = 4\pi^2\nu_i/h$, and N_{v_i} is a normalization constant. The eigenvalues are

$$E_i = \hbar\omega_i(v_i+\tfrac{1}{2}) \tag{14}$$

with v_i = 0, 1, 2,. . . ; the ω_i are given'by Eq. (6). For the doubly degenerate vibration ν_2 where two of the o's are the same, each of the mutually degenerate pair of vibrations gives its contribution $\omega_2/2$ to the zero-point energy, therefore,

$$E_2 = \hbar\omega_2(v_2+1) \tag{14a}$$

and the corresponding eigenfunction is

$$\Psi_2 = N_{v_{2a}}H_{v_{2a}}(\sqrt{\alpha}_2\xi_{2a})\,H_{v_{2b}}(\sqrt{\alpha}_2\xi_{2b})\exp(-\alpha_2/2)(\xi_{2a}^2+\xi_{2b}^2) \tag{15}$$

In the harmonic approximation, the selection rules for both the JR and Raman transitions in a polyatomic molecule are the same as those for the diatomic molecule, that is, $\Delta v_i = \pm 1$ for each normal vibration. The occurrence of certain fundamentals in the IR or Raman spectrum depends on the presence of a change of either the dipole moment or the polarizability, respectively. Under symmetry operation, only the symmetric vibration ν_1 of the CO, molecule can change its quantum number v_1 by ± 1 owing to the Raman effect, whereas the bending ν_2 and asymmetric ν_3 vibrations of the CO, molecule can change their quantum numbers only by $\pm$ 1 owing to electric dipole interaction.

If the anharmonicity is taken into account, the total vibrational eigenfunction Ψ_v will include an additional term $\chi(\xi_1,\xi_{2a},\xi_{ab},\xi_3)$, which is small compared with the product $\Psi_1\Psi_{2a}\Psi_{2b}\Psi_3$. The term values for the vibrational energy as a result of anharmonicity are given by

$$G(v)=\sum_{i=1}^{3}\omega_i\left(v_i+\frac{d_i}{2}\right)+\sum_i\sum_k x_{ik}\left(v_i+\frac{d_i}{2}\right)\left(v_k+\frac{d_k}{2}\right)+\sum_l g_{ii}\ell_i^2 \tag{16}$$

where d_i = 1 for nondegenerate and 2 for doubly degenerate vibrations. The first summation in Eq. (16) is the dominant one; the double sum gives the higher-order correction terms which arise from cross

coupling between different modes of vibration through the anharmonic force constants x_{ik}; the last summation is called the ℓ-type doubling, where g_{ii} represents small constants of the order of the x_{ik}. For non-degenerate vibrations, $\ell_i = 0$ and $g_{ii} = 0$. In the case of CO_2, only one degenerate vibration is excited. This mode of vibration is doubly degenerate on account of the equivalence of the two directions of the angular momentum ℓ. This double degeneracy can be removed by increasing rotation as a result of the Coriolis effect. Thus, for each J a splitting into two components occurs whose separation increases with increasing J.

For every vibrational state there exist a set of rotational levels, but with slightly different spacings for the different vibrational levels. It must be realized that for degenerate vibrational levels, J must be larger than or equal to ℓ, as $J = \ell, \ell + 1, \ell + 2, \ldots$; in other words, the first $\ell - 1$ rotational levels are missing in the degenerate vibrational state. Figure 3 gives the energy level diagram of a few low-lying vibrational states of the CO, molecule. Table 2 lists both the measured IR absorption and Raman spectra for transitions between levels corresponding to those shown in Fig. 3, as well as to a few neighboring levels. Two extremely strong absorption bands at 667.3 and 2349.3 cm^{-1} belong to the bending mode ν_2 (species π_u) and the asymmetric mode ν_3 (species Σ_u^+), respectively. The intense Raman spectrum consists of two lines at 1285.5 and 1388.3 cm^{-1} with an intensity ratio 1: 0.6, which correspond well with the ν_1 and $2\nu_2$ modes.

It should be pointed out that the lower laser levels 02^00 and 10^00 are almost in resonance, which leads to a perturbation of the energy levels, as recognized first by Fermi(*121*), owing to the anharmonic terms in the potential energy. As a result, the 10^00 level is shifted up and the 0200 level is shifted down so that the actual separation of the two levels is much greater than expected. At the same time a mixing of the eigenfunctions of the two levels occurs. The smaller the original energy difference of the two levels, the stronger the mixing. In addition, the magnitude of the perturbation depends on the value of the corresponding matrix element $E_{1,2}$ of the perturbation function V' as

$$E_{1,2} = \langle 10^00|V'|02^00\rangle \tag{17}$$

where V' is given essentially by the anharmonic terms in the potential energy, and $\Psi_{10^00}, \Psi_{02^00}$ are the zero approximation harmonic oscillator eigenfunctions of the two interacting vibrational levels. The perturbed energy E is given by

$$E = \tfrac{1}{2}(\delta_+) \pm \tfrac{1}{2}(4|E_{1,2}|^2 + \delta_-^2)^{1/2} \tag{18}$$

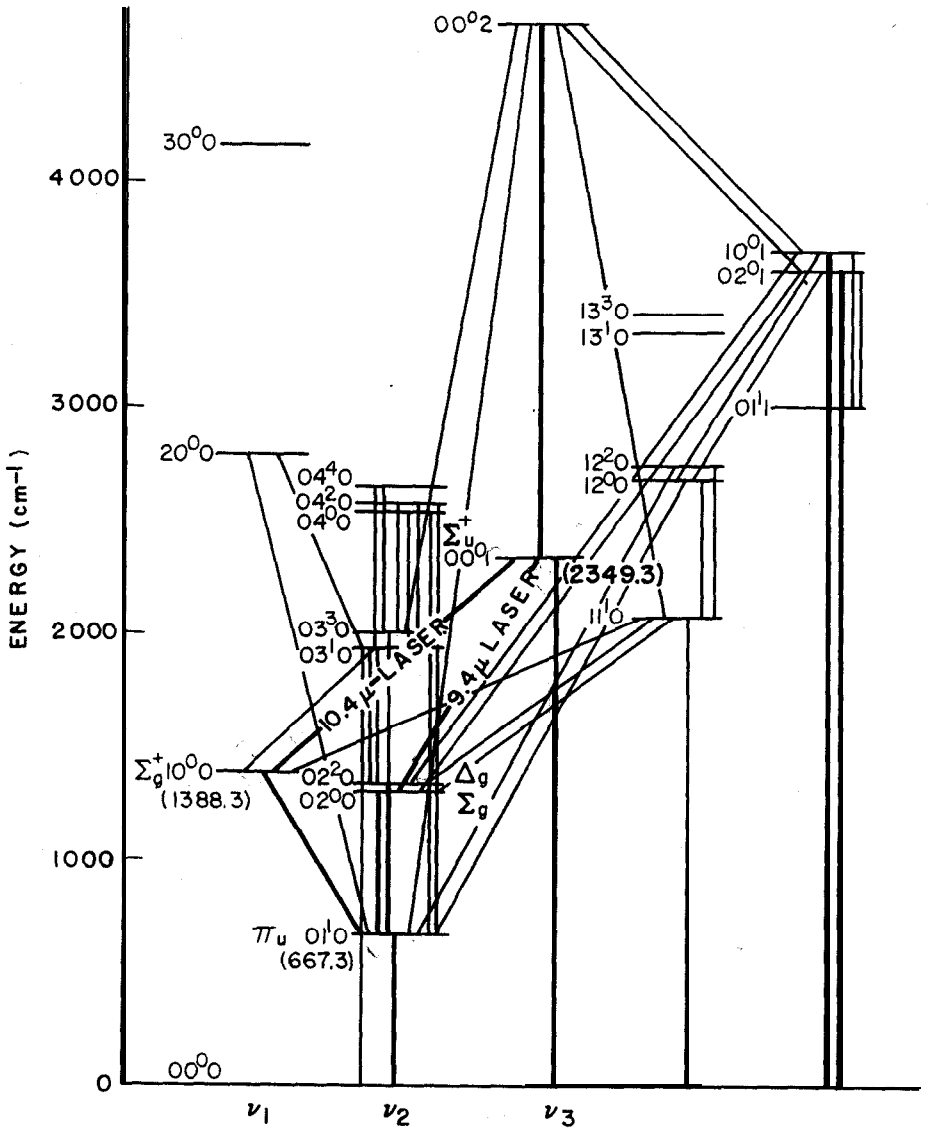

Fig. 3. Energy level diagram of low-lying vibrational levels of the CO_2 molecule.

when δ_+ and δ_- are the sum or difference of the two unperturbed eigenvalues of the 10^00 and 02^00 levels, respectively. It should be noted that 02^00 is only one of the two sublevels belonging to the $2\nu_2$ mode. The other sublevel, 02^20 (species Ag) also lies very close to the 10^00 level. Because of the symmetry operation, the rule requires that only two vibrational levels of the same species can interact with the other; therefore only the Σ_g^+ (02^00) sublevel of the 020 level can perturb the $1\ 0^00$ level which has the species Σ_g^+. The energy level values of the two states 10^00 (I 388.3 cm^{-1}) and 02^00 (1285.5 cm^{-1}) as given by Eq. (18) differ considerably from $2\nu_2$ (ν_2 = 667.3 cm^{-1}). For the same

TABLE 2

Low Lying Infrared and Raman Bands of CO,

Upper state		Lower state		ν_{vac} Observed (cm-') (114)
$\nu_1\nu_2\nu_3$	Species	$\nu_1\nu_2\nu_3$	Species	
01'0	π_μ	00°0	Σ_g^+	667.3
0200	Σ_g^+	00°0	Σ_g^+	1285.5
10^00	Σ_g^+	00°0	Σ_g^+	1388.3
03'0	π_μ	00°0	Σ_g^+	1937.5
$00^0 1$	Σ_u^+	00^00	Σ_g^+	2349.3
0200	Σ_g^+	01^10	π_μ	618.1
02^20	Δ_g	01^10	π_μ	668.3
10^00	Σ_g^+	01^10	π_μ	720.5
03'0	π_μ	01^10	π_μ	1264.8
0400	Σ_g^+	01_1^10	π_μ	1886
2000	Σ_g^+	01^10	π_μ	2137
03'0	π_μ	02^20	Δ_g	596.8
03'0	π_μ	0200	Σ_g^+	647.6
00^0 I	Σ_u^+	10^00	Σ_g^+	960.8
00^0 I	Σ_u^+	0200	Σ_g^+	1063.6
04^20	Δ_g	02^20	Δ_g	1242
04^20	Δ_g	0200	Σ_g^+	1305. I
2000	Σ_g^+	0200	Σ_g^+	1528

reason, the splitting of the two sublevels $\ell_2 = 0$ and 2 of the 020 state is anomalously large (49.9 cm^{-1}). As a consequence of the strong perturbation (Fermi resonance), a strong mixing of the eigenfunctions of the two levels occurs so that the two observed levels can no longer be unambiguously designated as 10^00 and 02^00. Each actual level is a mixture of two. The corresponding eigenfunctions of these two mixed states $(10^00, 02^00)'$ and $(10^00, 02^00)''$ can be expressed in terms of a linear combination of Ψ_{10^00} and Ψ_{02^00} as

$$\begin{aligned}\Psi_{(10^00,\,02^00)'} &= a_+\Psi_{10^00} - a_-\Psi_{02^00}\\ \Psi_{(10^00,\,02^00)''} &= a_-\Psi_{10^00} + a_+\Psi_{02^00}\end{aligned} \tag{19}$$

where

$$a_\pm = \left(\frac{(4|E_{1,2}|^2+\delta_-^2)^{1/2} \pm \delta_-}{2(4|E_{1,2}|^2+\delta_-^2)^{1/2}}\right)^{1/2} \tag{20}$$

These results are valid not only for the perturbation owing to the effect of one adjacent level but also for the integrated perturbing effect of a large number of vibrational levels of which each can contribute a term in $|E_{1,2}|$ through the anharmonic terms in the potential

energy. We shall see the significance of these effects later in Section III.E and in Section IV.B on relaxation processes.

C. VIBRATIONAL-ROTATIONAL SPECTRA

The energy of a linear symmetric molecule can be obtained to a good approximation simply by adding the rotational $hcF(J)$ given by Eq. (8) and the vibrational energy $hcG(v)$ given by Eq. (16). Actually, the two types of motion occur simultaneously and give rise to the fine structure of IR and Raman bands. The coupling between the rotational and vibrational motions introduces additional terms in the energy expression which will be discussed later in Section I II .F.3.

We shall now briefly consider the symmetry properties of the eigenfunctions and the selection rules for vibrational-rotational transitions. The rotational levels of linear molecules are positive or negative depending on whether the sign of the total eigenfunction

$$\Psi_T = \Psi_e \Psi_r \Psi_v \tag{21}$$

remains unchanged or changed upon an inversion. The Ψ_e is the eigenfunction for the ground electronic state $^1\Sigma$ and is totally symmetric. In all symmetric excited vibrational levels (species Σ^+), the even rotational levels are positive and the odd are negative. In antisymmetric vibrational levels (species Σ^-), the converse is true. In $\pi, \Delta, \cdots$ vibrational levels, for each J value there is a positive and a negative level of slightly different energy whose order alternates as: +-, -+ +- . . . or -+ +- -+, . . . This double degeneracy for π, A vibrational levels, as mentioned before, is a result of the equivalence of the two directions of the angular momentum ℓ, thus a splitting into two components for each J occurs whose separation increases with increasing J. As an example, for species π, the /'-type splitting would give a term $g_{22}\ell_2^2$ in Eq. (16).

The selection rules for the vibrational-rotational transitions in the IR spectrum are

$$\begin{aligned} &\mathrm{Al} = 0, \pm 1, \qquad \Sigma^+ \leftrightarrow \Sigma^-, \quad \mathrm{g} \not\leftrightarrow \mathrm{g}, \quad u \not\leftrightarrow u \\ &AJ = 0, \pm 1, \qquad (J = 0) \not\leftrightarrow (J = 0), \quad + \not\leftrightarrow -, \quad s \not\leftrightarrow a \end{aligned} \tag{22}$$

where s and a designate the symmetric and antisymmetric Ψ_R and the symbols $\leftrightarrow$ and $\not\leftrightarrow$ represent "allowed" and "not allowed," respectively.

Specifically, two of the strongest CO, lasers arise from the vibrational-rotational transitions of the $\Sigma_u^+ - \Sigma_g^+$ vibrational bands ($00^0 1$–$10^0 0$) and ($00^0 1$–$02^0 0$), at laser wavelengths near their band edge 10.4

and 9.4 μ, respectively. Laser transitions have been obtained from both the P branch ($\Delta J = -1$) and the R branch ($\Delta J = +1$) of each band. The Q branch ($\Delta J = 0$) is not allowed because transitions occur between two Σ states for which $\ell = 0$. Figure 4 gives a detailed transition diagram for laser oscillations from both the P and R branches of the $00^0 1 - 10^0 0$ and $00^0 1 - 02^0 0$ bands.

D. CO, LASER TRANSITIONS

The most complete measurements on laser transitions were made by Frapard et al.(122) using a prism inside the cavity in order to avoid the strong competition between rotational levels, especially in a

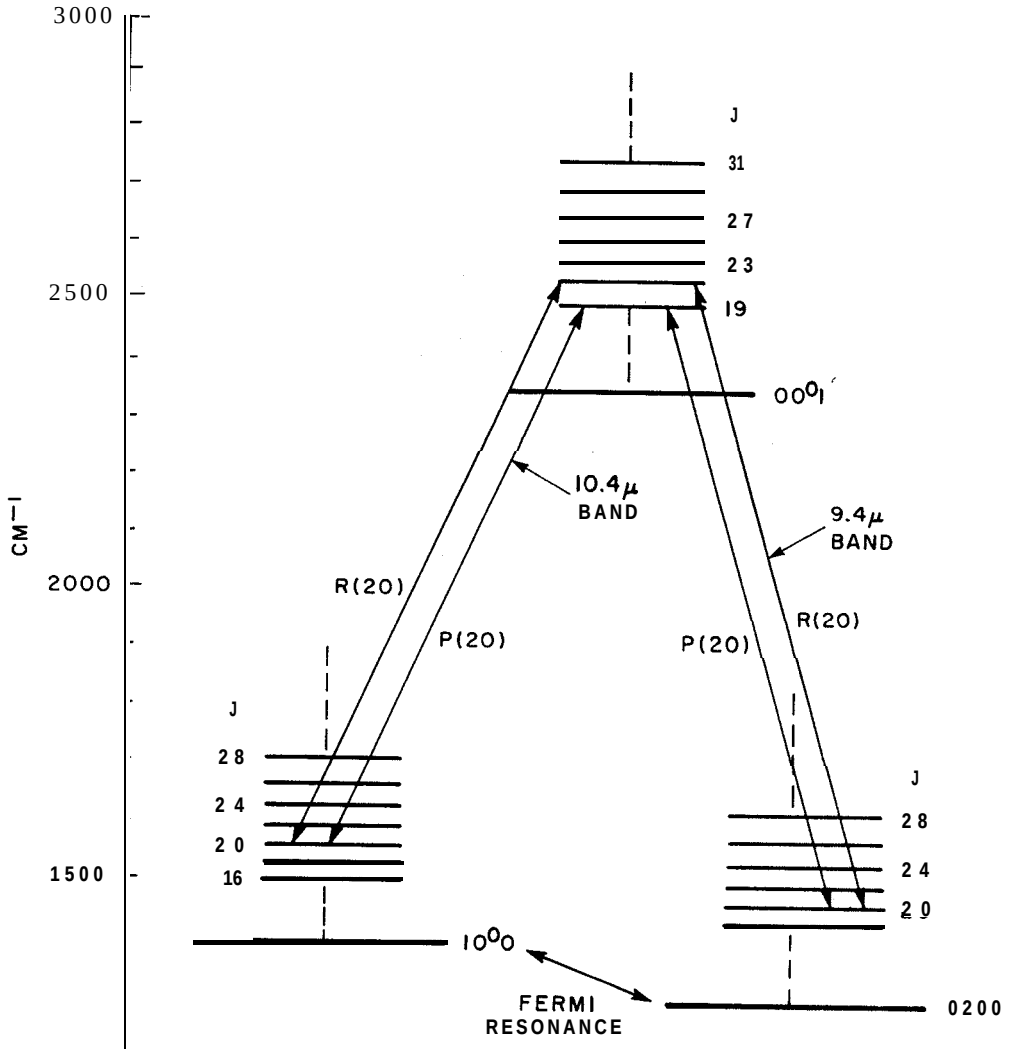

Fig. 4. A detailed laser transition diagram for the 00° I -10°0 and 00" 1-02°0 bands. including rotational levels.

high-power CO, laser system (these competition effects will be discussed in great detail later). Their results along with the measurements by Pate1 (2) are given in Tables 3-6. Early investigations (I-I I) of CO, laser spectroscopy were performed with laser systems which did not incorporate a dispersive element in the feedback 'interferometer. In these systems the larger the number of simultaneous laser transitions, the weaker the laser output. For example, Patel(2) observed a total of 14 simultaneously oscillating laser lines in the *P* branch of the

TABLE 3

Measured CO_2 Laser Wavelengths of the *P* Branch of the $00^01 - 10^00$ Vibration-Rotation Transitions

Measured laser wavelength in vac. (μ)	Frequency (cm^{-1})	Transition[a,b] $(00^0\ 1)$-$(10^00$
10.4410	957.76	P(4)
IO.4585	956.16	*P*(6)
10.4765	954.52	*P*(8)
10.4945	952.88	*P*(10)
IO.5135	951.16	*P*(12)
10.5326	949.43	P(14)
10.5518	947.70	*P*(16)
10.5713	945.96	*P*(18)
10.5912	944.18	*P*(20)
10.6118	942.35	*P*(22)
10.6324	940.52	*P*(24)
10.6534	938.67	*P*(26)
10.6748	936.78	*P*(28)
10.6965	934.88	*P*(30)
10.7194	932.89	P(32)
10.7415	930.96	P(34)
10.7648	928.95	P(36)
10.7880	926.95	*P*(38)
10.8120	924.90	*P*(40)
10.8360	922.85	*P*(42)
10.8605	920.77	*P*(44)
10.8855	918.65	P(46)
10.91 IO	916.51	P(48)
10.9360	914.41	*P*(50)
10.9630	912.16	*P*(52)
10.9900	909.92	P(54)
11.0165	907.73	*P*(56)

"See Ref. (2). A total of 14 laser transitions, *P*(12) to *P(38)*.
*See Ref. (122). Additional 13 laser transitions, *P(4)* to *P*(10) and *P*(40) to *P(S6)*.

TABLE 4

Measured CO, Laser Wavelengths of the R Branch of the 00^0 1- 1 $0^0$0 Vibration-Rotation Transitions

Measured laser wavelength in vac (μ)	Wave number (cm-')	Transition[a,b] (00^01)–(10^00)
10.3655	964.74	R(4)
10.3500	966.18	$R(6)$
10.3335	967.73	$R(8)$
10.3190	969.09	$R(10)$
10.3040	970.50	$R(12)$
10.2860	971.91	$R(14)$
10.2855	972.24	$R(16)$
10.2605	974.61	$R(18)$
10.2470	975.90	$R(20)$
10.2335	977.18	$R(22)$
10.2200	978.47	$R(24)$
10.2075	979.67	$R(26)$
10.1950	980.87	$R(28)$
10.1825	982.08	$R(30)$
10.1710	983.19	$R(32)$
10.1590	984.35	$R(34)$
10.1480	985.42	$R(36)$
10.1370	986.49	$R(38)$
10.1260	987.56	$R(40)$
10.1150	988.63	$R(42)$
10.1050	989.61	$R(44)$
10.0955	990.54	$R(46)$
10.0860	991.47	$R(48)$
10.0760	992.46	$R(50)$
10.0670	993.34	$R(52)$
10.0585	*994.18*	$R(54)$

[a] See Ref. (124). A total of 7 laser transitions, $R(14)$ to $R(26)$.
[b] See Ref. (122). Additional 19 laser transitions, R(4) to R(12) and R(28) to R(54)

00^01–10^00 band from a laser using only CO_2 as the active medium; the laser output was only in the milliwatt range. However, when a mixture of gases such as CO,-N,-He is used, the laser output increases more than four orders of magnitude as demonstrated by the work of Pate1 et al.(11) When the output was examined by a rapid scanning technique (123) a few laser lines, namely, P(18), P(20), and P(22), were found to oscillate at one time. The first observation of CO, laser oscillations in the R branch of the 00^01–10^00 band was made by Howe(124) in a flowing CO,-air laser system. Howe's laser oscillated

TABLE 5

Measured CO, Laser Wavelengths of the P Branch of the $(00^0\ 1)$–$(02^0 0)$ Vibration-Rotation Transitions

Measured laser Wavelength in vac. (μ)	Wave number (cm^{-1})	Transition".[b] $(00^0 1)$–$(10^0 0)$
9.4285	1060.61	P(4)
9.4425	1059.04	$P(6)$
9.4581	1057.30	$P(8)$
9.4735	1055.58	$P(10)$
9.4885	1053.91	$P(12)$
9.5045	1052.13	P(14)
9.5195	1050.47	$P(16)$
9.5360	1048.66	$P(18)$
9.5525	1046.85	$P(20)$
9.5690	1045.04	$P(22)$
9.5860	1043.19	$P(24)$
9.6035	1041.29	$P(26)$
9.5210	1039.34	$P(28)$
9.6391	1037.44	$P(30)$
9.6575	1035.46	$P(32)$
9.6760	1033.48	P(34)
9.6941	1031.56	P(36)
9.7140	1029.44	P(38)
9.7335	1027.38	$P(40)$
9.7535	1025.27	$P(42)$
9.7735	1023.17	P(44)
9.7940	1021.03	P(46)
9.8150	1018.85	$P(48)$
9.8360	1016.67	$P(50)$
9.8575	1014.46	$P(52)$
9.8790	1012.25	$P(54)$
9.9010	1010.00	$P(56)$
9.9230	1007.76	$P(58)$
9.9465	1005.38	$P(60)$

[a] See Ref. (6). A total 14 laser transitions, **P(** 10) to **P(36).**
[b] See Ref. (122). Additional 15 laser transitions, **P(4)** to **P(8)** and **P(38)** to $P(60)$.

in seven transitions and had a low power output. Laser oscillations in the P branch of the $00^0\ 1$–$02^0 0$ band, on the other hand, were first observed by Barchewitz et al. (5,6). In addition to these $00^0\ 1$–$10^0 0$ and $00^0\ 1$–$02^0 0$ bands, Frapard et al. (122) have reported CO_2 laser oscillations in the P branch of the $01^1 1$–$03^1 0$ band near 11 μ. These results are given in Table 7. Other laser transitions in the wavelength range from 11 to 18 μ also have been reported (125, 126). A total of 16

TABLE 6

Measured CO, Laser Wavelengths of the *R* Branch of the $(00^0\ 1)$–$(02^0 0)$ Vibration--Rotation Transitions

Measured laser wavelength in vac. (μ)	Wave number (cm-')	Transition[a,b] $(00^0\ 1)$-$(10^0 0)$
9.3677	1067.50	*R*(4)
9.3555	1068.89	*R*(6)
9.3420	1070.43	*R*(8)
9.3295	1071.87	*R*(10)
9.3 172	1073.28	R(12)
9.3055	1074.63	*R*(14)
9.2937	1076.00	*R*(16)
9.2825	1077.30	*R*(18)
9.2715	1078.57	*R(20)*
9.2605	1079.85	*R*(22)
9.2500	1081.08	*R*(24)
9.2397	1082.29	*R*(26)
9.2295	1083.48	*R*(28)
9.2197	1084.63	*R*(30)
9.2103	1085.74	*R*(32)
9.2010	1086.84	*R*(34)
9.1920	1087.90	*R*(36)
9.1830	1088.97	*R*(38)
9.1740	1090.04	*R*(40)
9.1660	1090.99	*R*(42)
9.1575	1092.00	*R*(44)
9.1490	1093.01	*R*(46)
9.1420	1093.85	*R*(48)
9.1340	1094.81	*R*(50)
9.1265	1095.71	*R*(52)

[a] See Ref. (4). A total 7 laser transitions, *R(* 16) to *R*(28).
[b] See Ref. (122). Additional 18 laser transitions, *R(4)* to *R(14)* and *R(30)* to *R(52)*.

laser transitions has been precisely measured (125) and assigned to the *P* branch of the 01^11–11^10 band as given in Table 8. Thirteen additional laser transitions have been assigned (126) to 14^00–$05^1 0$ (13.2,x), 21^10–12^10 (13.5 μ), 14^00–13^10 (16.6 μ), 03^11–02^21 (17.0 μ), and 24^00–23^10 (17.4 μ) bands. Laser intensities from these bands are much weaker than those oscillating in the 00^01- $10^0 0$ and $00^0 1$ –$02^0 0$ bands and most of them oscillate only in the pulsed mode. Detailed information concerning these weaker CO, laser transitions can be found in Ref. (126). With present day technology, only a few additional laser lines can be added(l27) to those that have already been observed.

TABLE 7

Measured(l22) CO, Laser Wavelengths of the P Branch of the $01^{0}1$ - 03^{1} 0 Vibration-Rotation Transitions

Wavelength in vac. (μ)	Wave number (cm^{-1})	Transition
10.9735	911.29	$P(19)$
10.9951	909.50	$P(21)$
11.0165	907.73	$P(23)$
11.0300	906.62	$P(24)$
11.0385	905.92	$P(25)$
11.0535	904.69	$P(26)$
11.0610	904.08	$P(27)$
11.0760	902.85	$P(28)$
11.0850	902.12	$P(29)$
11.1000	900.90	$P(30)$
11.1070	900.33	$P(31)$
11.1235	899.00	$P(32)$
11.1315	898.35	$P(33)$
11.1485	896.98	$P(34)$
11.1555	896.42	$P(35)$
11.1736	894.97	$P(36)$
11.1791	894.53	$P(37)$
11.1980	893.02	$P(38)$
11.2035	892.58	$P(39)$
11.2235	890.99	$P(40)$
11.2295	890.51	$P(41)$
11.2495	888.93	$P(42)$
11.2545	888.53	$P(43)$
11.2770	886.76	$P(44)$
11.2804	886.49	$P(45)$

E. VIBRATIONAL TRANSITION PROBABILITIES AND RADIATIVE LIFETIMES

The radiative transition probabilities between two states m and n are given by the Einstein A coefficient

$$A_{mn} = \frac{1}{2J_m + 1}\left(\frac{64\pi^4}{3h\lambda^3}\right)S_{mn} \tag{23}$$

where S_{mn} is the line strength. It is given by the sum of the squares of all matrix elements,

$$S_{mn} = \sum_{m,n} |\langle J_m M_m | p | J_n M_n \rangle|^2 \tag{24}$$

TABLE 8

Measured(12.5) CO_2, Laser Wavelengths of the *P* Branch of the $01^{1}1$–$11^{1}0$ Vibration-Rotation Transitions

Wavelength in vac. (μ)	Wave number (cm^{-1})	Transition
10.9730	911.33	*P*(19)
10.9856	910.28	*P*(20)
10.9944	909.55	*P*(21)
I 1.0078	908.45	*P*(22)
11.0164	907.74	*P*(23)
11.0300	906.62	*P*(24)
11.0385	905.92	*P*(25)
11.0529	904.74	*P*(26)
11.0610	904.08	*P*(27)
11.0762	902.84	*P*(28)
11.0840	902.20	*P*(29)
11.0999	900.91	*P*(30)
II.1073	900.31	*P*(31)
Ii.1238	898.97	*P*(32)
11.1309	898.40	*P*(33)
11.1483	897.00	*P*(34)

where *J* and *M* are the angular momenta and the *z* components, respectively, and *p* is the dipole operator.

Statz et al. (128) have calculated the line strengths for a number of transitions among the low-lying vibrational levels of CO_2. Instead of the usual perturbation approach, they constructed the eigenfunction by a linear combination of a large number of levels which are connected by "matrix elements" with the levels of interest, i.e., $00^{0}0$, $01^{1}0$, $10^{0}0$, $02^{0}0$, $00^{0}1$. This involves the diagonalization of large Hamiltonian matrices, in some cases as large as 30 **x** 30. In the Hamiltonian. anharmonic forces were included and the potential energy contains terms up to fourth order. Contributions from these terms are significant in that some of the forbidden transitions in the harmonic approximation become partially allowed. The magnitude of the dipole moment as a function of various normal coordinates also enters in the determination of transition probabilities. Quadratic and higher-order terms in the normal coordinates are involved, especially for the forbidden transitions. However, they do not contribute to the calculated line strength significantly. Of all the levels considered, only the $00^{0}1$–$00^{0}0$, $00^{0}2$–$00^{0}1$, $01^{1}0$–$00^{0}0$, and $02^{2}0$, $02^{0}0$–$01^{1}0$ transitions are allowed in the absence of anharmonicities. Table 9 presents the Einstein coefficients

TABLE 9

Einstein A Coefficient (128) for Some Vibrational Transitions in CO,

Transition		Transition probability (sec^{-1}) Untrapped	Trapped
$00^0 1 \rightarrow 00^0 0$	R	2.0×10^2	8.8
	P	2.1×10^2	10.1
$00^0 1 \rightarrow 02^0 0$	R	0.19	
	P	0.20	
$00^0 1 \rightarrow 1000$	R	0.33	
	P	0.34	
$0002 \rightarrow 00^0 1$	R	3.9×10^2	
	P	4.1×10^2	
$01^1 0 \rightarrow 0000$	R	0.48	0.48
	P	0.46	0.46
	Q	0.94	
$02^0 0 \rightarrow 01'0$	R	0.22	
	P	0.26	
	Q	0.48	
$02^0 0 \rightarrow 01^1 0$	R	1.07	
	P	0.84	
	Q	1.89	
$10^0 0 \rightarrow 01'0$	R	0.20	
	P	0.23	
	Q	0.44	

for several transitions calculated (128) by choosing suitable values for anharmonic force constants to best fit the experimental data. Table 10 gives the radiative lifetimes calculated(l28) from the A coefficients. The transition lifetime for the 00^0 l-l $0^0 0$ band, on the other hand, has been determined to be 4.7 sec from the absorption measurements (29, 30) using the CO, laser (as discussed in the following subsection). From these results it is clear that radiative processes cannot account for the laser action since the radiative lifetimes of the lower laser levels are two to three orders of magnitude longer than that of the upper laser level. Relaxation of these lower laser levels $10^0 0$ and $02^0 0$ with relatively long radiative lifetimes by collisions with other molecules or atoms must play an important role in the CO, laser. A detailed discussion is given in Section IV. B.

TABLE 10

Radiative Lifetimes (128) of Some Vibrational Levels in CO,

Level	Lifetime sec	
	Untrapped	Trapped
00^0I	2.4×10^{-3}	5.0×10^{-2}
0002	1.3×10^{-3}	
01^10	1.1	2.8 (even J), 1.1 (odd J)
0200	1.0	
02^20	0.26	
10^00	1.1	

F. CO, LASER SPECTROSCOPIC MEASUREMENTS

The extremely narrow linewidth of CO, lasers as radiation sources allows spectroscopic studies of the CO, molecule with high precision. In this section we shall present both the absorption and transmission spectra of a CW CO, laser through and absorption cell filled with CO, gas and the measurements of the rotational constants of the CO, molecule by a heterodyne of two stable CW CO, lasers operating on any two by a heterodyne of two stable CW CO_2 lasers operating on any two neighboring transitions.

1. *Absorption Spectra*

The absorption coefficient has been measured(29,30) by using a single vibration-rotation laser line, 10.6 μ $P(20)$ transition, through an absorption cell filled with pure CO, gas. For an inhomogeneously or Doppler broadened line, the absorption coefficient a at the line center is given by

$$a(\lambda_0) = -\frac{1}{8\pi}\frac{\lambda_0^3}{c\tau_r}\left(\frac{Mc^2}{2\pi kT}\right)^{1/2}\left[n_u - \frac{g_u}{g_\ell}n_\ell\right] \tag{25}$$

where τ_r is the radiative lifetime of the vibration-rotation transition, k is the Boltzmann constant, T is gas temperature, M is the mass of the CO_2 molecule, n_u and n_ℓ are the upper- and lower-level population, respectively, and g_u and g_ℓ the corresponding statistical weights. For a collision-broadened case, a is given by

$$a(\lambda_0) = -\frac{1}{8\pi}\frac{\lambda_0^2}{\tau_r\nu_c}\left[n_u - \frac{g_u}{g_\ell}n_\ell\right] \tag{26}$$

where ν_c is the collision frequency and all other symbols have their

usual meanings. I n the Doppler broadened region a is proportional to the gas pressure P because both n_u and n_ℓ are directly proportional to P. But in the case of collision broadening, a should be independant of P because ν_c is also proportional to P. The measured absorption coefficient (30) as a function of the CO, gas pressure is shown for the $P(20)$ line in Fig. 5. The combined Doppler and collision contour which best fits the data is represented by the solid curve. These measurements yield a collision frequency $\nu_c = 7.8 \pm 0.8 \times 10^9$ sec^{-1}, an optical broadening cross section of 5.7×10^{-15} cm^2 for collisions with CO, molecules and a transition lifetime $\tau_r = 4.7 \pm 0.5$ sec. The break in the absorption curve occurs at P = 5.2 Torr of CO_2, indicating that if the gas pressure in a CO, laser exceeds this value, the linewidth would be homogeneously broadened.

2. *Transmission Spectra*

The transmission spectra of the 00^0 I-I 0^00 laser lines in both the P and R branches for i?(2) to R(40) and $P(4)$ to $P(42)$ have been measured(l29) by using a White absorption cell with a total path length of IO m. From data on transmission vs. CO, gas pressure, one can determine the line intensity S_J and the half-width A,. Figure 6 shows typical transmission data for both the P- and R-branch laser lines at a fixed CO, pressure of 300 Torr. The upper curve is the scan of laser frequencies in the absence of absorbing gas and the lower curve shows the attenuation of these lines. It is noteworthy that strong lines near the band center are absorbed more strongly than the weaker ones in the wings. This observation suggests that it may be more desirable for laser communication through atmosphere to use laser lines in the wings of the band at which the least absorption loss is assumed.

The spectral transmittance t at the peak of the collision-broadened line is given by

$$t = \exp\left[\frac{-S_J L}{\pi \Delta_J}\right] \qquad (27)$$

where L is the total path length through the absorption cell. The transmittance was found to be independent of gas pressure for pressures above 50 Ton-. Careful measurements of t were made(129) for a number of selected lines in the 10.4-μ band in the collision-broadened region. The values S_J/Δ_J (in cm^{-1}) at 300" K for these lines are deduced from the transmittance measurements. Results are summarized in Table 11, for which each of those values represents about 10 independent measurements. The dependence of linewidth A, (cm^{-1}–atm^{-1}) at

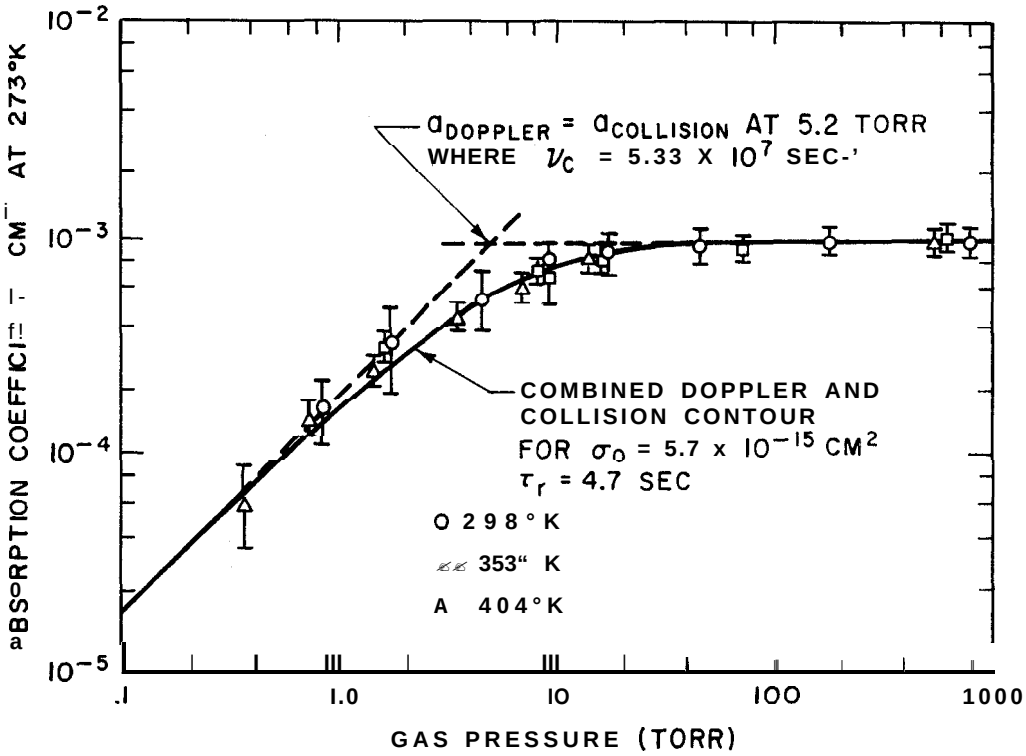

Fig. 5. Absorption coefficient of CO, gas for the 10.6-p CO_2 laser as a function of CO, density. The absorption coefficients are scaled to 273" K, using the equilibrium temperature dependence for the lower state J = 20. The expected temperature dependence is verified by the fact that the data lie on a single curve, while the measured absorption coefficients in the high density limit varied by a factor of five for the temperature range shown. See text. [After Gerry and Leonard(30).]

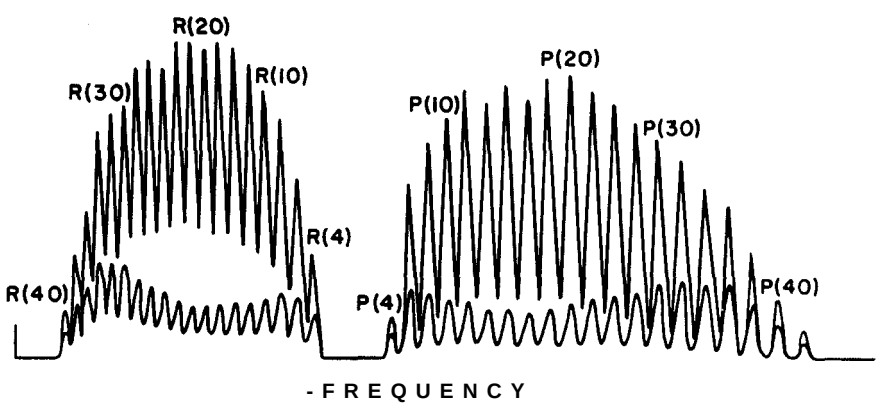

Fig. 6. The upper traces show CO, laser emission in the P and R branches of the 00"1 - 10°0 band without attenuation. These spectra were obtained by rotating a diffraction grating as one of the cavity mirror. The lower traces show the same emission after attenuation by a I O-m path of pure CO, (300 Torr), equivalent to a path of approximately 30 km of air. [After Oppenheim and Devir(129)

TABLE 11

Ratios of Laser Line Intensity S_J to the Half-Width Δ_J for Selected CO, Laser Transitions in the 10.4-p Band at 300" K (129)

'Transition	S_J/Δ_J (10^3 cm^{-1})
$P(4)$	2.00 ± 0.11
$P(8)$	3.72 ± 0.12
$P(18)$	5.84 ± 0.16
$P(32)$	2.83 ± 0.05
$P(40)$	1.35 ± 0.05
$R(2)$	1.54 ± 0.10
$R(6)$	3.53 ± 0.09
$R(16)$	5.87 ± 0.13
$R(26)$	4.75 ± 0.18
$R(30)$	3.34 ± 0.18
$R(40)$	1.30-to.11

300" K on the rotational quantum number m for the 10.4-p band CO, laser is shown in Fig. 7, where $m = -J$ for the P branch and $m = J + 1$ for the R branch. For the P(20) line, one obtains from Oppenheim and Devir's results(l29) a value of $\sim$ 3.3 MHz/Torr as the collision-broadened linewidth. Similar measurements were made earlier by Rossetti et al. (130), and are shown in Fig. 7.

3. *Rotational Constants*

The advantage of the narrow laser linewidth can be utilized also to obtain reliable information about the fine structure constants of the molecule. The coupling between the rotational and vibrational motion results in a slight modification of B and D values in Eq. (8) both of which vary with v_i. The change in B_v is owing to a change in the moment of inertia I during a vibration so that I does not equal I_e (value for the equilibrium position or the rigid rotator). The change in D_v is caused by the effects of centrifugal stretch; however, for practical purposes its dependence on v usually can be neglected. The modification of B takes on the form similar to that for diatomic molecules,

$$B_v = B_e - \sum_{i=1}^{3} \alpha_i \left(v_i + \frac{d_i}{2} \right) \tag{28}$$

where d_i = 1 for nondegenerate and 2 for doubly degenerate vibrations,

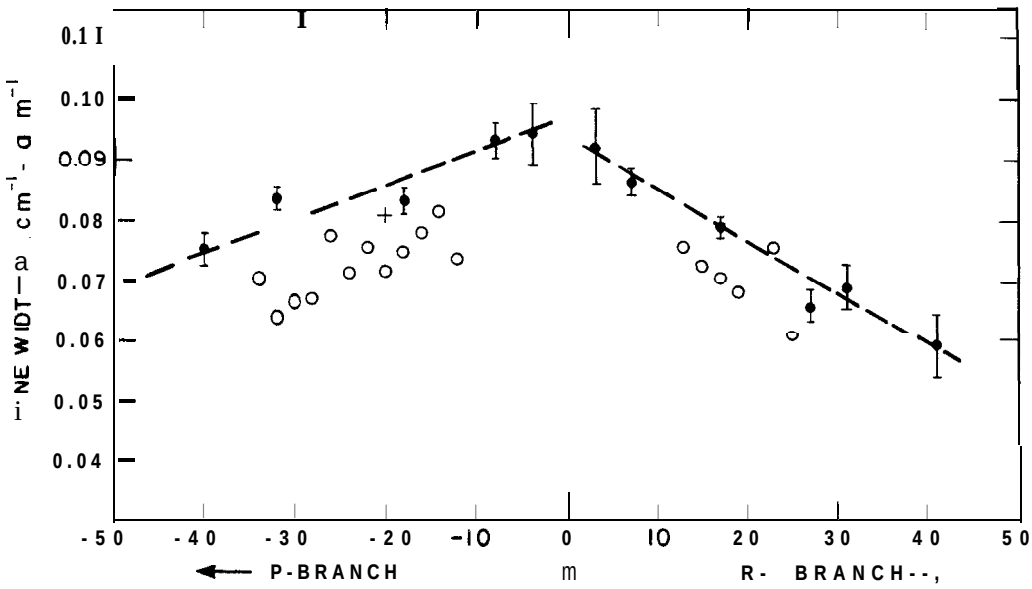

Fig. 7. Dependence of line width $\Delta_J(\mathrm{cm^{-1}\ atm^{-1}})$ at 300°K on rotational quantum number m for the 10.4-μ band of CO_2. ●, Oppenheim et al. (*129*); 0, Rossetti et al. (*130*); +, McCubin et al. (29).

and α_1 are the fine structure constants. Other interactions, such as the Coriolis effect, would also contribute (*114*) a small correction to these constants; however, we shall not go into details here.

The B_v and D_v values recently (131) have been measured accurately using two stabilized CW CO, lasers. The experiment involves a mixing of stabilized vibration-rotation laser lines in a GaAs mixer. The beat frequencies, in the millimeter-wave region of 50–80 GHz, are measured for 37 pairs of transitions to an accuracy better than I MHz. An expression for beat frequencies, f, can be derived (131) from the term values $T(v, J)$ of vibrational-rotational energy levels which are the sum of Eqs. (8) and (16) as

$$\begin{aligned} f_P &= T(v_u, J-2) - T(v_\ell, J-1) - T(v_u, J) - T(v_\ell, J+1) \\ f_R &= T(v_u, J+2) - T(v_\ell, J+1) - T(v_u, J-2) - T(v_\ell, J-3) \end{aligned} \tag{29}$$

where f_p and f_R are the beat frequencies in $\mathrm{cm^{-1}}$ of two adjacent laser lines in the P and R branches, respectively, and J is the rotational quantum number (a running odd integer). The measured beat frequencies for 37 pairs of transitions were analyzed by a digital computer using a multiple regression method. The deduced rotational constants for 00^0 1, 10^00, and 02^00 levels are presented in Table 12, along with the best values obtained from the conventional spectroscopic data.

TABLE 12

Rotational Constant Measurements from Mixing CO_2 Lasers

Constant	CO_2 Laser Measurement (This Work)		Previous best value[a,b]
	(MHz)	(cm^{-1})	(cm^{-1})
B_{00^01}	11606.180 ($\pm$0.011)	387140.44 ($\pm$0.37) $\times 10^{-6}$	387132 ($\pm$40) $\times 10^{-6}$
D_{00^01}	39.728 ($\pm$0.063) $\times 10^{-4}$	13.252 ($\pm$0.021) $\times 10^{-8}$	13.45 ($\pm$0.50) $\times 10^{-8}$
$B_{10^00}-B_{00^01}$	91.3584 ($\pm$0.0014)	3047.389 ($\pm$0.046) $\times 10^{-6}$	3069 ($\pm$10) $\times 10^{-8}$
$D_{10^00}-D_{00^01}$	-5.506 ($\pm$0.011) $\times 10^{-4}$	-1.8366 ($\pm$0.0035) $\times 10^{-8}$	-0.65 ($\pm$0.7) $\times 10^{-8}$
$B_{02^00}-B_{00^01}$	100.1534 ($\pm$0.0019)	3340.757 ($\pm$0.063) $\times 10^{-6}$	3344 ($\pm$10) $\times 10^{-6}$
$D_{02^00}-D_{00^01}$	7.140 ($\pm$0.016) $\times 10^{-4}$	2.3816 ($\pm$0.0053) $\times 10^{-8}$	2.65 ($\pm$1.2) $\times 10^{-8}$

[a]C. P. Courtoy, *Can. J. Phys.*, **35**, 608 (1957).

[b]R. Oberly and K. N. Rao, *J. Mol. Spect.*, **18**, 73 (1965).

IV. Population Inversion Mechanisms

In this section we shall be concerned mainly with the processes that produce population inversion between the $00^0 1 - 10^0 0$ and $00^0 1 - 02^0 0$ vibration-rotation levels of CO_2. According to the laws of thermodynamics, external excitation of some kind is required for all laser systems.[7] In the case of the CO, laser, collisional relaxation processes also play a vital role in the over-all inversion scheme. Collisional relaxation by itself is a rather complicated and thoroughly investigated field which involves a large number of kinetic processes. Before discussing the collisional processes of relevant CO, levels, especially $10^0 0$, $02^0 0$, and $01^1 0$, we shall consider the processes which produce the $00^0 1$ upper laser level population.

A. EXCITATION PROCESSES

It was suggested early by Patel[3] that population inversion may exist among certain vibration-rotation transitions in the $00^0 1$ and $10^0 0$ bands even though the population $n_v = \Sigma_J n_J$ of the upper vibrational level is slightly less than that of the lower laser level. The main argument rests on the fact that within a given vibrational state, n_J is distributed according to Eq. (9). Although this argument may lead to a small population inversion among some of the vibration-rotation transitions between two vibrational levels, it cannot possibly yield very high gain because only a small fraction of population density satisfies this condition known as "partial inversion." The two principal pumping mechanisms are now recognized as (I) direct electron impact and (2) resonance transfer of energy between N_2 ($v = 1$) and CO, ($00^0 0$).

1. Electron Impact

Measurements of rotational and vibrational excitation cross sections of CO, and N_2 by inelastic collisions of electrons at low energies (O-3 eV) have been reviewed by Phelps(132). Since then more accurate measurements have been made by Stamatovic and Schulz (233) for electron energy within 0.05 eV of threshold for all fundamental modes in CO_2. As a result considerable knowledge has recently been added concerning excitation processes and cross-section measurements relevant to CO, lasers. Figure 8 shows the cross sections

† Recently a chemical CO, laser without external excitation sources has been reported by T. A. Cool [see Ref. (*216*)]. However this laser still requires external power to maintain a high-speed gas flow through the laser interacting region.

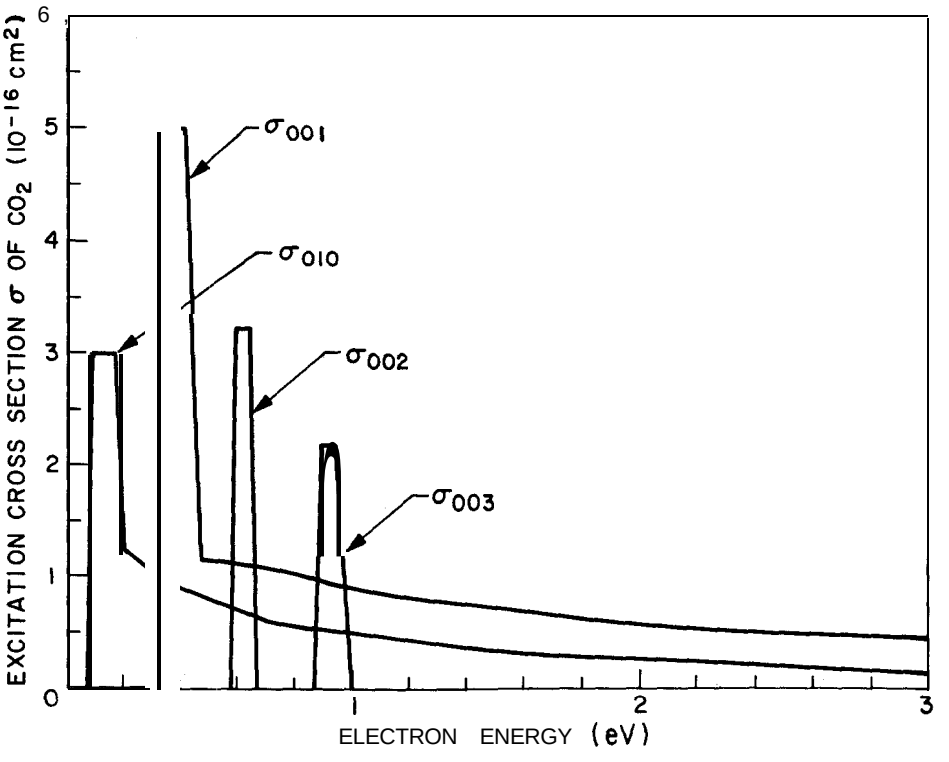

Fig. 8. Cross sections for vibrational excitation of CO, by electron impact. See text. [After Hake and Phelps(l7).]

which were derived by Hake and Phelps(17) for the vibrational excitation of CO, molecules by electrons. Results show that there exists a set of four resonances at 0.08, 0.3, 0.6, 0.9 eV, two of which have high energy tails.† The resonances at 0.3, 0.6, and 0.9 eV have been observed by Boness and Schulz(l8) who used high-resolution electron beam techniques. Hake and Phelps associate the 0.3, 0.6, and 0.9 eV energy loss processes with the three levels of the asymmetric mode (ν_3, $2\nu_3$, and $3\nu_3$) of the CO_2 molecule, and 0.08 eV is associated with the lowest bending mode (ν_2).

The unique feature of these results for CO, is that the resonances in each case occur very close to the threshold for onset of the particular energy loss process. This is quite different from the situation which is observed in diatomic gases, such as N_2, where the resonances occur at energies well above the ~ 0.3 eV threshold for $v = 1$ .as shown in Fig. 9. These results indicate that the probability of excitation of N_2 ($v = 1$) by

†A. V. Phelps has pointed out (private communication) that the cross sections given in Fig. 8 may be significantly in error with regard to their energy dependence. Only the over-all value of the sum of the 0.3, 0.6; and 0.9 eV energy loss processes and the threshold energy dependence of the 0.08 eV process are considered reliable.

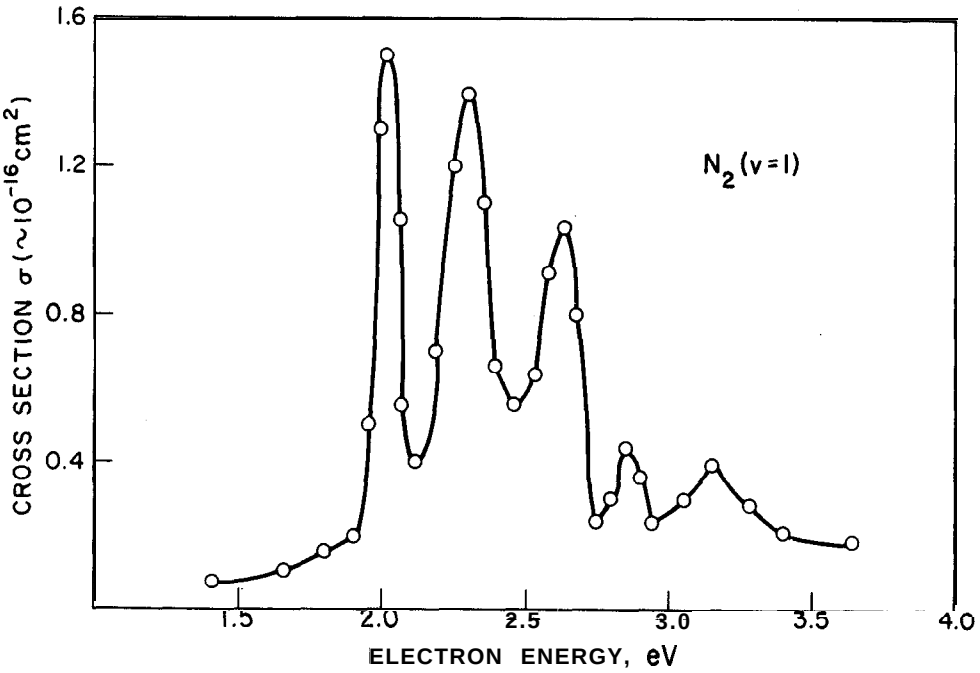

Fig. 9. Cross section for vibrational excitation of N_2 (v = 1) by electron impact. [After Schulz(*134*).]

electron impact at $kT_e > 1$ eV depends less critically on electron temperature than does that of CO, (00^0 1). The total excitation cross section σ_T of N_2 also has been investigated by Schulz(*134*), who showed that σ_T reaches a maximum value $\sim 3 \times 10^{-16}$ cm^2 at electron energy ~ 2.3 eV, as shown in Fig. 10. This high probability was attributed to a "resonance" effect between the energetic electrons and the N_2 molecular potential, causing the formation of a short-lived negative-ion compound N_2^-. In the case of CO_2, the resonance theory is necessary to explain the shape and magnitude of the vibrational excitation cross section near the threshold (within 0.05 eV). But in the energy range fat above threshold, the resonance theory cannot explain the behavior and magnitude of the excitation cross section. Thus one must attribute the excitation of the CO, (00^0 I) for electron energy in the range from I to 3 eV typically found(*16*) in a CO_2–N_2–He discharge to a "direct" process. Clearly the experimental conditions, such as gas pressure, mixture ratios, and electrical discharge current, must be adjusted so that the distribution of electron energy is most favorable for excitation of N_2 (v = 1) and CO, (00^0 1) but not CO, (0 1 ^{1}0). From the results of Figs. 8 and 9 and the electron temperature measurements (16) it is clear that excitation of CO, (00^0 1) level population by electrons is in the region dominated by the direct process and that a major portion of

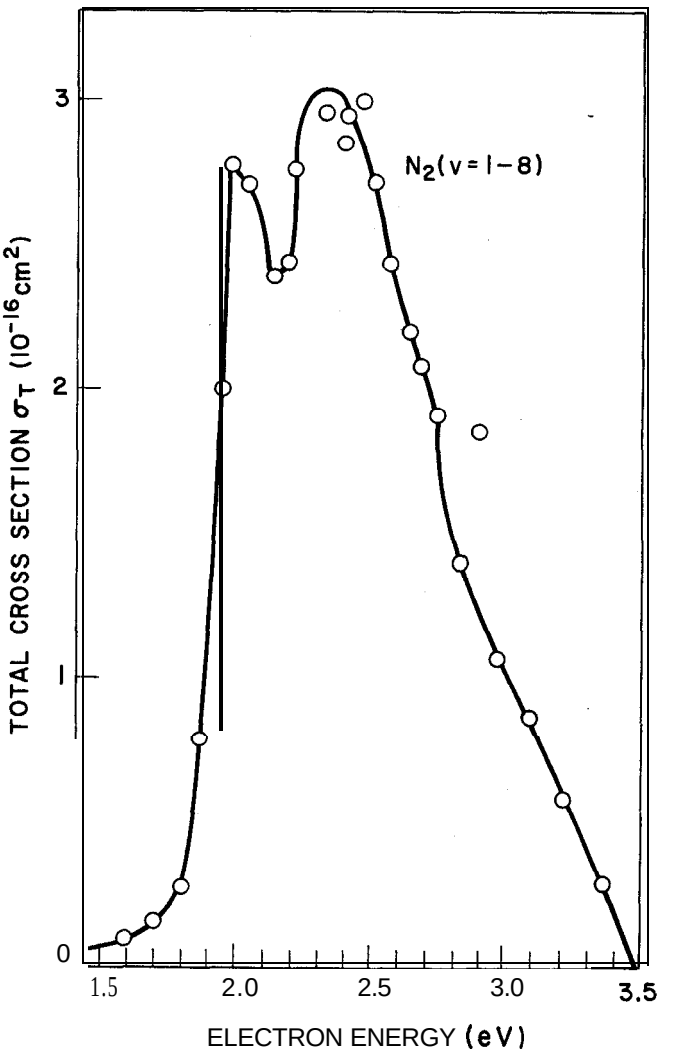

Fig. 10. Total effective cross section for vibrational excitation of N_2 (v = 1-8) by electron impact. [After Schulz (*134*).]

the electrons is used in the excitation of N_2 (v = 1), which in turn transfers its energy to excite CO, (00^0 1).

In the Born approximation, the vibrational excitation cross section σ is *(135)*

$$\sigma = \mu_{mn} \frac{3R_y}{8\pi a_0^2 \epsilon} \ln \frac{\epsilon^{1/2} + (\epsilon - E_i)^{1/2}}{\epsilon^{1/2} - (\epsilon - E_i)^{1/2}} \tag{30}$$

where $\mu_{mn} = \langle m|p|n\rangle$ are the, dipole matrix elements from 01^10 and 00^0 1 to the ground state, ϵ is the average electron energy, R_y is the Rydberg constant, and a_0 is the radius of the Bohr orbit. For $\epsilon \gg E_i$, the ratio of the cross sections σ_1/σ_2 for two vibrational states evaluated at

a particular electron energy ϵ is

$$\frac{\sigma_1}{\sigma_2} = \frac{f_1 E_2}{f_2 E_1} \frac{\ln(4\epsilon/E_1)}{\ln(4\epsilon/E_2)} \tag{31}$$

where f_1 and f_2 are thefnumbers or the IR absorption intensities of the two vibrational transitions. They are

$$f_{mn} = \frac{E_v}{3R_y a_0^2 e^2} |\mu_{mn}|^2 \tag{32}$$

Using f values given by Penner(*136*), i.e., $f_{010} = 7.9 \times 10^{-6}$, $f_{001} = 1.14 \times 10^{-4}$ and $f_{100} = 0$, Eq. (3 I) yields the ratios $\sigma_{010}/\sigma_{001} \simeq 0.35$ for $\epsilon = 1.9$ eV which is in fairly good agreement with recent experimental measurements (133) for 1.5" scattering at 1.9 eV. From the preceding results, one concludes that in a CO_2–N_2–He laser, the average electron energy must be chosen far above the threshold value for excitation of the $00^0 1$ CO, level in order to avoid direct pumping of the 01^10 level. In -this case only a small fraction of the electrons is used to pump the ground state CO, molecules to the $00^0 1$ upper laser level; but for the most part, electrons in the discharge are used to excite the first vibrationally excited state of nitrogen. On the other hand, the average electron must be limited to < 3 eV in order to avoid excessive dissociation processes. If one assumes that the entire energy stored in the vibrationally excited N_2 (v) molecules (up to $v = 4$) can be transferred to the CO, (00^0 1) level by a rapid resonant transfer process (to be discussed in detail later), it is possible to estimate the rate of excitation of the CO, (00^0 1) level population from the excited N_2 molecules alone by using the total effective excitation cross section of N_2 (see Fig. 10) and data(l37) on electron density n_e and drift velocity $\bar{v}_e$ in a positive column. At 1Torr of N_2 pressure, the rate of excitation of N_2 is **equal** to $N_0 n_e \sigma_{N_2} \bar{v}_e \simeq 1\ 0^{18}\ \text{sec}^{-1} - \text{cm}^{-3}$ for electrons with energies in the 1-2 eV range. In a laser tube 1m long and 2.5 cm i.d., this rate **could** produce a total $\sim 5 \times 10^{20}$ quanta/sec, corresponding to a maximum output power of the order 100 W.

2. Resonance Transfer

Excitation by resonance transfer (or collision of the second kind) was postulated as an important inversion mechanism in the first gas laser (He-Ne) by Javan et al.(*138*) using a helium metastable as the pump for Ne, the emitter. The importance of this process, however, was never completely convincing until the advent of the CO_2–N_2 laser (9). The selective excitation of CO, (00^0 1) from the ground state by the

first vibrationally excited N_2 (v = 1) occurs at a very rapid rate(25), $k_e = 1.9 \times 10^4$ Torr^{-1}-sec^{-1}, because of the extremely close coincidence between N_2 (v = 1) and CO, (00^0 1) as

$$N_2(v = 1) + CO_2(00^0 0) \xleftrightarrow{k'_e, k_e} N_2(v = 0) + CO_2(00^0 1) - 18 \text{ cm}^{-1} \quad (33)$$

and N_2 (v = 1) cannot otherwise decay to the ground state because N_2 has zero permanent dipole moment This resonance transfer, as given by Eq. (33), produces a mixed state in which the combined population of N_2 (v = 1) and CO, (00^0 1) are essentially in equilibrium. This, in effect, increases the effective lifetime of CO, (00^0 1) by almost a factor of two upon addition of a few Torr of N_2 pressure as measured by Cheo (24). Relaxation of this mixed state takes place subsequently at a slower rate(24,25) ($k_{\nu_3} \simeq 110$ Torr^{-1}-sec^{-1}) as compared with the relaxation rate of ν_3 in a pure CO, gas discharge ($k_{\nu_3} \simeq 385$ Torr^{-1}-sec^{-1}). We shall discuss the relaxation processes in detail later.

Vibrational energy transfer processes by collisions have been treated theoretically by Landau and Teller(139) and later extended by Schwartz, Slawsky, and Herzfeld (SSH)(*140*). Because of the nonadiabatic nature of vibrational motions during molecular collisions, it has generally been assumed that only the strong and short-range repulsive forces are effective in causing the energy exchange. The SSH theory has been very successful in explaining a wide variety of collisional processes, in particular the $V \rightarrow T$ vibrational-to-translational energy exchange as we shall discuss later. However, an exception to this theory, as pointed out by Sharma and Brau(*141*), is the near-resonant vibrational energy transfer reaction described by Eq. (33). Recent experimental results obtained by laser-induced fluorescence(25,142) and shock-wave techniques(l43) show that the cross section for this reaction has an anomalous inverse temperature dependence, in the temperature range below 1000°K, from that predicted by the SSH theory. Sharma and Brau(l41) proposed a long-range dipole-quadrupole interaction by which this anomalous behavior can be explained. For simplicity, they assumed the expression for the dipole-quadrupole interaction with a spherical potential,

$$V = \frac{pq}{2r^4(t)} \quad (34)$$

where p is the dipole moment of CO_2, q is the quadrupole moment of N_2, and r(t) is the classical trajectory describing the relative positions of the center mass of the molecules during the collision. These long-range forces are particularly important at low temperatures ($T <$

1000°K) and for processes of near-energy resonance. Using the interaction potential of the form given by Eq. (34), the probability $\mathscr{P}$ of vibrational energy transfer can be expressed as (141)

$$\mathscr{P} = \frac{1}{4h^2} |\mu_{10} q_{01}|^2 \left| \int_{-\infty}^{\infty} \frac{\exp(i\omega t/\hbar)}{r^4(t)} dt \right|^2 \tag{35}$$

where $\omega = \Delta E/\hbar$ (AE = 18 cm^{-1}), and $\mu_{10} = \langle 000|p|001\rangle$ and $q_{01} = \langle 1|Q|0\rangle$ are the dipole and quadrupole matrix elements between (000) and (001) states of CO, and between $v = 1$ and $v = 0$ states of N_2, respectively. In this approximation for rigid-sphere interaction, Sharma and Brau(*141*) obtained the formula for the total cross section of vibrational energy transfer in terms of the gas temperature, as

$$\mathscr{P}(T) = \frac{3\pi^3 m |\mu_{10} q_{01}|^2}{64 h^2 b^4 kT} \tag{35a}$$

where m is the reduced mass and b the closest approach $\simeq 3.9 \times 10^{-8}$ cm (hard-sphere collision diameter). Since the rate constant k_{vv} for the $V \rightarrow V$ processes and the probability $\mathscr{P}$ are related(l5) by

$$k_{vv} \propto \mathscr{P} T^{1/2} \tag{36}$$

the theory(l42) based on long-range forces provides an expression for the temperature dependence of the exchange rate as proportional to $T^{-1/2}$. This result is in excellent agreement with the measurements of Rosser et al.(*142*) in the temperature range from 300" to 1000°K. At higher temperatures ($T > 1000$" K), experimental results (141) show that the transfer rate is approximately proportional to $T^{3/2}$, which indicates that the interaction is dominated by the short-range forces as predicted by the SSH theory.

It is a known fact that a substantial amount of CO (~10% of the CO, pressure) is produced in a CO_2 gas discharge(19) as a result of dissociation of CO_2. Studies of CW and pulsed CO_2 laser amplifiers showed that CO increases the gain(35) and the effective lifetime(24) of the $00^0 1$ upper laser level substantially. These observations can be explained also by the same mechanism discussed above. The reaction

$$CO_2(00^0 1) + CO(v = 0) \xleftrightarrow{k_e(CO)} CO_2(00^0 0) + CO(v = 1) + 206\ cm^{-1} \tag{37}$$

appears to be important in a CO_2 laser, especially for a sealed-off laser system, even though the energy resonance for this reaction is not as close as that of Eq. (33). The $k_e(CO)$ has been measured(*144*) to be 0.79×10^4 $Torr^{-1}$-sec^{-1}. Relaxation of this mixed state resulting from the resonant transfer process (37) takes place via collisions with CO or

CO, molecules in the ground state at a much slower rate(*14*), k_{CO_2-CO} = 193 $Torr^{-1}$-sec^{-1}, which is a factor of about 2 less than $k_{CO_2-CO_2}$. It should also be pointed out here that helium, which is the other gas commonly used in a CO, laser, plays no important role, for all practical purposes, in the excitation or deactivation of the $00^0 1$ upper CO, laser level (24).

B. RELAXATION PROCESSES

To understand all the important aspects of population inversion in a CO, laser, one must not overlook relaxation processes which are comparable in magnitude to the resonance transfer processes for excitation of the upper CO, laser level. As mentioned before, the use of a CO,-He mixture in a CO, laser results in an equal or slightly higher power output than that of a CO_2–N_2 mixture. This is primarily owing to efficient relaxation of the lower CO, laser level by collisions with helium(24,25) while the upper CO, laser level lifetime is left unaffected. The presence of many relaxation processes makes the CO, laser a much more complex system than most other existing lasers because the theory of a multilevel ($00^0 1$, $10^0 0$, $02^0 0$, $01^1 0$, $00^0 0$) laser system is difficult to treat. The mechanism is further complicated by the rotational relaxation and competition effects which are especially important when the laser is operated on a single rotational line. The concept of using relaxation processes for creating population inversions, in addition to excitation processes, is by no means new and has been introduced earlier by Gould(145). His concept has become successfully realized in the CO,-N,-He laser. To produce a high efficiency and high power laser, the lifetimes of the upper laser level, τ_u, and the lower level, τ_ℓ , must satisfy the condition,

$$\tau_u^r \gg \tau_u^c \gg \tau_\ell^c \tag{38}$$

where τ^r and τ^c represent the radiative and collisional (or effective) lifetimes, respectively. Furthermore, the laser levels should lie near the ground state so that the power conversion efficiency can be high and the relaxation of the lower laser level can be greatly increased by collisions with gas additives. The calculated radiative lifetimes of the lower laser levels $10^0 0$, $02^0 0$ and the lowest bending mode $01^1 0$ are very long (see Table 9). Therefore, relaxation via collisions are vital in the establishment of an inversion.

I. Gas Kinetics in a CO_2 Laser

Vibrational relaxation in CO, and mixtures of CO, has been extensively investigated by ultrasonic(1.5) and shock-wave techniques (*143*), and most recently by means of CO, lasers(14,24,25,142). Ultrasonic measurements (*15*) yield mainly the relaxation time of the lowest bending mode 0 $1^1$0 of CO_2. As shown in Fig. 3, relaxation of this level involves a vibration-to-translation ($V \rightarrow T$) energy exchange, as described by

$$CO_2(01^10) + M \xrightarrow{k_{v_2}(M)} CO_2(00^00) + M + 667\,cm^{-1} \quad (39)$$

Other ($V \rightarrow T$) processes as well as vibration-vibration ($V \rightarrow V$) energy exchange are very important in the understanding of CO, lasers. For example, the Fermi resonance exchange between the two lower laser levels 1 0^0 0 and 02^00 is

$$CO_2(1\,0^00, 02^00)' + M \xleftrightarrow{k_F} CO_2(10^00, 02^00)'' + M + 102\,cm^{-1} \quad (40)$$

where, (10^00, $02^00)'$ and $(10^00, 02^00)''$ are two mixed states as discussed in Section III.B. Both of these levels can decay to the 0 1^1 0 level through resonant processes such as

$$CO_2(10^00, 02^00)' + CO_2(00^00) \xleftrightarrow{k(v_1, 2v_2)} 2CO_2(01^10) - 50\,cm^{-1} \quad (41a)$$

$$CO_2(10^00, 02^00)'' + CO_2(00^00) \xleftrightarrow{k(v_1, 2v_2)} 2CO_2(01^10) + 52\ \text{cm-*}. \quad (41b)$$

The upper laser level is coupled to the lower laser levels by collisions and by stimulated emission, as

$$CO_2(00^01) + M \xrightarrow{k_{v_3}} CO_2(n, m^\ell, 0) + M + E_{trans} \quad (42)$$

and

$$CO_2(00^01) \xrightarrow{S_u I_{laser}} CO_2(10^00) \text{ or } CO_2(02^00) + h\nu \quad (43)$$

Because a large amount of experimental information has been compiled on relaxation rates of $V \rightarrow T$ processes, the theory for the $V \rightarrow T$ process is fairly well established. On the other hand, the theory for the $V \rightarrow V$ process is less developed, and only very recently, with the advance of the CO, laser, has the experimental information on the $V \rightarrow V$ processes become available. In general, theoretical arguments indicate a faster rate for a $V \rightarrow V$ process than for a $V \rightarrow T$ process because the former involves a resonant exchange. It turns out, as we shall discuss in greater detail later, that the $V \rightarrow T$ rate for the lowest

bending mode $01^1 0$ is one of the dominant factors in controlling the gain and power of CO, lasers.

Transfer of energy between two vibrational states or one vibrational and one translational degree of freedom occurs only through inter- or intramolecular collisions. The average number of collisions, Z, required to deactivate one vibrational quantum to its e^{-1} value is defined by

$$Z = \tau/\tau_c \tag{44}$$

where τ is the relaxation time or the effective lifetime of the state and τ_c is the time between successive collisions which is inversely proportional to gas pressure P. Therefore, l/Z is the probability of deactivation of vibrational energy in one collision. Since Z depends only on the kinetics of the colliding molecules, it is a function of gas temperature and independent of P.

The relaxation rate of a collisional process is related to the exponential relaxation time τ by the simple expression

$$k = (P\tau)^{-1} \tag{45}$$

where k is the rate constant of a given relaxation process. This fact is used widely in experimental investigations of relaxation time of excited vibrational states of CO, in a pure CO, gas mixture such as in Eqs. (39)-(42), etc.

In a mixture involving CO_2 and a foreign gas M, relaxation of a vibrationally excited CO, molecule can take place through the binary processes by collisions with either a ground state of CO, and/or with M. The relaxation rate for the binary collisions is given by

$$k = xk_{CO_2-CO_2} + (x-1)k_{CO_2-M} \tag{46}$$

where x is the mole fraction of CO_2, and $k_{CO_2-CO_2}$ and k_{CO_2-M} are the respective rates for CO,-CO, and CO_2–M collisions. This equation is useful in determining the relaxation rate constants of 01^10, $00^0 1$, and 02^00 or 10^00 levels by collisions with foreign gases such as H_2, He, H_2O, CO, and N_2 which are commonly used in CO, lasers.

In the cases of CO,-N, and CO,--CO mixtures, where resonant transfer is important, mixed states are formed as described by Eqs. (3 3) and (37). The formation of these mixed states is very rapid (typically $\sim 10^{-5}$ sec in a working CO, laser). Thereafter the combined population CO, (00^0 I) and N_2 ($v = 1$) or CO ($v = 1$) remains essentially in equilibrium. The relaxation of the mixed state in the case of a CO,-N, mixture occurs at a much slower rate by means of the processes.

$$CO_2(00^0 1) + N_2(v=0) \xrightarrow{\tau_{CO_2-N_2}} CO_2(n,m',0) + N_2(v=0) \tag{47a}$$

$$N_2(v = I) + CO_2(00^0 0) \xrightarrow{\tau_{N_2-CO_2}} N_2(v = 0) + CO_2(n,m^{\ell},0) \quad (47b)$$

The relaxation rates of Eqs. (47) can be computed from the measurements of the effective lifetime τ of CO, $(00^0\ 1)$ in a CO,-N, mixture, by the equation,

$$\frac{1}{\tau} = \frac{1}{x_1 + rx_2}\left[\frac{x_1^2}{\tau_{CO_2-CO_2}} + x_1x_2\left(\frac{1}{\tau_{CO_2-N_2}} + \frac{r}{\tau_{N_2-CO_2}}\right)\right] \quad (48)$$

where $r = \exp[-(E_{N_2} - E_{CO_2})/kT]$ and x_1 and x_2 are the mole fractions of the CO, and N_2 molecules, respectively. The fraction of excitation CO, $(00^0\ 1)$ is $x_1/(x_1 + k_e x_2/k_e')$, where k_e and k_e' are the rates for the reaction as described by Eq. (33). Therefore the number of collisions between CO, $(00^0\ 1)$ and CO_2 in the ground state is less than that in pure CO, gas by the factor $x_1^2/(x_1 + k_e x_2/k_e')$. Since the observed rates of the processes in Eqs. (47) are proportional to x_1x_2, they cannot be separated experimentally. Also in Eq. (48) a term owing to $N_2(v = 1)$–$N_2(v = 0)$ collisions has been neglected, since the relaxation time for this process is very long(146).

2. Relaxation of the 01^10 Level

Among all processes discussed above, the $V \rightarrow T$ process as described by Eq. (39) is the most widely studied in both theory and experiment. Before presenting various experimental measurements of the relaxation time of CO, levels and rate constants for the above mentioned collisional processes, we shall briefly discuss some theoretical developments and mechanisms on $V \rightarrow T$ processes. Several books (*147*–149) on this subject are available for more details. Landau and Teller (139) were the first to treat the theory of energy transfer in a collision. Even though the treatment is classical, it contributes significant insight into the physical mechanisms. They showed that the probability of energy transfer depends on the interaction potential between colliding molecules and on their relative velocities. If the relative change in strength of an external force is small during τ_c the process is adiabatic, otherwise it is nonadiabatic. According to Ehrenfest's principle, only the nonadiabatic process can cause a quantum transition. Since the repulsive intermolecular forces are of shorter range than all others and thus can produce a sufficiently strong interaction to cause a transition, they are the only ones that need be considered.

Based on that assumption and also assuming that the velocities of the colliding molecules obey Maxwell's distribution, Landau and Teller (139) obtained an expression for the probability that the vibrational energy E_v of one of the colliding pair is transferred to the translational

mode of the other. It is given by

$$\mathscr{P} \propto \exp[-(3E_v/kT)^{1/3}] \tag{49}$$

A quantum mechanical treatment of this problem was formulated by Schwartz et al.(140) about 16 years later, and they obtained some numerical results for Z from a priori calculation. In this treatment, they fitted the widely used Lennard-Jones potential(150), in which the dominant term, r^{-12}, is the strong repulsive part of the interaction between the two colliding particles, with an exponential form ($V \propto e^{-r}$), thus simplifying the mathematical analysis considerably. They obtained the probability $\mathscr{P}$ for a $V \rightarrow T$ process as given by

$$\mathscr{P} = 0.39V_{10}^2\left(\frac{8\pi^3\mu E_v}{\alpha^2h^2}\right)\sigma^{3/2}\left[1-\exp\left(\frac{-2\sigma}{3}\right)\right]^{-1}\exp(-\sigma) \tag{50}$$

where $V_{10} = \langle 01^10|V|00^00\rangle$, μ is the reduced mass of the colliding pair, and

$$\sigma = 3\left(\frac{2\pi^4E_v^2\mu}{\alpha^2h^2kT}\right)^{1/3} + \frac{E_v}{2kT} \tag{51}$$

The quantum mechanical results show a temperature dependence similar to that derived classically. Numerical results of these calculations are in better agreement with experimental data(*15*). Figure 11 shows both the experimental (ultrasonic) measurements and the SSH theoretical results for relaxation of 01^10 CO, level by collisions with unexcited CO, molecules and He atoms. As we shall see later, relaxation of this level is very important for the CO, laser because population inversion densities associated with the 00^01-10^00 and 00^01-02^00 laser transitions are essentially limited by the relaxation rate of the 01^10 level(14). Other gases such as H_2, H_2O, and to some extent CO (data on CO are not as abundant as for H_2 and H_2O) are known to enhance the relaxation rate of the lowest bending mode of CO,. Table 13 gives a list of the 01^10 relaxation rates k_{v_2} for CO, mixed with various gases.

Several considerations should be pointed out.

1. H_2 and H_2O are very effective in relaxing the 01^10 level, but they also relax the upper CO, laser level (00^01) very effectively. Therefore, these gases normally are not used intentionally in high-power CO, laser systems. lmprovements in performance with H_2 or H_2O additives have been reported with the sealed-off CO, laser(20,67). Even then, the concentration of these gases is extremely small compared with other constituents and must be carefully controlled in order to obtain consistent results.

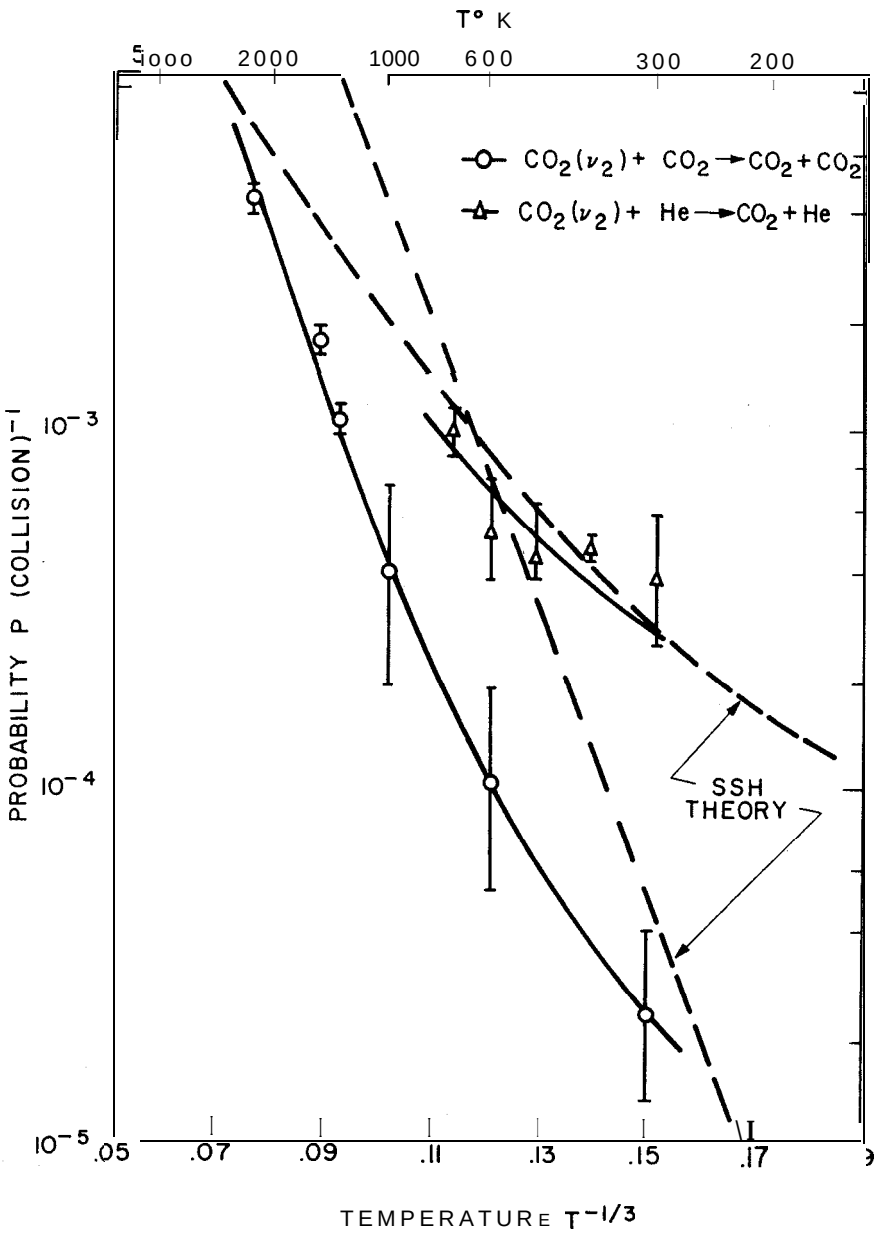

Fig. 11. Probability for vibrational-translational ($V \rightarrow T$) energy exchange between the lowest bending mode, 01'0, and the ground state of the CO, molecule. [After Taylor and Bitterman(*15*).]

2. Helium, even though less efficient in deactivating the 0 I ^{1}0 level than H_2 and H_2O, yields the highest gain(19) compared with any other single gas additives. This is mainly because the upper CO, laser level is essentially unaffected by the admittance of a large amount of helium into the laser ($\gtrsim$ 10 Torr), whereas the 10^00 level relaxation time is reduced drastically(24). At such high pressures the relaxation time of

TABLE 13

Relaxation Rate Constant k_{v_2} for CO, in Various Gas Mixtures at T = 300°K

Mixture	k_{v_2} (Torr^{-1} sec^{-1})	References
CO_2	194	15
CO,-H,	6.5 x 10^4	15
CO,-He	3.27 x 10^3	15
CO_2–H_2O	4.5x 105	15
co*-co	2.5 x 10^4	148"
CO_2–N_2	6.5 x 10^2	1.5"

"Ultrasonic data on CO and N_2 are not as accurate as other data given here.

the 01 ^{1}0 level is about 2 x 10^{-5} sec and is in fact shorter than $\tau_{CO_2-H_2O}$ (5 x 10^{-5} sec at 0.1 Torr of H_2O) in a typical working CO_2–H_2O laser.

3. In studies of the transient gain response of pulsed CO_2–H_2 and CO_2–H_2O laser amplifiers, Cheo(l4) observed a substantial absorption in the afterglow period as shown in Fig. 12. When a minute amount of

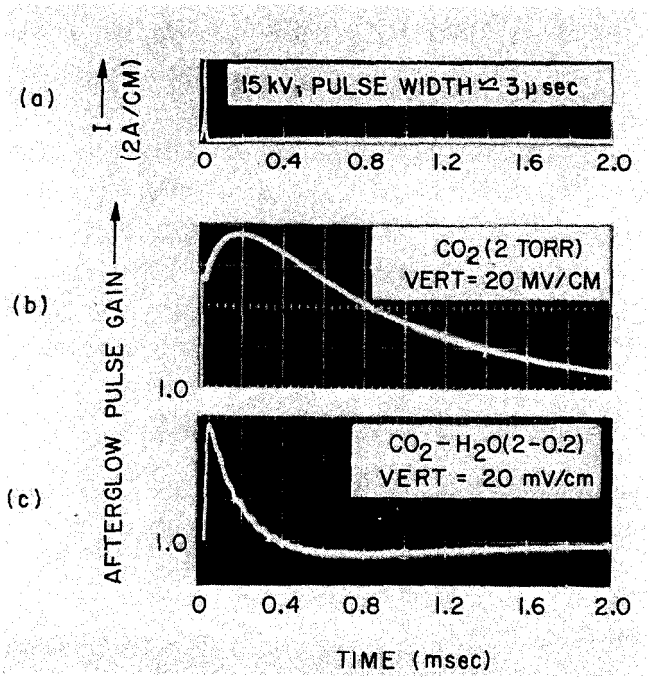

Fig. 12. Afterglow pulse gain measurements. (a) Discharge current pulse used to produce the optical gain pulse in curves b and c. (b) The 10.6-p gain pulse in a 22-mm-bore laser amplifier tube filled with 2-Torr of CO,. (c) The afterglow gain and absorption pulses at 10.6 μ in a 22-mm-bore laser amplifier tube filled with 2 Torr of CO_2 and 0.2 Torr of H_2O.

H_2O vapor (0.1-0.2 Torr) is introduced into the CO, laser amplifier, the afterglow gain decays rapidly at a rate more than one order of magnitude faster than that of pure CO,. However, the absorption pulse following the initial gain has a very long tail with a time constant typically of the order of 1 msec. The peak absorption increases with increasing H_2O pressure at a constant excitation. This has led to the conclusion that a bottleneck is formed at the $01^1 0$ level in the latter afterglow periods and relaxation of this long lifetime level is achieved primarily by the wall diffusion process. As we shall see later in discussions of deactivation of the 00^0 I and 1 $0^0 0$ and $02^0 0$ levels, relaxation of the lower CO, laser levels is essentially limited by the depletion rate of the $01^1 0$ level. The accumulation of population at the $01^1 0$ can occur through resonant intermolecular process as given by

$$\mathrm{CO,}\ (00^0 1) + H_2O\ (000) \rightarrow CO_2\ (01^1 0) + H_2O\ (010) + 87\ \mathrm{cm^{-1}} \qquad (52)$$

and the 010 level of H_2O molecules can subsequently transfer its energy to CO, through the process

$$H_2O\ (010) + \mathrm{CO,}\ (00^0 0) \leftrightarrow H_2O\ (\mathrm{OOO}) + \mathrm{CO,}\ (10^0 0) + 207\ \mathrm{cm^{-1}} \qquad (53)$$

Available experimental data(l5) show that the probability $\mathscr{P}$ for deactivation of the $01^1 0$ level of CO, by collisions with H_2O has an opposite temperature dependence from that predicted by the SSH theory, a condition similar to that for the resonance transfer process observed in a CO_2–N_2 mixture. To date, there exists no satisfactory explanation of this anomalous behavior. If $V \rightarrow V$ resonant processes as described by Eqs. (52) and (53) play a significant role, assumptions made in the formulation of SSH theory would be inadequate. It is imperative that further experimental studies be carried out to verify the significance of these $V \rightarrow V$ processes by which H_2O interacts with the ν_1 and ν_2 modes of the CO, molecule.

4. Finally it should be stressed again that dissociation plays an important role in CO, lasers because CO can relax the $0\,1^1 0$ level of the CO, molecule very effectively as well as excite the 00^0 I level by a resonant transfer, as discussed earlier. The CO has not been among the most widely studied additives to CO_2, nevertheless, it is always present in a CO, gas discharge. In studies of early CO, lasers, when pure CO, was the main gas used in sealed-off tubes, the presence of CO or certain impurities in a CO, gas discharge was indispensible for causing the population inversion between the vibrational levels of the CO, molecules. This fact has been substantiated by the pulsed-gain measurements(I4) of relaxation times of the 00^0 1 and $10^0 0$ levels of the CO, molecule.

3. *Relaxation of $00^0 1$ Level*

The relaxation times of the 00" I CO, upper laser level in various gas mixtures commonly used in CO, laser systems have been measured by an induced fluorescence technique(25) with a Q-switched CO, laser and by the afterglow pulse gain technique(I4). The former was introduced by Hocker et al.(23) to study the relaxation time of the 00^0 1 level via CO,-CO, collisions. In this experiment, a small passive cell containing CO, gas or mixtures of CO, with other gases is placed inside a rotating-mirror Q-switched CO_2 laser cavity. During the Q-switching phase (typically the pulse width is 0.2 to 0.5 μsec in duration) the I $0^0 0 \rightarrow 00^0$ 1 transition is nearly saturated, and a small fraction ($\sim 10^{-3}$) of the CO, molecules in the passive cell is pumped to the $00^0 1$ level. The relaxation rate is determined by observing the spontaneous decay of the 00" $1 \rightarrow 00^0 0$ emission intensity (4.3 μ) from the side window as a function of CO, gas pressure. The relaxation times measured by this method were limited to a minimum of a few μsec by the laser pulse width and to a maximum of about 1 msec by the frequency of the rotating mirror. Because the fluorescence is very weak. rneasurements arc made usually at fairly high gas pressures. The advantage of this method. of course. is that it provides unambiguous measurements of gas composition because the interaction in the cell involves no discharges.

The afterglow pulse gain technique. on the other hand. can yield information concerning the relaxation times of both the upper $00^0 1$ and the lower- $10^0 0$ or $02^0 0$ CO, laser levels simultaneously. This technique is applicable to most high-power CW laser systems satisfying the condition described by Eq. (38). In a pulsed CO, laser amplifier with a very short electrical excitation pulse ($\sim$ 1 μsec), the transient gain response to a CW CO, laser first rises exponentially with a time constant τ_r and then decays exponentially with a time constant τ_d (see for example. Fig. 12b). Analysis(24) indicates that τ_r and τ_d correspond to the relaxation times of the lower and the upper laser levels, respectively. This technique not only permits a direct measurement ofeffective lifetimes of both the upper and lower laser levels, at a significantly higher signal-to-noise ratio than from fluorescence measurements. but also yields information concerning the energy transfer processes which are relevant to the population inversion between 00^0 1-l $0^0 0$ or 00^0 1 – $02^0 0$ levels in various mixtures containing CO,. However. it must be emphasized that relaxation time or rate measurements by this method were made in a pulsed laser amplifier- with a suitable electrical excitation for optimum gain. therefore a certain amount of impurities, such

as CO and O_2 (and in some cases NO, OH, etc.) is present and can cause complications in the interpretation of results. Nevertheless, information obtained in this way is much more relevant to CO, laser performance because the experimental conditions are similar to those for operating CO, lasers. For this reason we shall discuss here mainly the pulse-gain measurements and compare them with measurements obtained by other methods whenever appropriate data are available.

In a series of papers, Cheo(*14*,*24*) has reported the relaxation times of the 00^0 1 and 10^00 CO, laser levels by measuring the exponential rise and decay time constants of the afterglow gain pulse in CO_2, CO_2–H_2, CO_2,-He, CO_2–H_2O, CO_2–N_2, CO_2,-CO, and CO_2,-Xe nonflowing gas mixtures. Some measurements for CO_2,-He mixtures were made also in a flowing gas laser amplifier. In the cases of CO_2, CO_2,-H_2, and CO_2–H_2O, the product of the 00^0 1 level relaxation time constant τ_{00^01} and the additive gas pressure P for a fixed CO, concentration was found to remain at a constant value over a certain range of P. Thus the rate constant k_{ν_3} for relaxation of the 00" 1 level by collisions with these gases can be determined directly from the slopes of the linear plot of $1/\tau_{00^01}$ vs. P curves. These measured values of k_{ν_3} are listed in Table 14 along with fluorescence measurements(2.5) of $k_{,,}$. In general, k_{ν_3} values obtained from the two different methods are in fairly good agreement. For mixtures of CO_2–N_2 and CO_2,-CO, τ_{00^01} increases by almost a factor of 2 upon addition of a few Torr of CO and N_2 pressure(*14*) as a result of the rapid resonant transfer process.

TABLE 14

Relaxation Rate Constant k_{ν_3} of CO, in Various Gas Mixtures X at $T = 300°K$

Mixture	P_{CO_2} (Torr)	P_X range (Torr)	k_{ν_3} (Torr^{-1} sec^{-1})	
			Pulse gain(*14*)	Fluorescence[a]
CO_2	1-8	[b]	385	350
CO_2-H_2	3	0.5-3.0	4.5 x 10^3	3.8 x 10"
CO_2-He	1	1-8	O-50	85
CO_2–H_2O	2	0.05	4.2 x 10^4	2.4 x 10^4
CO_2- N_2	1	1-7	115[c]	106
CO_2-CO	2	1–5	193"	
CO_2-Xe	2	0.1-1.0	O-50	30

[a] Data by Moore et a1.(25,141) at much higher gas pressure than pulse gain measurements.

[B] Other species such as CO-O_2 are also present owing to dissociation of CO_2.

[C] Obtained for largest P_X values.

Relaxation of the mixed states, as described by Eqs. (33) and (37), is at a much slower rate through processes (47b) than that by CO_2-CO_2 collisions. These rate constants k_{v3} for CO_2-N_2, and CO_2-CO collisions are computed from Eq. (48) for mixture ratios 1 : 7 and 2: 5, respectively.

From Table 14 we see that both H_2 and H_2O relax the upper CO_2, laser level severely. These results, combined with the bottleneck formation at the 01 ^{1}0 and 1 0^00 levels as described by Eqs. (52) and (53), can account for the extremely critical pressure dependence on gain and power output encountered with CO_2-H, and CO_2-H_2O laser systems. In the cases of CO_2-He and CO_2-Xe mixtures, no significant change in τ_{00^01} from that of pure CO_2 was observed for $0 < P_{He} < 8$ Torr and $0 < P_{Xe} < 1$ Torr. In most cases, the relaxation of CO_2 (ν_3) takes place through the $V \rightarrow V$ coupling between ν_3 and ν_2 (or ν_1) modes as

$$CO_2(\nu_3) + M \longrightarrow CO_2(\nu_2) + M + 416\ cm^{-1} \tag{54}$$

However, it has been pointed out by Yardley and Moore(*151*) that in the case of noble gases the most favorable collisions for the deactivation of ν_3 occur when only a small amount of energy on the order of kT is exchanged with the translational mode. This argument is based on the fact that the measured(*151*) probability for deactivation of CO, (ν_3) by noble gases has a peak for those whose reduced mass μ, and hence velocity of the rare-gas collision partners, corresponds to a resonance between the collision time τ_c and the frequency difference between the two levels involved, or

$$\tau_c \simeq \frac{h}{\Delta E} \tag{55}$$

For $\tau_c \simeq 1.6$ Å/$(8\,kT/\pi\mu)^{1/2}$, one obtains the energy difference ΔE of a transition between the initial and final states within 20 $cm^{-1} \leqslant E \leqslant$ 300 cm^{-1}. Based on these arguments, deactivation of CO, (ν_3) by collisions with noble gases is attributed to the intramolecular energy exchange, for example,

$$CO_2(\nu_3) + M \longrightarrow CO_2(04^00) + M - 199\ cm^{-1} \tag{56}$$

and

$$CO_2(\nu_3) + M \longrightarrow CO_2(11^10) + M + 272\ cm^{-1} \tag{57}$$

It has been shown(*151*) that the highest transition probability for the intramolecular $V \rightarrow V$ energy transfer, when the difference of energy levels lies within a few hundred cm^{-1}, is owing mainly to a mixing of vibrational states through anharmonicity and Coriolis coupling terms. Therefore this process cannot be very efficient when compared with

other collisional relaxation processes among polyatomic molecules. For this reason the population density at the upper CO, laser level is relatively unaffected upon addition of a large amount of He or Xe.

Diffusion also plays an important role in the deactivation of the excited CO, molecules. This has been studied by Kovacs et al.(152), who measured the wall depletion rate of the excited 00^0 1 level of CO, by monitoring the decay of the spontaneous 4.3-p radiation arising from the 00^0 1 level of CO_2 molecules in an induced fluorescent cell excited by a rotating-mirror Q-switched CO_2 laser pulse. The measured diffusion coefficient for the 00^0 1 level was found to be different from the self-diffusion coefficient obtained from viscosity measurements. Several absorption cells of different diameters and wall materials were used in this experiment. The relaxation rate of the 00^0 1 level population is determined by both the collisional relaxation rate within the volume and the destruction rate of the wall. Thus

$$k_{\text{total}} = k_{\text{wall}} + k_{\text{volume}} \tag{58}$$

where $k_{\text{wall}} = \gamma^2 \mathscr{D}/r_0^2$ and $k_{\text{volume}} = k_{\nu_3}$ as given in Table 14. The symbol γ represents the roots of the boundary equation which is derived from the continuity equation at the wall, $\mathscr{D}$ is the diffusion coefficient, and r_0 is the radius of the absorption cell. For a cylindrical tube, the boundary equation is given by (*152*)

$$\gamma J_1(\gamma) - \frac{\bar{v} r_0}{2\mathscr{D}} \left(\frac{1 - \beta}{1 + \beta} \right) J_0(\gamma) = 0 \tag{59}$$

where β is called the wall reflection coefficient and $\bar{v}$ the average thermal velocity of the molecules. For CO, pressures greater than 1 Torr, k_{total} is dominated by k_{ν_3}, whereas for $P_{CO_2} < 1$ Torr, $k_{\text{total}} \simeq k_{\text{wall}}$, which increases rapidly and approaches a constant value $(\bar{v}/r_0) \times (1 - \beta/1 + \beta)$. Figure 13 shows the plot of k_{wall} vs. CO_2 pressure. The dashed curve represents the P dependence for the volume-quenching case, which is obtained by extrapolation from data taken above 1 Torr where diffusion is negligible. The measured diffusion constant $\mathscr{D}$ is 0.7 ± 0.01 cm²/sec which differs substantially from the self-diffusion constant (148) 0.119 ± 0.001 cm²/sec. Experiments with four different wall surfaces yield the same result, 0.22 ± 0.08, for the wall deexcitation probability $(1 - \beta)$. This result is attributed(152) to a common type of comtamination absorbed by the surfaces of the absorption cell.

4. *Relaxation of the 1 $0^0 0$ and $02^0 0$ Levels*

As mentioned before, because of Fermi resonance, relaxation of $(10^0 0, 02^0 0)'$ and $(10^0 0, 02^0 0)''$ takes place via processes (41) at a

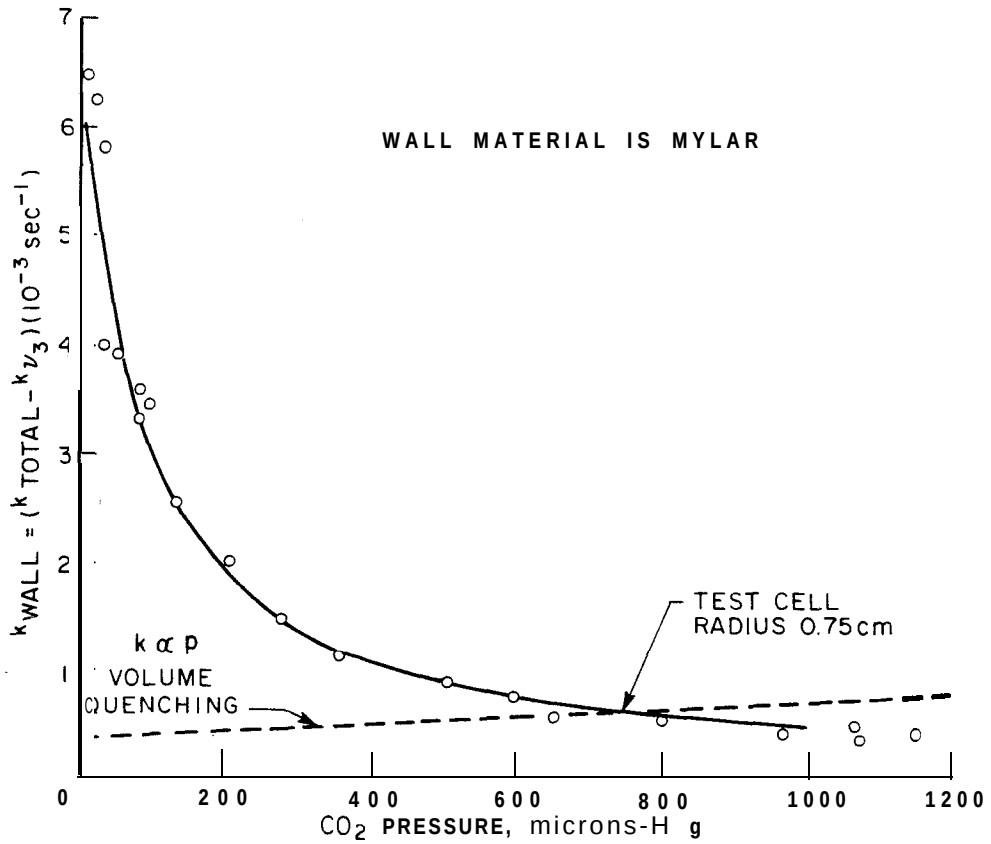

Fig. 13. Diffusion-decay rate of the $00^0 1$ CO, level as a function of CO, pressure. Data (open circles) were obtained from a cell with a 1.5-cm i.d. Mylar wall material. The dashed curve is the volume quenching rate as a function of CO, pressure. [After Kovacs et al. (*152*).]

rate $k_{(\nu_1,2\nu_2)}$ several orders of magnitude as fast (*153*) as a second-order transition, such as $1\ 0^0 0 \rightarrow 01^1\ 0$, which would require a Raman-like perturbation ($1\ 0^0\ 0 \rightarrow 00^0 0 \rightarrow 01\ ^1 0$). To date no direct rate measurements have been made of either the Fermi resonance, Eq. (40), or the $V \rightarrow V$ processes, Eqs. (41). Pulse-gain measurements (14) provide only an effective relaxation rate of the lower laser level; because of the strong collisional coupling between the lower laser level and the bending mode ($0\ 1^1\ 0$ level), the measured rate constants $k^{\text{eff}}_{(\nu_1\ 2\nu_2)}$ are actually the trapped values owing to the accumulation of population at the $01\ ^1 0$ level. This is evident when the pulse-gain results as given in Table 15 are compared with the relaxation rates of the $01\ ^1\ 0$ level as given in Table 13. The measurements (Table 15), except for those taken with a pure CO_2 fill in which a considerable amount (> 10%) of CO is present owing to dissociation of CO_2, are reasonably close to the k_{ν_2} values. This indicates that the effective relaxation rates of the lower laser levels are essentially limited by that of the $01\ ^1\ 0$ level.

TABLE 1.5

Effective Rate Constant $k^{\text{eff}}_{(\nu_1,2\nu_2)}$ of CO, in Various Gas Mixtures X

Mixture	P_{CO_2} (Torr)	P_X range (Torr)	$k^{\text{eff}}_{(\nu_1,2\nu_2)}$ ($\text{Torr}^{-1}\,\text{sec}^{-1}$) Pulse gain (*14*)
CO_2	1-8	*a*	2.2×10^{n}
CO_2–H_2	3	0.5-3.0	3.3×10^{4}
CO_2-He	1	1-8	4.7×10^{3}
CO_2–H_2O	2	0.05	1.2×10^{6}
CO_2-N_2	1	1-7	26
CO_2-CO	2	1-5	4.1×10^{3}
CO_2-Xe	2	0.1-1.0	5×10^{3}

"Other species such as CO-O_2, are also present owing to dissociation of CO_2.

In the case of CO_2–CO_2 collisions, pulse-gain measurements (*14*) yield a $k^{\text{eff}}_{(\nu_1,2\nu_2)}$ value of 2.2×10^{3} Torr^{-1}-sec^{-1} which is about 10 times that for a k_{ν_2} value obtained by ultrasonic methods (*15*). This discrepancy could be owing to dissociation of CO_2 into CO and O_2. From ultrasonic data (*15*), O_2 does not relax the CO_2 (01^1 0) level very efficiently, but very little data on CO is available. According to pulse-gain measurements (*14*), the relaxation rate for the 10^00 and 02^00 levels is 4.1×10^{3} Torr^{-1}-sec^{-1}, obtained by collisions with CO. Therefore, the assumption of dissociation is a reasonable one and is consistent with other observations (*35*), such as enhancement of CO_2 laser gain and of power output by addition of CO, and also spectroscopic analysis of the side-light emission from a CO_2 laser discharge (*19*). Another interesting observation is that, in the case of a pulsed CO_2-N_2 laser, the effective lifetime of the lower laser level increases with increasing N_2 gas pressure similarly to the increased lifetime observed for τ_{00^01} in the same gas mixture as a result of resonance transfer between CO_2 (00^0 1) and N_2 (v = 1). It has been suggested (*15*) that since Ar also is known to be less efficient than CO_2 in deactivating mode ν_2, the same mechanism may be involved for these two cases.

Recently Rhodes et al.(28), using double-beam resonance techniques, observed a fairly fast rate of the order of 4×10^{5} Torr^{-1}-sec^{-1} in a CO_2 absorption cell by monitoring the decrease in absorption of a CW 10.6-p radiation immediately following a 9.6-p rotating-mirror Q-switched CO_2 laser pulse. From their experiment, it is not clear what reaction corresponds to the observed rate. They attribute this rate to the relaxation of the mixed state (10^00, 02^00) to the 0 1^10 level via Eq. (41). Herzfeld (*153*) has made extensive computations of the

vibrational relaxation rates in the presence of Fermi resonance, using an exponential repulsive interaction energy between the two colliding particles and eigenfunctions of the states $(10^00, 02^00)'$ and $(10^00, 02^00)''$ as given by Eq. (19). Mixing of nonresonant states was also taken into consideration, but symmetry rules were observed in this numerical analysis. Several of these numerical results, which are relevant to the CO_2 laser system, are tabulated in Table 16. Calculations of vibrational energy exchange rates, using Herzfeld's method, recently have been carried out by Gordietz et al.(154) for mixtures of CO_2-He, CO_2–N_2, and CO,-CO. The calculated results are given in Table 17. Several significant points emerge from these calculations. (i) The numerical calculation of the Z number for the $01^10 \rightarrow 00^00$ is in excellent agreement with the experimental results given in Table 13.

TABLE 16

Z Number(*153*) for Various Relaxation Processes in Pure CO,

Transition	300°K	600" K	1000" K	2000" K
$01^10 \rightarrow 0000$	58,400	2.900	430	43
$(1000, 02^00)' \rightarrow 00^00$	3.2×10^8	3.7 x IO"	2.0×10^5	5.600
$(10^00, 02^00)'' \rightarrow 00^00$	8.7×10^8	8.2×10^6	3.8×10^5	8,900
$(10^00, 02^00)' \rightarrow 01^10$	29,300	1,550	250	29
$(10^00, 02^00)'' \rightarrow 01^10$	75,500	3,330	480	49
$02^20 \rightarrow 01^10$	29,200	1.450	215	22
$(10^00, 02^00)' \leftrightarrow (10^00, 02^00)''$	290	145	85	40
$(10^00, 02^00)' \leftrightarrow 02'0$	140	70	42	21
$(10^00, 02^00)'' \rightarrow 02^20$	163	81	49	24
$(11^10, 03^10)' \rightarrow (10^00, 02^00)'$	22,300	1.141	180	19
$(11^10, 03^10)' \rightarrow (10^00, 02^00)''$	56.400	3.900	760	100
$(11^10, 03^10)'' \rightarrow (10^00, 02^00)'$	3.5 x IO"	1.2×10^5	14.300	880
$(11^10, 03^10)'' \rightarrow$ (10~0.0200)"	29,580	2,040	300	27
$(11^10, 03^10)' \rightarrow 02^20$	38,100	2,180	390	110
$03^30 \rightarrow 02'0$	19,500	970	140	14
$(11^10, 03^10) \rightarrow$ sum over all	5,800	320	52	< 10
$00^01 \rightarrow 00^00$	8.6×10^{12}	1.6×10^{10}	2.2×10^8	1.2×10^6
$0^01 \rightarrow (10^00, 02^00)'$, (0000)	2.6×10^9	4.7 x IO'	3.5 x IO"	1.5×10^5
$0^01 \rightarrow (10^00, 02^00)''$, (0000)	5.9×10^8	1.35×10^7	1.2×10^6	64,000
$0^01 \rightarrow (00^00), (10^00, 02^00)'$	6.8×10^9	1.2×10^8	9×10^6	3.9×10^5
$0^01 \rightarrow$ (0000). $(10^00, 02^00)''$	1.6×10^8	3.2 x IO'	3.2×10^6	1.7×10^5
$0^01 \rightarrow (01^10, 02^00)'$, (01' 0)	1.1×10^8	1.25 x IO'	3.3×10^6	6.9×10^5
$0^01 \rightarrow (10^00, 02^00)''$, (01^10)	1.4×10^7	$2.6 \times$ IO"	8.1×10^5	2.4 x IO"
$0^01 \rightarrow 01^10, (10^00, 02^00)'$	4.8×10^8	5.4×10^7	1.5 x 10'	2.9 x 10"
$0^01 \rightarrow 01^10, (10^00, 02^00)''$	6.4 x 10'	1.1×10^7	3.8×10^6	1.05×10^6
$0^01 \rightarrow$ sum over all	2.7×10^6	4.9×10^5	1.25×10^5	21,000

TABLE 17

Calculated(*154*) Vibrational Energy Transfer Rate Constants among CO_2, N_2, and CO Molecules

k ($Torr^{-1}\,sec^{-1}$)	300°K	600" K	1000° K
N_2 (v = 1) → $CO_2(\nu_3)$	1.0x 10^4	2.1 x 10^4	3.9 x 10^4
CO (v = 1) → $CO_2(\nu_3)$	1.38 x 10^3	7.3 x 10^3	2.6 x 10^4
k_{ν_3} (CO_2–N_2) for Eq. (44)	10	63	2.8 x 10^4
k_{ν_3} (He) for Eq. (38)	62	6.9 x 10^2	2.7 x 10"
k_{ν_2}(CO)	4.5 x 10^3	6.5 x 10^4	5.8 x 10^5
co (v = 1) → $CO_2(\nu_1) + CO_2(\nu_2)$	9.5 x 10^2	3 x 10^3	8.2 x 10^3
co (v = 1) → $CO_2(\nu_2)$	6	46	2.8 x 10^2

(ii) Only 290 collisions (corresponding to -4 x 10^4 $Torr^{-1}$-sec^{-1}) are required to achieve a mixed state among 10^00 and 02^00, the lower CO_2 laser levels; the formation of this state through Eq. (40) is at a rate about 300 times as fast as that derived from Eq. (39). (iii) Relaxation rates of the lower laser levels to the lowest bending mode (01^10) are of the same order of magnitude as that for the transition from $01\,^10 \rightarrow 00^00$. These results are about one to two orders of magnitude lower than that reported by Rhodes et al. (28) but are very close to the pulse-gain measurements of $k^{\text{eff}}_{(\nu_1,2\nu_2)}$ by Cheo(*14*). (iv) The transfer rate between (10^00, 02^00) and 02^20 is very rapid even though a direct mixing between 10^00 and 02^20 is not allowed because of the symmetry rule. Furthermore, the transfer rate between 02^20 and $0\,1\,^10$ is of the same order of magnitude as that for ($100, 02^00$) → $0\,1^10$; therefore the 02^20 level may be important also for the populations of 10^00, 02^00, and 01^10 to reach equilibrium(l.55).

It is clear from the above discussions that the vibrational energy exchange and collisional relaxation in CO_2 laser systems are very complex and further studies in this area are needed. However, for a typical CO_2 laser using a CO_2–N_2–He mixture, the four most important relaxation processes are given by Eqs. (39)–(42). The first three processes lead to the depletion of the population of the lower laser level which in general occurs at a rate ($\gg 10^2$) much greater than the process described by Eq. (42).

5. Rotational Relaxation

All the preceding discussions pertained to the relaxation of low-lying vibrational levels of the CO_2 molecule while assuming that rotational

relaxation within a given vibration state occurs at an extremely fast rate. Using viscosity data for CO_2, a simple calculation shows that the collision time for hard-sphere collisions is about 100 nsec at 1 Torr. This corresponds to a rate constant of 1 0^7 $Torr^{-1}$ sec^{-1} if rotational thermalization occurs in one collision. Previous relaxation-time measurements by the pulse gain (14,24) and by rotating-mirror Q-switched laser techniques(25,28) have been limited to about 0.3 μsec or greater because of either the duration of the electrical excitation in a pulsed discharge or the length of the rotating-mirror Q-switched CO_2 laser. Recent development(*56*) of a GaAs electrooptic switch for cavity dumping a 10.6-p Q-switched pulse of about 10 kW and 20 nsec duration has made direct measurement of the rotational thermalization time of the 00^0 1 upper CO_2 laser level possible. A single-frequency $P(20)$ 10.6-μ cavity dumped pulse (for details see Section V.E) was used to measure the rotational relaxation rate constants k_{rot} of the CO_2 (J, 00^0 I) level by collisions with CO_2(*26*), N_2, or He(27). This was accomplished by monitoring the transient change in the CW gain of a 9.6-p P(J) laser amplifier, where J = 17, 19, . . . , 39, induced by passage of a 20-nsec 10.6-μ $P(20)$ laser pulse through a pure CO_2, CO_2-N_2, or CO_2-He laser amplifier. Since the P(20) 10.6-μ and $P(20)$ 9.6-p transitions share a common upper level, ***J = 19 (see*** Fig. 4), the CW gain of the 9.6-p CO_2 laser amplifier will be suddenly reduced by the passage of the 10.6-k Q-switched pulse through the same medium. The recovery time of the gain at 9.6 μ is a direct measure of the rotational relaxation time of the J = 19 upper laser level. More significantly, one can obtain the selection rules for rotational transition if the Q-switched laser is fixed on $P(20)$ of the 10.6-p band but the 9.6-p CW laser transition is scanned over different J values.

Figure 14a shows the 10.6-μ, $P(20)$ Q-switched pulse. Figure 14b, c are the 9.6-p CW gain responses for the $P(20)$ and $P(30)$ transitions, respectively, when the medium is suddenly perturbed by the Q-switched 10.6-μ $P(20)$ laser pulse. Both traces b and c of Fig. 14 are obtained for a CO_2 pressure of 1.1 Torr. In Fig. 15, the measured rotational relaxation rate I $/\tau_{rot}$, or the recovery rate of the gain, is plotted as a function of CO_2, N_2, and He gas pressures. Rate constants k_{rot}, for CO_2–CO_2, CO_2–N_2, and CO_2–He collisions, are obtained from the slopes of these linear plots of $1/\tau_{rot}$ vs. CO_2, N_2, and He gas pressures and are given in Table 18. For pure CO_2, the value of $Z = \tau/\tau_{coll}$ (the number of gas kinetic collisions necessary to cause rotational thermalization) is equal to 0.6. This implies that collision-induced rotational mixing occurs more rapidly than simple hard-sphere collisions. Acoustical absorption experiments (1.56) show that $Z_{CO_2-CO_2}$ = 1 .5 for ground state CO_2 molecules. This result is the relaxation rate

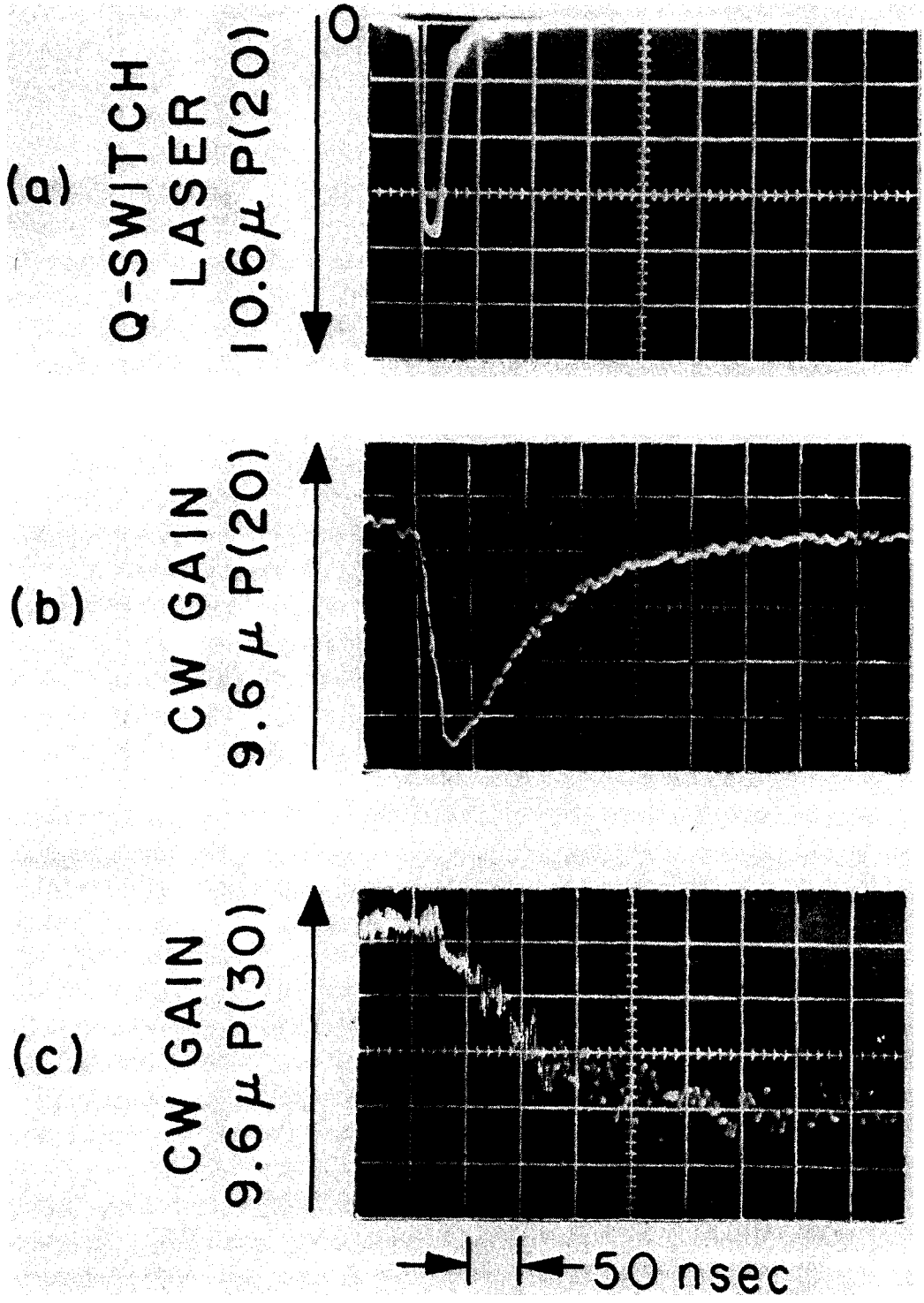

Fig. 14. Data on rotational relaxation in the 00° 1 CO_2 level. Trace (a) shows the cavity-dumped $P(20)$ 10.6-μ laser pulse as measured by a Ge: Cu(Sb) detector. Traces (b, c) show the responses of CW gain of the $P(20)$ and $P(30)$ transitions in the 00° I -02°0 band, respectively, after the medium has been perturbed by the passage of a cavity-dumped $P(20)$ 10.6-p laser pulse.

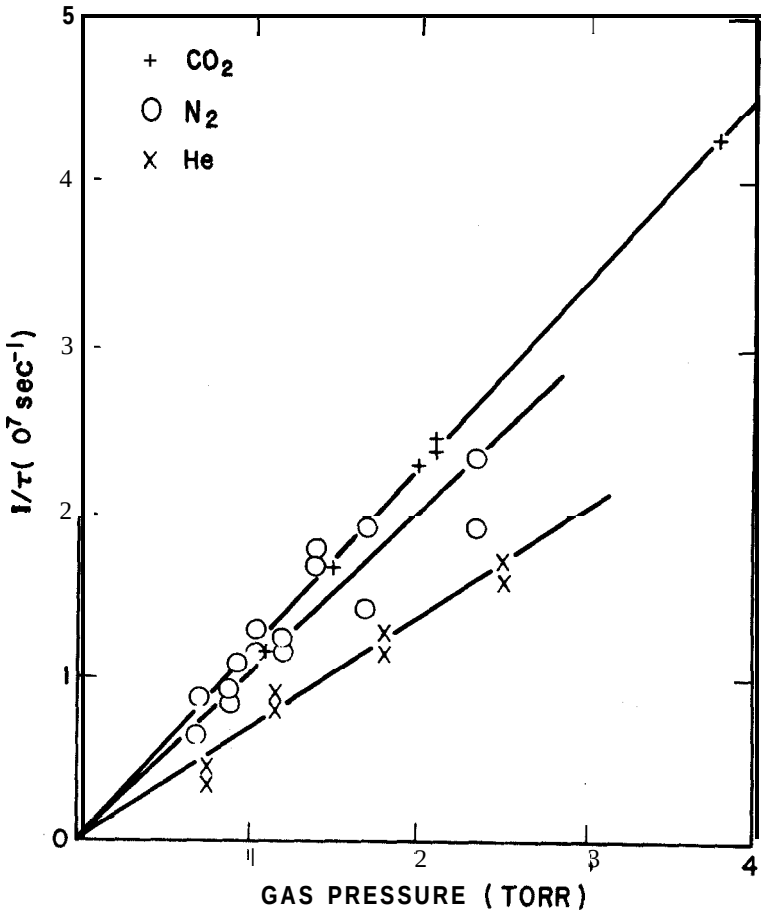

Fig. 15. Kelaxation rate $1/\tau_{rot}$ of the J = 19 rotational level of the 00" l CO, vibrational band as a function of CO_2, N_2, and He gas pressure.

of the average rotational energy when the entire distribution of the rotational levels is involved. On the other hand, the measurements made by using the double laser beam resonance technique(26,27)

TABLE 18

Rotational Relaxation Rate Constant $k^{rot}_{CO_2-X}$ of CO, (00^0 1, J = 19) for X = CO_2, He, and N_2 (*26,27*)

X	CO,	He	N_2
$k^{rot}_{CO_2-X}$ (10^7 sec^{-1} $Torr^{-1}$)	1.1 ± 0.2	0.7 ± 0.1	1.0 ± 0.2

involve a single perturbed J level in an excited vibrational state. The measured value(*29,30*) of the optical-broadening collision frequency by CO_2-CO_2 collisions yields a rate constant of approximately 1.0×10^7 $Torr^{-1}$ sec^{-1}, in good agreement with that obtained by the direct method described above, indicating that the 10.6-p linewidth is owing primarily to collisions causing rotational mixing. The relative effectiveness of CO_2. N_2, and He for optical broadening of the CO_2 absorption line also has been measured(*157*). From these measurements(*156*), one obtains $k_{CO_2-CO_2}/k_{CO_2-N_2} = 1.33$ and $k_{CO_2-CO_2}/k_{CO_2-He} = 1.69$, consistent with values given in Table 18.

Figure 14c shows the decay of CW gain for the 9.6-p $P(30)$ line when perturbed by the 10.6-p $P(20)$ Q-switched laser. Similar results were obtained also for transitions from $P(18)$ to P(38). The observed decrease in gain for the $P(30)$ line is owing to the collisional transfer of population from the $J = 29$ to the $J = 19$ rotational level. If rotational relaxation is a stepwise process, i.e., $\Delta J = \pm 2$, one would expect that the levels closest to $J = 19$ are most strongly coupled, so that there would be an increase in the time delay between the transient gain perturbation and the Q-switched laser pulse for either an increasing or decreasing value of J from $J = 19$. Experimentally, one finds that the observed waveforms for all transitions from $P(18)$ to $P(38)$ in the 00^0 1–02^00 band are very similar, with the exception of the $P(20)$. The decay times for all J's have almost the same value as the gain recovery time of the $P(20)$ line. This suggests that the rotational relaxation is J-independent, and only one collision is necessary to thermalize all rotational levels. From these measurements, it is clear that, in a CO, laser, all these tightly coupled rotational levels compete strongly for lasing. As a result, oscillation often switches from one line to the next, especially in a high-power laser system without a dispersive element. Further discussion on rotational level competition appears in Section V.C.

In summary, extensive investigations, both experimental and theoretical, have been carried out on various excitation and relaxation processes occurring in CO_2 discharges. Mechanisms responsible for population inversion of the two strongest bands, namely 00^0 I – 10^00 and 00^0 l-0200, are well understood; however, no attention has been given to other CO, laser transitions because they are weak and very little work has been done on them. Laser oscillations from those weak bands exist only under pulsed excitation. Measurements of colhsion cross sections and rate constants of the important processes allow reliable estimations on the performance of various CO, laser systems.

V. Conventional Laser Systems

Conventional CO_2 laser systems comprise either a sealed-off gas discharge or a low-speed longitudinal flow of CO_2 in a mixture along the discharge column. The gain and power characteristics of this type of laser have been investigated extensively, and the mechanisms are well understood. In this section we present the properties of these laser systems, such as the small-signal gain, gain saturation, linewidth and lineshape, CW and Q-switched laser output, and stabilization and life of a sealed-off CO, laser. A brief discussion of some nonlinear phenomena which have direct effects on the CO, laser is also included. Interpretation of experimental results is provided in terms of known physical processes and, in some cases, results are compared with theoretical models utilizing available information on lifetimes and collision cross sections of excitation and relaxation of the laser levels.

More recently concentrated effort has been devoted to laser systems involving high-speed (sub- or supersonic) transverse and longitudinal flow. Power output from these systems has exceeded that from conventional lasers by more than one order of magnitude, but the laser efficiency in general is lower. Experimental conditions for these high-flow systems are substantially different from the normal ones and involve either a high-speed exhaust channel at a flow rate greater than the relaxation rates of the laser levels or sudden expansion through a supersonic nozzle. We shall treat these subjects as well as some other novel systems in Section V 1.

A. SMALL-SIGNAL GAIN

The theory of the CO, laser, especially for the conventional types, is fairly well established. Historically it was the experimental investigation of various gain characteristics that led to insight into mechanism and provided the stimulus for theoretical development. Investigations of CO, laser amplifiers usually yield more information than do studies of laser oscillators because in the former the gain is directly proportional to the population inversion of the laser levels whereas the oscillators are inherently nonlinear systems involving positive feedback. Furthermore, one can extract a large amount of information from an amplifier with negative gain value. An oscillator, on the other hand, provides no information when the medium gain is less than the oscillator loss.

A small signal I propagating through an amplifying medium with an unsaturated gain coefficient α_0 will be amplified with a rate of increase

$$\frac{dI}{dL} = \alpha_0 I \tag{60}$$

where L is the length of the medium. From the principle of energy conservation, the increase in intensity per unit length, dI/dL, is related to the population inversion density $n_u - (g_u/g_\ell)n_\ell$ by

$$\frac{dI}{dL} = h\nu\mathscr{W}\left(n_u - \frac{g_u}{g_\ell} n_\ell\right) \tag{61}$$

where n_u and n_ℓ are the population densities of the upper and lower laser levels, g_u and g_ℓ are the level degeneracies, and $\mathscr{W}$ is the induced emission rate which is related to the spontaneous transition lifetime τ_r by (*158*)

$$\mathscr{W} = \frac{\lambda^2 I}{8\pi h\nu\tau_r} g(\nu) \tag{62}$$

where g(v) is the intensity distribution function describing the lineshape. Combining Eqs. (60)–(62) one obtains

$$\alpha_0 = \frac{\lambda^2}{8\pi\tau_r} g(\nu)\left(n_u - \frac{g_u}{g_\ell} n_\ell\right) \tag{63}$$

Equation (63) is equivalent to Eqs. (25) and (26) provided that a proper expression for g(v) is chosen. In the case of homogeneous broadening,

$$g(\nu - \nu_0) = \Delta\nu/2\pi[(\nu - \nu_0)^2 + \tfrac{1}{4}(\Delta\nu)^2] \tag{64}$$

where $\Delta\nu$ is the full width of the Lorentzian line at half-intensity and ν_0 is the center frequency of laser transition. At low gas pressure, the Doppler lineshape yields a better description which can be approximated by a Gaussian distribution $g(\nu_0)$ over ν_0 for a gas in thermal equilibrium as

$$g(\nu_0) = (\sqrt{\pi}\Delta\nu_0)^{-1} \exp\left[-\left(\frac{\nu_0 - \nu_0'}{\Delta\nu_0}\right)^2\right] \tag{65}$$

where $\Delta\nu_0$ is the half-width of the Doppler-broadened line **and** ν_0' is the line center at zero velocity.

A number of parameters such as excitation current, wall temperature, gas mixtures and mixing ratios, tube bore, and flow rates can affect the gain in a CO, laser in addition to pressure broadening or Doppler effects. In what follows we shall present experimental investigations of these effects which provide not only quantitative information about the CO, laser but also guidelines to achieve the optimum performance of this laser.

1. Current and Temperature Dependence

Parametric studies on the unsaturated gain coefficient of both the nonflowing(*19*) and flowing(*34*,*35*) CO, laser amplifiers have been made by measuring the power ratio of the net increase in the output to the input for a fixed length of amplifying medium. Figure 16 shows the effects of excitation power (discharge currents) on gain for a number of

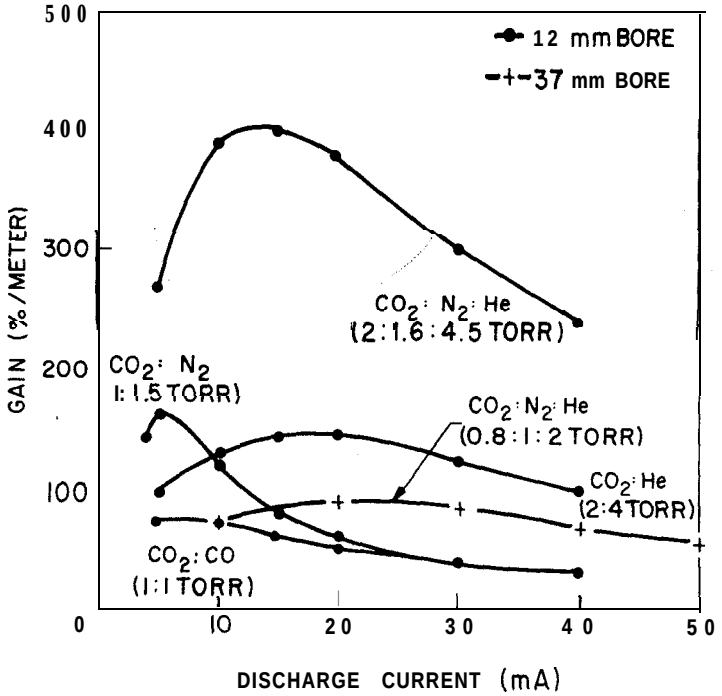

Fig. 16. Gain versus discharge current for various flowing CO, gas media at optimum mixture ratios and a constant CO, flow rate of 150 cm^3/min in 12- and 37-mm-bore amplifier tubes.

flowing gas mixtures. In general, optimum gain occurs at higher discharge currents for systems containing helium. Similar behavior is observed also for the nonflowing laser systems. At optimum discharge current, the gain of a nonflowing CO_2–He laser amplifier decreases with increasing wall temperature, as shown in Fig. 17. In general, the gain depends more critically on wall temperature for systems without helium but the temperature dependence is found to be less critical for flowing systems than for nonflowing laser amplifiers. One of the important effects of helium is to reduce the gas temperature in a discharge, owing to its high thermal conductivity. Similarly, gas temperature in a conventional laser also can be reduced by slowing the gas flow. Another important role played by helium is to increase the relaxa-

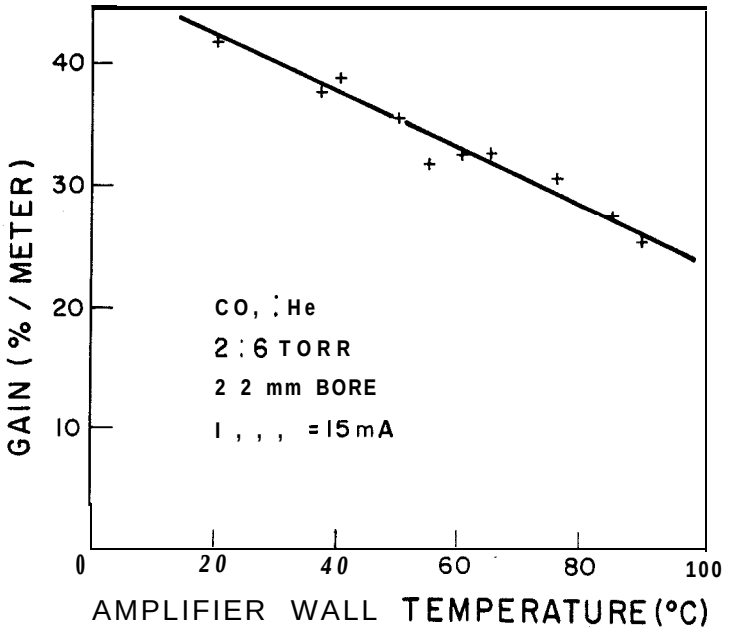

Fig. 17. Effect of wall temperature on optimum gain of a CO_2–He laser amplifier.

tion rate of the lower laser level. As shown in Fig. 16, an increase in discharge current leads to an increase in pumping rate, thus contributing to the initial increase of gain; however, it also leads to an increase in gas temperature, causing a rapid depopulation of CO_2 laser levels. With the addition of He the gas temperature decreases so that the depletion rate of the upper laser level population by collisions is decreased; furthermore the relaxation of the lower laser level is increased by CO_2-He collisions. Therefore, systems containing He usually can be pumped at higher discharge currents and thus yield a larger inversion density.

2. Pressure and Bore Dependence

For both flowing and nonflowing laser amplifiers, gain increases rapidly with increasing He pressure from 0 to about 3 Torr and thereafter gain becomes relatively insensitive to a further increase of helium pressure. However, gain depends critically on CO_2 partial pressure as shown in Fig. 18. This behavior can be easily explained from the measurements of volume quenching rate and wall destruction rate through diffusion of the vibrationally excited CO, molecules as shown in Fig. 13. It can be seen from Fig. 13 that the total decay rate of the 00^0 I level, k_{total}, has a minimum value at $P_{CO_2} \simeq$ I Torr, at which a maximum gain is obtained for the pure CO_2 and CO_2–N_2 laser

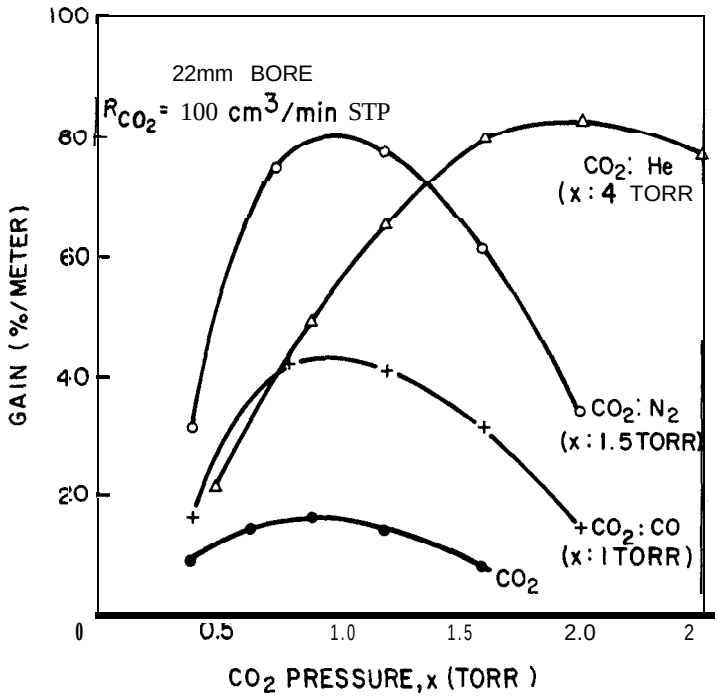

Fig. 18. Gain versus CO, pressure for various gas mixtures in a 22-mm-bore amplifier tube. The CO, flow rate is 100 cm^3/min.

amplifiers of approximately the same bore size (- 20 mm). This is expected because diffusion of CO, (00^0 1) through N_2 should have about the same coefficient as that measured in pure CO, gas (0.07 ± 0.01 cm^2/sec), since the rate of vibrational energy exchange between these two molecules is extremely high(25). The rate of deactivation of N_2 (v = 1) at room temperature is known to be very low(*15*). Furthermore, relaxation rates of both the upper and lower CO_2 laser levels by collisions with N_2 are much lower(*14*) than those with CO_2 (see Tables 14 and 15). For a CO,-He mixture, one can operate the laser at a higher CO, partial pressure by taking advantage of the fact that He relaxes the lower CO, laser level very effectively, especially at higher He pressure while leaving the-upper laser level population unaffected (14). Other effects of He, such as a shift in the electron energy distribution and a decrease of gas temperature in a CO, gas discharge, also are involved. In summary, the most important role played by He in a CO, laser is to remove the "bottleneck" 01^10 level which lies in the depletion path of the lower laser level population.

The dependence of optimum gain on tube bore(19,35) is shown on Fig. 19. For a flowing-gas laser amplifier the gain varies inversely as the bore, a weaker dependence is exhibited by the nonflowing gas systems. In general, the optimum gain and power output occur at a PD

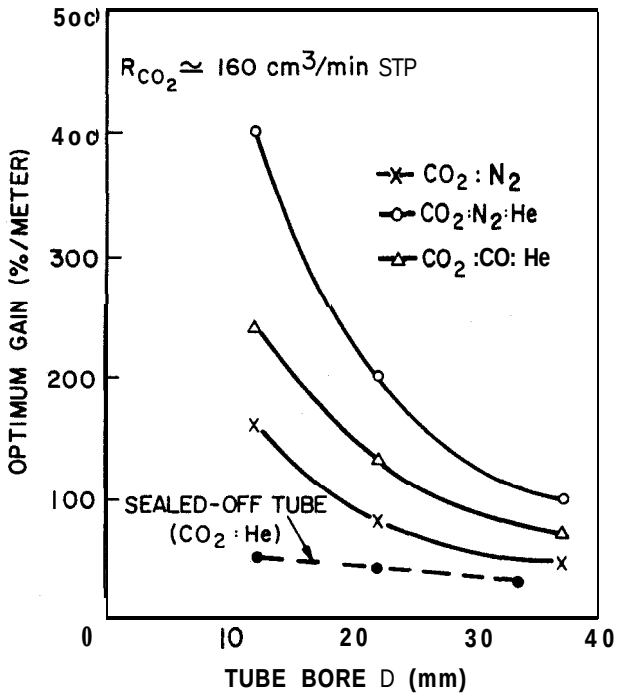

Fig. 19. Optimum gain of various flowing CO, gas media at CO, flow rate of 160 cm^3/min as a function of tube bore. The dashed curve is the maximum gain of a nonflowing laser amplifier versus tube bore.

product (19,35) of about 3 Torr-cm, where P is the CO_2 partial pressure and D is the bore of the tube. The highest gain reported for the nonflowing laser amplifier(*19*) is 1.7 dB/m from tubes with inner diameter less than 20 mm and with a CO,-He gas mixture, whereas a maximum gain of 7.8 dB/m can be obtained from a flowing CO_2–N_2–He laser amplifier(3.5) with a 12-mm bore. The radial gain profiles(*19*) across a nonflow amplifier tube diameter for CO_2, CO_2–N_2, and CO,-He are shown in Fig. 20. For CO_2 and CO_2-He discharges, the radial gain profiles have essentially the same shape with a fairly constant value near the center of the discharges and decreasing gradually toward the wall of the amplifier tube. In the case of CO_2–N_2, the flat portion of the gain extends further toward the wall. These radial gain profiles for various gas mixtures can be explained(l54) by the volume destruction of vibrationally excited CO, molecules, by the variation of the relaxation rate of the upper laser levels with gas mixtures, and by the nonuniformity of gas temperature as a function of the tube radius.

3. *Effects of Gas Flow*

The effects of gas flow on gain are shown in Fig. 21. These measurements(35) were made in water-cooled laser amplifiers with a dc

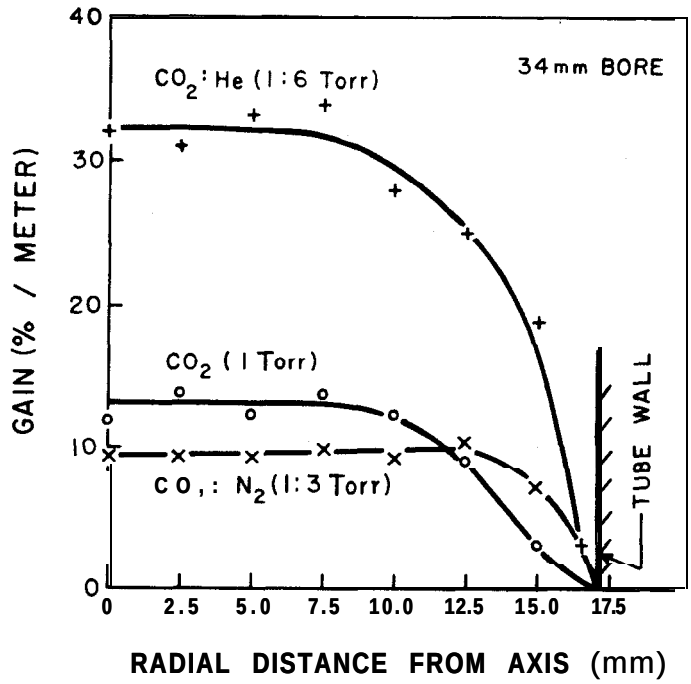

Fig. 20. Small-signal gain as a function of tube radius for CO_2, CO,-N,, and CO,-He mixtures in a 34-mm-bore amplifier.

electrical discharge and a longitudinal flow of gas mixture either from anode to cathode or vice versa. In a conventional laser with a low-speed longitudinal gas flow, the transit time of gas flow is much too long compared to the diffusion and collisional relaxation times; therefore, the gain enhancement by the gas flow in this case is owing simply to a reduction of the gas temperature by convection and by exhaustion of the hot gas at a higher temperature. This is consistent with the observation that the gain and power output of a flowing laser depend less critically on the discharge tube wall temperature. An enhancement of gain by a factor of nearly two is observed(35) merely by maintaining a continuous flow of gas through the amplifier at a very low flow rate ($\lesssim 20$ cm^3/min). A related phenomenon often observed in a freshly filled nonflow laser is that the output power increases slowly and reaches its maximum value in a time varying from a few minutes to several hundred hours depending on the gas mixture used in the discharge tube. In a sealed-off CO_2 gas discharge, a significant concentration of CO can be accumulated in the tube after a few minutes of operation(*19*). Dissociation and recombination processes continue until a quasi-equilibrium state is reached. Clearly other processes such as energy transfer(*146*) between CO and N_2 and a possible formation of complex molecules also could take place, thus making

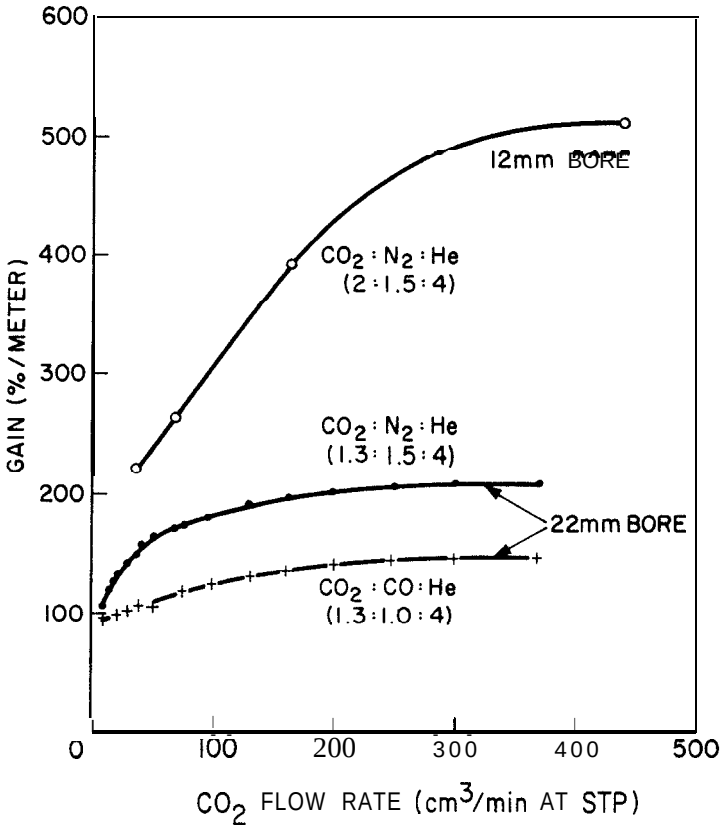

Fig. 21. Effect of gas flow on gain of CO,-N,-He and CO_2–CO–He laser amplifiers in 12- and 22-mm-bore tubes. Gas pressure and mixture ratio are near optimum in each case.

the nonflowing CO_2 laser a very complicated system to analyze. However, a continuous flow of gas at a very low rate (< 20 cm^3/min) is sufficient to remove the accumulation of CO which causes these complications in sealed-off lasers, and to produce a substantial gain enhancement by maintaining an optimum balance among various components of the gas mixture. Evidence of the accumulation of CO was obtained from the studies of spontaneous light emission of the CO angstrom band at 4835 and 5 198 Å in a CO_2 laser discharge as a function of gas flow rate. Results(*35*) shown in Fig. 22 indicate that the relative spectral intensity of CO, resulting from dissociation of CO_2, in a CO_2 gas discharge decreases rapidly to $\leq 20\%$ of that in a sealed-off CO_2 gas discharge as the CO_2 flow rate is increased from zero to about 20 cm^3/min STP. On the other hand, the relative spectral intensity of CO in a CO gas discharge is relatively insensitive to the flow rate.

The small-signal gain coefficient has also been measured(*87*) in a very high speed (500 m/sec) gas flowing laser amplifier. In this experiment a uniformly mixed CO_2–N_2–He mixture [with only the nitrogen

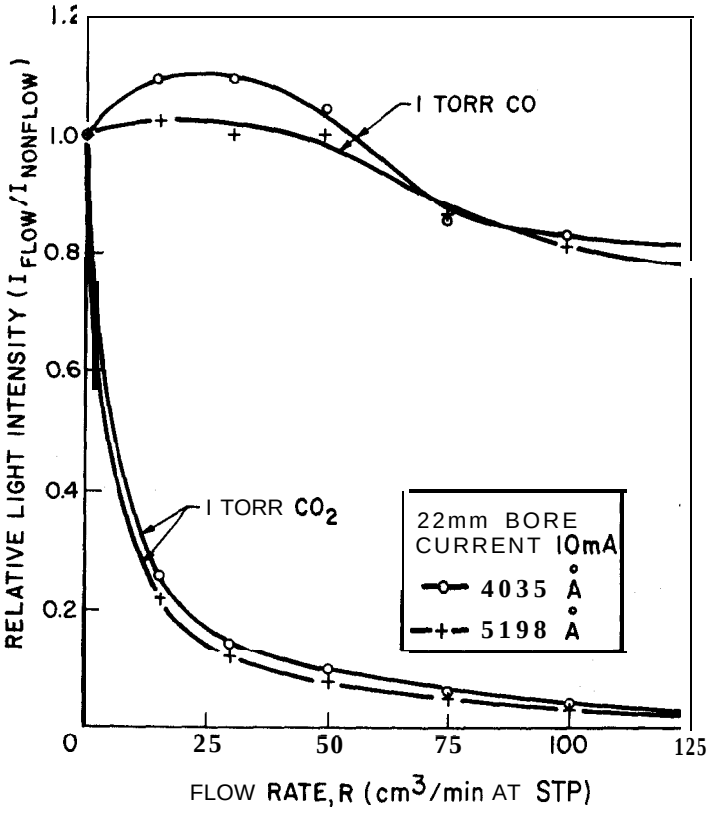

Fig. 22. Ratio of spontaneous light intensities ($I_{flow}/I_{nonflow}$) of 4835 Å and 5 198 Å. Angstrom system of CO versus flow rate for both CO, and CO gas discharges in a 22-mm-bore tube.

being excited (pumped) prior to mixing] was injected into an amplifier column with an optical axis along the direction of flow. There was no glow discharge in the column and CO, molecules were pumped entirely by the N_2 excited in a separate chamber. Because the resonant transfer time is short compared with the fluid mixing time, the optical gain reached a maximum value at a short distance ($\simeq$ 2 cm) downstream from the points of injection. For a 2.54-cm-bore amplifier tube with an active length of 18.5 cm, an average gain of 4.2 dB/m was obtained. Although the average gain value in this device was not unusually high, and was essentially limited by the development of a boundary layer downstream, the experiment demonstrated that high gain can be realized in a high-speed tranverse-flowing laser in which the gain should be independent of the length. In fact this system has been investigated recently by Targ and Tiffany(l59) who have measured the small-signal gain as well as the gain-saturation parameter (to be discussed in Section VI) in an amplifier with an optical axis transverse to the flow.

4. Gain Distribution

From Eq. (63), one can derive the gain coefficients α for $P[(J-1) \rightarrow J]$ and $R[(J+1) \rightarrow J]$ branch vibration-rotation transitions between the 1 0^00 and 00^0 1 vibrational levels. Assuming that all rotational levels are in thermal equilibrium with the translational gas temperature T, and that the linewidth is Doppler broadened, one obtains(38) the gain coefficients α_P and α_R as given by

$$\alpha_P = AJT^{-3/2}\left\{\frac{n_1B_1}{n_2B_2}\exp\left[-F_1(J-1)\frac{hc}{kT}\right]-\exp\left[-F_2(J)\frac{hc}{kT}\right]\right\} \tag{66}$$

$$\alpha_R = A(J+1)T^{-3/2}\left\{\frac{n_1B_1}{n_2B_2}\exp\left[-F_1(J+1)\frac{hc}{kT}\right]-\exp\left[-F_2(J)\frac{hc}{kT}\right]\right\} \tag{67}$$

where 1 and 2 denote the upper 00^0 1 and the lower 10^00 laser levels, respectively. The parameter A is given by

$$A = \frac{8\pi^3}{3k}\left(\frac{Mc^2}{2\pi k}\right)^{1/2} n_2B_2S_{12} \tag{68}$$

where S_{12} is the line strength of the transition in question and is related to the transition lifetime τ_r by

$$\frac{1}{\tau_r} = \frac{1}{2J_1+1}\frac{64\pi^4}{3h\lambda^3}S_{12} \tag{69}$$

From a numerical analysis for the gain distribution with J, Patel(*3*) showed that population inversion can exist among these vibration-rotation transitions even though $n_1 < n_2$ where n_1 and n_2 are total population densities in the upper 00^0 1 and the lower 10^00 laser levels, respectively. The relative population inversion for the P branch is much larger than that for the R branch. In an experiment in which the small-signal gain coefficients α_P and α_R were measured for each individual transition, Djeu et al.(*38*) have obtained the actual gain profiles as shown in Fig. 23. The total gas pressure used in the experiment was about 5 Torr (CO_2 = 0.65, N_2 = 1.4, He = 2.9 Torr) so that the gain coefficient derived for Doppler broadening is appropriate(30). These measured gain values are somewhat smaller than previously measured values(35), largely owing to the use of low gas pressures which are far below the optimum value for the tube bore used in the experiment. They provide, however, a lower bound of the ratio of population densities for the 00^0 1 and 10^00 levels in a typical CO_2–N_2–He laser with a longitudinal gas flow. The ratio n_{00^01}/n_{10^00} equals 2.27 for this laser medium in a I-in.-i.d. tube with a dc discharge current of 15 mA. Taking the measured(*29,30*) value of 4.7 ± 0.5 sec for the

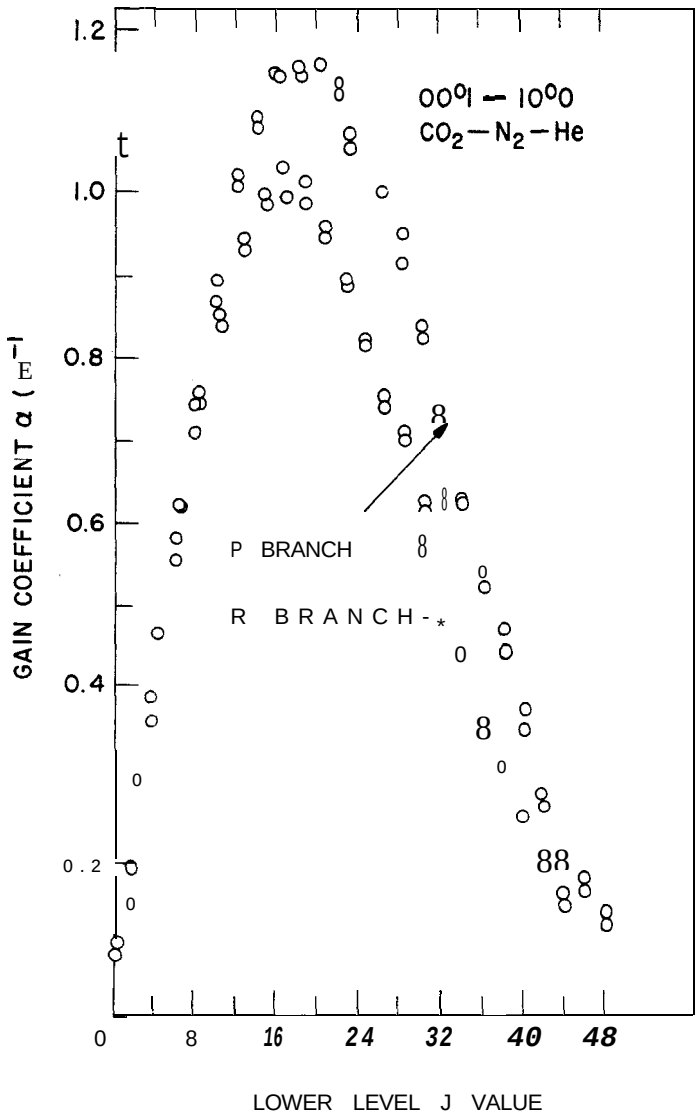

Fig. 23. Gain distribution for individual vibrational-rotational transition in the ***P*** and ***R*** branches of the 00" 1–10°0 band. Amplifier tube bore is 2.54 cm; gas mixture and flow velocity are: CO_2 (0.65 Torr), N_2 (1.4 Torr), and He (2.9 Torr); v = 192 cm/sec. [After Djeu et al. (*38*).]

spontaneous radiative lifetime of the $00^0\,1 \rightarrow 10^00$ transition, one obtains (38) the absolute population densities, in this case

$$n_{00^01} = 3.27 \times 10^{15}\ \text{cm}^{-3} \quad \text{and} \quad n_{10^00} = 1.44 \times 10^{15}\ \text{cm-3} \tag{70}$$

This corresponds to a lower bound of 17 and 8% of the total density of CO, molecules excited, respectively, into the $00^0\,1$ and 10^00 vibrational levels in a conventional flowing CO_2–N_2–He laser system.

5. Analysis -A Thermodynamic Approach

Various mechanisms leading to population inversion in the $00^0\ 1 - 1\ 0^0 0$ band have been presented in Section IV. A large amount of quantitative information on gain and its dependence on various parameters also has been presented. On the other hand, a number of theoretical analyses have been made (*22,25,42,46,154,160,161*) in the attempt to explain the gain and power characteristics of the CO, laser. Because of the large number of 'complex processes involved, an exact treatment is very difficult, and a number of assumptions must be made in order to obtain semiquantitative calculations. In general this problem can be approached by using either the usual rate equations or a thermodynamic model. Using the former approach, Moore et al. (25) have treated the problem by grouping a number of vibrational levels which are strongly coupled with the $00^0\ 1$ level into one combined upper laser level and similarly for the lower laser level. The other approach introduced by Gordietz et al. (*22,154*) is different from the usual rate equation analysis and will be discussed somewhat in detail here. This analysis has been further extended by Tulip (*160*) to include the effects of stimulated emission.

Gordietz et al. (*22,154*) have calculated the gain and population inversion of the vibrational levels in the CO_2 laser by a set of energy balance equations among various vibrational modes. In this model, a simple assumption is made that each vibrational mode can be characterized by a temperature, so that in each mode the Boltzmann distribution is established. This assumption is valid as long as the rate of exchange of the vibrational quanta within each mode is faster than excitation and transfer rates into other vibrational modes or translational motion. In this way a set of rate equations can be replaced by a reduced number of energy balance equations for the vibrational modes involved. Physical processes that are taken into account in the balance equations include (1) the electronic excitation of the N_2 ($v = 1$) and CO ($v = 1$) levels which subsequently transfer their energies to a CO_2 ($00^0\ 1$) level by the resonant exchange process and (2) the transfer of vibrational energy of CO_2 ($00^0\ 1$) to the bending mode and finally into the translational motion of molecules by collisions (for details see Section IV.B). In this analysis, effects of CO, arising from the dissociation of CO_2, on various vibrational modes of the CO_2 molecule also are emphasized. The direct transfer of the vibrational energy from ν_3 and ν_1 modes to the translational energy and both the spontaneous and stimulated processes have been ignored. The coupled energy balance equations for three vibrational modes of CO_2 and for the vibrationally

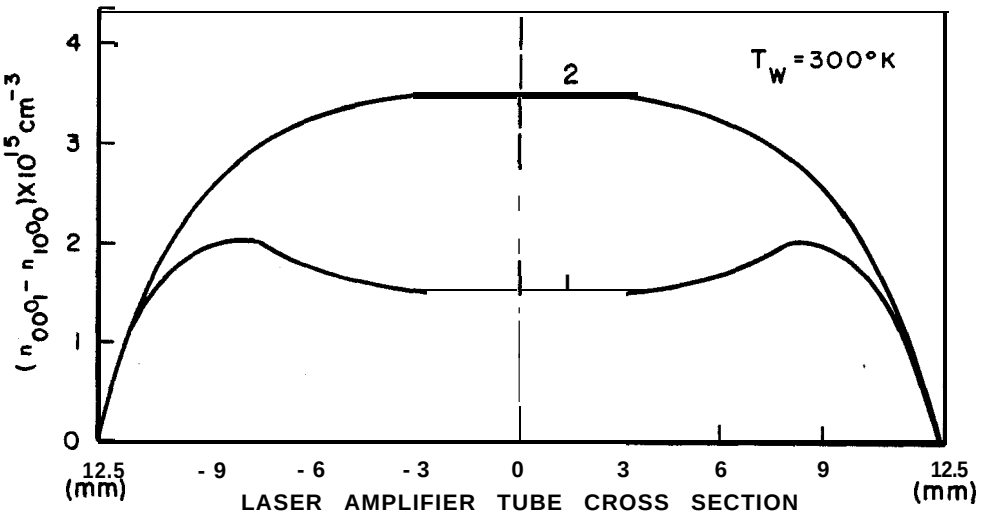

Fig. 24. The calculated radial profile of the population inversion density for (1) CO,-N, (2-2 Torr) and (2) CO,-N,-He mixture (2-2-6 Torr), for average electron density $\bar{n}_e = 6.5 \times 10^9\ cm^{-3}$. [After Gordietz et al. (*154*).]

excited N_2 and CO are too lengthy to present here. We shall simply present some of the numerical results and compare them with measured gain coefficients. Figure 24 shows the calculated (*154*) radial profiles of population inversion density for CO_2–N_2 and CO_2–N_2–He mixtures. These results are in excellent agreement with the experiments (Fig. 20). In the case of CO_2–N_2, the gain at the center of the tube can be even slightly less than that near the edge owing mainly to the high gas temperature on the axis of the discharge column. With the addition of He, the population inversion increases near the center of the tube as a result of a large (about a factor of two) reduction of gas temperature, which has a significant influence on the relaxation rates of vibrational levels (see Tables 16 and 17). Figures 25 and 26 show, respectively, the calculated current and pressure dependence on gain. These results are derived from the above theoretical model using rate constants given in Table 17 by assuming an average electron energy of 3 eV in a discharge tube of 12.5-mm bore. Again these computed values are in reasonably good agreement with experimental measurements (see Figs. 16 and 18) in that the optimum gain occurs at higher currents and high gas pressure for systems containing He. Furthermore the calculated inversion number density is of the same order of magnitude compared with the values (38) deduced from the measurements of the gain distribution profile for each individual transition as given by Eq. (70).

The inclusion of the stimulated emission term in the energy balance equations by an analysis similar to that of Gordietz et al. (154) has been

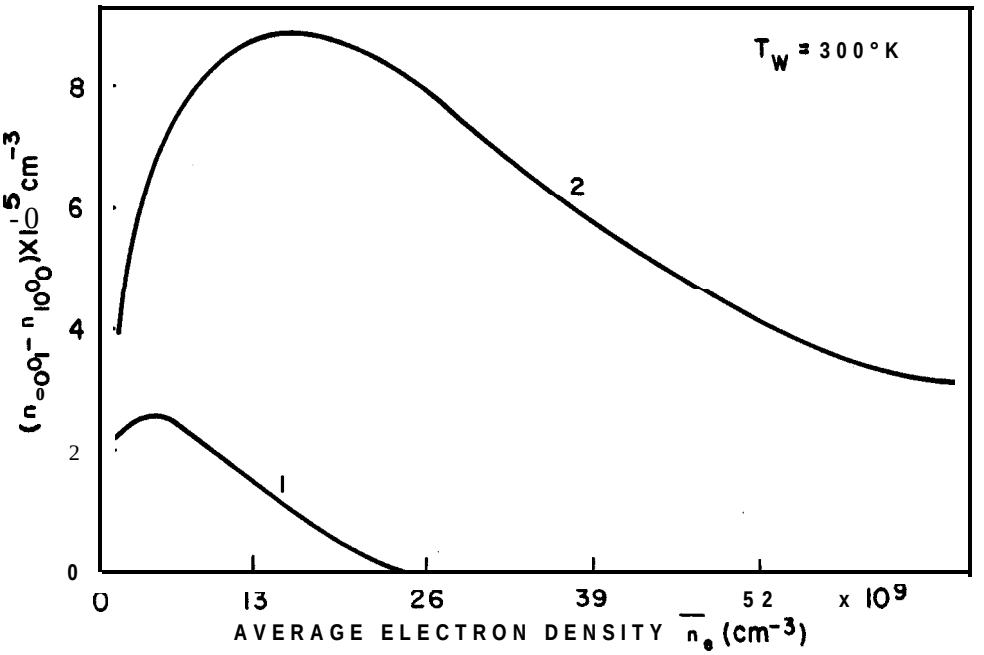

Fig. 25. The calculated population inversion density as a function of electron density for (1) CO_2–N_2 mixture (2-2 Torr) and (2) CO_2–N_2–He mixture (2-2-6 Tort-). [After Gordietz et al. (*154*).]

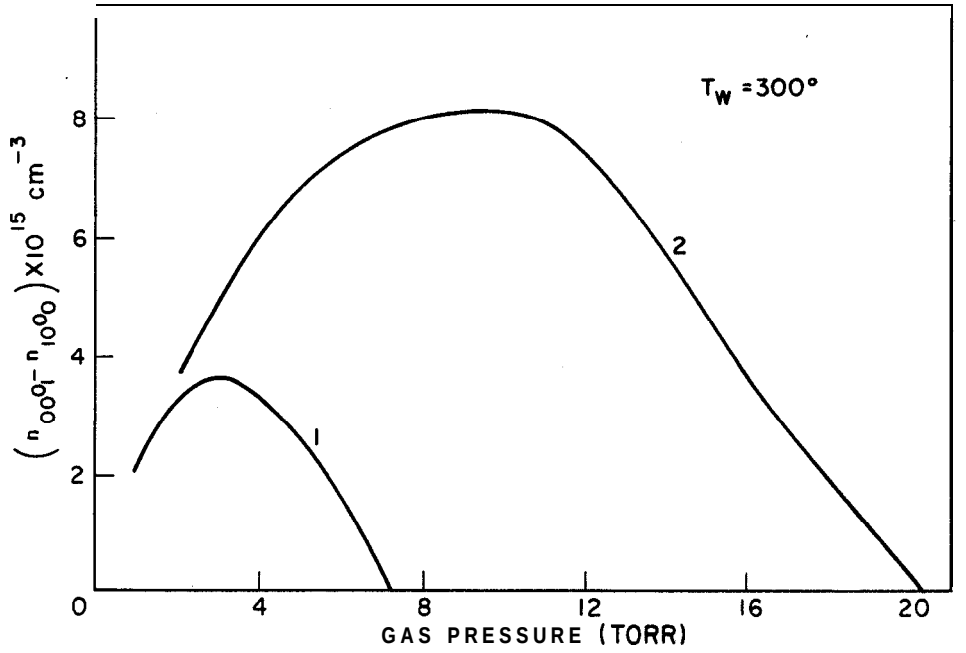

Fig. 26. The calculated population inversion density as a function of total gas pressure for (1) CO_2–N_2 mixture (I-1), A, = 6.5 x 10^9 cm^{-3}, and (2) CO_2–N_2–He mixture (I–1–3), $\bar{n}_e$ = 2.6 x 10^{10} cm^{-3}. [After Gordietz et al. (*154*).]

made recently by Tulip(*160*). In this analysis, assumptions are made to equate the vibrational temperatures of the antisymmetric ν_3 mode with the excited state of N_2 (v = 1), and those of the symmetric ν_1 and the bending ν_2 modes with the translational temperature. This in effect is equivalent to the assumption in the rate equation approach(25) of grouping a number of levels into a single laser level. Further simplifications are made by ignoring a number of relaxation and excitation, as well as dissociation and diffusion, processes. With these assumptions and approximations, the set of energy balance equations is reduced to only two equations, one of which describes the energy conservation of the ν_3 mode, E_3, and the other of the combined ν_1 and ν_2 modes, $E_1 + E_2$. They can be expressed as (160)

$$\frac{dE_3}{dt} n_0 n_e h\nu_3 X_T - \xi'(T_3, T') + \xi_3(T_2, T_3) - W h\nu \left(n_u - \frac{g_u}{g_\ell} n_\ell\right) \tag{71}$$

and

$$\frac{d}{dt}(E_1 + E_2) = \xi_2(T, T_2) - (1 - \Delta E)\xi_3(T_2, T_3) + h\nu_2 \mathscr{W}\left(n_u - \frac{g_u}{g_\ell} n_\ell\right) \tag{72}$$

In Eq. (71), the first term in the right-hand side represents electronic excitation, where-n,, and n_e are the number densities of CO, and electrons, respectively. The total excitation probability X_T of both the ν_3 mode and N_2 (v = I) is defined by $X(\nu_3) + (n_{N_2}/n_{CO_2})X(N_2)$. The second and third terms represent the rates of energy transfer from the vibrationally excited nitrogen N_2 (v = 1) characterized by a temperature T' to $CO_2(\nu_3)$ and from $CO_2(\nu_3)$ to $CO_2(\nu_2)$ levels, respectively. The functional form of $\xi_i(T_j, T_i)$ is (161)

$$\xi_i(T_j, T_i) = \frac{1}{\tau_{ij}}[E_i(T_j) - E_i] \tag{73}$$

where $1/\tau_{ij}$ is the transfer rate at a given gas pressure, and

$$E_i(T_j) = \frac{n_0 h\nu_i}{\left[\exp\left(\frac{h\nu_i}{kT_j}\right) - 1\right]} \tag{74}$$

The last term in the right-hand side of Eq. (71) is the stimulated emission rate, in which $\mathscr{W}$ is given by Eq. (62). In Eq. (72), $\Delta E \equiv h\nu_3 - (h\nu_1 + h\nu_2)$, and other symbols have their usual meanings. In the steady state condition that dE_i/dt = 0, solutions for Eqs. (71) and (72) have been obtained numerically (160). By using the measured vibrational lifetimes(*24*) of the upper ($\tau_u = 4 \times 10^{-3}$ sec) and lower ($\tau_\ell = 2 \times 10^{-4}$

sec) laser levels and by assuming a line-center value(*30*) $g(\nu_0)$ = 6.3 x 10^{-9} which corresponds to a collisional linewidth of 75 MHz and a Doppler width of 50 MHz, this analysis has led to some interesting results on gain saturation, which will be discussed in detail in the next section. The calculated(*160*) small-signal gain coefficient is 4.8 dB/m at an optimum excitation ($n_e X_T$ = 200) corresponding to an electron density of 4 x 10^9 cm^3. This result and the calculated(160) gain-vs.-excitation currents (data are not included here) are in good agreement with the measured values (Fig. 16), suggesting that this thermodynamic description of vibrational thermal equilibrium in the CO_2 laser is valid even in the presence of a high stimulated emission rate.

B. GAIN SATURATION

One of the interesting characteristics of the CO_2 laser is the extremely high gain saturation parameter which is the basic requirement for a powerful laser system. In the early studies of gain characteristics, Cheo and Cooper(19) observed that the gain remains unsaturated over a 30-dB input power range from a few milliwatts to several watts for a beam cross section ~ 6 mm diam. Subsequently a number of investigators(40,42) have reported values of the gain saturation parameter ranging from 22 to 100 W/cm^2. Recent work(*159*) on a transverse gas flow amplifier yielded a value as high as 250 W/cm^2. Clearly the gain saturation of a CO_2 laser is not unique and depends much on operating conditions of the laser. Work by Tulip(*160*) showed that the gain saturation parameter increases with increasing excitation rate. Another detailed study(42) of the effects of diffusion showed that the gain saturation of a sealed-off CO_2 laser amplifier decreases monotonically from 97 to 25 W/cm^2 as the average input beam radius increases from 0.9 to 2.5 mm in an 18-mm-bore amplifier tube with electrical discharges.

1. A Two-Level Model

According to Eq. (60), a small input signal, of intensity I,,. propagating through an amplifier with an unsaturated gain coefficient α_0, will be amplified according to the expression

$$I = I_0 \exp(\alpha_0 L) \tag{75}$$

where ***L*** is the length of the gain medium. However, the growth of radiation is limited by saturation of the medium. Gain saturation as a

function of radiation intensity I has been analyzed(l62) for both homogeneously and inhomogeneously broadened media. In the homogeneous case, the gain coefficient α at the line center decreases with increasing I according to the relation

$$\alpha = \frac{\alpha_0}{(1 + I/I_s)} \tag{76}$$

whereas for inhomogeneous broadening,

$$\alpha = \frac{\alpha_0}{(1 + I/I_s)^{1/2}} \tag{77}$$

where α_0 is the small-signal gain and I_s the saturation parameter, which is defined by that value at which α reduces to one-half of the α_0 value. In terms of the relaxation rates of a two-level system, I_s at the center of the Lorentzian line is (162)

$$I_s = 8\pi^2 h\nu\Delta\nu\tau_r \Big/ \lambda^2\left[k_u^{-1} + \frac{g_u}{g_\ell} k_\ell^{-1}\right] \tag{78}$$

where τ_r, is the radiative lifetime of the 001 $\rightarrow$ 100 transition, k_u and k_ℓ are the relaxation rates of the upper and the lower CO, laser levels, $\Delta\nu$ is the Lorentzian half-width of the transition, A is the wavelength, and g_u and g_ℓ are the degeneracies of the two levels. Since $k_u \ll k_\ell$ (g_ℓ/g_u), Eq. (78) can be approximated by

$$I_s = \frac{8\pi^2 h\nu\Delta\nu\tau_r}{\lambda^2} k_u \tag{79}$$

A comparison of Eq. (79) with the induced transition rate $\mathscr{W}$ as given by Eq. (62) shows that saturation occurs when the rate of induced transition becomes comparable to the relaxation rate of the upper laser level. The induced transitions depopulate the upper laser level population at a rate which is eventually limited by the relaxation processes in the medium. Therefore, the saturation parameter can be enhanced by increasing the relaxation or the induced transition rate and consequently the small-signal gain coefficient is reduced. This, at first, seems surprising, but the paradox is explained when one considers that the criterion for a laser system to reach saturation is for the rate of excitation to the upper laser level to be as fast as the stimulated emission rate from the excited state. By substituting values τ_r = 5 sec, τ_u = 1 msec, and $\Delta\nu$ = 50 MHz into Eq. (79) one obtains a saturation parameter of $\simeq$ 0.3 W/cm², which is about two orders of magnitude smaller than the measured values. Christensen et al.(*42*) pointed out that the main source of discrepancy between the theory and experiment is the fact

that the CO, laser is a multilevel system with both homogeneous and inhomogeneous broadening. We shall disregard for the moment a large variation of the measured saturation parameter reported by a number of workers, ranging from 22 to 2.50 W/cm^2. To reconcile this discrepancy one must replace the relaxation rate of the upper laser level k_u in Eq. (79) by the weighted relaxation rates $\left(\Sigma_i^m n_i k_i\right)/n_u$ of all the other closely coupled levels to the upper laser level. As discussed in the next section, this, in effect, will increase the relaxation rate k_u by m approximately a factor of which is the number of strongly coupled levels within the 00^0 1 band, or the number of ways that the molecule can rapidly leave the lasing level into other tightly coupled levels, each of which can relax at the rate k_i. This modification has brought the theory in closer agreement with experiments.

2. Multilevel System

Since CO, laser levels involve a large number of strongly coupled rotational levels via collisions, it is apparent that a multilevel description is called for, especially when operating conditions are such that level competition is involved. As pointed out above, a theory based on the description of a simple two-level model for a CO, laser system cannot adequately account for the gain saturation in a CO, laser amplifier. Here we shall present a summary of the analysis for a multilevel system, treated by Christensen et al. (*42*). In their treatment, assumptions were made that the laser action occurs only between one upper and one lower rotational level, each of which is coupled strongly with a set of m rotational levels, and that the lasing levels are homogeneously broadened. The rate equations for this system are of the form,

$$\frac{dn_J^u}{dt} = -k_J^u n_J^u - \sum_i K_{iJ}^u + \sum_i K_{Ji}^u n_i^u - \mathscr{W}\left(n_J^u - \frac{g_u}{g_\ell} n_{J'}^\ell\right) + \Gamma_J^u$$

$$\frac{dn_{J'}^\ell}{dt} = -k_{J'}^\ell n_{J'}^\ell - \sum_i K_{iJ'}^\ell + \sum_i K_{J'i}^\ell n_i^\ell + \mathscr{W}\left(n_J^u - \frac{g_u}{g_\ell} n_{J'}^\ell\right) + \Gamma_{J'}^\ell \qquad (80)$$

$$\frac{dn_j}{dt} = -k_j n_j - \sum_i K_{ij} n_j + \sum_i K_{ji} n_i + \Gamma_j \qquad (j \text{ represents all other rotational levels})$$

where k_J^u and $k_{J'}^\ell$ are the relaxation rates of the upper and lower laser levels; K_{iJ}^u and $K_{iJ'}^\ell$ are the relaxation rates among the upper and lower levels; n_j's are the population densities of the remaining rotational levels in either the upper or lower vibrational states; Γ_j represents the pump-

ing rate from ground to the jth level; and $\mathscr{W}$ is the induced transition rate as given by Eq. (62).

In the steady state condition, all the time derivatives are equal to zero. Equation (SO) reduces to a set of algebraic equations which can be solved for n_J^{u} and $n_{J'}^{\ell}$ in terms of rate constants and for $\mathscr{W}(I)$ by means of Cramer's rule. These solutions combined with Eq. (63) yield the gain coefficient as a function of radiation intensity I in a form similar to that of a two-level system, but the expression contains terms involving k_{u}'s and K_{ij}'s in a very complicated way. We shall not go into detail here. In the assumption that the coupling among the rotational levels is very strong compared with the vibrational relaxation rate, $k_j \ll K_{ij}$, one obtains a simplified expression (42) for the saturation parameter I, for a homogeneously broadened medium:

$$I_{\mathrm{s}} = 8\pi\tau_{\mathrm{r}} h\nu / g(\nu)\lambda^2 \left[n_J^{\mathrm{u}} \Big/ \sum_i k_i^{\mathrm{u}} n_i^{\mathrm{u}} + g_{\mathrm{u}} n_{J'}^{\ell} \Big/ g_{\ell} \sum_i k_i^{\ell} n_i^{\ell} \right]_I \qquad (81)$$

By comparing Eqs. (81) and (78), it may be noted that the behavior of the gain saturation parameter I, of a multilevel system is similar to that of a two-level system if one replaces the terms in Eq. (8 1) by

$$\frac{1}{n_J^{\mathrm{u}}} \sum_i^m k_i^{\mathrm{u}} n_i^{\mathrm{u}} = k_{\mathrm{u}}^{\mathrm{eff}} \qquad \text{and} \qquad \frac{1}{n_{J'}^{\ell}} \sum_i^m k_i^{\ell} n_i^{\ell} = k_{\ell}^{\mathrm{eff}} \qquad (82)$$

If all k_i's and n_i's are assumed to be equal, then $k^{\mathrm{eff}} = mk$, where m is the number of coupled levels in either the upper or the lower vibrational states. To bring the theory closer to experiment, a total of 50 levels must be actively involved in competing for population in a CO, laser. Actually n_i is a function of J and gas temperature as given by Eq. (9), therefore Eqs. (82) can be rewritten as

$$k_{\mathrm{u}}^{\mathrm{eff}} = k_{\mathrm{u}} \frac{kT}{2hc} \frac{\sum_i^m \exp(-h\nu_i/kTB_i)}{(2J+1)\exp[-BJ(J+1)hc/kT]} \qquad (83)$$

Again the assumption was made that all k's are equal. These relaxation rates are collisional in nature when diffusion is negligible, but become enhanced if the particles can diffuse into and out of the beam within a time comparable to the inverse collision relaxation rates. Effects of diffusion will be discussed in detail below. Based on collision effects alone, particles can leave the lasing level and move either into all the levels not explicitly included in the rate equations (80), directly at a rate k_{u}, or by a cross relaxation into any one of the m levels which subsequently relax to the lower vibration state at the rate k_{r}. Therefore a

particle has m effective ways of leaving the system of upper levels with an effective relaxation rate k_u^{eff} approximately equal to mk_u. This causes an increase in the saturation parameter. As pointed out before, the increased power density obtainable from such a system is achieved because the rate at which excitation of CO_2 molecules into the upper level also is increased accordingly.

3. *Effects of Excitation and Diffusion*

The measured values of the gain saturation I, reported by a number of investigators (*40–42,159,160*) vary over a wide range. The parameters which have the greatest effect on I_s are the excitation currents and the laser beam cross section. Figure 27 shows both the theoretical and measured results for I, as a function of the excitation parameter (discharge currents). The measurements were made (*1* 60) in a laser amplifier tube of 6-cm bore with a flowing CO_2-N_2-He gas (1 : 2: 3 Torr), excited by a dc electrical discharge. The laser beam, passed along the

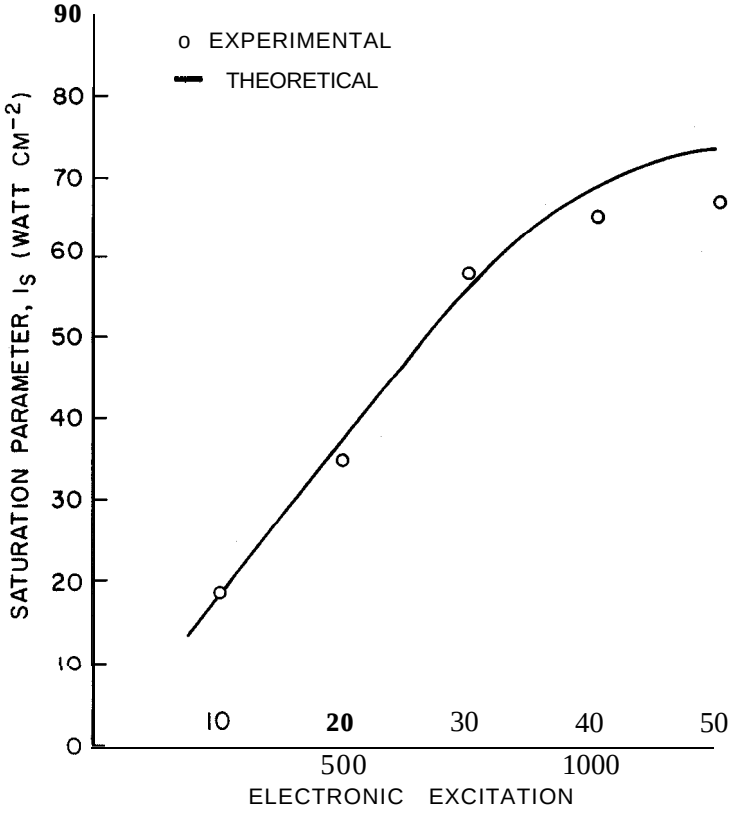

Fig. 27. The measured and calculated gain saturation parameter I_s as a function of excitation. The upper scale of the abscissa is the discharge currents in mA and the lower scale of the abscissa is the excitation parameter $n_e X_T$. [After Tulip (*160*).]

axis of this tube, had a Gaussian profile with radius of 3.9 mm at $1/e$ of maximum intensity. Detectors with l-mm aperture size were placed in the near field of the oscillator. The curve in Fig. 27 represents the theoretical results using the thermodynamic approach (*160*). At low excitation current, the gain of the amplifier obeys a homogeneous saturation function as described by Eq. (76). At high excitation levels ($n_e X \sim 1000$ or currents > 50 mA), theory and experiment begin to deviate, indicating that the theory based on thermal equilibrium may not be valid under these circumstances. Figure 28 shows both the theoretical and experimental results (*42*) of I_s as a function of average beam radius r_0 of the laser input to the amplifier. In this case the measurements were made in a laser amplifier with i.d. of I .8 cm and 70 cm of active length. The amplifier was filled with a sealed-off mixture of CO_2–N_2–He–H_2 (1.4 : 1.7 : 7.0: 0.2 Torr) and dc excited at a constant

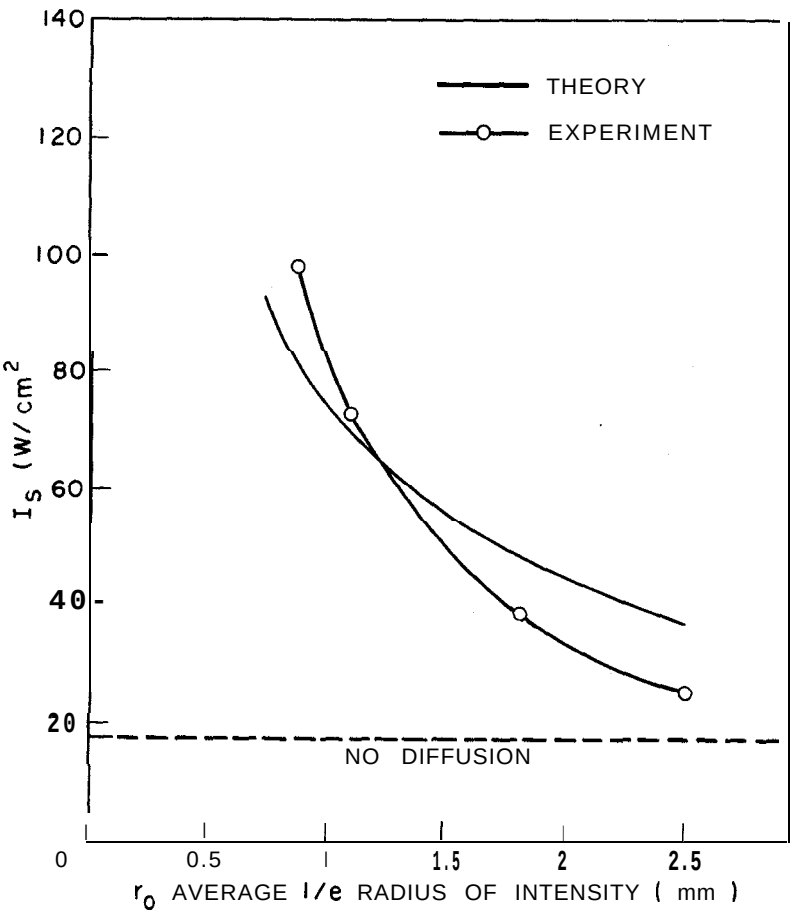

Fig. 28. The measured and calculated gain saturation parameter I_s as a function of average beam radius r_0. A multilevel system (for $n = 35$. $\Delta\nu = 43$ MHz) is assumed. [After Christensen et al. (*42*).]

discharge current of 26 mA for all the measurements. The measured saturation parameter varied from 2.5 to 97 W/cm² for four different average beam radii r_0 between 0.9 and 2.5 mm (measured to the l/e value of the intensity). The theoretical results in Fig. 28 were obtained (42) by inclusion in the rate equations (80) of a term $\mathscr{D}'\nabla^2 n_J$, where $\mathscr{D}'$ is defined heuristically by the same analogy as that of Eq. (82), namely

$$\mathscr{D}_u' = \frac{\mathscr{D}}{n_u} \sum_i n_i^u, \quad \text{etc.} \tag{84}$$

where $\mathscr{D}$ is the diffusion coefficient of the excited CO_2 molecules. In this way, a set of coupled equations including diffusion effects can be reduced to two equations similar to a simple two-level system,

$$\mathscr{D}'\nabla^2 n_u - k_u^{\text{eff}} n_u - \mathscr{W}\left(n_u - \frac{g_u}{g_\ell} n_\ell\right) = -\Gamma_u$$

and (85)

$$\mathscr{D}'\nabla^2 n_\ell - k_\ell^{\text{eff}} n_\ell + \mathscr{W}\left(n_u - \frac{g_u}{g_\ell} n_\ell\right) = -\Gamma_\ell$$

An analytic solution of Eqs. (85) for the input beam of a uniform intensity profile has been obtained(42) as a function of r_0 and results are plotted in Fig. 28 along with the measurements. Only qualitative agreement was found between theory and experiment, primarily owing to assumptions introduced in order to simplify the calculation. It should be pointed out that the actual beam intensity in a laser is Gaussian in the case of the TEM_{00} mode: however, solutions of Eqs. (85) for a Gaussian beam is quite difficult. Other work(*163*) on beam distortion caused by gain saturation is available in the literature.

From these results, it is clear that excitation and diffusion play an important role in determining gain saturation in a CO_2 laser. The depletion rate of the upper laser level population is proportional to the stimulated emission rate but is inversely proportional to the excitation rate. At a fixed excitation rate, the laser field depletes the upper laser level population and causes an excess population in the lower level. The excited CO_2 molecules from outside the beam region diffuse into the space occupied by the laser beam, and molecules in the lower laser level diffuse out of the interaction region. Diffusion effects become more significant when the diffusion rate of molecules is comparable to the relaxation rate of each of these coupled levels. Within the relaxation time τ_u (- 1 msec), the excited and deexcited CO_2 molecules can traverse optical beams of the order of a few millimeters in radius. Therefore it is easy to understand why the gain saturation parameter increases with decreasing beam size as shown in Fig. 28.

C. OTHER CHARACTERISTICS-ANOMALOUS AND NONLINEAR PHENOMENA

1. Linewidth and Lineshape

From absorption(29,30) and transmission (129, 130) measurements, one infers a much wider oscillation linewidth as a result of collisional broadening in a CO_2 laser (typically operating at a gas pressure above 5 Torr) than the usual Doppler width owing to merely the thermal motion of the gas molecules (- 60 MHz at a gas temperature of 400" K). A direct measurement(31) of the linewidth has been made in a laser amplifier by careful examination of the time response of the gain to a fast-rise step-input pulse. The homogeneous linewidth of this laser can be deduced also from the measurements of the depth of Lamb dip as a function of gas pressure. The former gives a direct measure of the homogeneous relaxation time T_2 and hence the bandwidth of the laser amplifier; the latter yields information not only on the linewidth, but also on the lineshape function g(v) and on level competition between adjacent rotational transitions. In the following discussion we shall present experimental measurements on the linewidth and lineshape of the CO_2 laser and point out some interesting aspects of Lamb-dip spectroscopy.

Direct linewidth measurements were made(31) by analyzing the time response of the amplifier gain for a step pulse with subnanosecond risetime. Figure 29 shows the oscilloscope traces of both the step input (top trace) and the gain response (bottom trace) of a multipath CO_2 laser amplifier. It may be noted that the shape of the gain pulse is considerably distorted owing to the limitation of the finite bandwidth of the amplifying medium. For an impulse function U_0, the electric field response of the amplifier $\mathscr{E}(t, z)$ with a homogeneously broadened line at the line center is (31)

$$\mathscr{E}(t,z) = U_0 + \frac{}{c}\left(\frac{Az}{ct-z}\right)^{1/2} I_1\left[2\left(\frac{Az}{c}\right)^{1/2}\left(\frac{t-z}{c}\right)^{1/2}\right] \times \exp\left[-\frac{\left(\frac{t-z}{c}\right)}{T_2}\right] \qquad t > \frac{z}{c} \tag{86}$$

$$\mathscr{E}(t,z) = 0 \qquad t < \frac{z}{c}$$

where A = $\alpha_0 c/2T_2$, α_0 is the small-signal gain coefficient, and I_1 the modified Bessel function of the first kind. The step response $G(t, z)$

can be obtained by squaring $\mathscr{E}(t, z)$ as described by Eq. (86), and integrating over the time period $0 \leqslant \tau \leqslant t$, as

$$G(t, z) = \left| \int_0^t \mathscr{E}(t-\tau, z)\, d\tau \right|^2 \tag{87}$$

Figure 30 shows some typical plots of the step response function $G(t, z)$ obtained by computer evaluation for a fixed gain coefficient

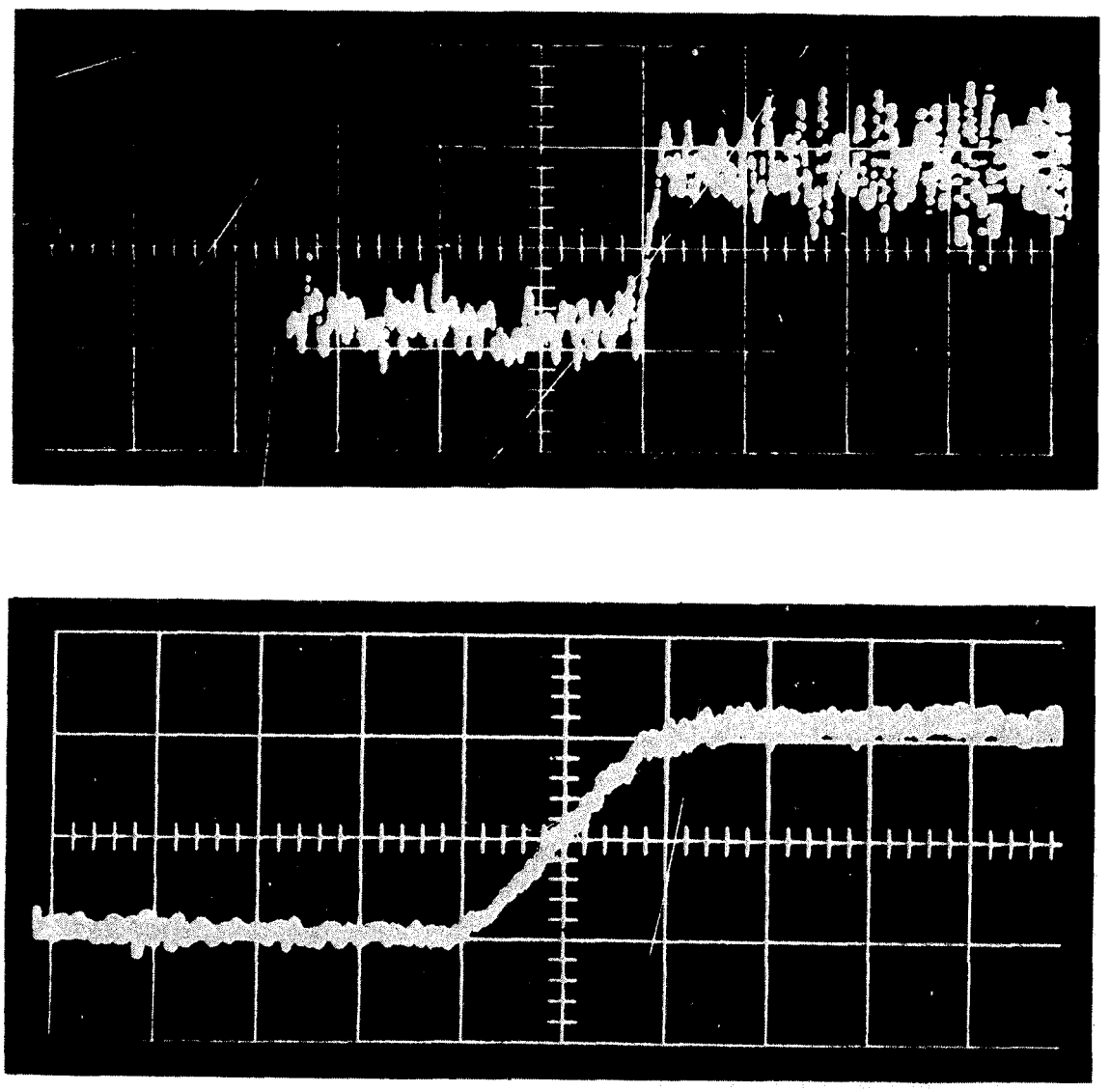

Fig. 29. Oscilloscope traces of time response of laser amplifier. Top trace shows the input signal with amplifier discharge off; bottom trace with discharge on horizontal scale 10 nsec cm. Vertical scales for the two traces are different. [After Bridges et al. (*31*).]

$\alpha_0 \simeq 4$ dB/m, but for three different T_2 values. Experimentally, for a given gas pressure, the measured result yields one net linewidth. A number of measurements were made at different amplifier gas pressures but with a constant mixing ratio of the three gases (CO_2-N_2-He). The measured gain values were fitted to the theoretical curves for a homogeneously broadened line from which one can infer a value of T_2.

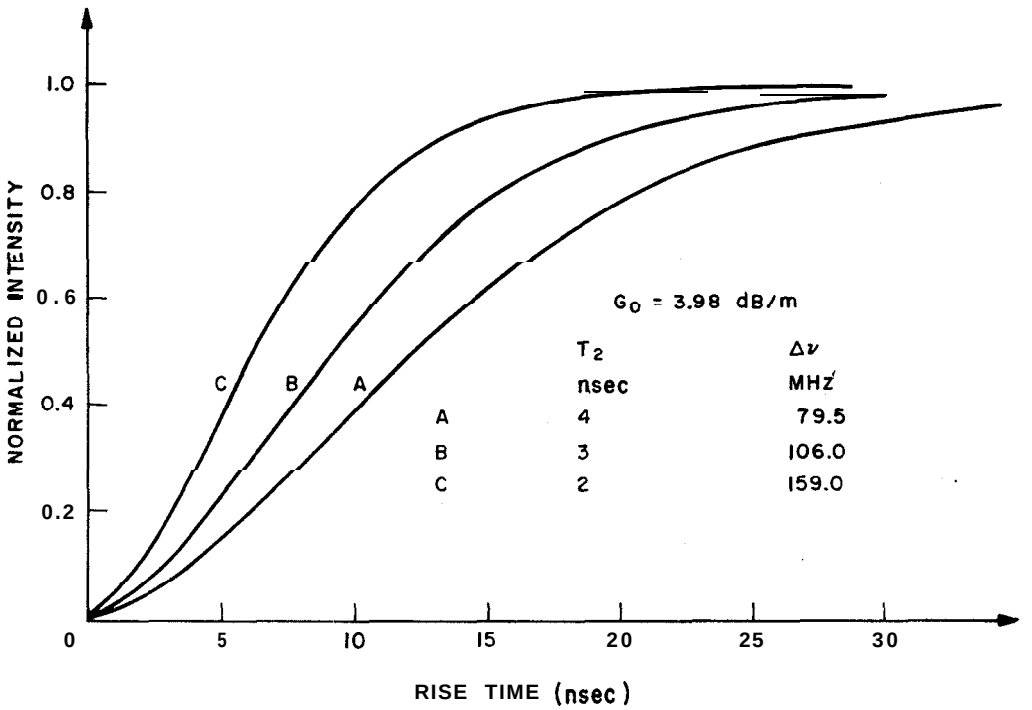

Fig. 30. The calculated step response for amplifying media with different bandwidths. [After Bridges et al. (*31*).]

Figure 31 shows a plot of the linewidth as a function of total gas pressure. The error bars indicate the uncertainty in the experimental values. The best straight line is drawn through the error bars and yields an intercepting value, 59 MHz at zero pressure, corresponding to the Doppler linewidth for a temperature of 372°K. The slope of this linear plot yields a collisional broadening of 4.67 MHz/Torr as compared with the absorption measurements(30) of 4.25 MHz/Torr for T = 372°K. The total bandwidth of a CO_2 laser under an optimum operating condition (P $\gtrsim$ IO Torr) is $\gtrsim$ 100 MHz, which is about twice that of the Doppler width, therefore the CO, laser lines are essentially homogeneous owing to many collisions of CO_2 (00^0 1) with other species during its lifetime.

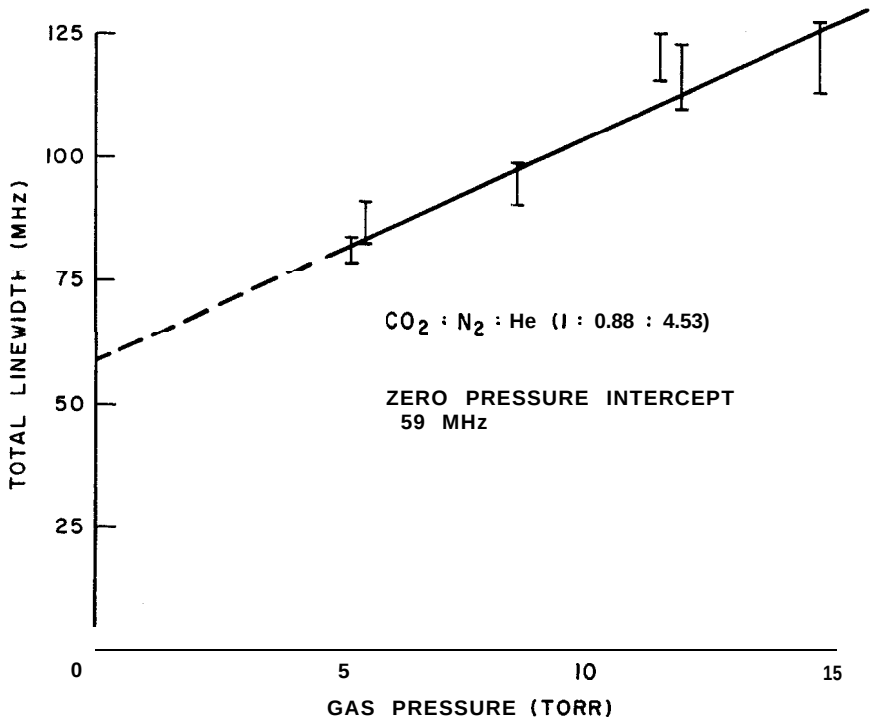

Fig. 31. The measured linewidths of a CO, laser amplifier as a function of gas pressure. The uncertainty in the experimental values is indicated by the error bars. [After Bridges et al. (*31*).]

Collision effects on gain saturation characteristics of the CO_2 laser have been studied (*164*) in a passive absorption cell inside the laser cavity. More recently the investigation of saturation characteristics in complex molecular systems, such as PF, and SF_6 gases, at CO_2 laser frequencies has led to the achievement of extremely high frequency stabilization for the laser (*165*,*166*). The advantage of using a passive cell instead of the usual method, frequency scanning over the linewidth of the oscillator, is that one can investigate the collisional effects over a much wider range of gas pressures. The effects of homogeneous broadening on gain are shown in Fig. 32. The dashed curve shows the gain profile of an inhomogeneously broadened line. It should be noted that collision broadening reduces the peak of the unsaturated gain but increases the linewidth, therefore the homogeneously broadened medium is a lossier system than the inhomogeneous case. When an intense field interacts with an inhomogeneously broadened line, "hole burning" occurs in the contour at the line center, reflecting the depletion of the upper laser level population by stimulated emission. In the case of a homogeneously broadened line, collisions tends to smooth out the hole-burning effect in the velocity distribution of the molecules. If the collision time $\tau_c \ll \tau_u$ which is the case

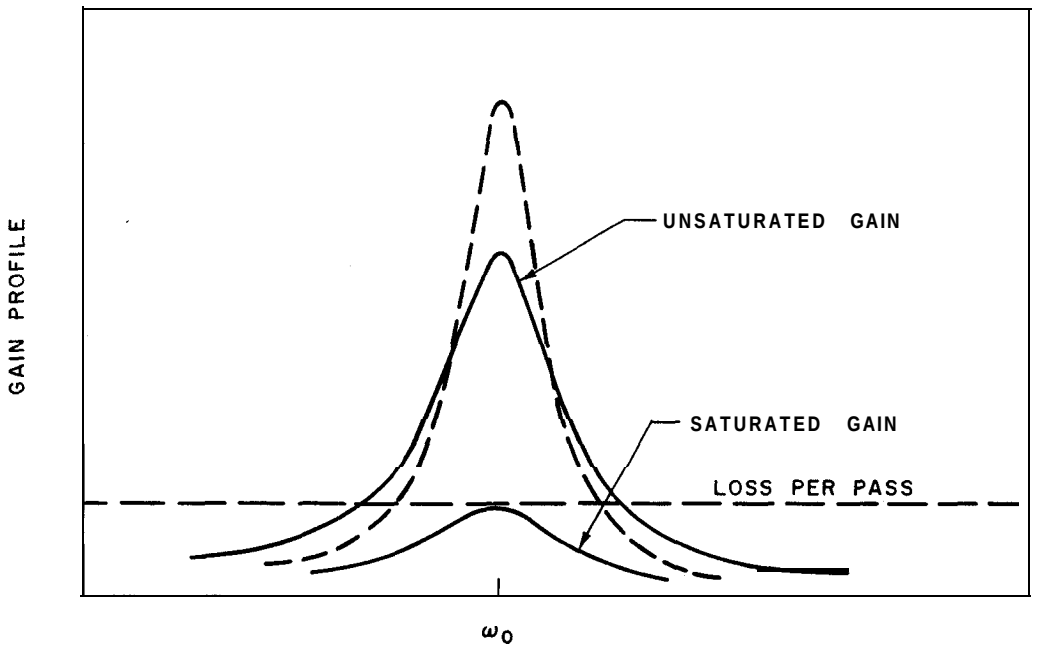

Fig. 32. Effects of homogeneous broadening on gain. Dashed curve represents the gain profile of an inhomogeneously broadened line.

in the CO_2 laser, washing out of the hole occurs, resulting in uniform reduction of the gain profile. Total saturation of the system is reached when gain is reduced below the total loss of the system.

At low gas pressure, the "Lamb dip" or hole burning has been observed(*32*,*167*) in the power tuning curve by a frequency sweep of the cavity with a piezoelectric ceramic transducer. For these experiments, the CO_2 laser must be constructed with a high degree of frequency and gain stability. Also a dispersive element such as a prism or a grating is required to eliminate the competition effects between tightly coupled rotational levels. Otherwise, these effects can cause complications in the interpretation of the results. Studies of the relative depth of the central tuning dip have been made(32) as a function of excitation current or gas pressure. Figure 33 shows the lineshape of the output of a P(22) 10.6-p CO_2 laser as a function of the cavity length. It may be noted that the relative depth of the central tuning dip increases with increasing excitation at a fixed gas pressure, consistent with the Lamb theory(l68). The depth of the dip was found(32) to decrease with increasing pressure. For pressures higher than 1 Torr the profile tends to be flattened. The pressure dependence of the intensity profile can be described by the expression given by Szöke and Javan (*169*),

$$I \propto \frac{G_0 - L \exp(\omega - \omega_0)^2/2\Delta\omega^2}{1 + \Delta\Delta'[\Delta'^2 + (\omega - \omega_0)^2]^{-1}} \tag{88}$$

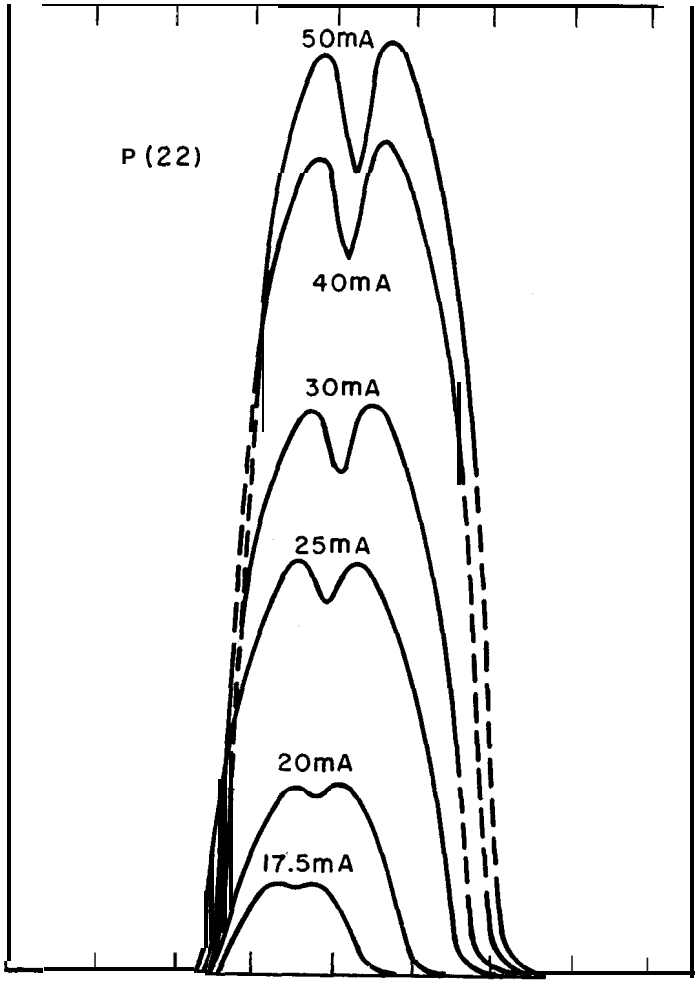

Fig. 33. Gain profile of the $P(22)$ 10.6-μ CO, laser line at different discharge currents. [After Bordé and Henry (*32*).]

where G_0 is the gain at the center of the Doppler line in absence of stimulated emission, L is the total loss per unit length, ω_0 is the frequency of the line center, ω is the oscillation frequency, A and A' are the "hard" and "soft collision" linewidth (*170*), and $\Delta\omega$ is the full width at half the maximum intensity. By fitting the measured profiles with Eq. (88), Bordé and Henry(32) obtained a plot of A and A' as a function of the total gas pressure, as shown in Fig. 34. From these results, one obtains a collision-broadening linewidth $\sim$ 5 MHz/Torr, which is in reasonabie agreement with the measurements by others(30,31) who used entirely different methods.

Other interesting aspects involving the use of the Lamb dip are: (i) the studies of rotational competition effects resulting in asymmetric gain profiles when two or more vibration-rotation lines are allowed to

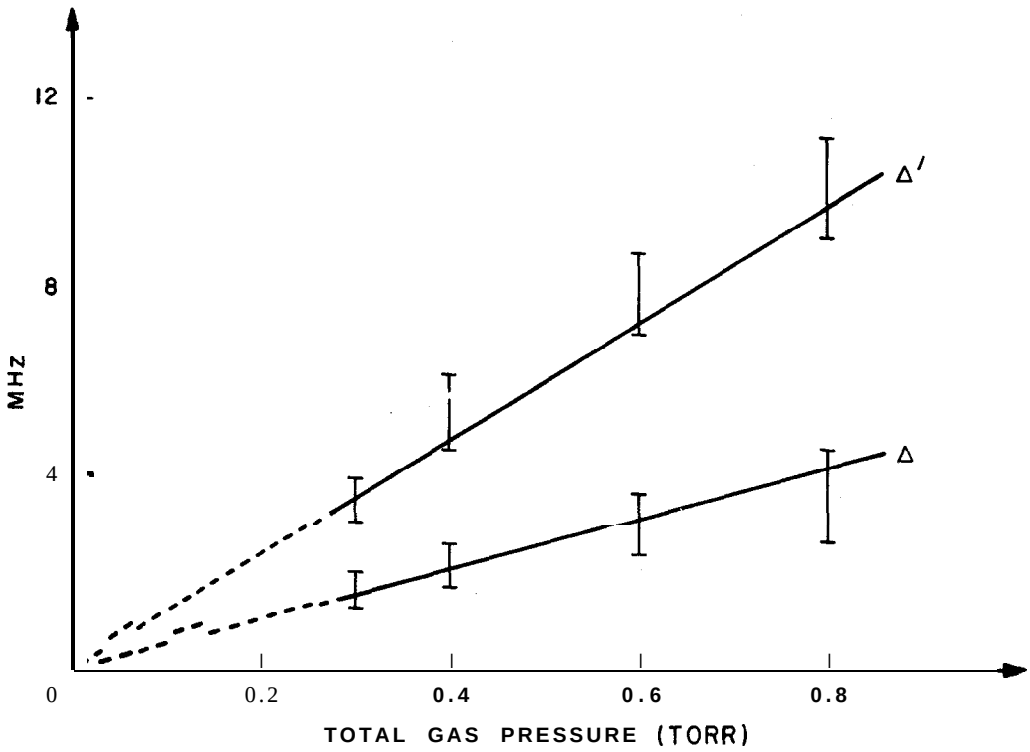

Fig. 34. The measured "hard" A and "soft" A' linewidths versus gas pressure for P(22) 10.6 μ CO, laser. [After Bordé and Henry (*32*).]

oscillate simultaneously, and (ii) the stabilization of the laser at the center of the dip by means of standard feedback techniques.

2. Rotational Level and Mode Competition

Previously we pointed out that rotational level competition plays an important role in the generation of high CW and Q-switched laser output in a single transition or in obtaining a high-gain saturation parameter in a CO_2 laser. Because of the strong collisional coupling responsible for the mixing of rotational levels, a small change in cavity length of a small CO_2 laser, whose cavity mode spacing is large compared to the linewidth, can cause the single-frequency oscillation to switch from one rotation level to another over a certain frequency interval. Level competition effects have been investigated in both stabilized standing-wave (*32*,*33*) and traveling-wave(33) lasers and in laser amplifiers (*26*,*27*) (see Section IV.B.5).

When two lines are oscillating simultaneously in a stabilized laser, a push-pull effect is evident from the central tuning curves of the two lines when their centers are swept simultaneously (Fig. 35). The profile

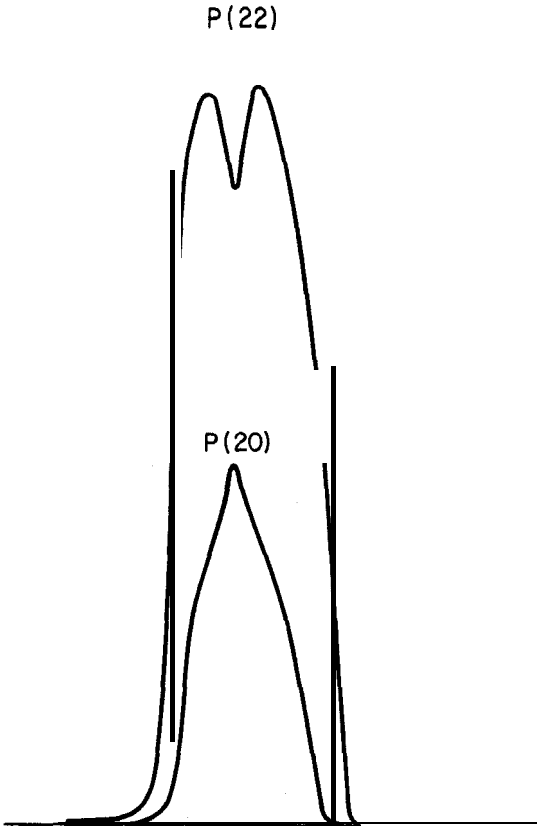

Fig. 35. Gain profile of the $P(20)$ and $P(22)$ 10.6-μ CO, laser lines when centers of the two lines are scanned simultaneously. [After Bordé and Henry (*32*).]

of the lower gain line, $P(20)$, shows only a sharp symmetric peak whereas the higher gain line, $P(22)$, shows a larger dip. Under high pressure, the dip in the P(22) line profile normally would not be so distinct in the absence of strong level competition. Oscillation can occur on a number of lines simultaneously only at low pressure. The rotational relaxation rate increases proportionally with pressure-and causes strong mixing among the levels so that eventually, at high pressures, only one line can oscillate at a time.

Quantitative investigations (33) were made of level competition effects both by the synchronous detection of a low-frequency variation of the heterodyne beat signal of two stabilized CO_2 lasers and by means of precise frequency control and biasing techniques of a ring laser oscillating with two opposite traveling waves. The bistable traveling-wave oscillations in a ring reveal several interesting characteristics of level competition effects and power-dependent gain profiles. In a ring laser, the Doppler shift owing to the gas flow is sufficient to cause a gain anisotropy as a function of frequency. By proper tuning of the

cavity the laser can be operated as a unidirectional oscillator. However, over a narrow frequency interval, two rotational levels can be made to oscillate with two opposite traveling waves, one in a clockwise and the other in a counterclockwise (ccw) direction around the ring-, with an intensity crossover between the two line centers. The measured gain profiles indicate that both the gain and intensity-dependent anomalous dispersion play a role in crossing from one rotational level to another. The power-dependent gain and index for a homogeneously broadened transition can be expressed by the equations (*171*),

$$\alpha(\nu) = \frac{1}{I}\frac{dI}{dx} = \frac{\alpha_0 \Delta^2}{\Delta^2(1 + I/I_s) + 4\pi^2(\nu_0 - \nu)^2} \tag{89}$$

and

$$n(\nu) = 1 - \frac{c}{\nu}\frac{\alpha_0 \Delta(\nu_0 - \nu)}{\Delta^2(1 + I/I_s) + 4\pi^2(\nu_0 - \nu)^2} \tag{90}$$

where α_0 is the small-signal gain coefficient, A the linewidth, ν_0 the center frequency of the transition, and I_s the saturation parameter. From these equations we see that both the gain and the refractive index profiles are strongly dependent on I and flattened with increasing I. If the frequency of oscillation is at line center, the dispersion effect vanishes and Eq. (89) reduces to Eq. (76). The power-dependent dispersion represents a mode-pushing term pushing the oscillation frequency away from the line center. Thus by tuning the cavity away from the line center, a point is reached where a different transition with an equal gain will compete for the total population in the laser medium.

The frequency tuning curves were obtained (33) for a ring laser which is made of a solid quartz block with a triangular shape. The perimeter of the active loop was 50 cm in length corresponding to a longitudinal mode spacing of 600 MHz. The laser medium consisted of a flowing CO_2–N_2–He gas mixture, introduced at one of the vertices, streaming down through both legs with flow rates either identical or biased in the two directions. The cavity can be tuned over a wide frequency range by means of a piezoelectric transducer attached to one of the three cavity mirrors. With an equal flow rate in the two legs, i.e., $v_{cw} = v_{ccw}$, the gain profiles for the two opposite traveling waves were identical and both were broadened as a result of the superposition of an up-shifted and a down-shifted gain profiles. The introduction of an asymmetric flow, i.e., $v_{cw} > v_{ccw}$, changed the gain profiles of the two waves 'significantly. The cw traveling wave had higher gain in the higher flow path and its center frequency ν_0 was up-shifted by $\Delta\nu$ and that in the lower gain path down-shifted by Au' with $\Delta\nu > \Delta\nu'$. Similar considerations

applied to the ccw wave whose gain profile is a mirror image of that of the cw wave.

By tuning the cavity length from the high frequency side in the case of an asymmetric flow, the cw wave with a higher gain was brought into oscillation unidirectionally. As the cavity was being continuously tuned, a point was reached at which the ccw wave had an equal gain on a different rotational line. Over a few hundred KHz range, two oppositely directed traveling waves were made to oscillate on two different rotational transitions. Figure 36 shows the intensity of the relative amplitudes of the cw $P(16)$ and the ccw $P(18)$ lasers as a function of frequency excursion in the competition region. In addition, the frequency width of the competition region increases with increasing laser intensity. These results confirm that the competition effects are owing to intensity-dependent anomalous dispersion arising from gain saturation.

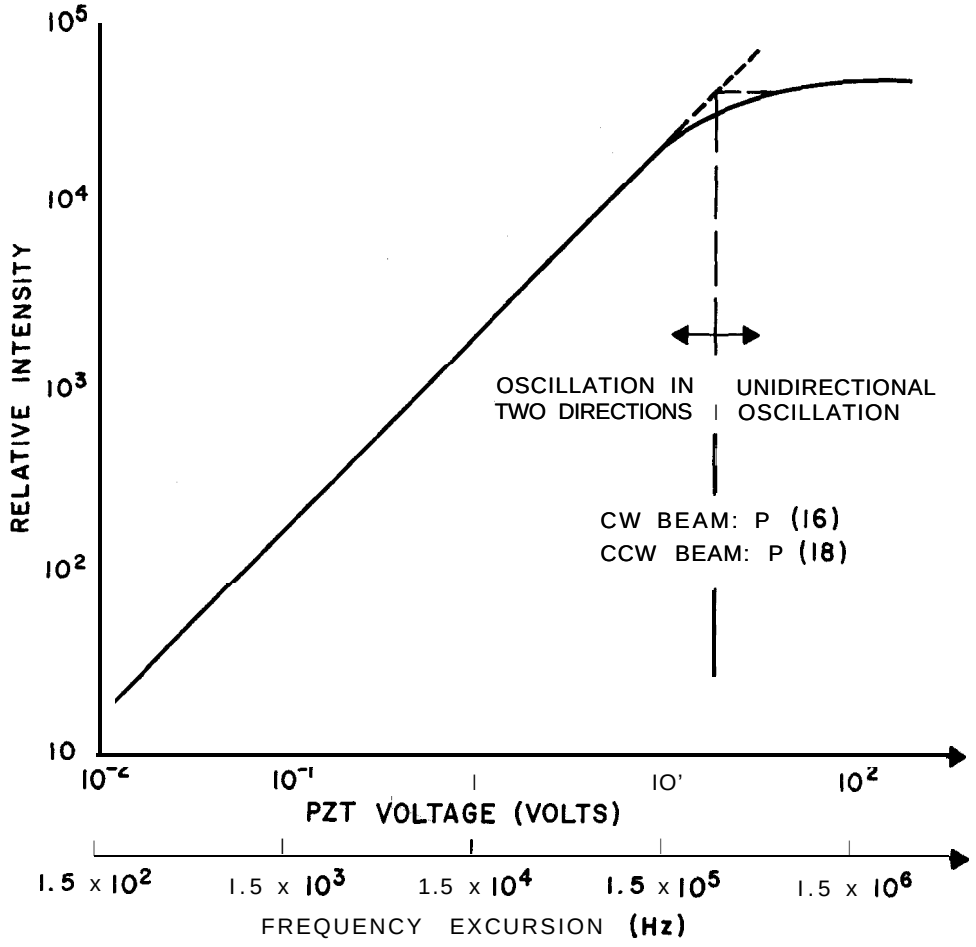

Fig. 36. Relative intensity versus frequency excursion in the competition region between clockwise (cw) $P(16)$ and counterclockwise (ccw) $P(18)$ transitions in a ring laser. [After Mocker(*33*).]

The interaction of modes in a CO_2 laser has been studied by Witteman(172) using a phenomenological approach rather than the usual density matrix formulation(168). In this analysis, competition between $TEM_{,,}$ and TEM_{01} modes owing to spatial overlap of the two fields E_1 and E_2 was treated. The rate equations for population inversion densities n_1 and n_2 associated with the two modes are(172)

$$\frac{dn_1}{dt} = \Gamma_1 - An_1 - \frac{c^3A}{16\pi h\nu^3}[g(\nu_1)\rho_1 n_1 + \tfrac{1}{2}g(\nu_2)\rho_2 n_1]$$
$$\frac{dn_2}{dt} = \Gamma_2 - An_2 - \frac{3c^3A}{64\pi h\nu^3}[g(\nu_2)\rho_2 n_2 + 2g(\nu_1)\rho_1 n_2] \tag{91}$$

where Γ_i is the excitation rate of the ith mode and An_i is the decay rate of the inversion density (where A is the Einstein A coefficient). The last term represents the mixing of the two modes, where $g(\nu_i)$ is the lineshape function of the ith mode, and ρ_i is the radiation flux density ($P_i = \frac{1}{2}\epsilon\mathscr{E}_i^2$). Solutions of Eqs. (91) were obtained from which estimations for the oscillation conditions could then be made. Figure 37 is a

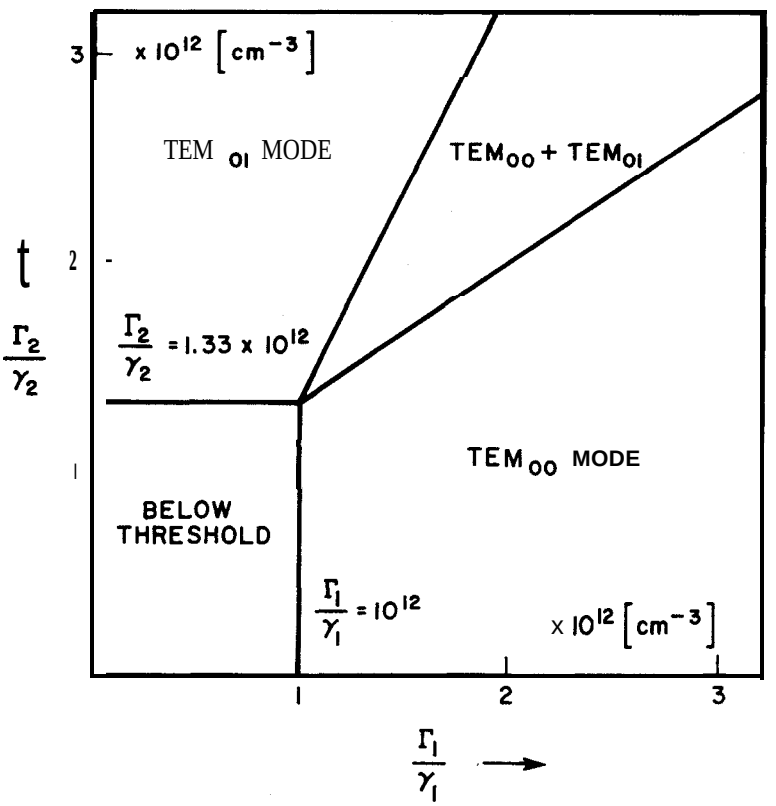

Fig. 37. The ratio of excitation parameter Γ to loss factory for the TEM_{00} mode versus that for the $TEM_{,,}$ mode. There are three oscillation regions, $TEM_{,,}$ or $TEM_{,,}$ separately or both modes together. [After Witteman(*172*).]

plot of the ratio of excitation parameter Γ to the loss factor γ for TEM,, mode against that for TEM_{01} mode. The threshold values for excitation are shown in Fig. 37 where ρ_i/γ_i is equal to $A/\alpha_i h\nu$ with estimated values for α_1 and α_2 taken as 5×10^5 and 3.75×10^5 erg^{-1} sec^{-1}, respectively. Above threshold, only the TEM_{00} mode oscillates if $\Gamma_1/\Gamma_2 > 1.5$, and only the TEM,, mode oscillates if $\Gamma_1/\Gamma_2 < 0.5$. In the region where $1.5 < \Gamma_1/\Gamma_2 < 0.5$, both modes can be made to oscillate. These results are in qualitative agreement with the observations(l72) that in a high-power single-mode CO_2 laser, the oscillating mode switches from TEM_{00} to TEM_{01} when the discharge current is increased from 25 to 36 mA.

3. Frequency Fluctuation

The oscillating frequency of a CO_2 laser can be changed by varying the operating parameters such as pressure and discharge currents. A 5-8 MHz/Torr downshift in frequency owing to an increase in total pressure, and a 0.5-0.9 MHz/mA upshift in frequency owing to an increase in discharge current have been observed(Z74) upon heterodyning two stabilized linear CO_2 lasers (3 parts in 10^{10}), both oscillating in a single axial and transverse mode on the *P* branch of the $00^0\ 1\text{-}1\ 0^0 0$ band. From two independent experiments, Mocker (*1* 74) concluded that the pressure-dependent frequency shift is caused by a change in the index of refraction of the gas discharge. The largest pressure-dependent shift, 7.4 MHz/Torr, was observed at a CO_2 partial pressure of 3.6 Torr which is near the optimum value for a small 8-mm-bore laser tube. On the other hand, the oscillating frequency increases with increasing discharge current and has a higher shift (900 KHz/mA) at lower current (5 mA/cm^2) and a lower shift (500 KHz/mA) at higher current (15 mA/cm^2). The amount of frequency shift caused by excitation was found to be independent of the location of the cavity resonance with respect to the line center. The current-dependent frequency shift is attributed also to the change in the index of refraction caused by the change in the electron density of the plasma. In a CO_2 gas discharge, the refractive index n is determined by all constituents in the plasma such as the neutral molecules and electrons:

$$n = 1 - \frac{1}{2}\frac{n_e e^2}{m_e \epsilon_0 \omega^2} + 2\pi\alpha_m n_m \tag{92}$$

where n_e and m_e are the electron density and mass, respectively; α_m and n_m are the polarizability and density of the molecular gas, respectively. For gas mixtures and pressures typically used in a CO_2 laser,

the change in the refractive index contributes a shift in frequency of I O-I 2 MHz/Torr compared with the measured values of 5-8 MHz/Torr. On the other hand, the calculated frequency shift owing to electron density in the plasma (assuming $n_e \simeq 1\ 0^{10}\ cm^{-3}$) is a somewhat higher value than the measured frequency shift but is within a reasonable range of values for the large current densities and pressures used in the experiments(l74). It should be pointed out that a significant reduction of the refractive index may arise from dissociation of CO_2 molecule which may account for the difference in the calculated and measured results.

Optical line modulation by electron-plasma oscillations at 4 GHz has recently been observed (I 76) in an argon plasma tube which was placed in a microwave resonantor. By exciting the plasma oscillation in the Tonks-Dattner (TD) resonances (177) at two microwave frequencies, f_1 and f_2, such that the difference frequency Δf is much less than either f_1 or f_2 or the linewidth of the TD resonances, one can measure directly the local oscillations in the spontaneous emission intensity of the plasma. These local oscillations correspond to the localized fluctuations in the plasma density. By means of such an efficient nonlinear mixing between plasma oscillations in gases, this technique allows direct measurements (176) of the microwave-modulated CO_2 laser beam scattered from the plasma oscillation. From these experiments much information can be obtained about the plasma characteristics.

4. Nonlinear Phenomena

Coherent interaction between an intense CO_2 laser field and a resonant medium has resulted in a number of interesting phenomena including (i) passive Q switching and mode locking of the CO_2 laser, (ii) self-induced transparency, (iii) photon echo, (iv) free-induction decay and edge echo, (v) optical transient nutation, and (vi) parametric amplification. The physics of these phenomena involve coupled nonlinear differential equations describing the fields and the induced polarization by the fields. Detailed analysis of these topics is beyond the scope of this chapter; however, we shall present here some experimental results and give qualitative explanations of those which appear to have some practical interest in terms of CO_2 laser systems and devices.

Spontaneous Q switching and mode locking of CO_2 lasers by use of SF_6 gas as a saturable absorber inside the laser cavity was first observed by Wood and Schwarz(*47*,*52*) (detailed discussion will be given in Section V.E). This has subsequently led to an intensive study of the coherent interaction between the CO_2 laser and SF_6 or other media in

resonance with the CO_2 lasers. Passing a rotating-mirror Q-switched CO_2 laser beam through an SF, cell, Patel and Slusher(99) observed self-induced transparency, a phenomenon which is similar to that observed earlier by McCall and Hahn(178) using an intense ruby laser pulse through a ruby inhomogeneous absorbing medium. The optical energy in the first portion of the input pulse, which is absorbed by the medium to create induced dipoles, returns entirely back to the field through a stimulated emission of these dipoles in the presence of the latter portion of the optical pulse. For the case of two nondegenerate quantum states with an inhomogeneously broadened line, McCall and Hahn(l79) have studied theoretically the self-induced transparency problem, with emphasis on the existence of stable conditions by propagation. Results show that a stable solution exists for an input pulse of arbitrary shape with an intensity corresponding to a pulse angle $\theta = 2\pi$, where θ is defined by

$$\theta \equiv \frac{2\mu}{\hbar} \int_{-\infty}^{\infty} \mathscr{E}\, dt \tag{93}$$

In Eq. (93), μ is the dipole moment of the absorbing medium, and $\mathscr{E}$ is the field amplitude. For $\theta = 2\pi$, the input pulse will traverse the absorbing cell without suffering any loss in strength and will develop into a hyperbolic secant pulse I_t with a time delay τ_d from the peak of the input pulse, as given by

$$I_t \propto \operatorname{sech}^2 \frac{t}{0\tau_\omega} \tag{94}$$

and

$$\tau_d = T\frac{aL}{2} \tag{95}$$

where τ_0 and τ_ω are the pulse width of the input and the transmitted pulses, respectively, and a is the absorption coefficient of the medium.

Using a short and flat-topped CO_2 laser pulse from a laser with an electrooptic switch(56), Cheo and Wang(l07) have examined these characteristics by careful study of the dynamic evolution of this pulse through an optically thin as well as thick SF_6 absorbing medium. Figure 38 shows the waveforms of both the input and the output pulses. The width of the cavity-dumped pulse is about 20 nsec, which corresponds to the round-trip transit time of light in the cavity. Trace b shows the output waveform for an input pulse intensity corresponding to a "π" pulse. Trace c shows the waveform of a "2π" pulse. It is evident from traces b and c that both the pulsewidth and pulse delay decrease as the pulse angle increases from π to 2π. As θ approaches 2π, the pulse

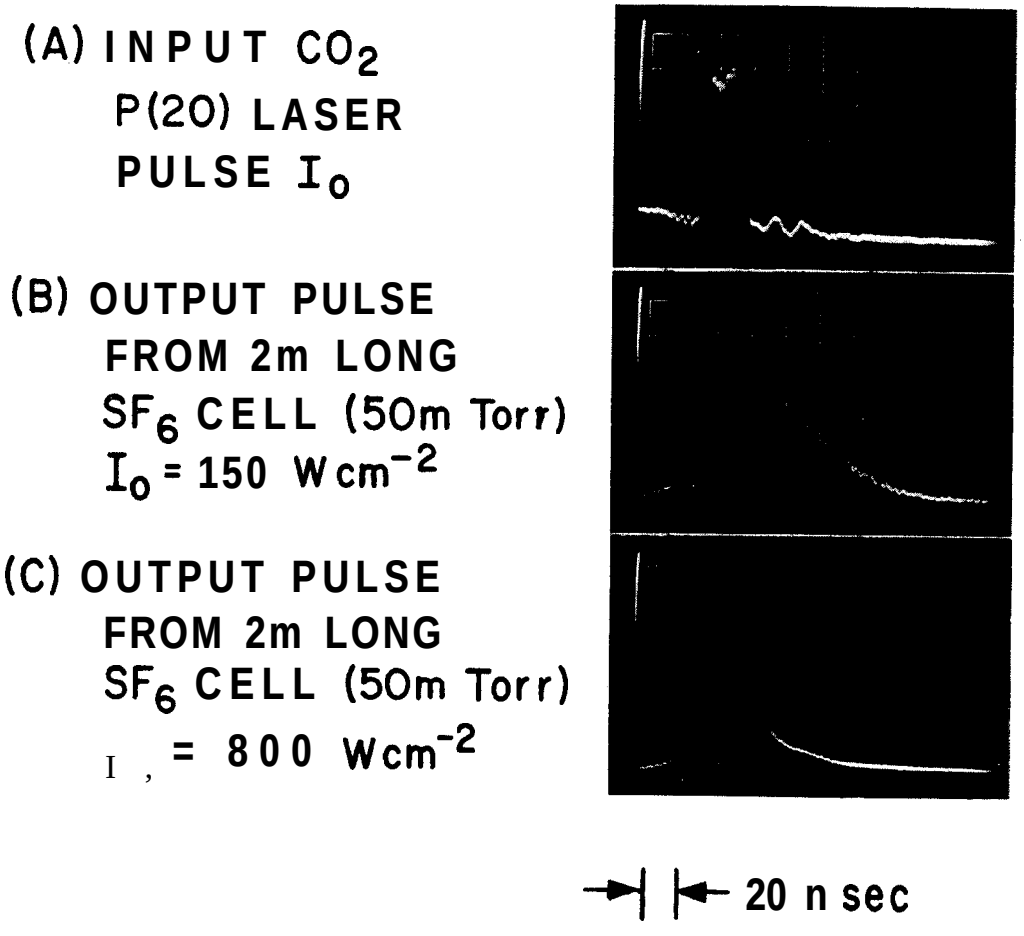

Fig. 38. (a) Waveform of a cavity-dumped CO, laser pulse at $P(20)$ 10.6 μ. (b) Output pulse shape from a 2-m-long SF, cell at 50 mTorr pressure for an input pulse intensity nearly corresponding to a π pulse. (c) Output pulse shape from the same absorption cell for a 2π pulse.

shape becomes more symmetric with the exception that a long tail is always associated with each transmitted pulse. This tail is attributed (107) to a phenomenon which is an optical analog of the nuclear magnetic resonance (NMR) phenomenon known as free induction decay and occurs in an inhomogeneous magnetic field(l80). It arises from the decay of the induced dipoles while undergoing free precession. The effects of propagation(l79) could also produce such a tail on the transmitted pulse but a detailed study(l07) of the pulse shape as a function of SF_6 gas pressure rules out this possibility. An examination (107) of the shape of the completely transmitted pulse reveals that the measured pulse shape is somewhat steeper than the ideal $\mathrm{sech}^2(t/\tau_\omega)$ function. The deviation is likely caused by the participation of the absorbing lines of higher angular momentum states in SF_6 *(105,181).*

The measurements(1O7) of pulsewidth and pulse delay time as a function of input pulse intensity I_0 indicate that local maxima in τ_ω and τ_d exist at I_0 corresponding to a π pulse. This result is consistent with the calculation(106) based on a simple model involving two nondegenerate quantum states.

Photon echo is also an optical analog of an NMR phenomena known as spin echo. When two Q-switched CO_2 laser pulses were passed colinearly through a 4-m-long SF_6 cell with a time separation $\tau_s \lesssim 1$ μsec between the two pulses, Pate1 and Slusher(*100*) observed that a small echo pulse occurred at a time about τ_s after the second excitation pulse. The optimum echo occurred when the intensities of the two excitation pulses, having identical polarization ($\Delta\phi_p = 0$) vectors, were ~ 1 W/cm^2 and 4 W/cm^2, corresponding to a $\pi/2$ and a π pulse, respectively. The echo amplitude decreased with either decreasing or increasing input pulse intensity and with increasing $\Delta\phi_p$. The echo polarization was always along the polarization of the second input pulse. Analysis (202) showed that the levels responsible for producing the observed echo (100) in a molecular gas such as SF_6 must arise from either $J = 1 \leftrightarrow J = 0$ or $J = 1 \leftrightarrow J = 1$ transitions. In performing this analysis one must consider the spatial degeneracy of the molecular energy levels.

Optical transient nutation(*101*) is another interesting phenomenon which occurs because the intense CO_2 laser pulse drives the SF_6 molecules successively from the lower state to acoherent superposition state where the induced dipoles oscillate in phase and result in a large microscopic polarization before undergoing the transition to the upper state. Similar steps are followed in the returning path. The cycle repeats but is subject to damping by the relaxation processes in the medium. This oscillation in the population between states reacts back on the field, resulting in an amplitude modulation of the incident laser signal. The frequency of the modulation Ω is proportional to the product of the dipole moment μ and the input field amplitude $\mathscr{E}$

$$\Omega = \frac{\mu \mathscr{E}}{\hbar} \tag{96}$$

Measurements(*101*) were made on the nutation frequency Ω as a function of $\mathscr{E}$. The dipole moment of the transition responsible for the coherent interaction with the $P(20)$ 10.6-μ CO_2 laser was found from the slope of the linear plot of Ω vs $\mathscr{E}$ to be 0.032 ± 0.003 D.

Parametric amplification of a CO_2 laser in an SF_2 cell has been reported by Gordon et al.(*182*). This phenomenon is attributed to the interaction between two optical waves in a resonant medium whose microscopic polarization is not linearly proportional to the fields.

Consequently energy of one wave (i.e., the "pump" field) is transferred to another (the "signal" field). In the experiment (182) the pump for the SF_6 parametric amplifier is provided by an intense CW CO_2 laser. The signal beam consists of a weak CO_2 laser beam with an amplitude modulated by means of a chopper prior to amplification. After the two beams are recombined into a single parallel beam within 1 mrad and are propagating through the SF_6 cell, the amplitude of the sidebands is increased with decreasing modulating frequency. Analysis based on a simple two-level model with a homogeneously broadened line shows that the gain α for the sidebands with frequency $\omega_s \ll T_2^{-1}$ is (182)

$$\alpha = \frac{a}{(1 + I_0/I_s)} \frac{(I_0/I_s)^2 - [1 + (\omega_s T_1)^2]}{(1 + I_0/I_s)^2 + (\omega_s T_1)^2} \tag{97}$$

where a is the absorption coefficient of the medium, I_0 is the intensity of the pump, I_s is the saturation parameter of the medium, and T_1 is the collisional relaxation time of the absorber. From Eq. (97), it is clear that a has a positive value, provided that

$$\omega_s T_1 < \left[\left(\frac{I_0}{I_s}\right)^2 - 1\right]^{1/2} \tag{98}$$

From measurements of the fluorescent decay time T_1 (2.6 msec) and the saturation parameter of SF_6 (1.8 W/cm^2), Eq. (97) yields gain values in good agreements with the measured results. In addition to the phenomena described, work on second harmonic generation (*94–96*), adiabatic rapid passage(Z83) of 10.6-μ CO_2 laser pulses through SF_6, and possibility of generating ultrashort CO_2 laser pulses (184) can be found in the literature.

D. CW POWER OUTPUT

In this section experimental results are presented on the CW power output from a conventional low-flowing CO_2–N_2–He laser and the variation of power yield versus various experimental parameters, such as flow rates, gas pressure of each mixture, discharge currents, coolants, and output coupling schemes. Also included in this section are discussions on the operating characteristics, lifetime, and stabilization in output power spectrum of small sealed-off CO_2 lasers.

1. *Flowing Laser Systems*

Early studies on CO_2 laser systems yielded power outputs varying over a wide range (a few watts to 40 W/m discharge length), owing

primarily to inefficient output coupling. With advances in thin-film technology, low-loss (< 1%) mirrors with thin dielectric layers increased the optimum output coupling to about 80 W with a multimode (transverse) spectrum from a 1 -m discharge column. For a flowing CO_2 laser, tube construction is extremely simple, consisting of a straight pyrex tube surrounded by a water jacket. Near the ends of the tube, cold hollow-cathode electrodes of nickel, molybdenum, or simply kovar (glass-to-metal) seal can be used for a reasonable length of time without causing too much sputtering. The ends of the tube are usually sealed with windows of KCl, NaCl, or other IR transmitting materials such as Ge, GaAs, TI-I 173 glass, or Irtran II set at the Brewster angle. Typically, the voltage-current requirement for a l-m discharge tube with a 5-cm bore is about 4 kV and 100 mA, and about IO kV and 40 mA for a 2-cm bore tube. The efficiency (ratio of output optical power to the input electrical power applied to the discharge tube) can be as high as 20%.

The investigation and optimization of CO_2 laser power and efficiency have been done by many workers during the past few years, and it is hardly possible to give complete references. A report prepared by Whitehouse(62) presents the state-of-the-art on mainly large conventional CO_2 laser systems (3-20 m in length). In a sequence of experiments, tests on mode control and output coupling were made involving the use of three mirrors of different radii of curvature (R = 4, 10, and 25 m). The total reflecting mirror was mounted directly on one end of the 3-m long and 2-in.-bore tube with a NaCl Brewster window on the other end. The output coupling was obtained from a NaCl flat, dielectrically coated on both surfaces to provide 35% transmission. The total cavity length L was 3.6 m corresponding to a longitudinal mode spacing $c/2L$ = 41.6 MHz. The spot sizes ω_1 and ω_2 of the fundamental mode at, respectively, the curved and flat mirrors are(*185*)

$$\omega_1 = \left(\frac{\lambda}{\pi}\right)^{1/2}\left[\frac{R^2L}{R-L}\right]^{1/4} \qquad \omega_2 = \left(\frac{\lambda}{\pi}\right)^{1/2}[L(R-L)]^{1/4} \qquad (99)$$

The cavity with R = 25 m provides a fundamental mode spot that best fills the tube volume. For the cavity with R = 10 m, the fundamental was sufficiently small but higher order transverse modes had the necessary gain to oscillate by filling the entire 2-in. bore. Table 19 gives the outputs for optimum gas mixtures and discharge currents and for a gas flow rate of 100 cu ft/min. At a discharge current of 120 mA, the cavity with R = 10 m yields an output of 80 W/m as opposed to 58 W/m with R = 25 m. With R = 4 m, the spot size is very small in the tube and is biggest at the spherical mirror. In this case the higher-

TABLE 19

The Optimum Output Power from Three CO_2-N_2-He Lasers with Different Cavity Configuration (62)
(L = 3.6 m, bore = 2 in.; flow rate = 100 ft^3/m)

R (m)	ω_1 (cm)	ω_2 (cm)	Power (W/m)	Mode
25	0.59	0.53	58	~ 1 in. fundamental
10	0.49	0.39	80	Fundamental + higher order
4	0.62	0.20	50	~ 0.5 in. fundamental

order transverse modes are not allowed to oscillate and output is limited to only 50 W/m.

Power dependence on pressure, flow rate, and discharge current have also been investigated (62), and values at which the maximum laser power can be achieved are in general very similar to those obtained in the unsaturated gain measurements (19,35) (see Section V.A.) The output power depends critically on the partial pressure of CO_2, and to a lesser extent on the partial pressure of He and N_2. The optimum CO_2 partial pressure for a 2-in. bore is about 0.5 Torr. The values of 6 Torr for helium and I .5 Torr for N_2 are reasonably close to the optimum condition for maximum power output. For a flowing gas laser operating at maximum output, a relatively weak dependence on wall temperature is observed (a 20-40% decrease in power output if the water flow is shut off) However, with an increase in tube diameter, the power is greatly decreased, indicating that water cooling is inadequate in the case ot larger-bore tubes (i.d. $>$ 2 in.). Water cooling is extremely important for sealed-off lasers. Without water cooling, the gain of a sealed-off tube becomes so low that in most cases oscillation cannot be maintained. Other processes, such as dissociation and spontaneous radiation losses also can contribute to the reduction of gas temperature, in addition to the conduction through the tube wall and convection by gas flow, but they are negligibly small compared with the conduction and convection losses.

The power dependence on excitation voltage and current is shown in Fig. 39 for two laser tubes. In this figure the peak power is reduced by ~ 25% from the maximum power achieved with the same tube when the dielectric coating on the NaCl mirror was not deteriorated owing to continuous use at high power level. Nevertheless the V–I characteristics and the power dependence are clearly demonstrated. Results with two tube-bore sizes show that the output power is relatively independent of tube diameter D, in contrast with the small-signal gain measurements

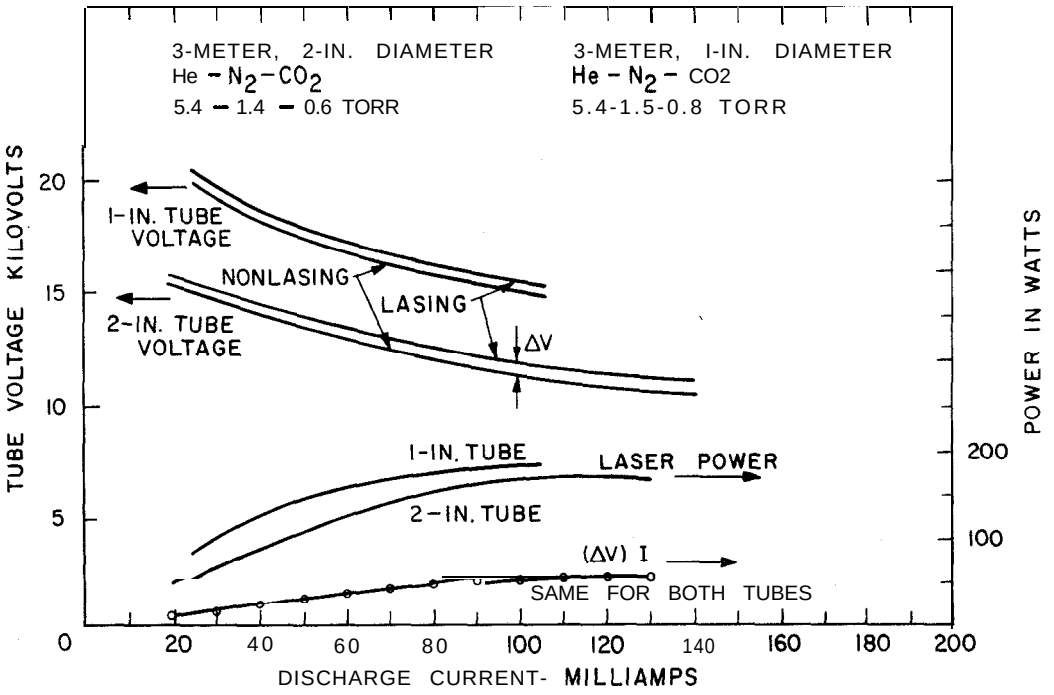

Fig. 39. Voltage, laser power, and incremental electrical power versus current for two laser tubes. Both tubes have the same length (3 m) and same pumping speed (65 ft^3/m). A I-in.-diam tube has two NaCl Brewster windows, one total reflecting mirror (50 m), and a flat mirror with $T = 65\%$. A 2-in.-diam tube has one NaCl Brewster window, one total reflecting internal mirror (10 m), and a flat mirror with $T = 35\%$. [After Whitehouse (*62*).]

which show a l/D dependence. This result and the requirement of higher discharge currents (about a factor of two) for obtaining optimum output power constitute the principal differences between an unsaturated and a saturated CO_2 laser system.

It should be pointed out that the discharge tube has a negative dynamic resistance of approximately 20-200 $k\Omega$ which requires the use of a series of ballast resistances. From Fig. 39, it is clear that laser action affects the V-I characteristics by a noticeable increase in excitation power. This is caused by the radiative power density generation in the lasing medium, acting as a heat sink. The actual increase in electrical power accounts for about $\frac{1}{3}$ of the laser power extracted from the tube. Other heat loss mechanisms include conduction loss to the wall and convection by gas flow, in addition to the radiative loss. By additional measurements on the power dissipated via the cooling water, Whitehouse (62) showed (Table20) the relative importance of the three dominant heat loss mechanisms for a 3-m-long, 2-in.-bore discharge tube at a flow rate of 65 cu ft/min. Results indicate that when a certain

TABLE 20

The Principal Heat Loss Mechanisms in a Conventional CO_2 Laser(62)

	Nonlasing		Lasing	
	Power (W)	Efficiency (%)	Power (W)	Efficiency (%)
Laser power	0	0	200	15
Power dissipated by H_2O cooling	880	70	790	60
Power dissipated by gas flow	370	30	330	25

amount of power can be coupled out off the cavity in a laser beam, other power losses, such as conduction by water coolant and convection by gas flow, are substantially reduced (> 10%). A simple calculation using the equation of heat flow shows that the gas temperature on the axis is approximately 400°–450°K and the average temperature in the discharge is about 400°K. Coolants other than water also have been attempted but they do not lead to a substantial increase in output power

2. *Large Laser Systems*

The first large CO_2 laser system was constructed at the Raytheon Company in Waltham, Massachusetts in 1967 with a folded 20-m-long water-cooled discharge tube. Each leg consists of a lo-m-long 2-in.-diam Corning conical pyrex pipe with one end joined by a brass pumping port through which the flowing CO_2–N_2–He mixture is pumped out and also serves as the common cathode. Mounted on the other end is a brass flange with holes through the edge for admitting the gas. It serves also as the anode for the discharge tube. The two identical 10-m sections are placed side by side on the same physical structure and optically connected in series by means of two flat total reflecting mirrors (gold coated on sapphire or copper) oriented at 45° with respect to the incident beam. A totally reflecting mirror with radius of curvature R = 50 m and a freshly polished NaCl flat for the output coupling were used in this folded laser. A CW laser power of 1.2 kW was achieved with an effective pumping speed of ~ 15 cu ft/min. This corresponds to an average power of 50 W/m and an efficiency of 17%. At present, it appears that only salt flats such as NaCl and KC1 are

suitable for output coupling at kilowatt power levels. Several shortcomings of these materials, in addition to their hygroscopic nature, were observed under high-power conditions: (i) dust particles tend to "burn in," (ii) the internal surface acquires an "orange peel" texture causing serious deterioration in optical transmission quality, (iii) the blank loses its flatness under thermal strain, and (iv) it cracks after several hours of continuous operation. Without the salt flat, an output of 100 W over an area about 1 in. diam was obtained in the form of superradiance. Spectrum analysis showed that this output consisted mainly of a single rotational line of the $P(20)$ 10.59-p transition. The fact that only one transition oscillates is a possible indication that a cavity mode has been built up by feedback from scattering at the Brewster window.

This work was further extended by Roberts et al. (*63*) who constructed a laser over 170 ft in length. The entire system consisted of 18 modules, each 9 ft 8 in. long. The operating characteristics and the output of this laser as a function of length are given in Table 2 1. The highest output from this giant laser with 18 modules was reported to be 2.3 kW, and 1.45 kW with only one mirror (total reflecting mirror). Other large CO_2 laser systems (*43*,*64*,*65*), involving the combination of a small CO_2 laser source and a large laser amplifier, will be discussed in Section V. E.

3. *Sealed-Off Lasers*

Several advantages for operating a sealed-off laser, instead of flowing gas, are that (i) a nonflow laser is inherently more stable in its output spectrum, (ii) it can be made more compact and portable, and (iii) it conserves gases, thus reducing operating and maintenance costs, a factor especially significant in countries where He and other gas components are not abundant. The difficulties with a sealed-off laser lie, of course, in the fact that the gain is considerably reduced and that the operating life is limited. In 1966, Cheo (*186*) carried out a life test on a sealed-off CO_2-He discharge tube with a water-cooled wall and obtained a total life of ~450 hr under continuous operation at a constant current of 25 mA, which was the optimum current for maximum laser power (26 W/m) when the tube was freshly filled. This tube (1 m in length with a 22-mm bore), which has been extensively used for the studies of CO_2 laser amplifiers (*19*), consisted of a pyrex envelope with a large ballast (~10 liters) attached to the tube. Two internal mirrors, one total-reflecting and the other dielectrically coated (T = 10%), were bonded (Torr-Seal) onto brass bellows at the two

TABLE 21

Operating Characteristics and Power Output as Functions of Length(63)

Number of modules	$P(CO_2)$ (Torr)	$P(N_2)$ (Torr)	$P(He)$ (Torr)	I mpedence (Ω)	Power in (kW)	Efficiency (%)	Power out (W)	Current (mA)
2	0.45	0.75	4.80	1.1×10^5	1.77	13.4	237	125
3	0.45	0.75	4.85	1.75×10^5	2.9	12.3	358	130
6	0.45	0.75	4.85	4.1×10^5	6.4	10.0	640	125
8	0.46	0.74	6.7	6.1×10^5	9.3	10.5	980	125
10	0.47	0.73	5.82	7.1×10^5	11.15	10.4	1160	12.5
12	0.40	0.80	4.80	8.6×10^5	14.7	9.7	1440	127
14	0.45	0.75	4.85	9.1×10^5	14.4	10.6	1540	127
16	0.45	0.75	4.80	—	—	—	1760	125
18	0.45	0.75	5.8	10.3×10^5	24.3	9.4	2300	150

ends. Two cold hollow Mo electrodes were used to maintain a dc discharge. The choice of using internal mirrors is that the life and performance would not be affected by a gradual deterioration of the salt windows. No special high vacuum processing was undertaken other than that the tube was cleaned by running a discharge for a period of a few minutes, and then evacuated down to a pressure of 10^{-6} mm Hg several times prior to the final filling. Similar results were obtained also by Bridges et al. (*61*), Whitehouse(*62*), and Carbone(66).

Another test was performed by Reeves(68) who repeated the previous experiment(l86) by using a CO_2–N_2–He mixture. In this case the discharge current was set at 40 mA throughout the entire experiment. The initial output power was 30 W and reached a maximum of 35 W after 200 hr of continuous operation and then gradually decayed to zero in about 580 hr. At the maximum power point, the CO_2-He laser (186) yielded an efficiency of about 16% and the CO_2-N_2–He laser operated at about 10% efficiency. The side-light emission spectra from the CO and N_2 species were monitored during the entire life test by a photomultiplier through a grating spectrometer with a 2.8 f number and a horizontal entrance slit. Almost all the identified lines in the range 3000-6000 Å were found to belong to the Angstrom ‘and third positive bands of CO or second positive bands of N_2. When the discharge was initially activated, a marked decrease in current by a factor of about $\frac{1}{3}$ was observed during the first minute. A corresponding increase in CO side-light’ intensity was also observed, indicating that the increase in impedance which causes a decrease in current was owing to the dissociation of CO_2 into CO and O_2. The intensities of the CO and N_2 spectra remained relatively constant during the life of the laser, although CO showed a slight increase and N_2 a slight decrease. One noticeable observation was the gradual development of a dark film deposited on the cathode glass envelope, owing to sputtering of the Mo electrode. The other interesting observation was the occurrence of cataphoresis. This process becomes so severe, especially within a few hours after the laser oscillation has stopped, that the visible glow discharge changes from blue (primarily CO Angstrom) to pink (primarily N_2 second positive), and in less than six hours of continuous operation the discharge color- changes from pink to orange (solely He line spectra). The migration of the pink–orange interface takes place from anode to cathode over a period of about I min. These results indicate that gas cleanup at the cathode by the sputtered film causes nonequilibrium in the CO_2 dissociation-recombination process and an eventual depletion of CO_2 and the cessation of laser output.

By keeping the cathode and its envelope at an elevated temperature (71) (- 300°C), the rate of absorption of CO_2 and the dissociated products at or near the cathode can be reduced, thus prolonging the life of a sealed-off laser by over 1000 hr. A different approach suggested by Witteman(69) is to use an inert metal such as platinum for the electrodes and to add a small amount of water vapor (or 0.2 Torr of H_2 and 0.1 Torr of O_2) to the CO_2–N_2–He mixture. Water vapor was believed to produce OH radicals in the discharge, which combine with CO_2 the dissociated product, to form CO_2 and H. Witteman showed that not only can the life of an operating CO_2–N_2–He–H_2O (or H_2) laser be extended beyond 2000 hr, but also the output power can be increased by a factor of nearly two over the same laser filled without H_2O. This large increase in output power is attributed to the effective relaxation of the lower laser level by collisions with H_2. The laser tubes used in this experiment were made of fused quartz and filled with 1 Torr of CO_2, 2.5 Torr of N_2, 11 Torr of He, and 0.2 Torr of H_2O (the gas mixture ratios used by Witteman differ somewhat from those by other investigators). A germanium flat (uncoated) was used as the output coupling mirror arid was shown to yield the best output (63 W/m) and highest efficiency (15%) when used with a 3-m-long laser tube. Work by Clark and Wada(*72*), on the other hand, showed that long life (- 2800 hr) can be achieved also with a pyrex tube (1 cm i.d. and 50 cm long) and cold nickel and oxidized-tantalum electrodes (instead of a quartz tube and Pt electrodes) when a small amount of Xe (1 Torr) is added to a CO_2-He (3.5-12 Torr) mixture instead of N_2 and H_2O. The effect of Xe is attributed to a reduction of electron temperature, which thus retards the CO_2 dissociation rate. The maximum output from this small laser is about 6 W.

Some of the conflicting reports on the use of H_2O (or H,) and electrode materials have been resolved by Deutsch and Horrigan(73) who performed a series of life tests by using various approaches and concluded that H_2 is essential for achieving long life of sealed-off CO_2 lasers. By using a very clean system (well baked at 300°C) filled with a CO_2–N_2–He–Xe mixture, they found that the tube life is very short (- 170 hr) even though heated nickel cathode electrodes were used. However, the initial laser power can be as high as that reported by Witteman(69) using a CO_2–N_2–He–H_2O mixture. With an unbaked system which has been contaminated by H_2 (by running an H_2 discharge for several hours prior to filling), a steady laser output at a relatively high power level was observed for almost 900 hr with no indication of failure. This laser was made of pyrex tubing with water cooling and with hollow cathode nickel electrodes fitted over with a glass sleeve to

minimize the sputtering owing to collisions of ions with sharp edges of the cylinder. The cathode envelope was thermally insulated to maintain a temperature of 2.50" to 300°C and a discharge current of 40 mA. The termination of this test was caused by a leak at one of the cemented mirrors. It was also concluded (*73*) that heating of a cathode alone cannot lead to long life unless the cathode has been processed under an H_2 atmosphere. Results of various investigators, as shown in Fig. 40,

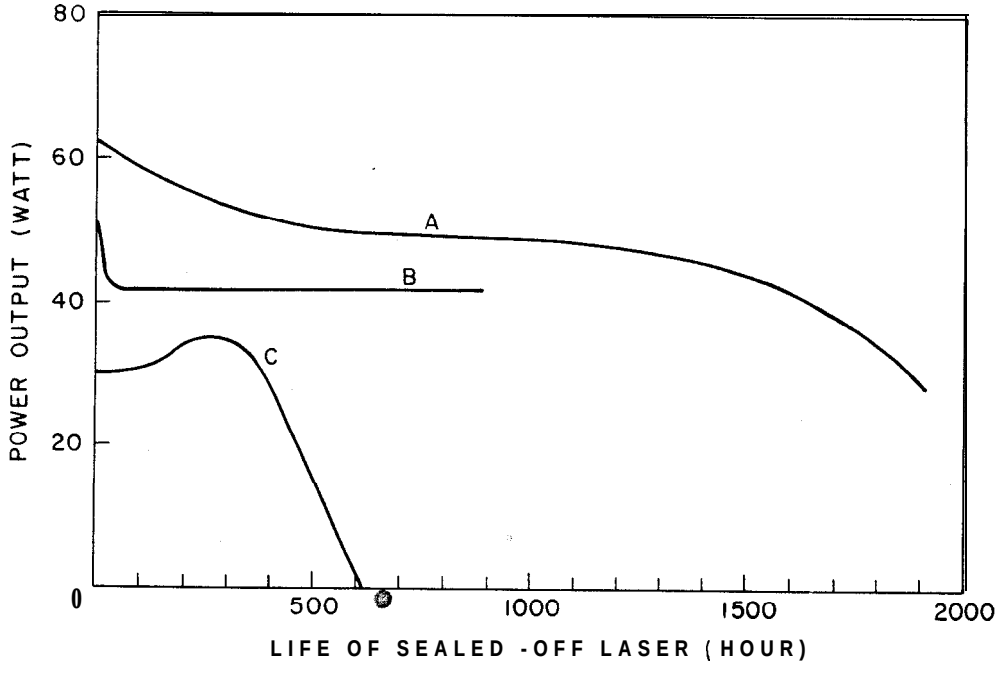

Fig. 40. The laser output versus continuous operating time of the sealed-off CO, laser. Curve A [Witteman(*69*)] uses a 1 .5-m-long quartz tube filled with 1 Torr CO_2, 2.5 Torr N_2, 1 1 Torr He, 0.2 Torr H_2, and 0. 1 Torr O_2. Curve B [Deutsch and Horrigan(*73*)] uses a 1 .23-m-long 2.5-cm i.d. pyrex tube filled with 1 .6 Torr CO_2. 2.2 Torr N_2, 11 Torr He, and 1. 1 Torr Xe. Curve C [Reeves(*68*)] uses a 1 -m-long 2.2-cm i.d. pyrex tube filled with 2 Torr CO_2, 1 Torr N_2, and 6 Torr He.

clearly indicate that the life of a sealed-off CO_2 laser can be made longer than 1000 hr under continuous operation provided that the tube is satisfactorily processed, a proper mixture of gases is selected, and the electrode material is correctly chosen. Questions in regard to quartz versus pyrex and the total life of a laser including the time that the laser is not in use still remain to be answered. Reynolds (*219*) reports a sealed-off CO, laser with over 10,000 hr of operation. The tube is made of quartz and has two self-heated electrodes. The initial output was about 2 W; after 10,000 hr of continuous operation the power output decreased by a factor of about $\frac{2}{3}$.

As mentioned in the previous section, water cooling is extremely important for a sealed-off laser. Results show that when wall temperature T_w is above 20°C, both the gain(*19*) and power output(73) decrease rapidly with increasing T_w. However for $T_w < 20°C$, the power output of a sealed-off laser increases slowly with a further decreasing T_w (as low as $-60°C$)(*57*), indicating that little can be gained by cooling the tube wall below 15°C.

4. Frequency and Intensity Stabilization

A number of applications in communications and in basic research require stable CO_2 lasers with extremely small fluctuation in both amplitude and frequency. An ideal laser would be one oscillating in a single cavity mode with a Gaussian profile far above threshold. Furthermore, under ideal operating conditions, the spectral width of this laser would be limited only by the phase fluctuation caused by the quantum noise(187). For a homogeneously broadened line operating above the threshold of oscillation, the linewidth $\Delta\nu_{osc}$ may be approximated by the Schawlow-Townes formula(l88) as

$$\frac{\Delta\nu_{osc}}{\nu} \sim \frac{\pi h}{P_\ell}(\Delta\nu_{cav})^2 \tag{100}$$

where $\Delta\nu_{osc}$ and $\Delta\nu_{cav}$ are full widths at half the maximum intensity, and P_ℓ is the power in the beam. Under ideal operating conditions of the CO_2 laser, $\Delta\nu_{osc}$ is of the order of $1\,0^{-3}$ sec^{-1}, which corresponds to a frequency stability of one part in 10^{16}. However, this limit has never been reached. For He-Ne or ion lasers, the Doppler linewidth is so wide (- 1.5 GHz) that a large number (> 10) of axial modes would oscillate in a typical I-m-long laser cavity even though the Fresnel number is chosen so that the higher-order transverse modes are suppressed by diffraction losses. Single-mode oscillation often is achieved by either shortening the laser tube or operating the laser near threshold. With these schemes the power output is severely limited. The situation is quite different for the CO_2 laser. It is quite easy to maintain a single-mode and single-frequency output at a high power level (> 20 W) because the linewidth of this laser is of the order of 100 MHz under typical operating conditions. Nevertheless, the cavity resonance is, in most cases, narrower than the molecular resonance and consequently the instability in' the laser medium owing to fluctuation in refractive index (as discussed in Section V.C.3) as well as the fluctuation in cavity resonance have a large effect on the stability of the laser frequency. Therefore it is imperative to operate a CO_2 laser with a well

regulated power supply, and closely controlled gas pressure and temperature. Changes in ambient temperature and mirror vibrations owing to environmental conditions are also a source of instability and lead to both long-term and short-term drifts in cavity resonance. At a given time, the deviation of frequency $\Delta\nu$ from the resonance frequency v is determined by the fluctuations in the refractive index Δn and cavity length ΔL as given by

$$\frac{\Delta v}{v} = \frac{\Delta n}{n} + \frac{\Delta L}{L} \tag{101}$$

A frequency shift on the order of 0.5-I MHz/mA and 5– 10 MHz/Torr is expected as a result of the change in refractive index. On the other hand, a 1-Å displacement of a mirror in a 50-cm-long cavity owing to acoustic noise or thermal instability will cause a frequency shift $\simeq$ 6 kHz. Therefore in addition to maintenance of a very stable discharge, adequate isolation from thermal and acoustic disturbances must be provided. A small change in cavity length or in refractive index can also cause the single-frequency oscillation to switch from one rotational level to another because of strong collisional coupling between rotational levels. Hence it is desirable to use a dispersive element(58) such as a diffraction grating as one of the cavity mirrors and to operate the laser in a single transverse mode.

Several review articles on laser stabilization techniques are available (*189–191*), therefore discussions will be limited to those which have already been applied to CO_2 laser systems. For ordinary laboratory use, the usual feedback technique by means of a piezoelectric translator (PZT) attached to one of the cavity mirrors, a lock-in stabilizer providing a small modulated signal and high voltage correction signals to the PZT, and a detector is sufficient to stabilize the cavity length. The work on frequency stabilization of sealed-off CO_2 lasers by stabilization of the cavity structure has been done extensively by Freed(*75*). Other techniques, either by utilization of competition effects between the cw and ccw waves in a ring laser(33) or by means of laser-saturated molecular absorption in SF_6(*165,166*), also have been used to stabilize the CO_2 laser.

The most widely used methods of determining the relative stability of lasers is to examine the time variation of the beat frequency of two independently free-running and stabilized lasers by recombining the two beams onto a photodetector(*192*), usually liquid-nitrogen-cooled gold-doped germanium ($\tau \gtrsim$ 30 nsec) or liquid-helium-cooled Cu- or Hg-doped germanium (I $\leqslant \tau \leqslant$ 20 nsec) with a 50-Ω load. The spectral analysis of the beat signal yields information concerning both the long-

and short-term stability of the lasers. By this technique Freed(75) showed that sealed-off CO_2 lasers, without any feedback stabilization and subjected to the normal laboratory environment, have a short-term stability of about 5 parts in 10^{12} for an observation time of 0.05 sec, and about 5 parts in 10^{13} if the 60-Hz disturbance owing to the power supply ripple is disregarded. Typical results of the beat frequency spectrum are shown in Fig. 41. The total frequency excursion

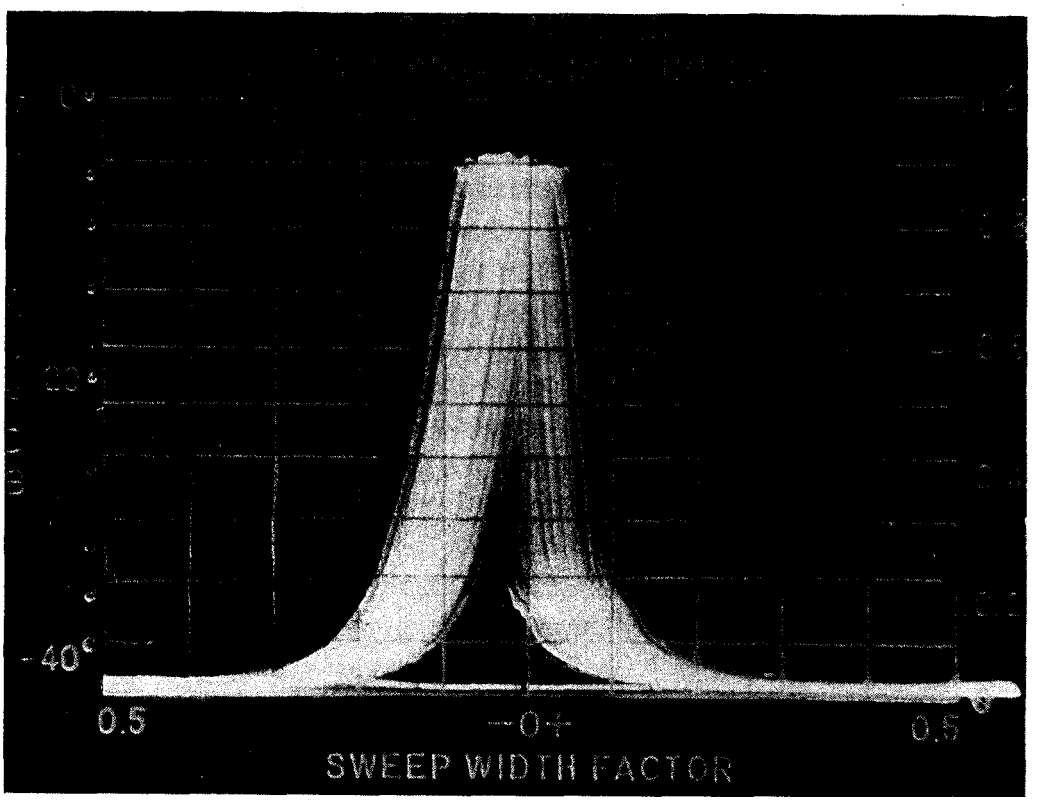

Fig. 41. Multiple-spectrum analyzer traces of the beat frequency of two stable lasers. Film exposure time, 4 sec; horizontal scale, 2 kHz/div; scanning rate, 60 sec. [After Freed (*75*).]

in this figure covers less than 2 kHz for 4 sec exposure time. The lasers used in these measurements were dc-excited discharge tubes with internal mirrors supported by four superinvar bars. At room temperature, the coefficient of thermal expansion of this alloy is claimed to be at least one order of magnitude lower than fused silica and passes through zero near room temperature. These rods are covered with acoustic and thermal insulating materials. The total length of the lasers is about 50 cm.

In the case of a ring laser, the intensity ratio of the two oppositely directed traveling waves oscillating on two adjacent rotational levels

(see Section V.C) is a function of frequency excursion. Therefore a discriminant can be derived without modulation of any of the laser parameters. This was achieved (*33*) by amplitude modulation of both beams alternatively external to the cavity before recombining. A phase-lock amplifier receives either a positive or negative signal, depending on whether the cw or the ccw beam is larger in intensity, and closes a feedback loop on a piezoelectric transducer on the ring laser. The operation can be understood with reference to Fig. 36. A slight increase in frequency from the equal-intensity point, 1.50 kHz, can cause the ring laser to change from dual-beam oscillation to unidirectional oscillation. Since a difference in intensity of 10^{-3} can be easily detected with a lock-in amplifier, a stabilization to ~ 5 parts in 10^{12} can be achieved. Other unique features of this operation are that this laser yields two different rotational lines locked in at the inter-rotational level competition region, and that changes in excitation will affect both transitions to an equal extent if the competition region lies exactly half-way between the two line centers, thus providing a first-order cancellation of the instabilities produced by fluctuations in the discharge.

Research on the stabilization of the CO_2 laser by means of locking the laser to the Lamb dip of a closely matched resonant line in SF_6 gas is presently in progress. This technique is similar to that used by Barger and Hall (*193*) for the 3.39-μ He-Ne laser with CH_4 as the resonant medium. However, exact measurements of the frequency stability of the CO_2 laser by this technique are not available at this time.

E. Q SWITCHING

The Q switching technique by which very intense laser pulses can be generated from a lasing medium is usually applicable when the upper level lifetime τ_u is long compared with the round-trip transit time τ_R of light in the cavity. The process in general involves a time-varying Q (quality factor) of the resonant cavity by means of an intracavity switch. The energy stored in the medium during the quiescent phase will build up far beyond the steady-state power level and then decay to the CW value when a high Q condition is suddenly established. This technique was first proposed by Hellwarth (*194*) for use with solid-state lasers and recently has been successfully applied to the CO_2 laser.

To understand the transient behavior for the rise and decay of the inversion process, Garrett (195) has presented a simplified analysis similar to that of Hellwarth (*194*), adaptable to a gas laser. The rate of change of the field $\mathscr{E}$ in a given mode and the rate of change of the upper

state population n_u are given by

$$\frac{d\mathscr{E}}{dt} = \left(An_u - \frac{1}{2}\frac{\omega}{Q}\right)\mathscr{E} \tag{102}$$

and

$$\frac{dn_u}{dt} = \Gamma_u - \left(\frac{1}{\tau_u} + \frac{\epsilon A\mathscr{E}^2}{4\pi h\nu}\right)n_u \tag{103}$$

where the assumption is made that the lower-level population relaxes very rapidly so that terms containing $n_\ell (\ll n_u)$ have been neglected. The coefficient A is given by

$$A = \frac{c\lambda^2}{8\pi\tau_r} g(\omega) \tag{104}$$

where g(ω) is the lineshape function as given by either Eq. (64) or Eq. (65) depending upon the line broadening process. The term Γ_u in Eq. (103) is the pumping rate, expressed as molecules/cm³/sec. Equation (102) is closely related to Lamb's equation of the form,

$$\frac{d\mathscr{E}}{dt} = \alpha\mathscr{E} - \beta\mathscr{E}^3 \tag{105}$$

where the cubic term in $\mathscr{E}$ is contained in the first term on the right-hand side of Eq. (102) through the first-order saturation effect. The last term in Eq. (103) represents the loss term owing to stimulated emission.

By solving these coupled equations, Garrett (*195*) showed that, as the feedback is suddenly introduced, the $\mathscr{E}$ field in a cavity of length L will build up exponentially in time to a peak intensity I_{max}, given by

$$I_{max} \simeq h\nu n_u L\left(\frac{\alpha_0}{\tau_R}\right) \tag{106}$$

which is the product of energy per photon $h\nu$, the number of available molecules in the upper state per cm² of cross-sectional area, and the single-pass gain per round-trip transit time. The field will then decay exponentially to the CW level as given by

$$I_{CW} \simeq \frac{h\nu n_u L}{\tau_u} \tag{107}$$

where τ_u is the effective lifetime of the upper level. By combining Eqs. (106) and (107), one obtains

$$I_{max} = \frac{\alpha_0\tau_u}{\tau_R} I_{CW} \tag{108}$$

Equation (108) shows that I_{max} is increased from I_{CW} by a factor $\alpha_0\tau_u/\tau_R$ which is the gain and lifetime product divided by the round-trip transit time.

For a 1 -m-long 20-mm-bore laser tube, $\alpha_0 \simeq 3$, $\tau_R \simeq 6$ nsec, $I_{CW} \simeq 20$ W/cm^2. With the assumption $\tau_u = 10^{-3}$ sec in a typical CO_2–N_2–He gas mixture, $I_{max} \simeq 10$ MW/cm^2 if Q switching is performed with an ideal switch under an optimum coupling condition. This value, however, has never been achieved in practice. The maximum peak power of a Q-switched CO_2 laser achieved to date is about two orders of magnitude below the above theoretical limit and the average power of the Q-switched laser is always less than the available CW power from the same laser.

It must be pointed out that the analysis by Garrett (195) is based on a simple two-level model, and was carried out by making a number of approximations. One important consideration which has been overlooked is that since the CO_2 laser is a multilevel system, the energy stored in the laser medium must be distributed among all the rotational sublevels. This is in a way completely opposite to the problem encountered in the analysis of the gain saturation of the CO_2 laser. As discussed in Section V.B, the two-level model cannot explain the gain saturation for the case of CW oscillation, and the expression derived from this model must be modified by a weighted average of the relaxation rate owing to the cross-coupling effects among all the sublevels. In the case of very fast Q switching, thermal equilibrium in all the rotational sublevels simply does not exist as in the continuous case so that Q switching can occur on any one of the rotational transitions independent of the others in the band. Therefore the energy stored in the vibrational level of CO_2 (00^0 1) cannot be extracted completely in a short duration. The effects of cross relaxation become important only if the switching time and pulse width are relatively long. In spite of these complications, a modest amount of peak power on the order of a few kilowatts, corresponding to a few millijoules of energy per pulse, can be obtained from a l-m-long CO_2 laser. The repetition rate can be made as fast as the cross-relaxation rate (- I 0^7 Torr^{-1} sec^{-1}) as in the case of spontaneous pulsing (or mode locking), or at a lower rate (- 10^3 sec^{-1}) for a longer (high average power) Q-switched pulse. In the following we shall present several Q-switching techniques and discuss in detail the characteristics of Q-switched CO_2 laser output in terms of pulse shape, width, energy and repetition rates, and the physical processes associated with these pulsing phenomena.

I. Pulsed Discharge

The CO_2 laser action was first observed(*1*,*2*) in a pulsed discharge with a few-microsecond-long excitation pulse. It is therefore reasonable to assume that the gain of a CO_2 laser transition in a pulsed lasing

medium may be somewhat higher than that in the CW condition. This has in fact been confirmed by Cheo(24) and subsequently by others (64,196). A large enhancement in gain (about one order of magnitude) is observed in the afterglow period owing to a rapid relaxation of the lower laser level before the relaxation of the upper laser becomes significant. By pulsing the discharge with a relatively long current pulse (- 100 μsec), laser pulses with peak power on the order of 1 kW and 150 μsec in duration have been obtained by Frapard(l97). Using very high excitation voltage in the range of 200 kV–1 MV and long pulse-width (6-50 μsec), Hill(*88*) obtained a large increase in laser peak power output on the order of 200 kW, corresponding to about 5 J per pulse at repetition rates of about 50 pps from a 2.5-m-long, 3-in.-bore tube filled with a flowing CO_2-N_2-He mixture at high concentration. The typical gas pressure used in these experiments exceeds 50 Torr. Efficiency varies from 4 to 10% depending on tube bore and gas mixtures. Figure 42 shows the waveforms of the excitation currents and laser pulse. The laser-pulse waveforms, Figs. 42b and 42c, can vary substantially upon variation of the gas-mixture ratio. In high-pressure gas discharges, it is expected that plasma instabilities can occur, causing a nonuniformity in the laser output across the tube diameter.

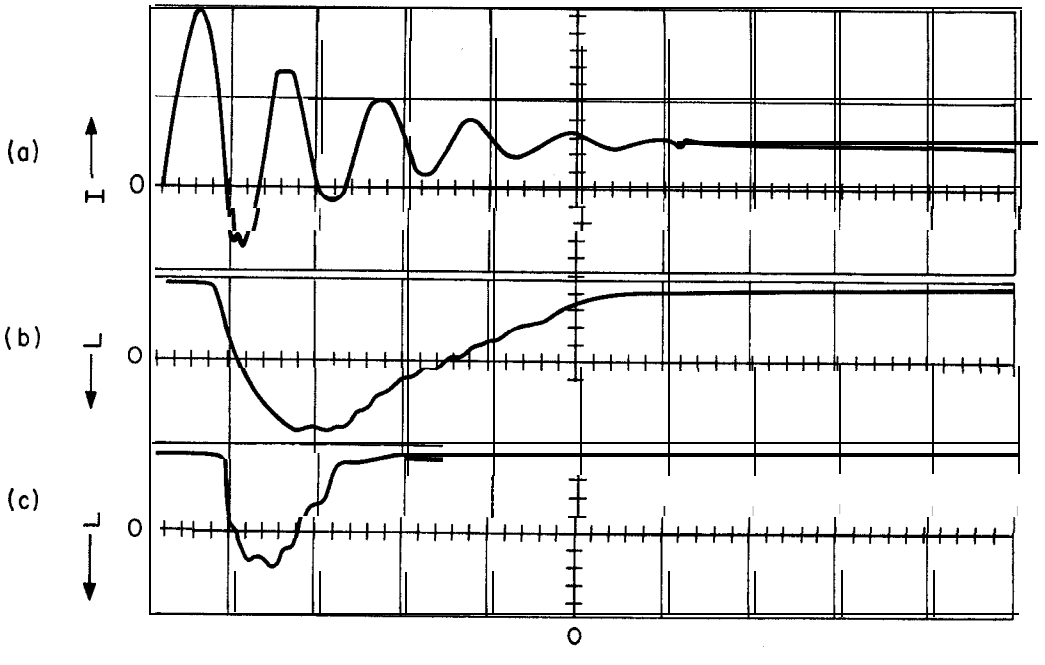

Fig. 42. (a) The excitation-current waveform I in a 2-in. bore, 6-ft-long laser tube filled with 5 Torr CO_2, 13 Torr N_2, and 30 Torr He at a flow rate 40 ft^3/hr. The initial breakdown voltage is ~ 500 kV and I, ≃ 40 A. (b) The laser output *L* caused by the excitation (a). (c) Variation of the laser pulsewidth by change of CO,-N, mixing ratios. Horizontal scale, IO μsec/division. [After Hill(*88*).]

Recently, Beaulieu(220) has reported the development of an electrically pulsed, atmospheric-pressure CO_2 laser with 20-MW peak power in a submicrosecond pulse. The efficiency is 17%.

2. *Mechanical Q Switching*

The most straightforward method of spoiling the cavity Q is either by rotating one of the cavity mirrors with a synchronous motor or by chopping the beam in the cavity with a mechanical shutter. The rotating-mirror technique has been commonly used in solid-state lasers, and was first applied to obtain Q-switched CO_2 laser pulses by Kovacs et al.(*44*). From a 2-m-long laser, they reported laser pulses with a peak power in excess of 10 kW corresponding to a few mJ of energy per pulse up to a maximum rotation rate of 500 Hz. A typical output pulse from a rotating-mirror Q-switched CO_2 laser cavity is shown in Fig. 43. With a single transverse mode operation, the optimum rotating

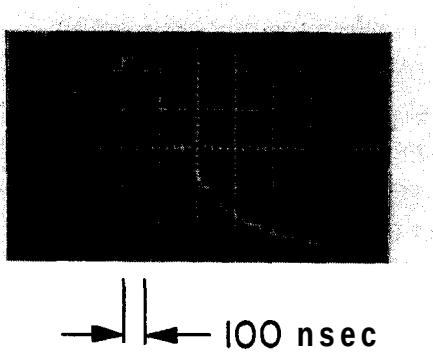

Fig. 43. **Output waveform of a rotating-mirror Q-switched CO_2 laser** pulse. The laser **cavity consists of a l-m-long flowing CO_2–N_2–He discharge tube terminated by two KCl Brewster-angle windows. The rotating mirror is coated with gold film and has R = 10 m. Power is coupled out from the diffraction grating mirror at** zeroth order. **Horizontal scale, 100** nsec/division; **peak power,** $\simeq$ 1 kW.

speed occurs at 200 Hz. As the rotation rate is increased from the optimum value, both-the pulse width and the pulse energy decrease sharply and reduce to zero at a rate of around 400 Hz. The output pulse shape is asymmetric with a full width at half power of about 300 nsec. Let a_1 and a_2 be the radii of the laser beam on the rotating and the stationary mirrors, respectively. The rotating mirror reflects an image of the stationary mirror back on itself in a time $t \simeq 2a_2/\omega L$ where ω and L are the angular velocity and length of the cavity, respectively. For a 10-mm spot size on the stationary mirror, ω = 1800 rad/sec and L = 2 m, one obtains an average time t_Q of about 300 nsec during which the rotating

mirror is aligned with the stationary mirror, consistent with the observed pulsewidth. The buildup time τ_b is typically of the order of 200 nsec, as shown in Fig. 43, and depends on the net gain and the turn-on time of the switch.

One complication with the rotating-mirror technique is the occurrence of time-varying. frequency or chirping in the output pulse spectrum. During the pulse buildup and decay, the cavity mirror continuously rotates and the cavity length as well as the modes change as a function of time. Workers(*1* 98,199) have observed this effect in a rotating-mirror Q-switched CO_2 laser pulse by heterodyning the *Q*-switched laser output with a stable CW local oscillator. The beat frequency ν is found to be a linear function of time. The measured(l99) value of $d\nu/dt$ is 70.4 MHz/μsec for a mirror rotation rate of 120 Hz. The result is consistent with a simple estimate of $d\nu/dt = -\nu r\omega/L$ where $r \simeq 3$ mm is the offset of the mirror from tube axis, ω is the angular velocity of the mirror, and L is the cavity length.

Using a mechanical shutter in the cavity near the flat mirror at which the laser beam is focused by two lenses to a very small spot, Meyerhofer(46) was able to produce pulses of about the same energy as those obtained with a rotating-mirror technique but at much higher repetition rates up to 5000 pps. The beam size at the focus between two antireflecting coated germanium lenses is about 95 μm so that the shutter-opening time can be minimized to about 700 nsec. By means of appropriate notches cut into the chopping wheel, any pulse repetition rate can be obtained; however, pulse energy will decrease in amplitude (Fig. 44) with decreasing pulse separation.

3. Reactive and Passive Q Switching

An approach that differs from the conventional Q-switching technique, and is known as the "reactive" process for obtaining high repetition rate Q switching in a CO_2 laser, has been described by Bridges(*45*). By moving one of the cavity mirrors along the laser axis at velocities between 16 and 30 cm/sec. he could obtain Q-switched pulses at repetition rates between 30 and 60 kHz in a single transition [$P(20)$ at 10.6 μ] with a width in the order of 1 μsec and an average power about the same as the CW output. To achieve a series of uniform single-transition pulses, the mirror speed must be maintained above 16 cm/sec, as shown in Fig. 45a. At higher speed (> 30 cm/sec) the pulses begin to alternate in size, a large pulse occurring for every complete wavelength of motion, as shown in Fig. 45b. The recovery time between pulses is attributed to the relaxation time of

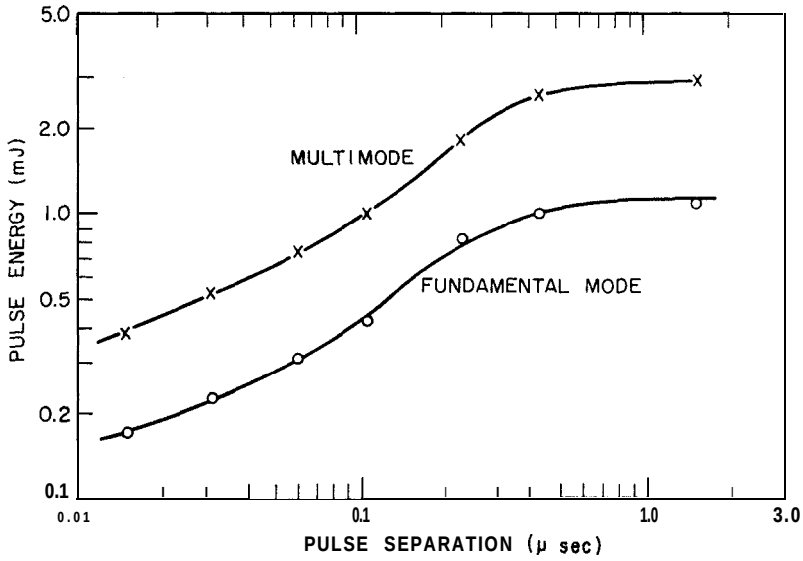

Fig. 44. Measured values of pulse energy as a function of pulse separation. The linear velocity of the mechanical shutter is maintained at a constant value (0.8 x 10^4 cm/sec) in all cases. [After Meyerhofer (*46*).]

the lower laser level. The measured time (~ 30 μsec) between pulses at the onset of a single-line oscillation is consistent with pulse-gain measurements on the lower-laser lifetime (at $P \sim 7$ Torr) made by Cheo (24).

At lower speed (< I6 cm/sec), the situation becomes rather complex. The output pulse spectrum consists of a number of lines during a half-wavelength movement, as shown in Fig. 45c. The pattern repeats itself but the process is subject to hysteresis effects. At slow speeds, the time required to travel a half-wavelength is much longer than the relaxation time of the lower laser level. A quasi-CW operation is maintained therefore, and switching occurs over several lines, owing to conditions more favorable for that particular transition in coincidence with a longitudinal mode at that instant.

Passive Q switching is another technique which can be used to obtain short CO_2 laser pulses by means of a saturable absorber. The first successful operation of passive Q switching in a CO_2 laser, using SF_6 gas as the saturable absorber, was reported by Wood and Schwarz (47). Subsequently similar phenomena were observed by various investigators using other gases, such as formic acid vapor, propylene, heated CO_2 (*48*), vinyl chloride (*49*), BCl_3 (*50*), CH_3F, PF_5 (*51*), CF_2Cl_2, and C_2F_3Cl (*200*). Undoubtedly many more can be found to produce Q-switched CO_2 laser pulses. The requirements for passive Q switching are that the medium must possess a strong absorption

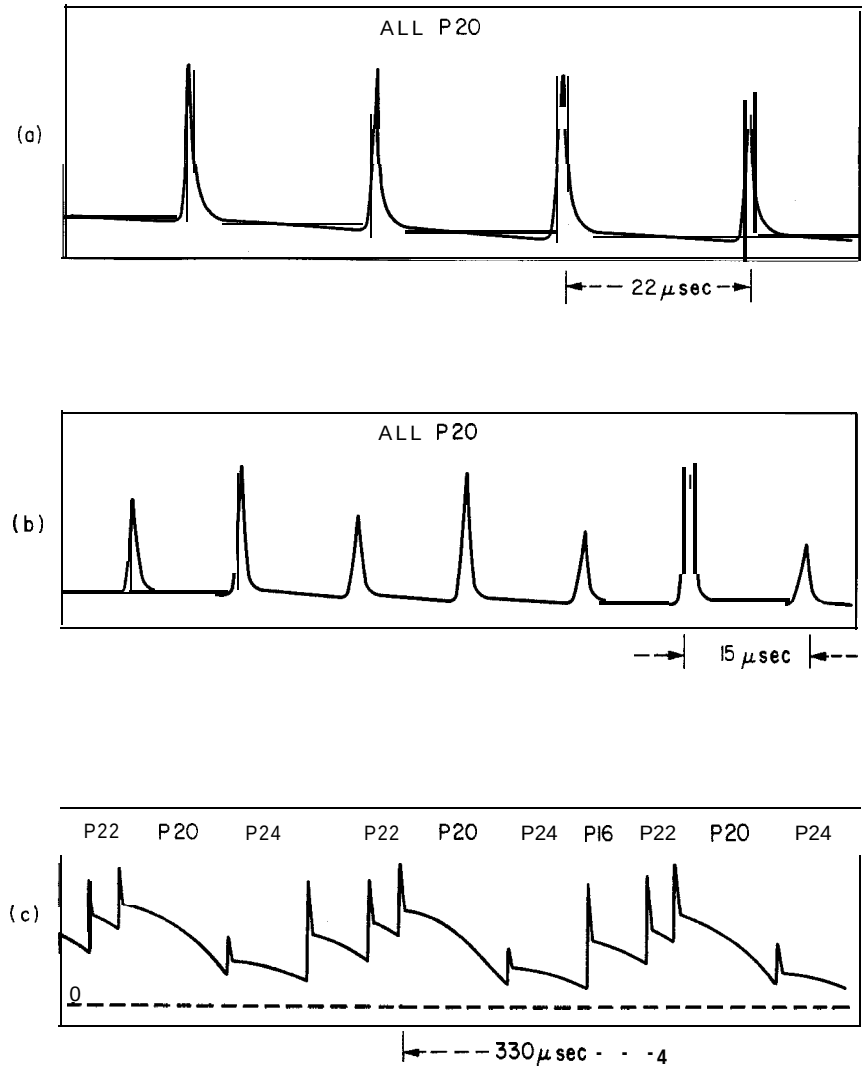

Fig. 45. Typical output of a CO_2 laser with one end mirror moving along the laser axis at the following speeds: (a) 24 cm/sec, (b) 35 cm/sec, (c) 1.6 cm/sec. The time taken for the mirror to travel a half wavelength is indicated. [After Bridges (*45*).]

cross section σ at CO_2 laser wavelengths and a long relaxation time T_1 for the upper state of the absorber so that $I/I_s \gg 1$, where I is the laser intensity and $I_s = h\nu/\sigma T_1$ the saturation parameter. In the case of SF_6, the I_s has a value of a few watts per cm^2 at a pressure of about 100 mTorr. When the absorbing gas is placed inside the laser cavity where I is in the order of 10^2 W/cm^2, bleaching will occur repetitively at a time period (- 500 μsec) corresponding to the collisional relaxation time T_1 of the upper vibrational state of SF_6. The repetition rate can be increased to some extent by the addition of buffer gases such as helium. With the help of a prism or a diffraction grating, the bleaching,

similar to that observed in other laser systems (*201*), can permit a burst of laser radiation at a wavelength in resonance with the absorber. The typical pulse is about 0.5–2 μsec in duration and has a peak power 20-200 times that of the CW output, depending on the gain of the laser medium and the concentration of the absorbing gas. Table 22 gives the performance of passive Q switching by various absorbers. Upon extension of the cavity length to 16.25 m, corresponding to an axial mode spacing of 9 MHz, self locking of a number of longitudinal modes has been observed (*52*) in a CO_2–N_2–He laser with an SF, absorber inside the cavity. However, mode locking of the CO_2 laser had been reported (*53*) earlier through the use of a GaAs intracavity acoustooptic switch as will be discussed in the following section. With the bieachable gas SF_6 inside the cavity, laser pulses as short as 20 nsec, as shown in Fig. 46a, with peak power in excess of 10^4 W have been obtained. The duration of the mode-locked pulses increases with increasing cavity length and decreasing absorber concentration. The fast rise and slower fall of these mode-locked pulse trains cover a period of approximately 1 μsec or longer (Fig. 46b), which is comparable to that of a passive Q-switched pulse. The situation repeats

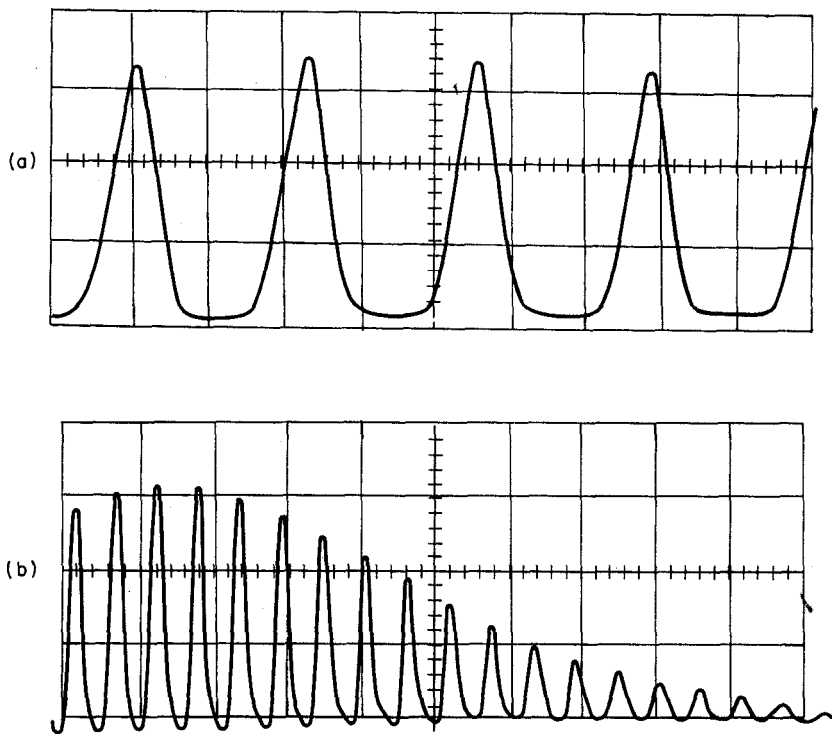

Fig. 46. Oscilloscope traces (reproduced) of mode-locked operation of a CO_2 laser with a cavity length L = 16.25 m. Horizontal scale: (a) 50 nsec/division, (b) 200 nsec/division. [After Wood and Schwarz (*52*).]

TABLE 22

Performance and Operating Characteristics of Passive Q Switching in a CO, Laser by Various Saturable Absorbers

Absorbing gas	Absorber transition	Abs. coef. (Ton--' cm-r)	Cell length (m)	Pressure (mTorr)	Temp (" C)	Laser tube length (m)	Laser transition	Pulsewidth (μsec)	Pulse separation (μsec)	Peak power	Ref.
CH_3F	$Q_{Q(12)}$	0.018	1	15-20	300	1	$P(20)$, 9.6 μ	1-2	40-100	$12P_{CW}$	51
	$Q_{R(4)}$	0.0033	1	40-160	300	1	$P(32)$, 9.6 μ	1-2	40-100	$12P_{CW}$	51
CO_2-propylene			0.75	500–500	450	1	$P(18)$, $P(20)$, 10.6 μ	1-2	18		48
Formic acid			0.2	~500	300	1	~9.2 μ			$\sim P_{CW}$	48
Vinyl chloride		0.01	0.1	2000	300	3.4	$P(18)$, $P(20)$, 10.6 μ	2	20	$4P_{CW}$	49
BCl_3 (He, NH_3, or air)		0.01-0.02	0.2	~1000	300	0.8	P and R branches 10.4 μ		40– 100		50
PF_5		0.02-O. 12	1	5-70	300	1	$P(2)$–$P(38)$, 10.4 μ	0.6-1	150-500	$\sim 50P_{CW}$	51
SF_6		0.1-0.5	0.1	20-50	300	3	$P(18)$–$P(26)$, 10.4 μ	0.4-2	250-450	$\sim 20P_{CW}$	47,49
C_2F_3Cl		0.019	0.25	500	300	2.5	$P(6)$–$P(20)$ $R(22)$–$R(26)$ 9.4 μ	1.8–5	15-40	$\sim 10P_{CW}$	200
CF_2Cl_2		0.076	0.25	20-50	300	2.5	$P(16)$–$P(46)$, 10.4 μ	0.8–3	15-100	$\sim 20P_{CW}$	200

every millisecond. Cavity dumping of a CO_2 laser by means of a bistable Fabry-Perot resonator filled with a saturable absorber (SF_6 gas) has been attempted(202). Preliminary results show that this technique can be used to achieve dumping but requires considerable improvement. Furthermore, passive Q switching and mode locking by use of saturable absorbers coupled with the present cavity dumping techniques do not allow simple control over the operating parameters and consequently the laser output. The most desirable methods are either by acoustooptic or by electrooptic means, which, as discussed below, provide a convenient way to control the shape and repetition rate of Q-switched CO_2 lasers.

4. *Acoustooptic and Electrooptic Q Switching*

Mode locking of a small (4 m long) CO_2 laser corresponding to an axial mode of 36 MHz was first reported by Caddes et al. (*53*), using a GaAs crystal as an intracavity acoustooptic loss modulator. These authors claim that mode locking of as many as five axial modes can be obtained by transferring energy from the fundamental oscillating mode to nearby below-threshold modes by sweeping the frequency back and forth across the oscillating linewidth (FM)-instead of the usual mode-locking operation (AM) by driving the cavity resonance at half the fundamental frequency $c/2L$ as first introduced by Hargrove et al.(*203*). In the AM case, the cavity loss is periodically modulated by the standing acoustic waves at a frequency $\nu_m = c/4L$, causing all excited cavity modes within the atomic linewidth to be phase locked. The observation by Caddes et al. (53) has been analyzed by extending the work on FM of McDuff and Harris(204) to include the effects of saturation. For homogeneous saturation, the ratio of the peak intensity I_p of the mode-locked laser to that of the CW laser I_{CW} is given by(*53*)

$$\frac{I_p}{I_{CW}} = \frac{\left[\left(\frac{\alpha_0}{\ell}\right) - \left(1+\frac{2d}{\ell}\right)^{1/2}\right](1+\gamma)^2}{\left[\left(\frac{\alpha_0}{\ell}\right) - 1\right]\left(1+\frac{2d}{\ell}\right)^{1/2}(1-\gamma)^2} \tag{109}$$

where α_0, ℓ, and d are the small-signal gain coefficient, the unmodulated loss parameter, and the depth of modulation. The parameter γ describing the below-threshold modes is given by(*204*)

$$\gamma = 1 - \left[\left(1+\frac{2d}{\ell}\right)^{1/2} - 1\right]\frac{\ell}{d} \tag{110}$$

Equation (109) is plotted in Fig. 47 as a function of α_0/ℓ. Notice that

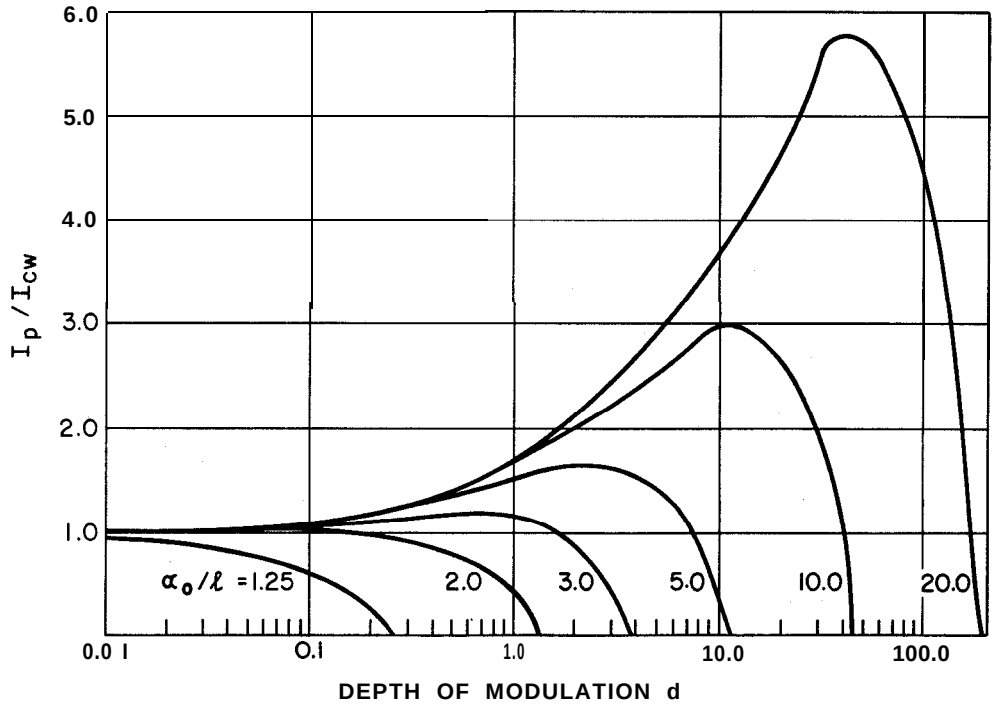

Fig. 47. The calculated intensity ratios of a mode-locked laser to the CW laser as a function of the depth of modulation d for various values of the gain α_0 over loss [parameters (α_0/ℓ). [After Caddes et al. (53).]

an enhancement of 5.7 in peak power from that of CW power is expected for a homogeneously broadened medium with $\alpha_0/\ell = 20$. On the other hand, no peak power enhancement is expected for an inhomogeneously saturated medium (results are not included here). Using a GaAs acoustooptic modulator driven by a quartz transducer at 18 MHz in a 4-m-long CO_2 laser cavity, an attempt was made(53) to produce short mode-locked laser pulses; unfortunately the photoconductive detector used to monitor the laser output did not have the bandwidth to detect the mode-locked pulses directly. However, Caddes et al. (53) were able to obtain beat signals at frequencies corresponding to $c/2L, c/L, \ldots, 5c/2L$. From the measured intensities of the beat signals, the ratio of d/ℓ is found to be 2.5, corresponding to an estimated pulsewidth of 5 nsec. It should be pointed out that the frequency response of a similar detector (SBRC 9145-Sb compensated Ge:Cu) has been shown(192) to have a 3-dB rolloff at 150 MHz, therefore the poor frequency response of the particular detector used in the above experiment is owing strictly to a unique situation of that detector.

In another experiment Bridges and Cheo(56) observed spontaneous self-pulsing in a CO_2 laser without a saturable absorber, using an intra-

cavity GaAs crystal as an electrooptic Q switch. Each Q-switched pulse contains a train of 10 or more 20-nsec pulses with a total duration of ~ 400 nsec in a single $P(20)$ transition in the 10.4-μ band. The switch is capable of dumping any one of the short pulses from the train out of the cavity through an output coupling polarizer, to produce a single output of ~ 10 kW peak power and ~ 20 nsec duration. Figure 48

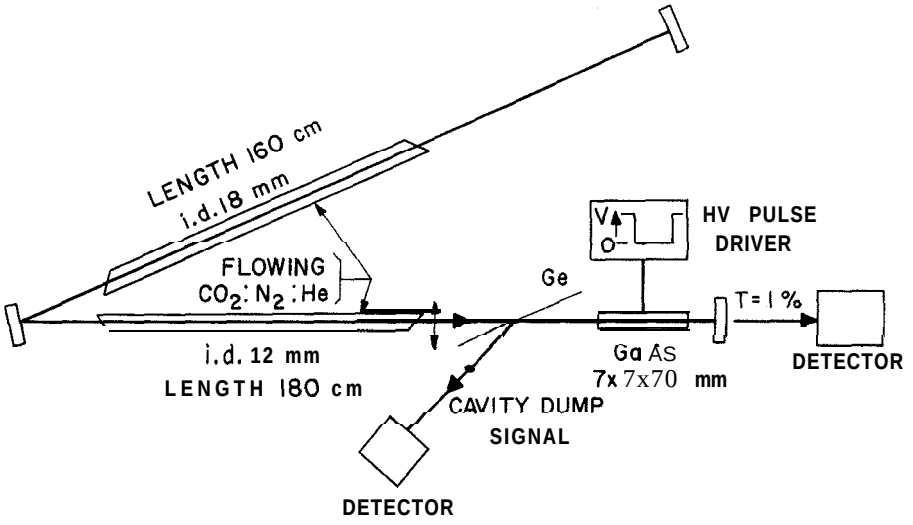

Fig. 48. Experimental arrangement for self-pulsing and dumping in a CO_2 laser with a GaAs electrooptic Q switch.

shows the experimental arrangement. The laser cavity consists of two discharge tubes filled with a flowing gas mixture of CO_2-N_2-He, a Brewster-angle Ge plate polarizer, a GaAs electrooptic crystal, and two end mirrors (one a totally reflecting mirror with **IO-m radius of** curvature and the other a plane mirror with 1% transmittance). Two cavity lengths, 5.5 and 8.2 m, were used in this study. The total available single-pass small-signal gain was 15 dB at 10.6 μ. Because of optical inhomogeneities in the GaAs, the net gain **was considerably** lower than this value, but the exact amount was not measured. The crystal, when suitably pulsed in conjunction with the polarizer. provided Q switching and cavity dumping. Similar arrangements have **been** used for solid-state lasers (205).

A spark gap pulser produced the switching voltages. During the **qui** escent phase, 5.5 kV dc was applied to the GaAs (7 **x** 7 **x** 70 mm) converting the normally isotropic crystal into a quarter-wave plate. The combination of biased crystal and polarizer prevented oscillation **by** introducing a large coupling loss to the resonator. The Q switching was achieved by pulsing the voltage to zero in less than 10 nsec

(10–90%). The coupling loss was then reduced to the 1% of the plane mirror. Output signals were detected with a GE: Cu: Sb photoconductor and a Tektronix-454 oscilloscope, with a combined time response of ≈ 2.7 nsec, which is limited primarily by the rise time of the scope. A typical signal observed at the slightly transparent end mirror is shown in **Fig.** 49(a). Following the Q switch, after a delay of ≈ 100 nsec, a

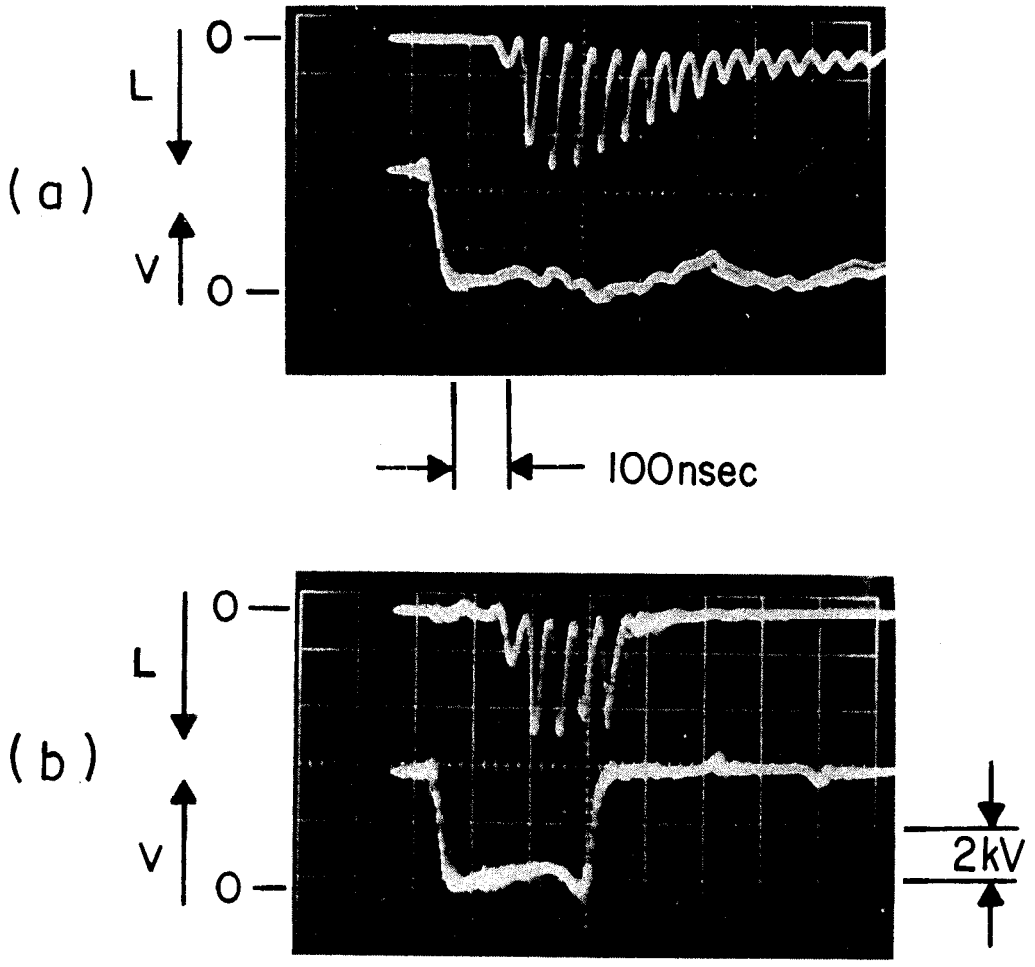

Fig. 49. Oscilloscope traces of the self-pulsing waveforms in a CO_2 laser as observed from the partially transmitting plane mirror (t = 1%). (a) The cavity Q is suddenly switched on by a GaAs electrooptic intracavity modulator. (b) The cavity Q is switched on and then switched off in a time approximately 250 nsec. Cavity length = 5.5 m; horizontal scale: 100 nsec/cm.

train of 10 or more short 20-nsec pulses is seen, rising to a peak intensity after ≈ 250 nsec and falling gradually to zero in about 500 nsec. This envelope is comparable to the single long (> 200 nsec) pulse typically obtained with other types of Q switching. The period between

the short pulses was the round-trip transit time in the resonator, about 37 nsec for the 5.5-m and 55 nsec for the 8.5-m resonator. The pulses were locked to the voltage pulse and were stable and repetitive from one Q-switch even to the next. Tests with a spectrometer showed that the output under these conditions consisted of only the strongest, $P(20)$, vibration-rotation line.

It was noticed that the pulse train appeared only when the oscillation built up to its peak in less than ≈300 nsec. The buildup time t_b was minimized by the use of small external coupling during the Q-switching phase, and by careful adjustment of the resonator. A sharp minimum in t_b was observed as the mirrors were brought into correct alignment. Cavity length tuning also varied t_b periodically, the behavior repeating with each half-wavelength displacement of the mirror. Close to the optimum points, $P(20)$ pulse trains were noted, while at intermediate points the oscillation built up in a much longer time (> 500 nsec) and consisted of several lines with no rapid pulsing. Related effects were noticed with length tuning in CW CO_2 oscillators. The optimum adjustment corresponds to the best coincidence between resonator modes and the strongest line, P(20). The oscillation on P(20) then builds up rapidly and, because of strong collisional coupling(26,27), takes precedence over other lines. The decay of the pulses after the peak is attributed to depletion of the vibrational inversion.

During the period preceding pulsing, a dc bias voltage is applied to the GaAs intracavity electrooptic Q switch which spoils the cavity Q. When the bias voltage is switched off, radiation builds up to its peak from the noise after about six round-trip passes (see Fig. 49). By pulsing the dc voltage on again in a time within ~ 10 nsec of the peak of oscillation, the resonator energy could be dumped via the germanium polarizer. After dumping, the Q is again spoiled and oscillation ceases. Without spontaneous self-pulsing, the dumped pulsewidth would equal the round-trip transit time of light in the resonator with a square-topped pulse shape as shown in Fig. 38a. When spontaneous pulsing was present and reapplication of the dc voltage occurred at a null between pulsations, a single short laser pulse of about 25-nsec duration and about 10-kW peak power was obtained as shown in Fig. 50a. When voltage was reapplied near a peak of the pulsation rather than near a null, a split pulse output was obtained as shown in Fig. 50b. The output power, coupled from the 1% transmitting mirror when dumping occurred, is shown in Fig. 49b. Optical inhomogeneities in the GaAs reduced the power output considerably from that potentially available. By replacing the 1% transmitting mirror with a diffraction grating, a short cavity-dumped CO_2 laser pulse from any one of the transitions

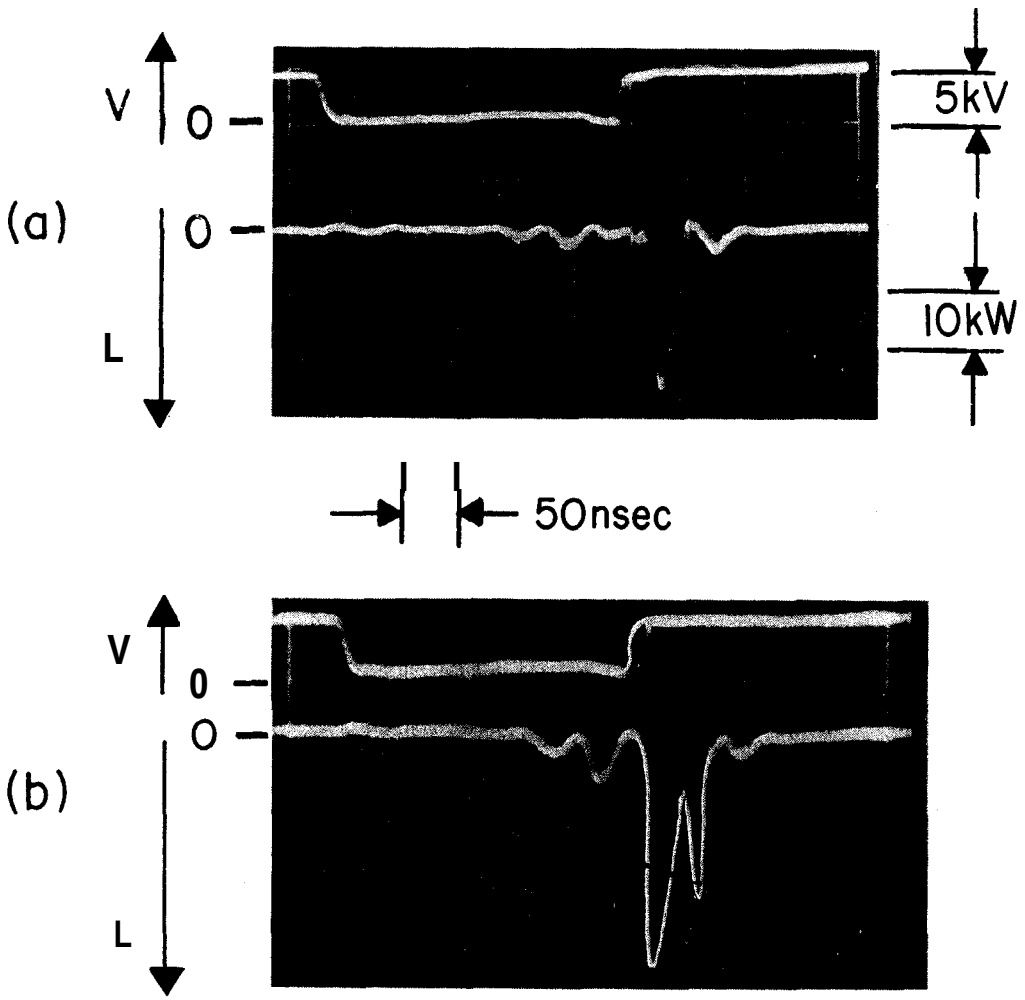

Fig. 50. Oscilloscope traces of a cavity-dumped CO_2 laser pulse coupled out of the cavity from the germanium polarizer. (a) Dumping occurs at a null of pulsations (cavity length = 5.5 m), (b) Dumping occurs near the peak of pulsations, resulting a split pulse (cavity length = 8.2 m). Horizontal scale: 50 nsec/division.

$P(14)$ to $P(30)$ of the 10-μ and 9-μ bands, with a 180-cm-long CO_2–N_2–He flowing-gas discharge tube, has been obtained as shown in Fig. 38a. Pulses from the R branch of both bands also can be obtained, but the number of rotational lines is reduced.

Since no saturable absorber was present during observation of self-pulsing, it was concluded that the effect results from nonlinear saturation phenomena in the laser medium itself. Spontaneous self-pulsing of this type has been previously reported for other gas lasers (*206*), and has been explained in terms of phase locking of a number of longitudinal modes, or in terms of a π pulse circulating in the resonator (207, 208) These may be considered equivalent interpretations of the same phenomenon in the frequency and time domains, respectively. The

observations will be compared with the circulating pulse picture as follows.

It was previously assumed(207) that the circulating pulse duration (τ) had to be less than T_2 (the average molecular dephasing time). This is believed to be an unnecessary restriction and the short pulse train, where $\tau = 8T_2$ [Ref. (31)], also can be described as π pulses. In the closely related problem concerning the buildup of a steady-state π pulse in a homogeneously broadened amplifier, theory(208) shows that the pulse duration is unrestricted and depends not only on T_2, but also on the gain and loss parameters of the system. The definition of a π pulse (for linear polarization), independent of pulse length is

$$\pi = \frac{\mu}{\hbar} \int_{-\infty}^{+\infty} \mathscr{E}\, dt \tag{111}$$

where μ is the dipole moment and $\mathscr{E}$ is the electric field amplitude of the pulse. Assuming that similar considerations apply to the oscillator, we can now compare the experimental results(56) quantitatively with the circulating v-pulse theory. From Eq. (111) the electric field strength required for a π pulse can be calculated using a graphical integration of the observed pulse shape. The value of $\mu/\hbar$ is derived from the measured (30) value (5 sec) of the 001-100 transition lifetime. The calculated peak field strength is 1.4×10^5 V/m corresponding to a power density of 2.4 kW/cm². Estimating the average beam diameter (multimode) as 1.5 mm and the peak power of the strongest pulse as 10 kW gives an actual peak field strength 1.5 times the calculated values for the π pulse. This is close enough to be significant in view of the approximate nature of the theory, which neglects diffraction, variation of field strength across the beam, and cross-relaxation effects.

As mentioned previously, the observed laser pulses were synchronized with the switching pulse. Recent computer simulation studies showed how spontaneous pulses can build up from noise(209) or from a small Gaussian disturbance(210). In the experiment with an electrooptic switch, the pulse builds up in a similar way from a "noise step" produced when the GaAs switch is turned on. About six round trips are required for this initial disturbance to build up to peak oscillation. The major difference between this experiment (56) and previous studies with a rotating mirror is that the electrooptic switch has a switch-on time less than the round-trip transit time. The recovery (in ~37 nsec) of population inversion (pumping) between the short pulses can be accounted for by the rapid transfer(26,27) of the rotational energy from other rotational states to the oscillating rotation-vibration level.

5. High-Power Pulsed Radar Systems

As discussed previously, high-power pulsed CO_2 laser output can be obtained from a high-pressure gas ($P > 50$ Torr) breakdown by using very high voltage at E/P values ranging from 12 to 70 V/cm Torr. Laser outputs under these conditions have very high energy (on the order of several joules per pulse) from a relatively compact system, but are very unstable. Therefore, it is not suitable for certain applications, such as in communication and pulsed Doppler radar systems. Work toward the development of a high average power (> 1 kW) IR radar system to be installed at the optical radar facility (*92*) of Lincoln Laboratory in Westford, Massachusetts was begun in 1967 almost simultaneously at Raytheon(64) and at Hughes Research Laboratories (65) in Malibu. The coherent laser source at 10 μ offers several advantages over conventional microwave radar systems in terms of beam divergence, large backscattered cross sections at optical frequency (*211*), jamming, and other interference effects. The transmitter was designed for signal processing at low signal-to-noise ratios backscattered from a moving target over periods of between 10 to 100 μsec, depending on the nature of the target. The Doppler frequency-shifted signal is detected by heterodyning with that of the transmitted pulse, which must be maintained at a constant and stable frequency with a well-defined wavefront at the transmitting plane. The most straightforward way to achieve these requirements is to use a low-power frequency-stabilized oscillator whose output pulse train is subsequently amplified through a sequence of laser amplifiers.

Figure 5 1 shows the design of the 1 -kW transmitter. A 25-W, single-mode output from a small CW oscillator is collimated by an array of reflectors and first directed through two stages of amplification to yield a maximum output of 400 W. This output is then modulated by a mechanical chopper at high repetition rates (up to 12 kHz) using a focusing technique similar to that described in Section V.E.2. These rectangular pulses of $\gtrsim 0.2$ mJ energy are then directed into the 50-m-long power amplifier with a small-signal gain of ~ 60 dB, a value chosen to avoid self-oscillation. At each end of the four-power amplifier sections, irises are used to minimize off-axis scattering. The folded amplifier-tube design is similar to those described in Section V.D.2. The performance of this transmitter is shown in Fig. 52. The average output power reaches 1 kW at a pulse repetition rate above 7 kHz, and continuously increases toward the equivalent CW level near 1400 W if the mechanical modulator is removed from the system. When operated in multimode oscillation, this system is capable of delivering an output

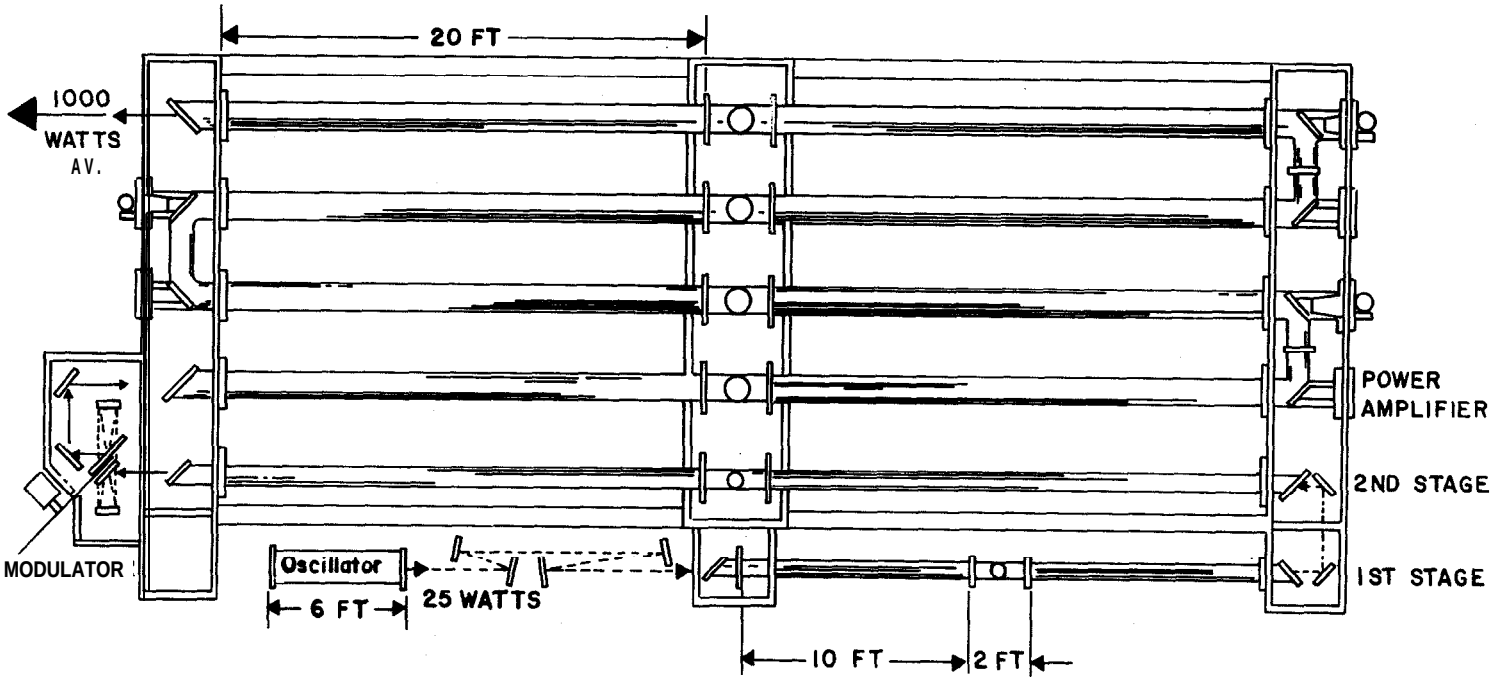

Fig. 51. Design of a 1-kW transmitter, which consists of a single-mode 30-W (CW) laser oscillator, first- and second-stage simplifiers, the modulator section, and the power amplifier section. [After Miles and Lotus(64).]

CW power in excess of 2.5 kW. The "self-oscillation background" line (in Fig. 52) refers to the spurious oscillations in the power amplifier. This is caused mainly by diffuse scattering from the mechanical chopper blade during the quiescent phase of operation. However, these spurious oscillations can be suppressed at pulse-repetition rates above 5 kHz. A test of beam divergence in the focal plane showed that the angular spread is less than 3×10^{-4}, 6×10^{-4}, and $1 0^{-3}$ rad at respective CW power levels of 100, 200, and 500 W. In this system, there is a considerable amount of backscattered signals from various optical components within the first two amplifying stages and in particular from the chopper blade; therefore, for heterodyne detection of weak return signals this spurious noise in the output channel must be reduced by either an efficient isolator between the oscillator and the amplifier array or replacement of the mechanical shutter with an electrooptic switch.

VI. Novel Laser Systems

Previous sections dealt mainly with conventional CO_2 laser systems, employing the usual electrical discharges in either a nonflowing or a low-speed longitudinal flowing gas mixture. For these systems, considerable advances have been made during the past few years both in the understanding of the physical processes involved in various lasing materials and in their optimum performance. Continuous-wave power as high as 8.8 kW(212) with efficiency of $\sim 25\%$, Q-switched pulses of $\gtrsim$ 0.2 MW peak power(*213*,*214*), and a single-pass unsaturated gain of 7.8 dB/m(*35*) have been achieved. On the other hand, concentrated effort has been placed on the development of various novel laser systems with the aim of producing high average power ($\gtrsim$ 1 kW) from a small and compact laser system by means of nonconventional approaches, for example, systems employing either a continuous transverse flow at supersonic speed(*82*,*87*), or a sudden expansion of hot gas through a nozzle in a shock tube(*215*). The concept of utilizing thermal pumping and rapid adiabatic cooling for production of population inversion in CO_2 molecules was first introduced by Basov et al. (78) as early as 1966. Experimental results on these systems are in general not available, and information which recently appeared in literature(*87*,*214*) are of a preliminary nature. However, experiments with transverse flow at subsonic speeds have shown that high power(86) and gain(159) can be obtained from a relatively compact laser system. Other ap-

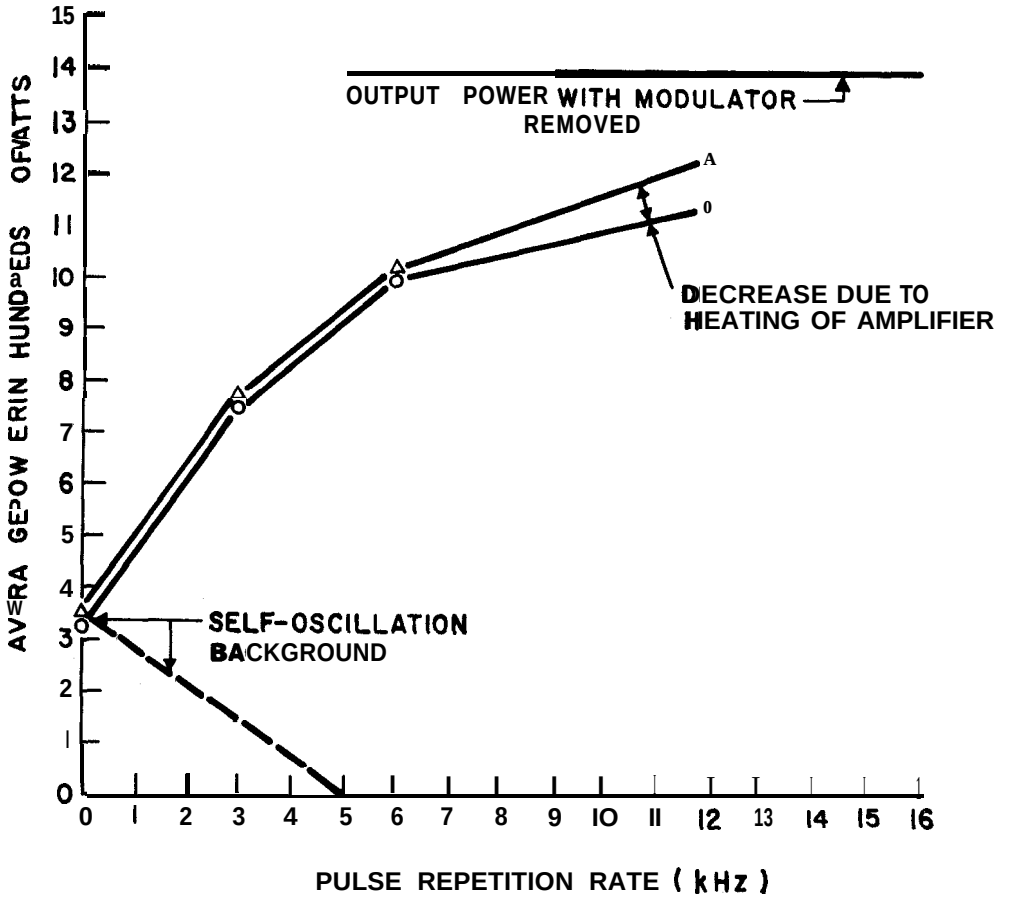

Fig. 52. Measured average power output of the transmitter shown in Fig. 51 versus repetition rate of the 10-μsec CO_2 laser pulse train. [After Miles and Lotus (*64*).]

proaches involving chemical(83,216) and thermal(77-82) pumping also have led to some significant advances.

The basic principles of a high-speed transverse-flowing-gasdynamic laser are based on differences in relaxation times for energy levels in the subsystems and the exchange rates of internal energies to translational temperature in the lasing medium. The rapid cooling of the translational temperature of the gas by sudden expansion or high flow rate is particularly important for thermally pumped lasers. Relatively high speed is also essential for chemically pumped lasers because reactions which are suitable for laser action are time dependent, and the chemical species are controlled by the gas flow. In the following a brief discussion of the physical mechanisms involved in each of these novel systems is given, and results on their performance under various experimental conditions are presented.

A. HIGH-SPEED SUBSONIC GAS FLOW

1. *Transverse Flow*

An analysis of power output and gain saturation characteristics of an idealized high-speed transverse-flow laser has been made by Cool (85). The assumption is made that the pumping process (electric discharge, flame, or vibrational energy transfer from various excited metastables of diatomic molecules such as N_2, DF, HCl, HBr, and HI) which establishes an upper laser level population occurs in the region located upstream before the gas enters the laser cavity. Laser action takes place within an optical cavity downstream where the vibrational relaxation occurs but excitation ceases with the exception of a resonant transfer from the metastables. Figure 53 describes the coordinates used

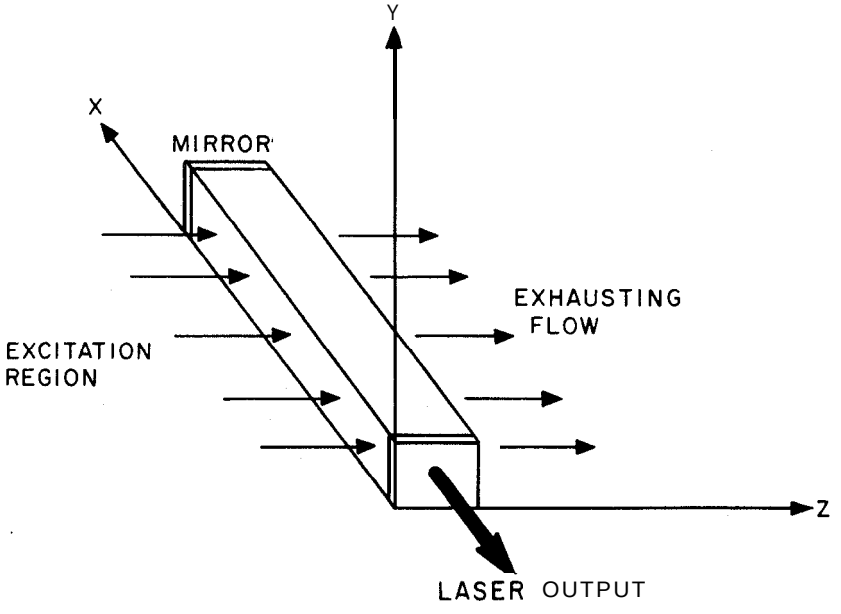

Fig. 53. Schematic diagram of a high-speed flow laser with the optical axis transverse to the gas flow. [After Cool (*85*).]

in the analysis. The gas flow is in the positive Z direction between two cavity mirrors which are aligned perpendicular to the X axis, and in this region ($Z \geqslant 0$) excitation is completed and the vibrational populations decay primarily by collisions and by stimulated emission within the laser cavity. A simple kinetic model (Fig. 54) as proposed by Moore et al. (*25*) is used by lumping a group of strongly coupled asymmetric vibrational states 00^0n, where n = 1.2, . . . , as the common upper laser level (designated by group 2), and similarly by combining a group

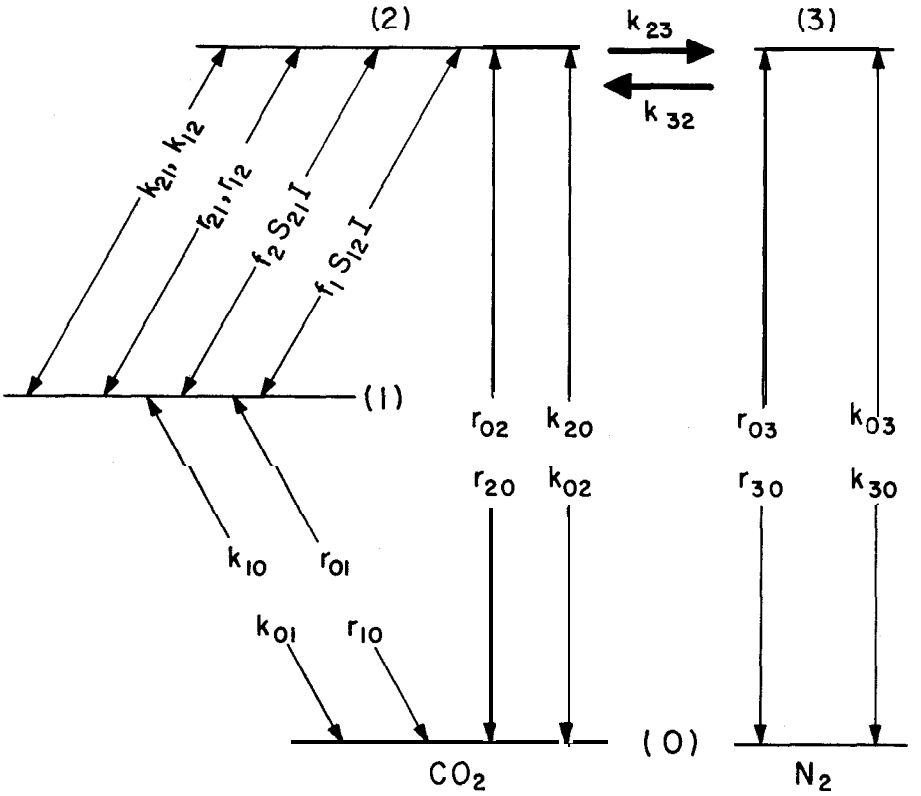

Fig. 54. Rate-controlling processes in a CO_2 laser. Groups 1 and 2 represent the collective lower and upper laser levels. Group 3 represents the excited metastables such as N_2, DF, HCl, etc.

of closely coupled states, i.e., 10^00, 02^00, 02^20, and 01^10 as the lower laser level (denoted by group 1) Group 3 represents the metastables of diatomic molecules with vibrationally excited states up to $v = 4$ that are strongly coupled to the $v = 1$ state through a rapid intramolecular $V \rightarrow V$ process. The energy stored in group 3 is subsequently transferred to group 2 via the resonant exchange process, as described by Eq. (33) for the case of a CO_2–N_2 mixture. Therefore the number densities n_2 and n_3 of the respective groups 2 and 3 quickly reach an equilibrium through the coupled equations

$$\frac{dn_2}{dt} = -\frac{dn_3}{dt} = k_{32}n_3 - k_{23}n_2 \tag{112}$$

where k_{32} and k_{23} are related by

$$k_{32} = k_{23} \exp\left(\frac{E_{N_2} - E_{CO_2}}{kT}\right) = 0.914\ k_{23} \tag{113}$$

The measured value (25) for k_{32} is 1.9×10^4 Torr^{-1} sec^{-1}. The rate equations describing the intramolecular coupling between groups 0, 1, and 2 are given by

$$\begin{aligned}
\frac{dn_0}{dt} &= -(r_{02} + r_{01})n_0 + r_{20}n_2 - k_{10}n_1 \\
\frac{dn_1}{dt} &= r_{21}n_2 + r_{01}n_0 - k_{10}n_1 + k_{21}n_2 + \mathrm{SI} \\
\frac{dn_2}{dt} &= r_{02}n_0 - r_{20}n_2 - (r_{21} + k_{21})n_2 - SI
\end{aligned} \tag{114}$$

where the rate coefficients are defined in accordance with those indicated in Fig. 54; $r_{ij} \equiv$ excitation or deexcitation rates from ith to jth level; k_{ij} are the effective or over-all relaxation rates of these groups, and SI is the stimulated emission rate which connects the upper and lower laser levels as

$$\mathrm{SI} = (x_2 S_{21} n_2 - x_1 S_{12} n_1) I \tag{115}$$

where S_{12} is the line strength of that transition as given by Eq. (69), x_1 and x_2 are mole fractions of molecules in group 1 and 2, respectively, and I is the stimulated photon energy flux within the cavity, expressed in W/cm^2. These equations provide the initial population inversion in the upstream region. As the fluid enters the cavity, only vibrational relaxation processes occur ($Z \geq 0$) and the relationships determining the performance of the high-speed transverse-flow laser can be derived from the continuity equations for the number densities of these groups of vibrational states. For a one-dimensional isothermal flow with a uniform constant velocity U, Cool (85) obtained a set of equations describing the relaxation behavior within the laser cavity as

$$\begin{aligned}
U\left(\frac{\partial n_3}{\partial Z}\right) &= -k_{30}n_3 - k_{32}n_3 + k_{23}n_2 \\
U\left(\frac{\partial n_2}{\partial Z}\right) &= -k_{21}n_2 - k_{23}n_2 + k_{12}n_1 + k_{32}n_3 - \mathrm{SI} \\
U\left(\frac{\partial n_1}{\partial Z}\right) &= k_{21}n_2 - k_{12}n_1 - k_{10}n_1 + k_{01}n_0 + SI \\
U\left(\frac{\partial n_0}{\partial Z}\right) &= k_{10}n_1 - k_{01}n_0 - k_{32}n_3 + k_{23}n_2
\end{aligned} \tag{116}$$

where the rate constants are the same as those defined in accordance with Fig. 54. In Eqs. (116), the relaxation rate k_{03} and spontaneous emission processes have been neglected during the relaxation period.

Also the population densities n_i and stimulated emission term SI are the total average values within a cavity of length L along the X axis. From Eqs. (116) one obtains an oscillation condition relating to the relaxation processes in a steady flow as given by(8.5)

$$\mathrm{SI} + U\lambda\left(\frac{dS}{dZ}\right) = d_2(k_{32}n_3 - k_{23}n_2) + d_1(k_{10}n_1 - k_{01}n_0) - (k_{21}n_2 - k_{12}n_1) \tag{117}$$

where

$$\lambda = (x_1S_{12} - x_2S_{21}), \qquad d_1 = \lambda x_1 S_{12}, \qquad d_2 = \lambda x_2 S_{21} \tag{118}$$

From Eq. (117), we see that contributions to the population inversion are provided by the first (resonant transfer to group 2) and second (collisional relaxation of group 1) terms on the right-hand side. The last term represents the dissipative effect owing to a direct collisional coupling between groups 1 and 2. The solution of Eqs. (117), for a special case of constant mirror reflectances, yields the following relationship:

$$S = \frac{S_0}{(1 + I/I_S)} \tag{119}$$

where

$$S_0 I_S = C_1 \exp\left[\frac{-\alpha(1+\beta)Z}{U}\right] + C_2 \exp\left[\frac{-\alpha(1-\beta)Z}{U}\right] + C_3 \tag{120}$$

and

$$I_s = C_4 \exp\left[\frac{-\alpha(1+\beta)Z}{U}\right] + C_5 \exp\left[\frac{-\alpha(1-\beta)Z}{U}\right] + C_6 \tag{121}$$

with constants C_i, a, and β expressed in terms of various rate constants. The quantity I, is the local saturation parameter at Z, and $h\nu S_0$ is the unsaturated gain at the optical frequency ν. Since the inversion density is a function of Z, it is also practical to use a nonuniform reflecting mirror R(Z). The total laser power output P_ℓ per effective cavity volume V can be obtained by integrating Eqs. (120) and (121) over the cavity width W along the flow as

$$\frac{P_\ell}{V} = \frac{h\nu U}{W}\left(\frac{t}{a+t}\right)\left[\int_0^{W/U} S_0 I_s d\xi + \frac{\ln(1 - a - t)}{h\nu L}\right]_0^{W/U} I_s d\xi \tag{122}$$

where $\xi \equiv Z/U$, a, and t are dissipation loss and transmission coefficients of the laser cavity. Figure 55 shows the dependence of the local saturation parameter I_s along the flow direction Z as calculated

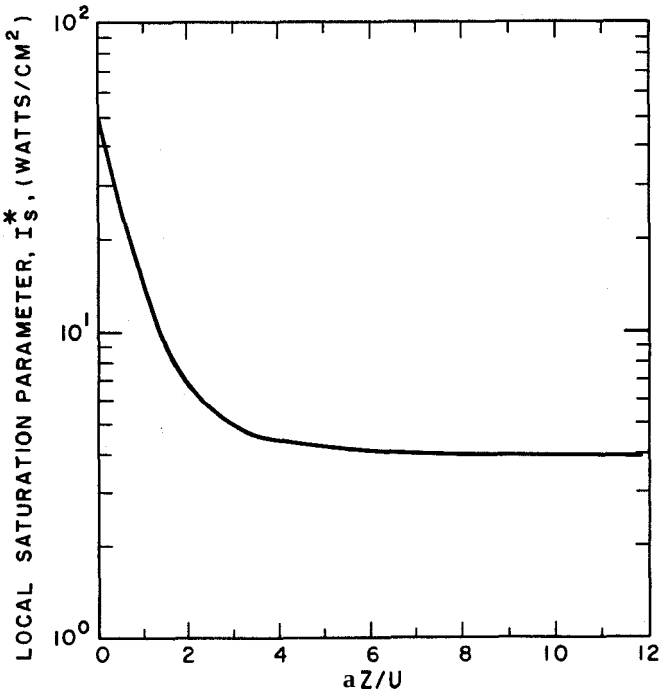

Fig. 55. Calculated local saturation parameter I, as a function of $\alpha Z/U$, where $\alpha = 1.36 \times 10^4\ \text{sec}^{-1}$, Z is the distance along the direction of gas flow, and U is the fluid velocity. [After Cool (*85*).]

from Eqs. (120) and (121). The initial value $I_s(0)$ is determined mainly by the transfer rate constant k_{32}; further downstream, I_s is primarily limited by the $V \rightarrow T$ relaxation rate of level 1 characterized by the rate constant k_{10}.

The optimized laser output coupling t_m can be obtained from Eq. (122) by setting $\partial P_\ell / \partial t = 0$. The optimum coupling parameter S_m is given by

$$S_m = -\frac{1}{h\nu L} \ln (1 - a - t_m) \tag{123}$$

Equation (123) yields the maximum power outputs for given values of L/a. The total radiation energy per optimum cavity volume HW_mL is given by

$$E = h\nu \int_0^{W_m/U} \text{SI}\, d\xi \tag{124}$$

and the total laser output per optimum cavity cross-sectional area HW_m is shown in Fig. 56 for $a = 0.04$ as a function of the cavity length L. The results of Figs. 55 and 56 were obtained by using rate constant measurements, most of which were made in an absorption cell (*25*)

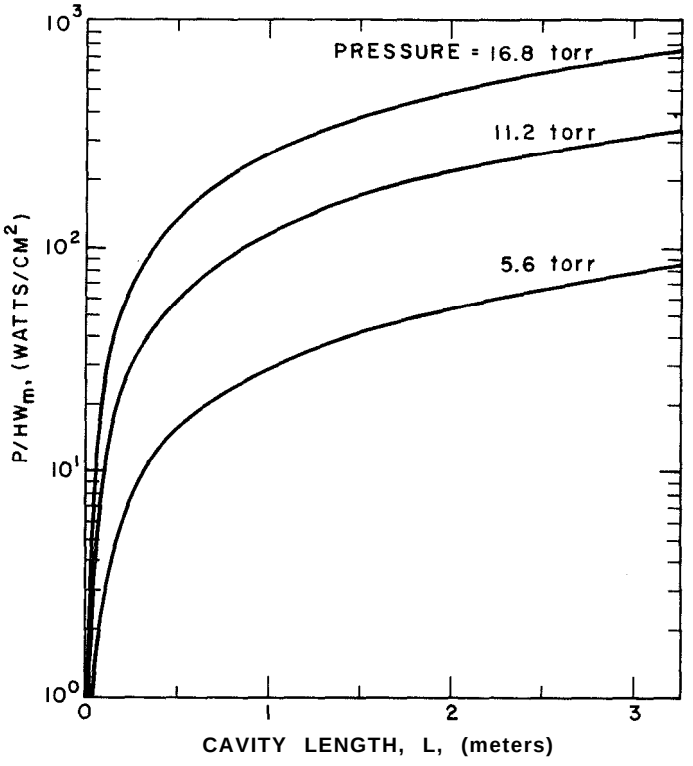

Fig. 56. Calculated laser output per effective cavity cross-sectional area (P/HW_m) as a function of the cavity length L. [After Cool (85).]

near room temperature and employing a laser system(85) with relatively low gain coefficient $\alpha = (1/I)(\partial I/\partial X) = 5.5\ \mathrm{m}^{-1}$. These values can vary substantially from one laser system to another depending upon the experimental conditions, such as gas flow rate and temperature. In addition. the treatment of gain saturation and power output, as discussed in Section V. B, must take into account the cross relaxation and diffusion effects. Despite these uncertainties the calculated results of Figs. 55 and 56 indicate some interesting characteristics of the high-speed flowing CO_2 gas laser, namely:

(a) The power output is directly proportional to the flow velocity U.

(b) The ratio of optimum laser output to cavity volume varies as the square of the gas pressure, provided that the gas temperature and mixture are fixed and a constant percentage of excited molecules is maintained.

(c) The localized power output and saturation parameter decay exponentially in two stages with increasing Z. The initial decay is characterized by a time constant associated with the rate of energy transfer to the upper CO_2 laser level, and the second stage overlaps the first and

has a time constant associated with the relaxation rate of the lower laser level.

(d) For high speed flow, where flow transit time is short compared with the buildup time for the boundary layer and molecular diffusion time, the gain is independent of the Y coordinate and the power output is directly proportional to the cavity height.

Almost concurrently Tiffany et al. (*86*) have obtained a very impressive CW power output in excess of 1 kW from a self-contained CO_2 laser with 1 -m active length, by using a recirculated forced-convection flow of a CO_2–N_2–He mixture transverse to the optical cavity. The major difference between this experiment and the above theoretical model is that the electrical discharge is used in the laser cavity. The flow velocity U used in this experiment is above 30 m/sec corresponding to a transit time across a few centimeters of active region within the lifetime of the upper laser level. Since gas cooling in a transverse-flow laser does not depend upon a diffusion process, higher gas pressure can be used, thus providing higher gain and power output. Figure 57 shows the power output for several gas mixtures as a function of electrical input power to the discharge. For a gas mixture of 2 Torr CO_2, 11 Torr N_2, and 5 Torr He, an output in excess of I kW/m in a beam of 40 mm diam can be coupled out of the cavity through a 35% transmitting

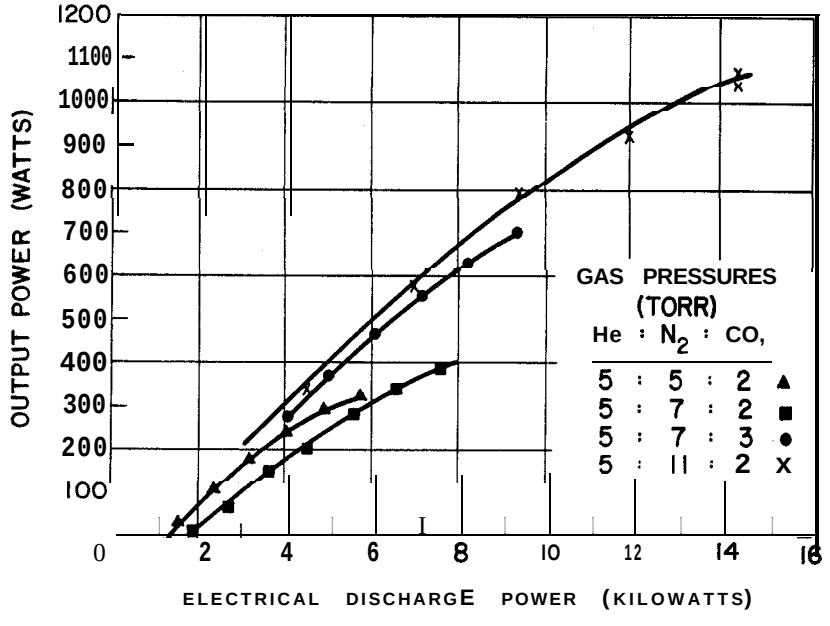

Fig. 57. Measured CO_2 laser output (CW) power for several gas mixtures as a function of electrical input power in a high-speed (- 30 m/sec) transverse-flow laser. [After Tiffany et al. (*86*).]

Ge mirror at an input electrical power of 14 kW. This corresponds to an efficiency of about 7%. The large amount of working gas (- 4000 ft^3/m) is recirculated in a closed cycle by a blower and a heat exchanger at a total power consumption of about 200 W.

Subsequently, measurements on gain and saturation parameter have been made (*159*) in a l-m-long subsonic transverse-flow laser amplifier using a stable low-power laser as the input signal source, with a beam diameter of 6 mm. Figure 58 shows the small-signal gain of the transverse-flow laser amplifier as a function of distance downstream (in the

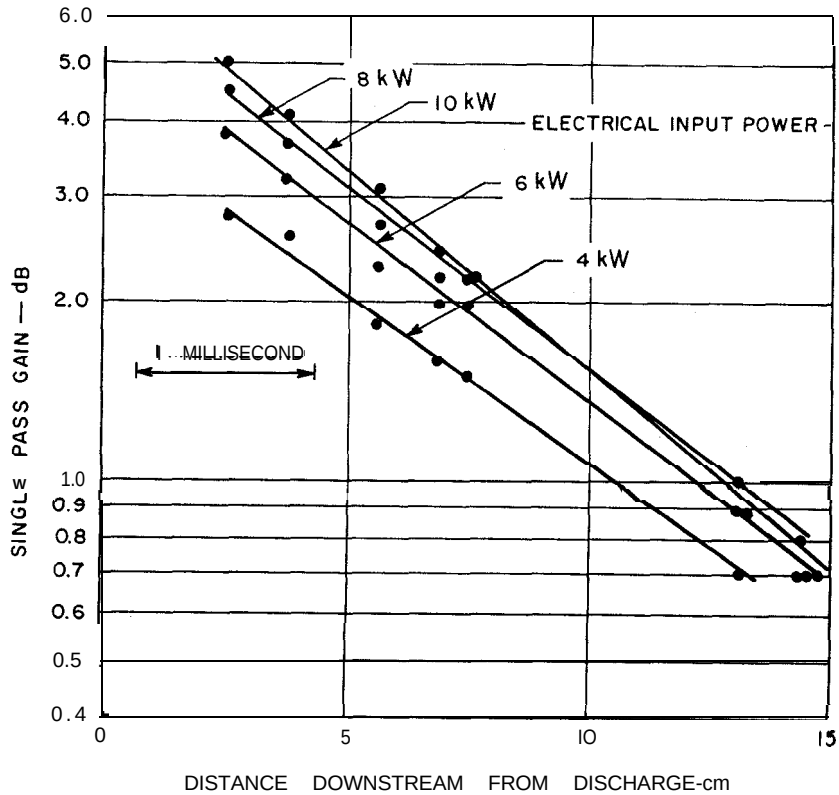

Fig. 58. Measured small-signal gain (dB) as a function of Z, the distance (cm) downstream from the electrical discharge at various input power levels in a high-speed (- 35 m/sec) transverse-flow laser. [After Targ and Tiffany (*159*).]

flow direction) from the discharge region for a number of input electrical power levels. The gas-flow velocity in this case is 35 m/sec and gas mixture consists of 2 Torr CO_2, 11 Torr N_2, and 5 Torr He. Results show that the gain decreases exponentially with increasing distance from the excitation region and drops to its $1/e$ value at a length of about 7 cm which corresponds to a time constant of about 2 msec, consistent with the collisional relaxation time of the upper CO_2 laser level. The

measured gain (*159*) and power output (86) dependence on gas pressure, flow velocity, and distance Z downstream are only in qualitative agreement with those characteristics as predicted by the theory(85). From the measurements of the small-signal gain (7.6 dB/m) in the discharge region and the corresponding power output (1 100 kW) that can be coupled out through a 35% transmitting mirror under the same experimental conditions, a gain saturation value of 246 W/cm² has been estimated(86) for the transverse-flow laser. Clearly this laser system represents one of the most significant advances in the CO_2 laser in recent years, and undoubtedly more information and an improved theoretical model about this system will soon become available.

Recently Buczek et al.(221) have reported a transverse flowing, magnetically stabilized CO_2 laser. Premixed gas flows through a rectangular channel transverse to the axis of a cylindrical discharge. If the discharge is unstabilized, the perpendicular gas flow forces the discharge to assume a curved path between the electrodes. However, by application of a transverse magnetic field the discharge can be forced back into a straight line coincident with the optical axis of the oscillator.

2. *Longitudinal Flow*

High CW power (140 W at about 10% efficiency from a IO-cm-long discharge tube) has been obtained from high pressure (10– 120 Torr) and high-speed (several hundred meters/sec) flowing CO_2–N_2–He lasers, although the direction of gas flow is along the optical axis. In a similar experiment, Brown and Davis (*222*), obtained a power output of 2300 W at 13% efficiency in a l-m by 3.8-cm discharge. The laser configuration is shown in Fig. 59. A water-cooled copper drift section about 30 cm in length is attached to the discharge tube and provides a continuous transfer of energy from N_2 (v = 1) to CO_2 molecules. Actually, for this purpose the drift section is much longer than needed, because, at the pressures used in this experiment, the vibrational transfer time is of the order of a few microseconds, corresponding to about l-cm path length at the maximum pumping speed of the system. The same laser device was used also in another experiment by injecting CO_2 about 10 cm downstream from a N_2–He discharge section. This scheme produced a CW output of 98 W at 1 1.7% efficiency, but required a higher flow rate (by a factor of about four) for CO_2 gas than for CO_2 injected directly into the discharge region. The measured values for saturation parameter varied from about 40 W/cm² at low pressure (- 10 Torr) to about 600 W/cm² at high pressure (- 100 Torr). The increase in gain saturation at higher gas pressure

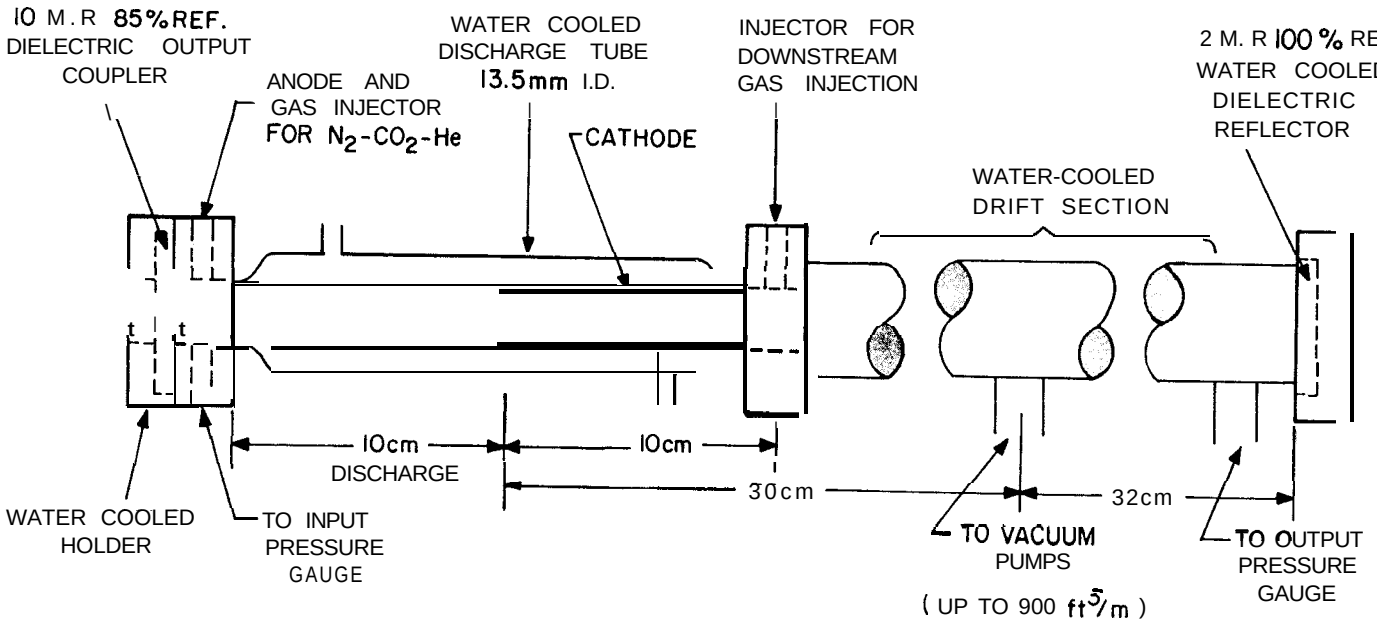

Fig. 59. Design of a high-pressure longitudinal-flowing laser tube. [After Deutsch et al. (*89*).]

is owing primarily to an increase in the relaxation rate of the upper laser level. The corresponding small-signal gain values were found to be 3.7 dB/m (high pressure) and 10.6 dB/m (low pressure). The fact that the laser output is relatively insensitive to the discharge length and the drift tube length (from 30 cm to 82 cm) indicates that the laser action occurs only within a short distance downstream from the discharge section, and suggests that a much shorter and compact laser can be made with the configuration shown in Fig. 59 but with much reduced lengths both for the discharge and drift sections. It must be realized that both schemes discussed in this section, i.e., transverse and longitudinal high-speed gas flow, as well as those in the following sections, require enormous pumping capacity and consequently consume a tremendous amount of gas (in excess of several hundred liters per minute). For this reason a closed-loop recirculating system is extremely desirable and should be incorporated as an integral part of such a laser.

In another investigation in which CO_2 was introduced downstream from a N_2–He discharge section DeMaria(223) reported a CW power output of I 1.2 kW at 13% efficiency in a 1-m by 2-cm channel.

B. THERMAL PUMPING AND SUPERSONIC FLOW

Since the first proposal of thermal pumping and adiabatic cooling of CO_2 gas mixtures by Basov et al.(78), several attempts have been made both in the United States and in the Soviet Union to achieve population inversion between the $00^0 1$ and $10^0 0$ vibrational states of the CO_2 molecules, using various techniques. Fundamental processes in these gasdynamic lasers involve initial thermal pumping of CO_2 molecules by either burning or heating the gas or mixture of gases followed by a sudden expansion of the heated gas mixture through a nozzle. The rapid change in the translational temperature of the gas mixture causes the excited vibrational states of the molecules to relax toward an equilibrium through various $V \rightarrow V$ processes at different rates (see Section IV for details), resulting in a temporary population inversion immediately following the expansion. In these laser systems, N_2 and He are often found to be useful for the same reasons as in conventional lasers. To date, both CW and pulsed laser actions at relatively high power level have been achieved by expansion of the heated gas through a supersonic nozzle. Gerry(224) has recently reported 30 kW of CW power from a gasdynamic laser operating in a limited beam close to diffraction. In a mode-divergent beam he obtained 60 kW of CW power.

1. Some Early Experiments

In 1967, Makhov and Wieder(79) demonstrated that the upper CO_2 laser level $00^0 1$ can be pumped by heated nitrogen. In the meantime Wieder(77) also reported the observation of CW oscillation (~ 1 mW) at the 10.6-μ by exciting the CO_2 molecules with a CO-air diffusing flame at a temperature of -3000°K. The laser linewidth in this system was deduced from the absorption measurements to have a value roughly one to two orders of magnitude higher than that in a conventional discharge tube. The apparatus used in this experiment consisted of a 4-m-long quartz tube with a 24-mm bore. Two burners were placed on either side of the tube in the parallel direction. By heating N_2 in an oven initially to a temperature $\sim$ 1150°C at pressures ranging from 0.1 to 1.5 atm, Wisniewski et al.(*80*) have attained population inversion in the $00^0 1 - 1\,0^0 0$ CO, vibration-rotation transitions upon mixing CO_2 with heated N_2 molecules. With some modification of the experimental arrangement (Fig. 60), Fein et al.(*81*) have obtained pulsed laser action with a peak power output of 20 mW and a peak small-signal gain of 11%. As shown in Fig. 60 the N_2 flow velocity at the inlet is about 0.25 m/sec at a pressure of 400 Torr and reaches a value of $\sim$ 1.25 m/sec in the oven before passing through the nozzle. At these low flow rates, there is sufficient time to allow the

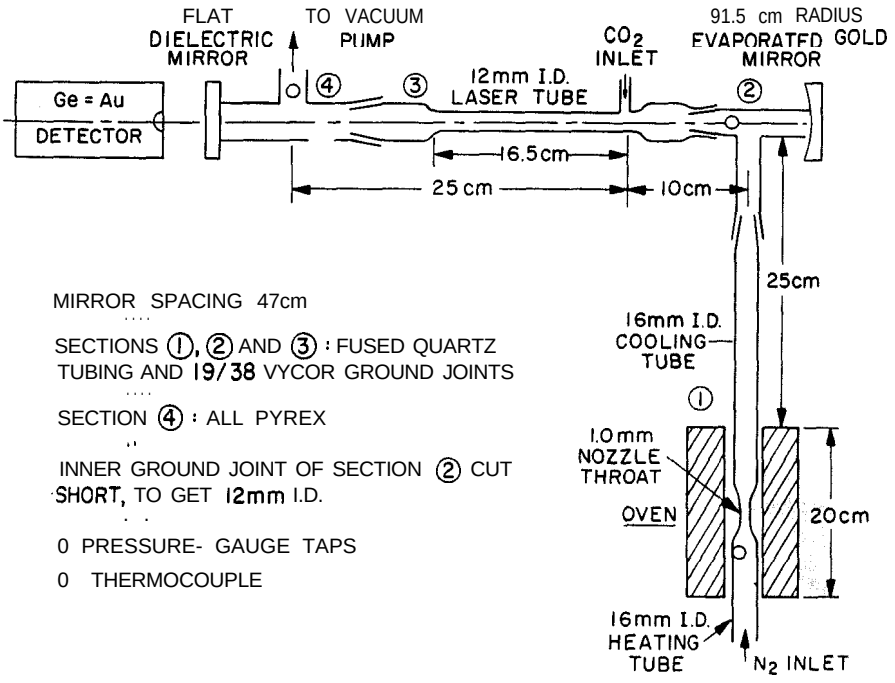

Fig. 60. Thermally-pumped CO_2-N_2 laser at a subsonic flow velocity $\sim$ 30 m/sec. [After Fein et al.(*81*).]

vibrational temperature to come to equilibrium with the translational temperature T_t. After expansion of N_2 through the nozzle, T_t reduces to near room temperature through the diffusion process in the cooling tube. Therefore, more than half of the excited N_2 molecules are lost before reaching the laser cavity. Note that this experiment does not utilize rapid cooling near the nozzle at which the fluid is accelerated to a supersonic speed. We shall see later that laser action with considerable increase in output power has been achieved in the region immediately following a sudden expansion of a heated gas mixture.

As the excited N_2 enters the laser tube at a flow velocity of about 30 m/sec, its pressure reduces to about 6 Torr, and it is mixed with 1 Torr of CO_2 at room temperature. Resonant transfer of vibrational energy from N_2 to CO_2 occurs in a time in the order of 50 μsec. In this system, both R and P branches at 10.6 μ oscillate, suggesting that a "total inversion" has been achieved@) by this scheme. The laser power increases almost linearly with increasing flow velocity in the range from 20 to 35 m/sec for an optimum gas mixture. The maximum gain as shown in Fig. 61 occurs at a distance $5 < Z <$ I.5 cm from the inlet port of CO_2 gas and depends somewhat on the mixture ratio used. Since this thermal laser is relatively simple to construct and involves no electrical discharge, it can be a useful tool for studies of gas kinetics and molecular-energy transfer processes.

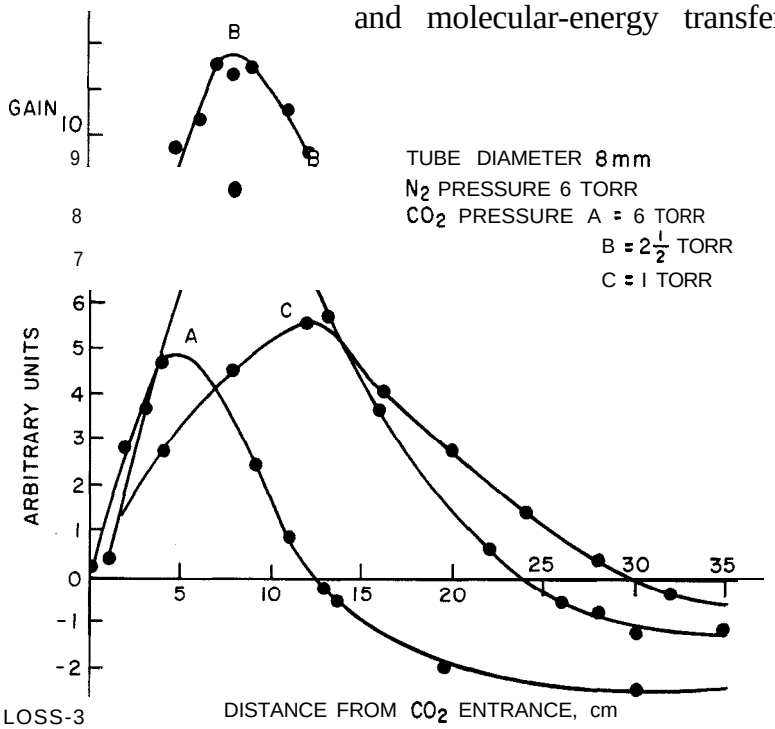

Fig. 61. Optical-gain distribution along the length of a thermally-pumped CO_2-N_2 laser tube from the CO_2 inlet. [After Fein et al. (*81*).]

2. *Supersonic Flow*

Two independent experiments on sudden expansion of a heated gas mixture through a supersonic nozzle have been reported recently. Kuehn and Monson(*215*) obtained pulse-laser energies up to ~10 J/cm² extracted from a 100-cm³ cavity with a gain path length of 14 cm; Bronfin and Hall(*87*) reported a CW laser power up to 60 W per 6 cm³ active volume.

The apparatus of the shock tube and the expansion chamber used for the pulsed-laser experiment is shown in Fig. 62. The heated gas

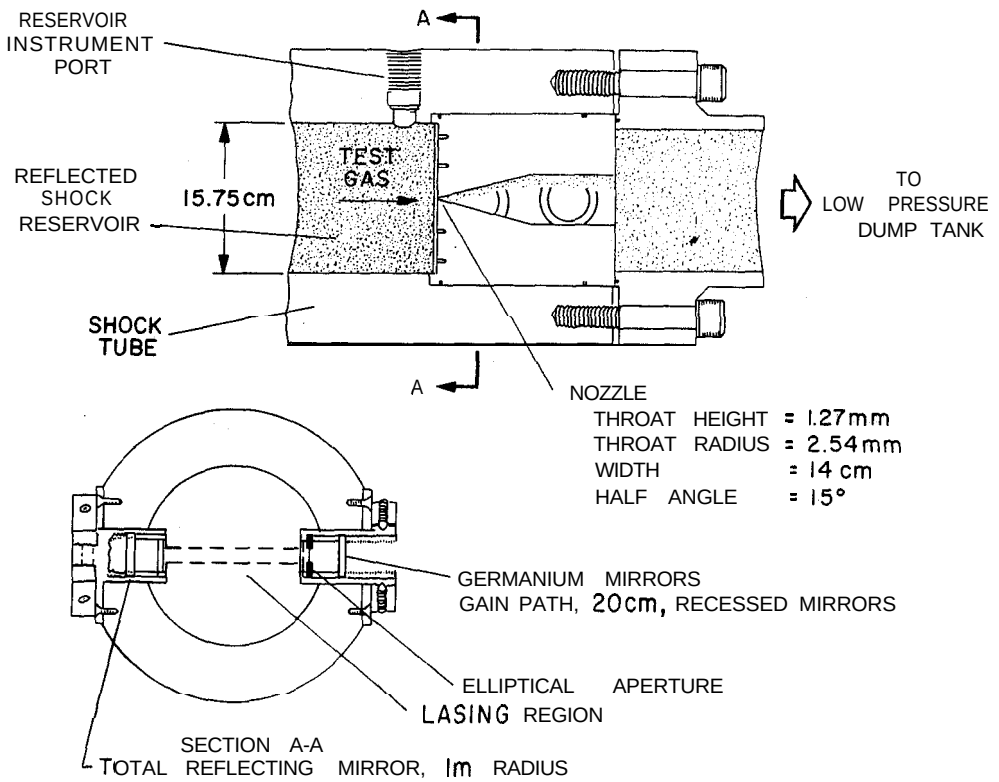

Fig. 62. Cross-sectional diagram of a shock-wave-generated supersonic flowing laser. [After Kuehn and Monson(*215*).]

mixture in a conventional shock tunnel is expanded through a two-dimensional supersonic nozzle with a slit width of 14 cm. The laser cavity is located behind the nozzle with an optical axis transverse to the direction of gas flow. The cavity mirrors are spaced 20 cm apart and recessed from the nozzle wall to avoid physical damage to the mirror surfaces by the solid particles generated by the shock waves. in this type of laser system, instabilities in the laser beam and extremely large

beam divergence are generated as a result of gas turbulences but improvements on the beam shape and instability to some extent can be made by using apertures. Two elliptical apertures (one 3 cm long and 1.27 cm diam; the other 3 cm long and 2.54 cm diam) were used in this experiment. Figure 63 shows the laser output as a function of the initial

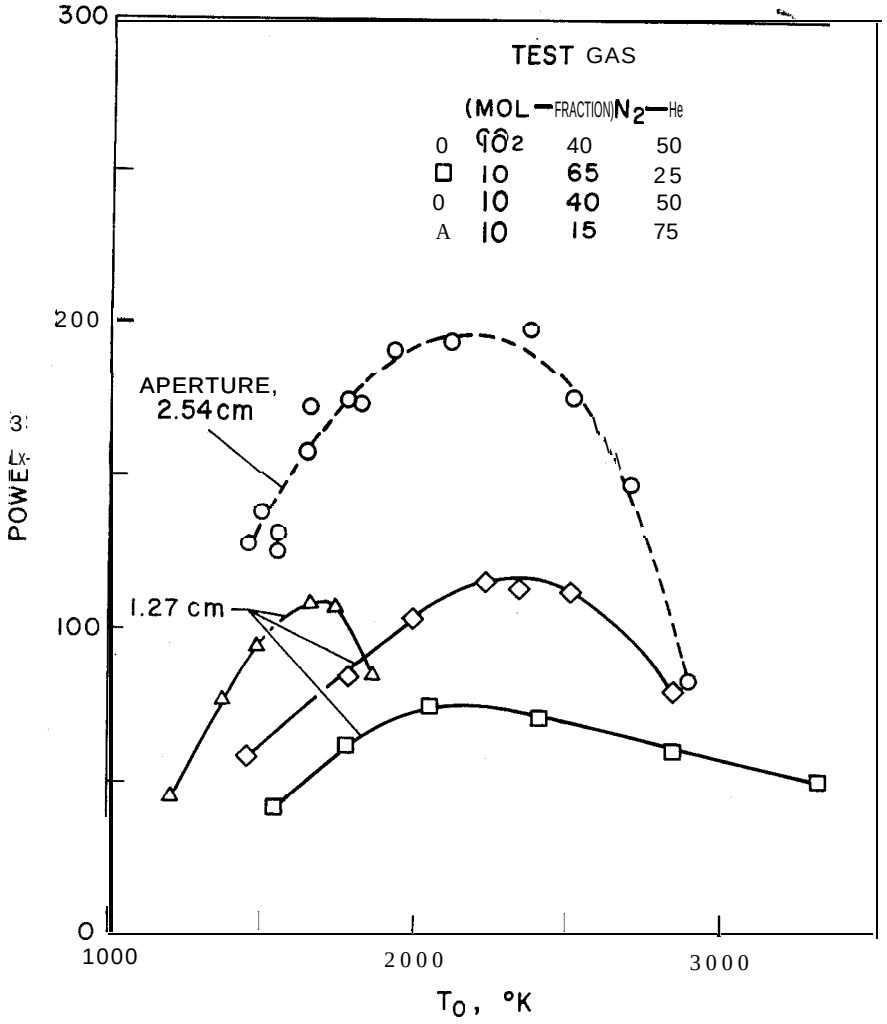

Fig. 63. Average power of the pulsed supersonic flowing laser as a function of the initial test-gas temperature before expansion through the nozzle. The output coupling mirror has a transmission of 7%. [After Kuehn and Monson(*215*).]

gas temperature before expansion. Data were obtained by using a 7% transmitting mirror in the laser cavity and for fixed total gas pressure $P_0 = 15.5 \pm 2.5$ atm before expansion. With optimum output coupling (- 12%), a maximum average output power of $\sim$ 250 W (with the aperture 2.54 cm diam) has been obtained from a heated CO_2–N_2–He mixture in the ratio I : 4 : 5.

Figure 64 shows the apparatus used to achieve a CW supersonic flow (- 10^3 m/sec). Arc-heated N_2 at a temperature of 1000-3000" K and a pressure of 1 atm is rapidly expanded through a two-dimensional supersonic nozzle 5 cm in length with 1 mm throat height, providing a Mach number of 3.4. Mixing of CO_2–He with the vibrationally excited N_2 near room temperature is accomplished by injection through two narrow slots positioned from both sides of the tunnel normal to the supersonic flow. The injection velocities are varied continuously up to sonic values. The typical total gas flow rates were about 10 liters per sec (STP) with a total gas pressure, measured downstream in the test chamber, of about 50 Torr at a mixing ratio of 1 : 2 : 2 (CO_2 : N_2 : He). The advantages of this arrangement over the previous experiments (Fig. 60) are that (1) very little loss of the vibrationally excited CO_2 or N_2 occurs through diffusion, (2) the present arrangement, by placing the laser cavity very near the nozzle slit, allows the use of high pressure, thus yielding much higher laser power, and (3) the high convection flow rate removes the bottleneck formation at the 0 1^1 0 level owing to thermal excitation. Under the experimental conditions, the transit time of fluid through the laser cavity is about 20 μsec, compared with $\sim$ 3 μsec resonant transfer time between CO_2 and N_2 and $\sim$ 75 μsec relaxation time of the upper laser level. Relaxation time of the 01^10 on the other hand is in the order of 10 μsec.

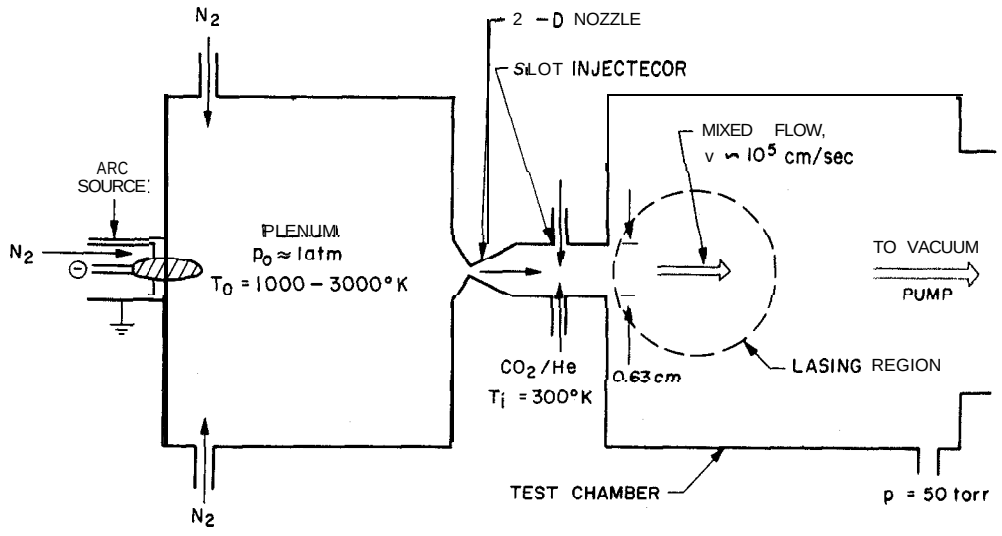

Fig. 64. Cross-sectional diagram of the thermal mixing laser. Optical gain, transverse to flow, is 5 cm; Z-dimensional nozzle throat height is I mm; and exit height is 6.3 mm (at 15" expansion angle). Injector slots for CO_2-He are 5 cm x 1 mm perpendicular to the expanded N_2 flow. The lasing region is indicated by the dotted circle. [After Bronfin et al. (*82*).]

Small-signal gain measurements as a function of flow rates R are shown in Fig. 65. The optical gain increases with increasing R_{CO_2} and R_{He}, and the highest gain value (about 0.8%/cm optical path length) is obtained at volumetric flow rate ratios R_{He}/R_{N_2} = 0.1 and R_{CO_2}/R_{N_2} = 0.3. These relatively low gain values for a supersonic flowing laser compared with those obtained from the conventional laser systems (35) indicate that gain saturation in a supersonic flowing laser must occur at much higher values. As mentioned before, both the stability and beam divergence in supersonic flowing laser are much more inferior than in

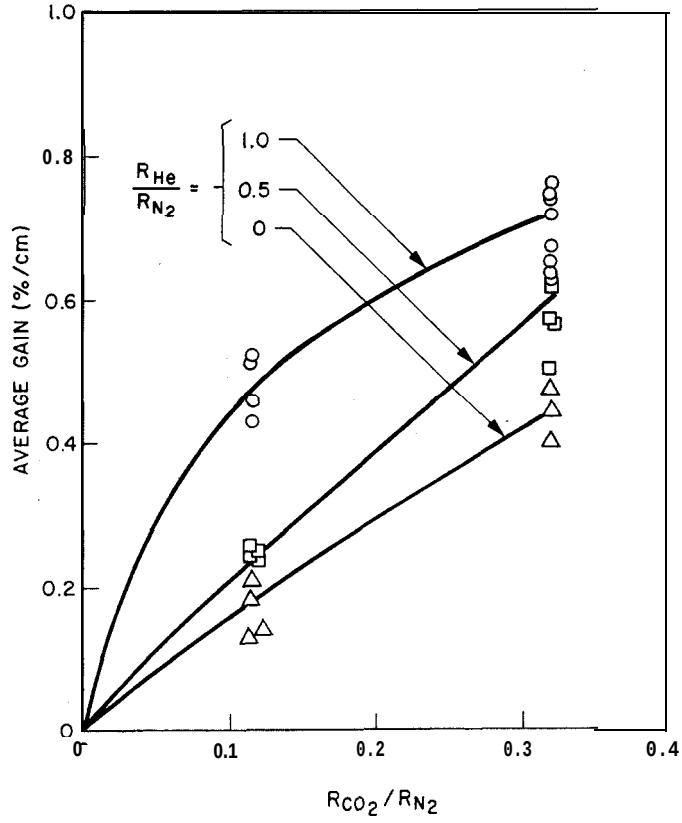

Fig. 65. Effect of composition on 10.6-μ gain. The N_2 flow rate is 3.63 liters/sec (STP), expanding from 2000° K, 1 atm. [After Bronfin et al. (*82*).]

the conventional low-speed CO_2 laser systems, owing primarily to the aerodynamic turbulences in the fluid. These turbulences which are properties of supersonic fluids limit the application of this laser.

C. CHEMICAL LASERS

Cool et al. (83) have obtained CW laser oscillation at 10.6 μ by means of chemical reactions forming vibrationally excited states of DF, HF,

and HCI molecules which subsequently transfer their vibrational energies to excite CO_2 molecules to the 00^0 1 level(*217,218*). In the early experiments(M), rf power was applied to the system through a side-arm tube to produce dissociated chlorine, fluorine deuterium, or hydrogen reactants before the mixture flowed into a coaxial Teflon reaction tube of 9-mm bore and 2 1 -cm length, located in the upstream portion of the laser cavity. Recently it has been found that this external rf energy source is unnecessary and it has been removed from the system(*216*). As shown in Fig. 66, the NO_2 F_2, and He gases are

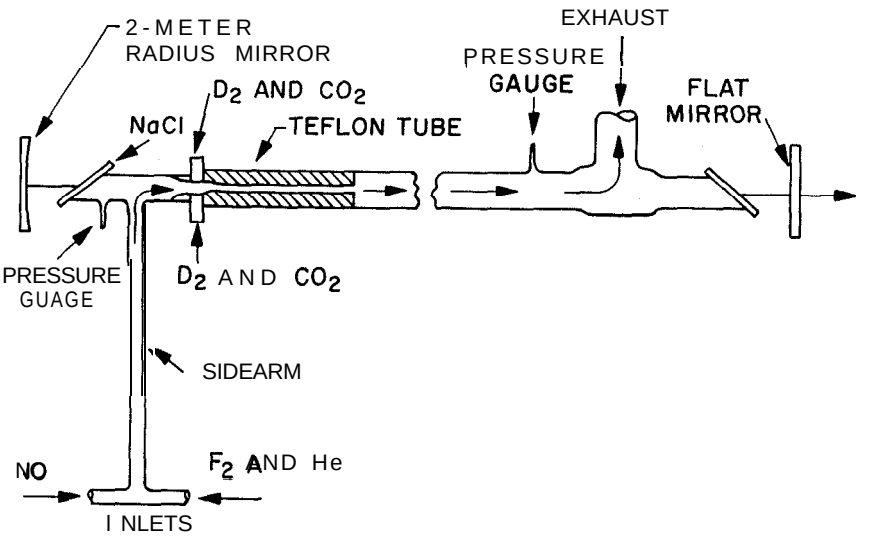

Fig. 66. A CW chemically pumped CO_2 laser with no external energy source. Laser action occurs mainly in the upstream portion of the tube. The cavity length is 1.5 m and the average flow velocity is ~ 600 m/sec(*83*).

injected into an 11-mm-bore quartz tube in which the reaction

$$F_2 + NO \longrightarrow NOF + F \qquad (I\,25)$$

takes place. The F and F_2 subsequently are mixed with D_2 in a 9-mm-bore Teflon tube to produce vibrationally excited DF molecules via the reactions

$$F + D_2 \longrightarrow (DF)^* + D \qquad (126)$$

and

$$D + F_2 \longrightarrow (DF)^* + F \qquad (127)$$

These excited DF molecules then transfer their energy to CO, molecules and produce a very impressive CW laser power of 8 W in a drift tube of less than 1 m in length. However, a supersonic speed (~ 600 m/sec) is required for the fluid flow in this CW chemical laser; therefore,

this laser consumes tremendous amounts of gases in order to sustain a continuous operation. Further studies on the chemistry and on the possibility of utilizing a recirculating loop are definitely required before a practical chemical laser can be realized.

LIST OF SYMBOLS

A	Einstein A coefficient for spontaneous emission
A_{mn}	transition probability between states m and n
a_0	Bohr radius
a_{ij}	internuclear force constants
a	absorption coefficient
a_1, a_2	mirror radius
B, B_v	rotational constant
b	distance of closest approach
C_{ij}	coefficients of quadratic terms of the kinetic energy
c	velocity of light
D, D_v	rotational constant (fine structure)
D_{ij}	coefficients of quadratic terms of the potential energy
$D_{\infty h}$	a point group
d	modulation depth
$\mathscr{D}$	diffusion coefficient
E_i, E_v, E_ν	vibrational energy of ith level or of ν mode
E_r	rotational energy
$\mathscr{E}$	electric field
$F(J)$	term values for rotational energy level
f_i	fnumber of ith emission line
f_P, f_R	beat frequencies in the P and R branch, respectively
$G(v)$	term values for vibrational energy level
$G(t, z)$	step response
g_l, g_u	statistical weight of the lower and upper level, respectively
$g(\nu), g(\omega)$	line-shape function
g_{ii}	ℓ-type doubling constants
$g(J)$	statistical weight of the Jth rotational energy level
H	width of a square laser cavity
H_v	Hermite polynomials
$\hbar = h/2\pi$	Plank constant times I $/2\pi$
I, I_e	moments of inertia
I	laser intensity
I_0, U_t	initial and transmitted laser intensities
I_S	gain saturation parameter

J	rotational quantum number
$K^{u}_{i,J}$	cross-relaxation rate constant between ith and Jth rotational levels in the upper laser level
$K^{\ell}_{i,J}$	cross-relaxation rate constant between ith and Jth rotational levels in the lower laser level
K_i, K_δ	valence-force constant
k	Boltzmann constant
k_e, k_e'	resonant exchange-rate constant
k_{vi}	vibrational relaxation-rate constant
k_{A-B}	collisional relaxation-rate constant between species A and B
k_{rot}, k^{rot}_{A-B}	rotational relaxation-rate constant
k_{ij}	vibrational relaxation-rate constant between states i andj
L	laser cavity length; also, patch length
ℓ	equilibrium internuclear distance between C and 0
ℓ_i	angular momentum quantum number
M	collisional partner *M;* also, magnetic quantum number
M_O, M_C	mass of oxygen and carbon atoms
m	reduced mass
$m = -J$	P-branch rotational quantum number
$m = J + 1$	R-branch rotational quantum number
N_e	average electron density
N_0	ground state population per unit volume
N_v	normalizing constant
n	index of refraction
n_e	electron density
n_i	population density of ith level
n_v	vibrational population density of Vth level
n_J	population density of Jth rotational level
$n_J{}^{u}$, $n_J{}^{\ell}$	population density of the upper and lower rotational levels
n_T	population density of Tth rotational level
P	gas pressure
P_ℓ	power output of laser beam
$P(J)$	P-branch vibrational-rotational transition
P	dipole moment
$\mathscr{P}$	probability of excitation or deexcitation processes
Q	quality factor of resonant cavity; also, quadrupole moment
R	mirror radius of curvature
$R(J)$	R-branch vibrational-rotational transition
R_x	flow rate of x specie
R_y	Rydberg constant

r_0	laser beam radius at 1 /e intensity
r_{ij}	excitation or deexcitation rates between states i and j
$r(t)$	classical trajectory
S_i	symmetric coordinates
S_{mn}, S	line strength between states m and n
STP	standard temperature and pressure; i.e., 273°K and 1 atm
T, T_t	translational temperature of gas
T_1	collisional or dissipative relaxation time
T_2	homogeneous relaxation (atomic or molecular dephasing) time
T_v	vibrational temperature of a given mode of oscillation
t, t_m	transmission coefficient of a mirror
t	spectral transmittance
U	fluid velocity
U_0	impulse response
V'	interaction potential
$\bar{v}$	average thermal velocity
v_i	vibrational quantum number
W, W_m	width of a square laser cavity
$\mathscr{W}$	induced emission rate
X	Cartesian coordinate
X_1	electronic excitation probability
x	mole fraction of a component in a mixture
x_{ij}	anharmonic force constants
Y	Cartesian coordinate
Z	average number of collisions; also Cartesian coordinate along the direction of gas flow
α_0	small-signal gain coefficient
α_m	polarizability of molecule
β	wall reflection coefficient
Γ_j	pumping rate of population from ground state to the jth level
γ_{ij}	excitation and deexcitation rates between states i andj
Δ_J	collisionally broadened linewidth
Δ, Δ'	hard and soft collisional linewidths
δ_+, δ_-	sum and difference, respectively, of energy between two states
ϵ	dielectric constant; also average electron energy
θ_{JM}	Jacobi polynomials
λ	wavelength

λ_i	roots of the secular determinant
μ	micron; also reduced mass of CO_2 molecule
μ_{mn}	dipole matrix elements between states m and n
ν	optical frequency
ν_0	center frequency of an optical line
ν_i	frequency of the three fundamental modes of vibration
ν_c	collision frequency
$\Delta\nu$	width of a spectral line at one-half maximum intensity
ξ_i	normal coordinates
ρ_i	radiative flux density of the ith mode
$\Sigma_g, \Sigma_u, \pi_u$	species associated with ν_1, ν_2, and ν_3 modes
$\Sigma, \pi, \Delta, \ldots$	spectroscopic notations to designate the vibrational levels
σ	cross section
τ_0	initial pulse width
τ_R	round-trip transit time of light in a cavity
τ_u, τ	collisional lifetimes of the upper and lower vibrational laser levels
τ_r	radiative lifetime of vibrational level
τ_ν	effective vibrational lifetime
τ_c	time between successive collisions
τ_w	width of a laser pulse
τ_d	delay time of a laser pulse
ϕ	azimuth angle about a spatially fixed axis
Ψ_e	wave function of an electronic state
Ψ_v	wave function of a vibrational state
Ψ_r	wave function of a rotational state
Ω	nutational frequency of induced dipoles
ω	angular frequency
ω_1, ω_2	mode spot size at flat and curved mirrors, respectively

ACKNOWLEDGMENTS

I wish to express my appreciation to the Bell Telephone Laboratories (Whippany) for encouragement and cooperation during the preparation of the manuscript. I am particularly grateful to T. J. Bridges, H. G. Cooper, and other members of the Laboratories for valuable discussions and comments, and to T. J. Bridges and W. B. Gandrud for proofreading the manuscript.

REFERENCES

1. C. K. N. Patel, W. L. Faust, and R. A. McFarlane, *Bull. Am. Phys. Soc.*, **9**, *500* (1964).
2. C. K. N. Patel, *Phys. Rev.*, **136A**, **1187 (I 964).**
3. C. K. N. Patel, *Phys. Rev. Letters*, **12,588 (1964).**
4. N. Legay-Sommaire, L. Henry, and F. Legay, *Compt. Rend., 260,339 (I 965).*
5. P. Barchewitz, L. Dorbec, R. Farrenq, A. Truffert, and P. Vautier, *Compt. Rend.*, 260,358 I (I 965).
6. P. Barchewitz, L. Dorbec, A. Truffert, and P. Vautier, *Compt. Rend., 260, 5491* (1965).
7. F. Legay and N. Legay-Sommaire, *Compt. Rend.*, **260**, 3339 *(I 964).*
8. C. K. N. Patel, *Phys. Rev. Letters*, **13**, 6 17 (1964).
9. C. K. N. Patel, *Appl. Phys. Letters, 7,* 15 *(1965).*
10. G. Moeller and J. D. Rigden, *Appl. Phys. Letters, 7,274* (1965).
11. C. K. N. Patel, P. K. Tien, and J. H. McFee, *Appl. Phys. Letters, 7,290 (1965).*

11a. A. J. DeMaria, to be published.

12. W. J. Witteman, *IEEE J. Quant. Electron., 2,375* (I 966).
13. M. J. Weber and T. E. Deutsch. *IEEEJ. Quant. Electron., 2,369* (1966).
14. P. K. Cheo, *Appl. Phys. Letters,* **11,** *38 (1967); IEEE J. Quant. Electron., 4, 587* (1 968).
15. R. L. Taylor and S. Bitterman, *Rev. Mod. Phys.*, **41**, 26 **(1969).**
16. P. 0. Clark and M. R. Smith, *Appl. Phys. Letters,* **9**, 367 (1966); for more recent measurements see D. C. Tyte and R. W. Sage, *Proc. IERE, Conf. On Lasers and Opto-Electronics, March, 1969, Southampton, England.*
17. R. D. Hake and A. V. Phelps, *Phys. Rev.*, **158**, 70 *(1967).*
18. M. J. W. Boness and G. J. Schulz, *Phys. Rev. Letters,* **21, 103** 1 (1968).
19. P. K. Cheo and H. G. Cooper, *IEEE J. Quant. Electron.,* **3**, 79 *(I 967).*
20. W. J. Witteman, *Phys. Letters,* **18,** *125 (1965); IEEE J. Quant. Electron.,* **QE-2,** 375 (1 966).
21. N. N. Sobolev and V. V. Sokovikov, *JETP Letters, 4, 204 (1966); ibid.,* **5**, *99* (1967).
22. B. F. Gordietz, N. N. Sobolev, and L. A. Shelepin, *Soviet Phys. JETP, 26, 1039* (1968).
23. L. 0. Hocker, M. A. Kovacs, C. K. R. Rhodes, G. W. Flynn, and A. Javan, *Phys. Rev. Letters,* **17,233 (1966).**
24. P. K. Cheo, *J. Appl. Phys.*, **38**, 3563 (1 *967).*
25. C. B. Moore, R. E. Wood, B. Hu, and T. J. Yardley, *J. Chem. Phys., 46, 4222 (1967).*
26. P. K. Cheo and R. L. Abrams, *Appt. Phys. Letters,* **14**, 47 **(1969).**
27. R. L. Abrams and P. K. Cheo, *Appl. Phys. Letters,* **15, 177 (1969).**
28. C. K. Rhodes. M. J. Kelly, and A. Javan, *J. Chem. Phys.*, **48**, 5730 (1968).
29. T. K. McCubbin, R. Darone, and J. Sorrell, *Appl. Phys. Letters, 8, I 18 (I 966).*
30. E. T. Gerry and D. A. Leonard, *Appl. Phys. Letters, 8,227 (1966).*
31. T. J. Bridges, H. A. Haus, and P. W. Hoff, *IEEE J. Quant. Electron., 4,777 (I 968).*
32. C. Bordé and L. Henry, *IEEE J. Quant. Electron., 4, 874 (I 968).*
33. H. W. Mocker, *IEEE J. Quant. Electron., 4,769 (1968).*
34. T. Deutsch, *ZEEE J. Quant. Electron., 3,* 15 I (1967).
35. P. K. Cheo, *IEEE J. Quant. Electron., 3,683 (1967).*

36. G. J. Dezenberg and J. A. Merritt, *Appl. Optics, 6.* 1541 (1967).
37. C. Rossetti and P. Barchewitz, *Campt. Rend., 262,* 1 *199* (*1966).*
38. N. Djeu, T. Kan, and *G.* J. Wolga, *IEEE J. Quant. Electron., 4,256 (1968).*
39. T. A. Cool and J. A. Shirley, *Appl. Phys. Letters,* **14.70 (1969).**
40. H. Kogelnik and T. J. Bridges, *IEEE J. Quant. Electron.. 3.95* (1 *967).*
41. D. F. Hotz and J. W. Austin, *Appl. Phys. Letters,* **11,** 60 **(1967).**
42. C. P. Christensen, C. Freed, and H. A. Haus, *IEEE J. Quant. Electron., 5, 276* (1969).
43. R. C. Crafer, A. F. Gibson and M. F. Kimmitt, *Brit. J. Appl. Phys., 2,* 1 *13.5 (1969).*
44. M. A. Kovacs, G. W. Flynn, and A. Javan, *Appl. Phys. Letters, 8.62 (1966).*
45. T. J. Bridges, *Appl. Phys. Letters, 9,* 174 (1966).
46. Dietrich Meyerhofer, *IEEE J. Quant. Electron., 4,762* 1 (I 968).
47. 0. R. Wood and S. E. Schwarz, *Appf. Phys. Letters,* **11,** 88 **(1967).**
48. P. L. Hanst, J. A. Morreal, and W. J. Henson, *Appl. Phys. Letters,* **12,** 58 (1968).
49. J. T. Yardley, *Appf. Phys. Letters,* **12,** 120 (1968).
50. N. V. Karlov, G. P. Kuzmin, Yu N. Petrov, and A. M. Prokhorov, *JETP Letters,* **7, 134 (1968).**
51. T. Y. Chang. C. H. Wang, and P. K. Cheo, *Appl. Phys.* Letters, **15, 157 (1969).**
52. 0. R. Wood and S. E. Schwarz, *Appl. Phys. Letters,* **12,263 (1968).**
53. D. E. Caddes, L. M. Osterink, and Russel Targ, *Appf. Phys. Letters,* **12,** 74 **(1968).**
54. T. Walsh, *RCA Rev., 27,323 (1966).*
55. J. E. Kiefer and A. Yariv, *Appf. Phys. Letters,* **15,** 26 *(1969).*
56. T. J. Bridges and P. K. Cheo, *Appf. Phys. Letters,* **14,262 (I 969).**
57. T. J. Bridges and C. K. N. Patel, *Appl. Phys. Letters, 7,244* (1965).
58. J. D. Rigden and *G.* Moeller, *IEEE J. Quant. Electron., 2,365 (1966).*
59. C. Frapard, *Phys. Letters, 20,384 (1966).*
60. J. Fantasia, Honeywell Inc., Syst. and Res. Div., Final Rept., HRC66-34, November (1966).
61. W. B. Bridges, P. 0. Clarke, and A. S. Halstead, *CFSTI,* Doc. No. AD807363, January (I 967).
62. D. R. Whitehouse. *CFSTI,* Doc. No. AD65303. May (I 967).
63. T. G. Roberts, G. J. Hutcheson, J. J. Ehrlich, W. L. Hales, and T. A. Barr, *IEEE J. Quant. Electron., 3,605 (1967).*
64. P. A. Miles and J. W. Lotus, *IEEE J. Quant. Electron., 4.8 I I* (1968).
65. M. R. Smith and D. C. Forster. 1968 International Quantum Electronics Conference, Miami, Florida, May 14– 17, 1968, Paper 10J-2.
66. R. J. Carbone, *IEEE J. Quant. Electron., 3.373 (1967).*
67. W. J. Witteman and H. W. Werner, *Phys. Letters,* **26A. 454 (1968).**
68. R. P. Reeves, unpublished work, 1967.
69. W. J. Witteman, *Appl. Phys. Letters,* **11,337 (1967).**
70. J. Fantasia, *CFSTZ,* Doc. No. N68- 13277, October (1967).
71. R. J. Carbone, *IEEE J. Quant. Electron., 4. 102* (1968).
72. P. 0. Clark and J. Y. Wada, *IEEE J. Quant. Electron., 4,263 (1969).*
73. T. F. Deutsch and F. A. Horrigan, *ZEEE J. Quant. Electron., 4,972 (1968).*
74. R. S. Reynolds, NASA Contract No. NAS5-10309, January (1968).
75. C. Freed, *IEEE J. Quant. Electron., 3,203* (1967); *ibid., 4,404 (1968).*
76. F. A. Horrigen, C. A. Klein, R. I. Rudko, and D. T. Wilson, Army Missile Command Contract No. DAAHO1-67-1589, September (1968); Laser Technology, Laser Optics Inc., Jan. 1969.

77. 1. Wieder, *Phys. Letters,* **24A, 759 (1967).**
78. N. G. Basov, A. N. Ordevskill, and V. A. Scheglov, *Soviet Phys. Tech. Phys.,* **12,** 243 (1967).
79. G. Makhov and I. Wieder, *IEEE J. Quant. Electron., 3,378 (1967).*
80. E. E. Wisniewski, M. E. Fein, J. T. Verdeyen, and B. E. Cherrington, *Appl. Phys. Letters,* **12,257 (I 968).**
81. M. E. Fein, J. T. Verdeyen, and B. E. Cherrington, *Appl. Phys. Letters, 14, 337* (I 969).
82. B. R. Bronfin, L. R. Boedeker, and J. P. Cheyer, *Bull Am. Phys. Soc.*, **14, 857** (1969), Paper FE-1 0; *Appl. Phys. Letters,* **16,** 2 14 (1970).
83. T. A. Cool, T. J. Falk, and R. R. Stephens, *Appl. Phys. Letters,* **15, 3** 18 **(1969);** T. A. Cool and R. R. Stephens,J. *Chem. Phys.,* **51,** 5175 **(1969).**
84. V. K. Konyukhov and A. M. Prokhorov, *JETP Letters, 3,436 (1966).*
85. T. A. Cool, *J. Appl. Phys.*, **40,** 3563 *(I 969).*
86. W. B. Tiffany, R. Targ, and J. D. Foster, *Appl. Phys. Letters,* **15,** 91 **(I 969).**
87. B. R. Bronfin and R. J. Hall, *Bull. Am. Phys. Soc.*, 14,857 (1969), Paper FE-I I.
88. A. E. Hill, *Appl. Phys. Letters,* **12,324** (1968).
89. T. F. Deutsch, F. A. Horrigan, and R. 1. Rudko, *Appl. Phys. Letters,* **15.88 (1969).**
90. N. McAvoy, H. L. Richard, J. A. McElroy, and W. E. Richards, "A 10.6 Micron Laser Communication System Experiment for ATS-F and ATS-G", Goddard Space Flight Center, Greenbelt, Maryland, *NASA TMX-524-68-206,* May (1968).
91. For a comprehensive evaluation and analysis, *see Deep Space Communication and Navigation Study,* Vols. 1, 11, and III, prepared by Bell Tel. Labs. for NASA, Contract No. NAS5-10293, May (1968).
92. For example, *see Lincoln Laboratory Optics Research Report,* Air Force Contract No. AF19(628)-5167, July (1969).
93. F. P. Gagliano, R. M. Lumley, and L. S. Watkins, *Proc. IEEE,* **57,** 1 14 (1969).
94. C. K. N. Patel, *Phys. Rev. Letters, 20, 1027* (1968); *ibid.,* **16,613** (1966).
95. C. K. N. Patel, P. A. Fleury, R. E. Slusher, and H. L. Frisch, *Phys. Rev. Letters,* 971 (1966).
96. G. D. Boyd, T. J. Bridges, and E. G. Burkhart, *IEEE J. Quant. Electron., 4, 5* 15 (I 968).
97. J. Warner, *Appl. Phys. Letters,* **12,222** (1968).
98. W. B. Gandrud, G. D. Boyd, J. H. McFee, and F. H. Wehmeier, *Appl. Phys. Letters,* **16,** 59 (1970).
99. C. K. N. Pate1 and R. E. Slusher, *Phys. Rev. Letters,* **19,** 1019 (1967).
100. C. K. N. Pate1 and R. E. Slusher, *Phys. Rev. Letters, 20.* 1087 (1968).
101. G. B. Hocker and C. L. Tang, *Phys. Rev. Letters,* **21,591** (1968).
102. J. P. Gordon, C. H. Wang, C. K. N. Patel, R. E. Slusher, and W. J. Tomlinson, *Phys. Rev.,* **179,294 (1969).**
103. C. K. Rhodes, A. Szöke, and A. Javan, *Phys. Rev. Letters,* **16,** 115 1 (I 968).
104. E. B. Treacy and A. J. DeMaria, *Phys. Letters,* **29A, 369** (1969).
105. C. K. Rhodes and A. Szöke, *Phys. Rev.* **184,** 25 (1969).
106. F. A. Hopf and M. 0. Scully, *Phys. Rev.,* **179,399 (1969).**
107. P. K. Cheo and C. H. Wang, *Phys. Rev.,* A 1,225 (1970).
108. See for example, C. B. Moore, *Acc. Chem. Rev., 2,* 103 (1969).
109. 1. Burak. A. V. Nowak, J. 1. Steinfeld, and D. G. Sutton, *J. Chem. Phys.,* **51,** 2275 **(1969).**
I IO. A. M. Ronn and D. R. Lide, Jr., *J. Chem. Phys.,* **47,** 3669 (1967).
11 1. C. K. N. Patel, *J. Chimie. Phys.,* **64,** 82 *(1967).*

112. V. P. Tychinskii, Soviet *Phys. – Usp.*, **10. 13 I (I 967).**
113. N. N. Sobolev and V. V. Sokovikov, ***Soviet Phys. – Usp.*, 10, 153 (1967).**
114. H. Herzberg, Molecular Spectra ***and*** Molecular *Structure–II*. Infrared ***and Raman Spectra of Polyatomic Molecules,*** Van Nostrand, Princeton, N.J., 1962.
115. J. B. Howard and E. B. Wilson, Jr., ***J. Chem. Phys., 2,620 (I 934).***
116. W. H. Shaffer and R. R. Newton,./. ***Chem. Phys., 10,405 (1942).***
11 7. P. E. Martin and E. F. Barker, ***Phys. Rev., 41.29 1*** (1932). [Ref. for ν_2.]
118. E. F. Barker and T. Y. Wu, ***Phys. Rev., 45, ((1934).*** [Ref. for ν_3.]
I *19.* I. Hanson, ***Phys. Rev., 46, 122 (I 93*** 1).
120. 1. Wieder and G. G. McCurdy, ***Phys. Reu. Letters, 16,565*** (1966).
121. E. Fermi, Z. ***Physik, 71,250*** (193 I).
122. C. Frapard, P. Lames, M. Roulot, X. Ziegler, and N. Legay-Sommaire, ***Compt. Rend., 262,*** 1340 (***1966).***
123. T. J. Bridges and A. R. Strnad, *IEEE J.* ***Quant.*** *Electron.*, **3**, 335 ***(1967).***
124. J. A. Howe, *Appl.* ***Phys. Letters, 7, 2 I (1965).***
12.5. J. A. Howe and R. A. McFarlane, *J.* ***Mol.*** *Spectry.*, **19,224** (1966).
126: B. Hartman and B. Kleman, *Can. J.* ***Phys., 44,*** 1609 (1966).
127. N. Djeu, T. Kan, C. R. Miller, and ***G.*** J. Wolga, *J.* ***Appl. Phys.,*** **39**, 2157 (1968).
128. H. Statz, C. L. Tang, and G. F. Koster, *J. Appl.* ***Phys.,*** **37**, 4278 ***(I 966).***
129. U. P. Oppenheim and A. D. Devir, *J.* ***Opt.*** *Soc.* ***Am., 58,585 (I 968).***
130. C. Rossetti, F. Bourbonneux, and P. Barchewitz, ***Compt. Rend., 262,*** 1684 ***(1966).***
131. T. J. Bridges and T. Y. Chang, ***Phys. Rev. Letters,*** **22**, 8 ***I I (1969).***
132. A. V. Phelps, ***Rev. Mod. Phys., 40,399*** (1968).
133. A. Stamatovic and G. J. Schulz, to be published.
134. G. J. Schulz, ***Phys. Rev., 116,*** 1141 ***(1959); ibid., 125, 229 (1962); ibid., 135, A988 (I 964).***
135. K. Takayanagi, ***Progr.*** *Theoret.* ***Phys. (Kyoto),*** **40**, 2 ***16 (1967).***
136. S. S. Penner, ***Quantitative Molecular Spectroscopy and Gas Emmissivities,*** Addison-Wesley, Reading, Mass., 1959.
137. S. C. Brown, ***Basic Data of Plasma Physics,*** **MIT** Press, 1959.
138. A. Javan, W. R. Bennett, and D. R. Herriott, ***Phys. Rev. Letters, 6, 106 (I96 I).***
139. L. Landau and E. Teller, ***Physik.*** *Z. Sowjetunion*, **10, 34** (1936).
140. R. N. Schwartz, Z. I. Slawsky, and K. Herzfeld, *J.* ***Chem. Phys., 20.*** 159 ***I (1952).***
141. R. D. Sharma and C. A. Brau, ***Phys. Rev. Letters,*** **19**, 1273 ***(1967).***
142. W. A. Rosser, A. D. Wood, and E. T. Gerry, 1968 International Quantum Electronics Conference, Miami, Florida, May 14–17, 1968, Paper 7G-4.
143. R. L. Taylor, M. Camac, and R. M. Feinberg, ***Proceedings Eleventh International Symposium on Combustion, Pittsburgh, Pa., 14-20 August (*** 1966).
144. C. B. Moore, ***Fluorescence (G. G.*** Guilbault, ed.), Dekker, New York, 1967, Chap. 3.
14.5. G. Gould, *Appl.* ***Opt.,*** *Suppl.* **2**, 59 ***(1965).***
146. R. C. Millikan and D. R. White, *J.* ***Chem. Phys.,*** **39**, 3209 (1963).
147. K. F. Herzfeld and T. A. Litovitz, ***Absorption and Dispersion of' Ultrasonic Waves,*** Academic Press, New York, 1959.
148. J. 0. Hirchfelder, C. F. Curtis, and R. B. Bird, ***Molecular Theory*** *of Gasses* ***and Liquids,*** Wiley, New York, 1954.
149. V. N. Kondrat'ev, ***Chemical Kinetics of Gas Reactions,*** Addison-Wesley, Reading, Mass., 1964.
150. J. E. Lennard-Jones, *Proc.* ***Roy.*** *Soc.* ***(London),*** **A106**, 441 **(1924).**
151. J. T. Yardley and C. B. Moore, ***J. Chem. Phys., 46,449 I (1967).***

152. M. Kovacs, D. R. Rao, and A. Javan, *J. Chem. Phys.*, **48**, 3339 *(1968).*
153. K. F. Herzfeld, *J. Chem. Phys., 47,743 (1967).*
154. B. F. Gordietz, N. N. Sobelev, V. V. Solovikov, and L. A. Shelepin, *IEEE J. Quant. Electron., 4,796* (1968).
1.55. R. D. Sharma, *J. Chem. Phys.*, **49**, 5 *195 (1968).*
156. R. Holmes, G. R. Jones, and R. Lawrence, *J. Chem. Phys.*, **41**, 2995 (1 **964).**
157. R. R. Patty, E. R. Manring, and J. A. Gardner, *Appl. Opt.*, **7**, 2241 *(1968).*
158. A. Yariv, *Quantum Electronics,* Wiley, New York, 1967.
159. R. Targ and W. B. Tiffany, *Appl. Phys. Letters,* **15,302 (1969).**
160. J. Tulip, *ZEEE J. Quant. Electron., 6,206 (I 970).*
161. W. J. Witteman, *IEEEJ. Quant. Electron., 2,375* (1966); *Philips Res. Rept.*, **21**, 73 *(I 966).*
162. W. W. Rigrod, *J. Appl. Phys.*, **36**, 2487 *(* 1965).
163. W. B. Bridges, *IEEE J. Quant. Electron., 4,820 (1968).*
164. Y. V. Brzhazovsky, V. P. Chebotayev, and L. S. Vasilenko, *IEEE J. Quant. Electron., 5, 146 (1969).*
165. P. Rabinowitz, R. Keller, and J. T. LaTourrette, *Appl. Phys. Letters,* **14, 376** *(1969); Bull. Am. Phys. Soc.*, **14,940** (1969).
166. Y. H. Pao, private communication, 1969.
167. T. Kan, H. T. Powell, and G. J. Wolga, *IEEE J. Quant. Electron., 5,299* (1969).
168. W. E. Lamb, Jr., *Phys. Rev.*, **134. Al429 (1 964).**
169. A. Szöke and A. Javan, *Phys. Rev., 145,137* (1966).
170. C. Bordé and L. Henry, *Compt. Rend., 265,* 125 1 (1967).
1 71. D. H. Close, *Phys. Rev.*, **153,360 (1967).**
172. W. J. Witteman, *IEEE J. Quant. Electron.*, **5**, 92 *(1969); ibid., 4,786* (1968).
173. H. Kogelnik and T. Li, *Proc. IEEE, 54, 13* 12 (I 966).
174. H. W. Mocker, *Appl. Phys. Letters,* **12**, 20 (1968).
175. J. B. Gerardo and J. T. Verdegen, *Proc. IEEE, 52.690* (1964).
176. R. A. Stern and *P.* **K.** Cheo, *Phys. Rev. Letters,* 23, 1426 (1969); 1970 Annual Joint Meeting of Am. Phys. Soc. and Am. Assoc. of Phys. Teachers, Chicago, Illinois (invited paper).
177. See, for example, P. Vandenplas, *Electron Waves and Resonances in Bounded Plasmas,* Wiley, New York, 1968.
178. S. L. McCall and E. L. Hahn, *Phys. Rev. Letters,* **18,908** (1967).
179. S. L. McCall and E. L. Hahn, *Phys. Rev.*, **183,457** (1969).
180. A. Bloom, *Phys. Rev., 98,* 1 105 (1955).
181. R. L. Abrams and A. Dienes, *Appl. Phys. Letters, 14. 237* (1969).
182. P. L. Gordon, S. E. Schwarz, C. 'V. Shank, and 0. R. Wood, *Appl. Phys. Letters,* **14,235** (1969).
183. E. B. Treacy and A. J. DeMaria, *Phys. Letters,* **29A**, **369 (1969).**
184. W. G. Wagner, H. A. Haus, and K. T. Gustafson, *IEEE J. Quant. Electron., 4, 267* (1968).
185. G. D. Boyd and H. Kogelnik, *Bell System Tech. J., 41, 1346 (1962).*
186. P. K. Cheo, unpublished work, 1966.
187. A. L. Schawlow and C. H. Townes, *Phys. Rev.*, **112,** 1940 (1958).
188. A. E. Siegman, B. Daino, and K. R. Manes, *IEEE J. Quant. Electron., 3, 180* (1967).
189. A. D. White, *IEEE J. Quant. Electron., 1,349 (I 965).*
190. G. Birnbaum, *Proc. IEEE, 55,* 1015 (1967).

191. T. G. Polanyi and 1. Tobias, Lasers- A Series of Advances, Vol. II (A. K. Levine, ed.), Dekker, New York, 1968.
192. T. J. Bridges, T. Y. Chang, and P. K. Cheo, *Appl. Phys. Letters,* **12,297 (1968).**
193. R. L. Barger and J. L. Hall, *Phys. Rev. Letters,* **22**, 4 *(1969).*
194. R. W. Hellwarth, *Advances in Quantum Electronics* (J. Singer, ed.), Columbia Univ. Press, New York, 1961.
195. C. G. B. Garrett, Gas *Lasers,* McGraw-Hill, New York, 1967.
196. R. C. Crafer, A. F. Gibson, M. J. Kent, and M. F. Kimmitt, *Brit. J. Appl. Phys., 2,* 183 (1969).
197. C. Frapard, *IEEEJ. Quant. Electron., 2,225 (1966).*
198. E. B. Treacy, *Proc. IEEE,* **46**, 2053 *(1968).*
199. R. L. Abrams, *IEEEJ. Quant. Electron,, 5.522 (1969).*
200. S. Marcus, *Appl. Phys. Letters,* 15.2 17 (I 969).
201. B. H. Soffer, *J. Appl. Phys.*, 35,255 I (1964); P. Kafalas, J. 1. Masters, and E. M. E. Murray, *ibid., 2349 (1964).*
202. A. Szöke, V. Daneu, J. Goldhar, and N. A. Kurnit, *Appl. Phys. Letters, 15. 376* (1969).
203. L. E. Hargrove, R. L. Fork, and M. A. Pollack, *Appl. Phys. Letters,* **5**, 4 *(I 964).*
204. 0. P. McDuff and S. E. Harris, *IEEE J. Quant. Electron., 3. 101 (1967).*
20.5. W. R. Hook, R. P. Hilberg, and R. H. Dishington, *Proc. IEEE, 54, 1954 (I 966);* R. N. Zitter, W. H. Steier, and R. Rosenberg, *IEEE J. Quant. Electron., 3, 6* 14 *(1967).*
206. P. W. Smith, *IEEE J. Quant. Electron., 3,627 (1967).*
207. A. G. Fox and P. W. Smith, *Phys. Rev. Letters,* 18,826 (1967).
208. J. A. Armstrong and E. Courtens, *IEEE J. Quant. Electron., 4. 4 I* 1 (1968); F. T. Arecchi and R. Bonifacio, *ibid., 1,* 169 *(I 965).*
209. J. A. Fleck, *Phys. Rev. Letters,* 21, 13 1 (I 968).
210. H. Risken and K. Nummedal, *J. Appt. Phys.,* **39**, 4662 *(I 968).*
211. P. K. Cheo and J. Renau, *J. Opt. Soc. Am.,* **59**, 82 1 (*1969).*
212. 8.8 Kilowatt CW Output Produced by Experimental CO, System. *Laser Focus, 4,* 3 (1968).
213. D. C. Smith, *IEEEJ. Quant. Electron.,* **5**, 29 *I (1969).*
214. A. F. Gibson, private communication.
21.5. D. M. Kuehn and D. J. Monson, *Appl. Phys. Letters,* **16**, 48 (1 *970).*
216. CW Chemical Laser Requires No External Energy Source, Editor, *Phys. Today,* Search and Discovery, **22**, 55, December (1969).
217. H. L. Chen, J. C. Stephensen, and C. B. Moore, *Chem. Phys. Letters, 2,* 593 (1968).
218. R. W. F. Gross, *J. Chem. Phys.. 50, 1889 (1969).*
219. R. S. Reynolds, International Electron Device Meeting, Washington, D.C., Oct. 28–30, 1970.
220. J. A. Beaulieu, *Bull. Am. Phys. Soc., 15, 808 (1970).*
221. C. J. Buczek. R. J. Wayne. P. Chenausky, and R. J. Freiberg, *Appl. Phys. Letters.* **16**, 32 1 (1970).
222. C. 0. Brown and J. W. Davis, private communication, 1970.
223. A. J. DeMaria, "Electrically Excited CO_2 Lasers," Meeting American Physics Society, Washington, D.C., April 1970, invited paper.
224. E. T. Gerry, "Gas-Dynamic CO_2 Lasers," Meeting American Physics Society, Washington, D.C., April 1970, invited paper.